# Activation of the human
Mediator kinase CDK8 by MED12
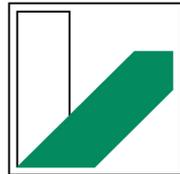
UNIVERSITÄT BAYREUTH

DISSERTATION

Submitted to the Bayreuth Graduate School Mathematical and Natural
Sciences (BayNAT) of the University of Bayreuth for
obtaining the academic grade of

Doctor rerum naturalium (Dr. rer. Nat)

by

Felix Klatt

from Berlin

September 2020

This doctoral thesis was prepared in the laboratory "Gene regulation by non-coding RNA" at the University of Bayreuth from December 2014 until September 2020 and was supervised by Dr. Claus-D. Kuhn

This is full reprint of the thesis submitted to obtain the academic degree of Doctor of Natural Sciences (Dr. rer. nat.) and approved by the Bayreuth Graduate School of Mathematical and Natural Sciences (BayNAT) of the University of Bayreuth.

Date of submission: 15.09.2020

Date of defense: 01.12.2020

Acting director: Prof. Dr. Markus Lippitz

Doctoral committee:

Dr. Claus-D. Kuhn	(reviewer)
Prof. Dr. Olaf Stemmann	(reviewer)
Prof. Dr. Clemens Steegborn	(chairman)
Prof. Dr. Angelika Mustroph	

Author contributions

Part of the results of this thesis were published in the following manuscript:

This thesis contains data from the following students:

- Franziska Langhammer, BSc (Master's thesis)
- Robin Weinmann, BSc (research module and Master's thesis)
- Melanie R. Müller, BSc (research module and Master's thesis)
- Bastian Jahreis, BSc (research module)
- Silas Amarell, BSc (research module)
- Meret Kuck (research module and Bachelor's thesis)
- Amelie Lindner (research module and Bachelor's thesis)

All of them were intensively supervised by myself and significantly contributed to this work. Presented data from these students are clearly defined in each figure legend.

Data from other scientist, which were relevant for this work, are separated in a distinct chapter. This comprises electrospray ionization mass spectrometry, crosslinking coupled to mass spectrometry and X-ray crystallography.

Summary

Eukaryotic transcription is regulated by the Mediator kinase module, which phosphorylates transcription-related targets and controls the association of Mediator and RNA polymerase II. The activity of its catalytic heart, cyclin-dependent kinase 8 (CDK8), is regulated by Cyclin C and the Mediator subunit MED12, with its malfunction contributing to numerous malignancies. To unravel how CDK8 activation is enhanced by MED12, I established recombinant expression and purification schemes that resulted in monodisperse, highly pure binary CDK8/Cyclin C and ternary CDK8/CycC/MED12 complexes. Using these complexes, I combined *in vitro* biochemistry, cross-linking coupled to mass spectrometry, and *in vivo* studies to decipher how the N-terminal portion of MED12 binds on the CDK8/Cyclin C complex and to gain mechanistic insights into the MED12-dependent CDK8 activation.

The data presented in my thesis demonstrate that the N-terminal part of MED12 wraps around CDK8, whereby it places an "activation helix" in direct proximity to the CDK8 T-loop for its activation. Interestingly, mutations in the activation helix that are frequently found in cancers do not alter the affinity of MED12 for CDK8, yet likely alter the exact positioning of the activation helix resulting in impaired CDK8 activity. Moreover, we find the transcriptome-wide gene-expression changes in human cells that result from a mutation in the MED12 activation helix to correlate with deregulated genes in breast and colon cancer. Finally, functional assays in the presence of kinase inhibitors reveal that MED12 binding reshapes the active site of CDK8 and thereby precludes the inhibition of ternary CDK8 complexes by type II kinase inhibitors. Taken together, these data establish that a newly identified activation helix in MED12 functionally replaces CDK8 T-loop phosphorylation and thereby likely remodels the active site. These data not only allow us to propose a revised model of how CDK8 activity is regulated by MED12, yet they have significant implications to drug development and will pave the road to new and specific CDK8 inhibitors that target CDK8 in its MED12-bound form.

Zusammenfassung

Das humane Mediator Kinasemodul reguliert eukaryotische Transkription durch die Phosphorylierung von Transkriptionsfaktoren und durch die Modulation der Interaktion des Mediatorkomplexes mit RNA Polymerase II. Die enzymatische Aktivität des Kinasemoduls basiert dabei auf der Cyclin-abhängiger Kinase 8 (CDK8), welche von Cyclin C und MED12 kontrolliert wird. Wichtig ist, dass viele Krebserkrankungen mit der Fehlregulation von CDK8 assoziiert sind. Um den MED12-abhängigen Mechanismus der CDK8 Aktivierung auf molekularer Ebene zu entschlüsseln, habe ich rekombinante Expressions- und Reinigungsmethoden für Proteinkomplexe etabliert, welche neben CDK8 und Cyclin C zusätzlich MED12 beinhalten. Diese gereinigten, monodispersen Proteinkomplexe wurden mittels *in vitro* Biochemie, chemischer Quervernetzung gekoppelt mit Massenspektrometrie und *in vivo* Experimenten dahingehend analysiert, um die Bindung des N-terminalen Segments von MED12 an den CDK8/Cyclin C Komplex zu charakterisieren und um mechanistische Details über die MED12-abhängige CDK8 Aktivierung zu erhalten.

Die Ergebnisse zeigen, dass sich MED12 um CDK8 herum windet. Dabei platziert MED12 eine „Aktivierungshelix" in der Nähe des T-loops von CDK8, was eine signifikante Stimulation der CDK8 Kinaseaktivität nach sich zieht. Darüber hinaus untersuchten wir besonders häufige, mit Krebs in Verbindung stehende MED12 Mutationen in der Aktivierungshelix. Interessanterweise stören diese Mutationen nicht die Interaktion von MED12 mit dem CDK8/Cyclin C Komplex, sondern sie veränderten höchstwahrscheinlich die exakte Platzierung der Aktivierungshelix, was mit einer deregulierten Kinaseaktivität korreliert. Zudem konnte gezeigt werden, dass durch eine Mutation in der MED12 Aktivierungshelix krebsartige Genexpressionsprofile von Brust- und Darm-Krebs in menschlichen Zellen hervorgerufen werden. Abschließende funktionale Studien mit Kinaseinhibitoren zeigten ferner, dass die Bindung von MED12 an CDK8 dessen aktives Zentrum strukturell verändert, wodurch die Bindungsaffinität und somit auch die Wirkung von Typ II Kinaseinhibitoren gegenüber CDK8 drastisch reduziert wird. Zusammengefasst wurde eine neue Aktivierungshelix in MED12 entdeckt, die auf funktionaler Ebene die allgemein notwendige Phosphorylierung des T-loops in CDK8 ersetzt, wobei das aktive Zentrum der Kinase verändert wird. Diese Ergebnisse sind Grundlage eines neuen Models der MED12-abhängigen Regulation der Kinaseaktivität von CDK8. Zusätzlich legt diese Arbeit nahe alle zukünftigen CDK8 Inhibitoren gegen MED12-gebundene CDK8 Komplexe zu entwickeln.

Contents

Figures

Abbreviations

AFF4	AF4/FMR2 familiy member 4
ATF1	Activating transcription factor 1
BRD4	Bromodomaincontaining protein 4
BRCA1	Breast cancer type 1 susceptibility protein
CAK	CDK-activating kinase
CDK	Cyclin-dependent kinase
CTD	C-terminal domain
Cyc	Cyclin
DSF	Differential scanning fluorimetry
DSIF	DRB sensitivity induced factor
E. coli	*Escherichia coli*
EMT	Epithelial-mesenchymal transition
GST	Glutathion S-transferase
hpt	Hours post transfection
IFN	Interferon
ITC	Isothermal titration calorimetry
MED12/13	Mediator of RNA polymerase II transcription subunit 12/13
MST	Microscale thermophoresis
NELF	Negative elongation factor
NGS	Next-generation sequencing
sgRNA	Single guide RNA
ssODN	Single stranded oligonucleotide donor
SHH	Sonic Hedgehog
Sirt-1	Sirtuin-1
SMAD	Mothers against decapentaplegic
STAT1	Signal transducer and activator of transcription 1
TAD	Transactivation domain
TF	Transcription factor
TFE	Trifluoroethanol
TGF/ß	Transforming growth factor beta
P2A	Porcine teschovirus-1 2A
Pol II	RNA Polymerase II
p-TEFb	Positive transcription elongation factor b
vCyc	Viral Cyclin
Wnt	Wingless and Int-1

Chapter 1: Introduction

1.1   Protein kinases

Eukaryotic proteins are regulated by post-translational modifications and the most widespread type of protein modification is phosphorylation (Ubersax and Ferrell, 2007). The reversibly nature of protein phosphorylation makes it an ideal candidate for the regulation of transient processes. The post-translational phosphorylation of proteins is mediated by protein kinases, all which catalyze the transfer of a gamma-phosphoryl group from ATP to a hydroxyl group of a serine, threonine or tyrosine residue. Protein kinases regulate a plethora of cellular processes and comprise the largest superfamily of eukaryotic enzymes. Already in the 1980s, protein kinases were shown to have important roles in oncogenesis and tumor progression and since have received increasing attention as targets for anticancer therapies (Hartwell et al., 1974; Manning et al., 2002; Rzymski et al., 2015). Accordingly, protein kinases are amongst the most critical and widely studied cellular signaling molecules.

Protein kinases differ in their ability either to phosphorylate serine/threonine or tyrosine residues. Thus, kinases are mechanistically classified into serine/threonine- and tyrosine-directed kinases. Cyclin-dependent kinases (CDKs) are serine/threonine kinases that were initially discovered as regulators of the cell cycle. The cell cycle contains several checkpoints to ensure the completion of the previous step, whereas cell cycle progression and regulation is tightly controlled by CDKs. Moreover, CDKs are engaged in fundamental processes such as transcription, epigenetic regulation, metabolism, neuronal differentiation, hematopoiesis, angiogenesis, stem cell self-renewal, and spermatogenesis (Lim and Kaldis, 2013; Malumbres, 2014; Morgan, 1997). Considering their broad biological functions, it is not surprising that malfunction or dysregulation of CDKs is a common feature of many cancers (Blume-Jensen and Hunter, 2001; Hanahan and Weinberg, 2011) Therefore, mechanistic information about CDK regulation is indispensable and the route to take that lead to novel, potent anti-cancer drugs (Blume-Jensen and Hunter, 2001).

1.1.1   Cyclin-dependent kinases

CDKs belong to the CMGC family, which is named for its primary constituent groups: Cyclin-dependent kinases (CDKs), mitogen-activated protein kinases (MAPKs), glycogen synthase kinases (GSKs) and CDK-like kinases (CLKs). It represent the largest protein family within the kinome (Varjosalo et al., 2013). CDKs can be subdivided into two broad groups: Those that mediate the progression of the cell cycle (e.g. CDK1, CDK2, CDK4 and CDK6, together referred as cell cycle-related CDKs) and those that regulate transcription (e.g. CDK7, CDK8, CDK9, together referred as transcription-related CDKs) (Fig. 1) (Espinosa, 2019; Malumbres, 2014). The enzymatic activity of CDKs is regulated by their partner proteins, the cyclins. Cell cycle-related CDKs can bind multiple cyclins, whereas transcriptional CDKs usually interact with one specific cyclin. Cyclin proteins vary in mass from 35 to 90 kDa and their amino acid sequence alters considerably, despite the fact that all of them are characterized by two conserved cyclin-box domains. Cell cycle-related cyclins are synthesized and destroyed at specific checkpoints during the cell cycle, thus regulating kinase activity in a timely manner (Malumbres, 2014). Tumor cells are often characterized by aberrant expression of cyclins rather than of the cell cycle CDKs themselves (Diehl, 2002). In contrast, cyclins that bind to transcription-related CDKs show a constant protein-level (Malumbres, 2014). During interphase, cell cycle progression is mediated by CDK4, CDK6, CDK2 and CDK3, whereas entry into mitosis is dependent on CDK1 (Malumbres and Barbacid, 2001). On the other hand, CDK7, CDK9 and CDK8 participate in promoting mRNA transcription by RNA polymerase II (RNA pol II), which directs the expression of protein-coding genes. Other CDKs regulate diverse processes including RNA splicing, transcript synthesis (CDK11, CDK12, CDK13) (Malumbres, 2014; Trembley et al., 2002) and neuronal function (CDK5, CDK10) (Lim and Kaldis, 2013).
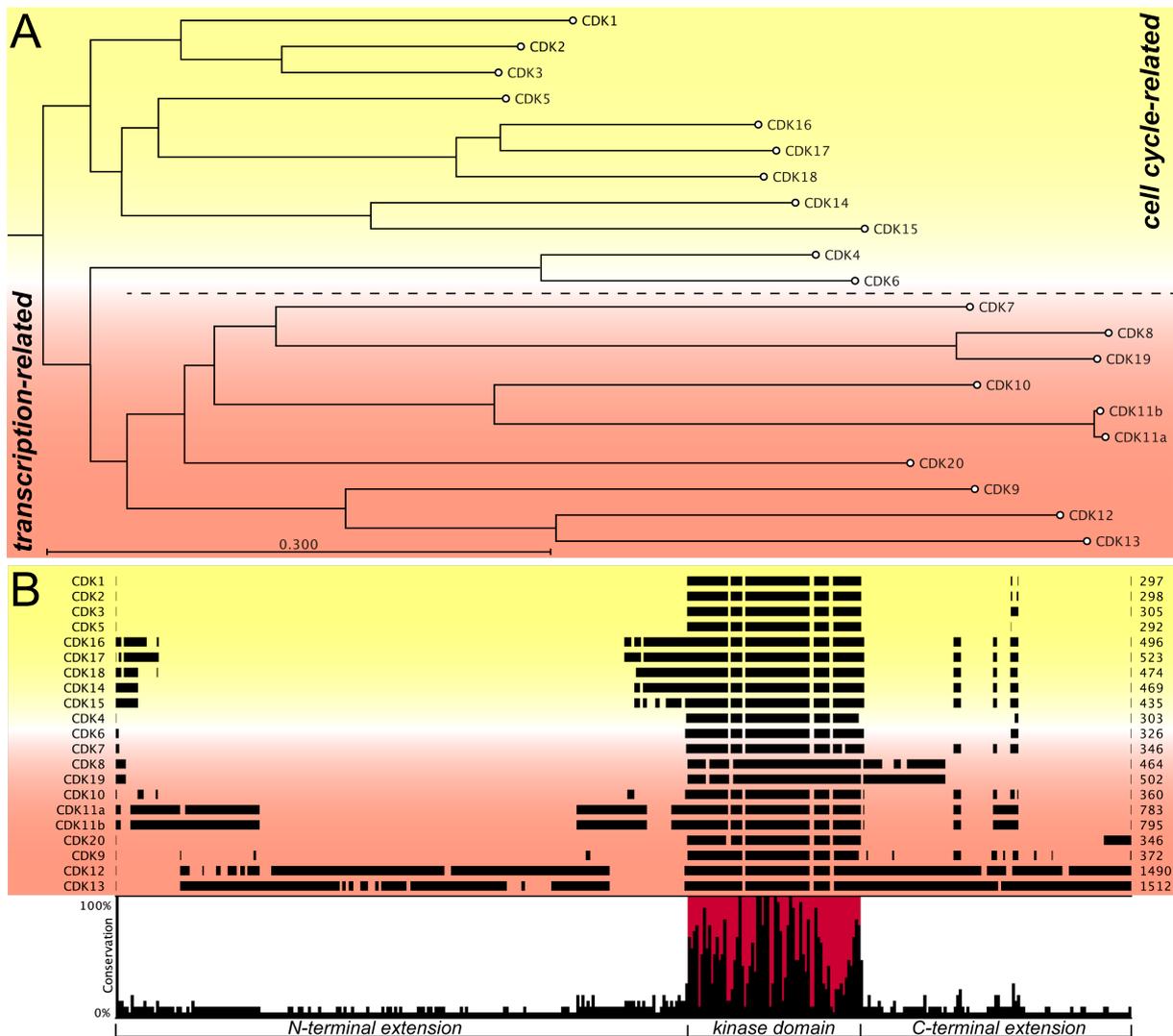
Figure 1: Evolutionary relationships among the human CDK subfamilies.

(**A**) Phylogenetic tree of all human CDKs. Cell cycle-related CDKs are shaded in green, transcription-related kinases are shaded in blue. (**B**) Sequence-alignment of all human CDKs. The conserved protein kinase domain is highlighted in red. The extend of conservation is represented by the height of the black bar beneath each residue. Coloring like in (A).The phylogenetic tree and the sequence-alignment was created with CLC Main Workbench 7 using canonical UniProt sequences.

1.1.1   Architecture of Cyclin-dependent kinases

CDKs range in size from approximately 250 amino acids, just harboring the conserved catalytic kinase domain, to proteins of more than 1500 residues with amino- and/or carboxy-terminal extensions of variable length (Fig. 1B) (Malumbres, 2014). Like all protein kinases, CDKs have a two-lobed structure: The N-terminal lobe is dominated by a series of ß-strands (often folded into an orthogonal barrel-like structure), with at least one absolutely conserved α-helix, the αC-helix. This helix was initially termed PSTAIRE-helix based on its amino acid composition in CDK1 and CDK2 (Fig. 2).
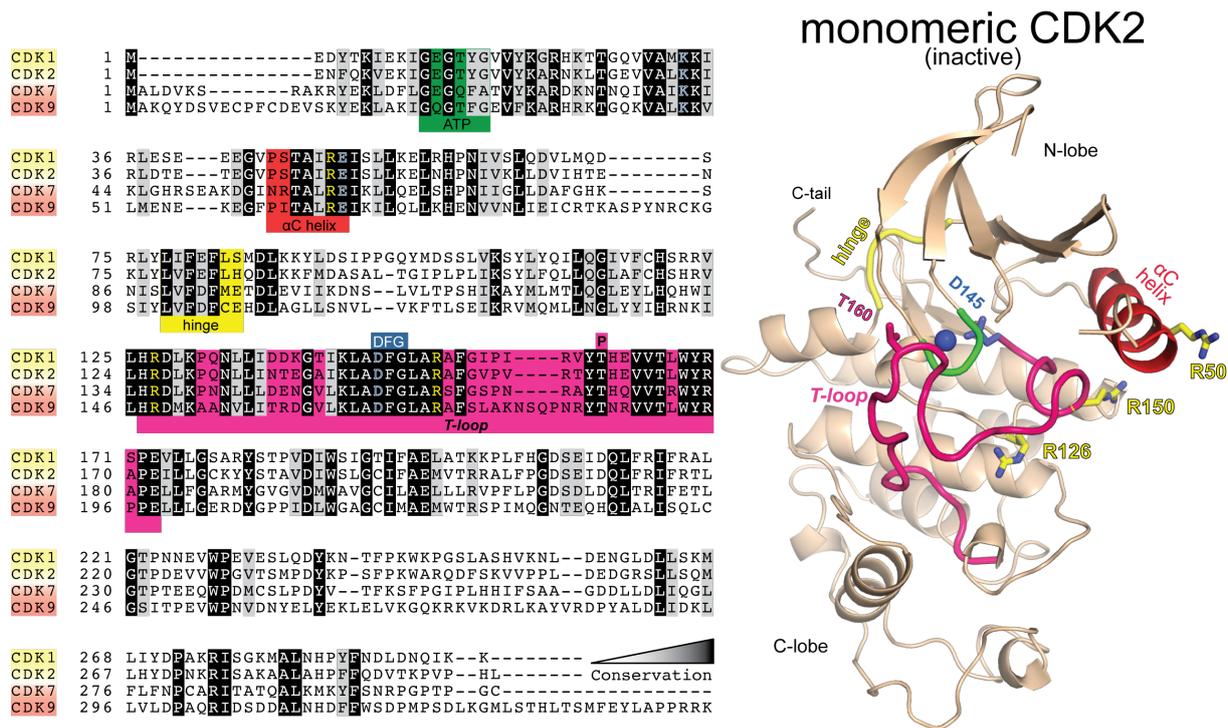
Figure 2: Sequence alignment and domain organization of prominent human CDKs.

Greyscale shading illustrates the extent of sequence conservation calculated from canonical UniProt sequences using Clustal Omega (Madeira et al., 2019). The ATP binding site is highlighted in green, the αC-helix in red, the hinge region in yellow and the T-loop in pink. The DFG motif is highlighted in blue within the T-loop, the activating phosphorylation site in pink. Residues that are part of the arginine triad are colored in yellow, residues that confine the catalytic triad are colored in blue. Please note that D145^{CDK2} belongs to both the DFG motif and the catalytic triad, and is shown as blue stick together with the Mg^{2+} ion (shown as a blue sphere). The activating phosphoresidue T160^{CDK2} is shown in pink within the T-loop. The alignment was exported into Expasy Boxshade. Structural features described are illustrated in their respective color on the fold of monomeric CDK2 (PDB code 1HCK). Shading of cell cycle- and transcription-related CDKs as in Fig 1.

The C-terminal lobe varies in size, sequence and topology. It is larger than the N-lobe and consists predominantly of α-helices. A short linker (commonly referred to as hinge region) connects the two lobes (Fig. 2). The linker region is a key element of the ATP nucleotide binding site, which lies in a cleft formed at the junction of the N- and C-terminal lobes. The conserved catalytic core is made up of the ATP-binding pocket, the αC-helix (which represent the cyclin binding domain) and a T-loop motif (Fig. 2) (Endicott and Noble, 2013; Malumbres, 2014). CDKs share additional characteristics, such as an arginine triad, a DFG motif and an activating phosphorylation site located in the T-loop and essential for full kinase activity. Collectively, all these features participate in CDK activation. In the cyclin-free monomeric state, critical residues within the CDK catalytic core are incorrectly positioned, preventing enzymatic activity. Lastly, the T-loop which binds the phospho-acceptor serine/threonine region of substrates is partially disordered in the inactive state (Jeffrey et al., 1995; Russo et al., 1996).

1.1.2   Activation of Cyclin-dependent kinases

The regulation of CDK activity is a multilayered process. It includes cyclin binding to its cognate CDK, inhibitory and activating phosphorylation and dephosphorylation events, and association of CDK-cyclin complexes with cellular cyclin-dependent kinase inhibitors or other cofactors that modulate the catalytic core of the CDK (Denicourt and Dowdy, 2004; Morgan, 1995; Pavletich, 1999; Pines, 1999). Many crystal structures of the CDK/cyclin family are available that revealed many of the aforementioned conserved features. The best-characterized CDK is CDK2, whose structure could be solved in multiple regulatory states. Therefore, the canonical CDK activation mechanism is based on comprehensive structural information on different activation states of CDK2 (Fig. 3) (De Bondt et al., 1993; Jeffrey et al., 1995; Russo et al., 1996).

In general, cyclin binding controls kinase activity and substrate specificity by the rearrangement of the αC-helix (Fig. 3A). This rearrangement releases a steric block to the catalytic site, formed by the DFG motif. In CDK2, the shift of the αC-helix upon cyclin binding causes the reorientation of $E51^{CDK2}$ into the binding cleft, where it comes close to $K33^{CDK2}$ and $D145^{CDK2}$ (the latter amino acid is the first of the DFG motif). These three residues constitute a catalytic triad that is conserved in all eukaryotic kinases and chelates the Mg^{2+}-ion necessary for ATP hydrolysis. For full CDK-activity, the T-loop has to be positioned in its catalytically competent conformation (Fig 3B). This is driven by T-loop phosphorylation. There, the introduced negative charge serves as an ionic organizing center to arrange the arginine-triad and thereby positions the T-loop in its fully active conformation (Huse and Kuriyan, 2002; Jeffrey et al., 1995; Nolen et al., 2004). Phosphorylation within the T-loop thereby completes the reorganization of the substrate binding site that was initiated by cyclin binding (Fig. 3C). In this regards, the transcription-related CDK CDK7 is of particular interest since it was identified as the CDK-activating kinase that mediates the T-loop phosphorylation of CDK1, CDK2, CDK4 and CDK6 and itself as well (Fisher, 2005; Liu and Kipreos, 2000).
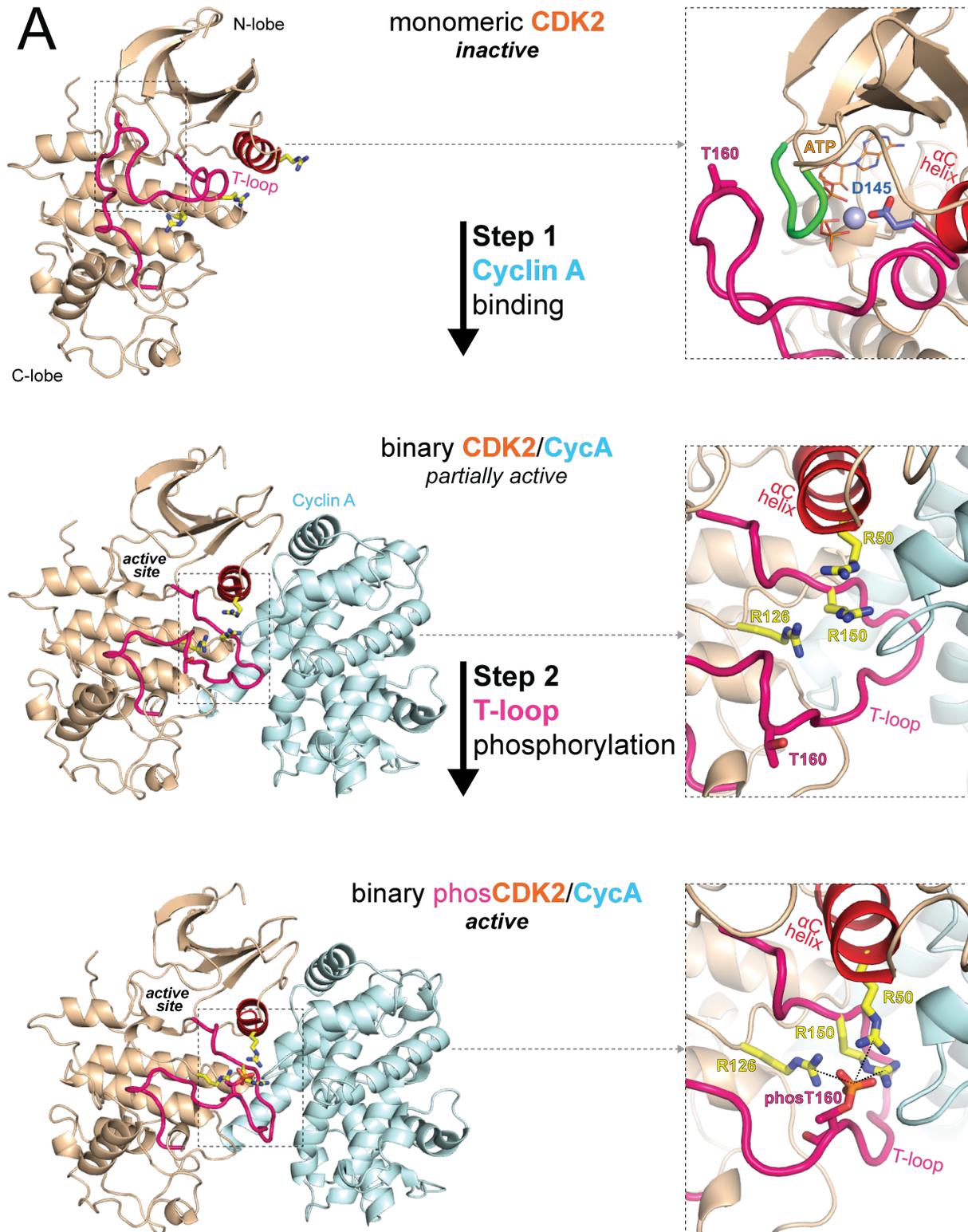
Figure 3: Canonical phosphorylation-dependent activation mechanism of the CDK/Cyclin family.
(**A**) The left side shows different CDK2 structures in cartoon representation that correspond to the non-activated (monomeric CDK2, PDB code 1HCK), the partially active (binary CDK2/CycA complex, PDB code 1FIN) and the fully active (phosphorylated CDK2/CycA complex, PDB code 1JST) CDK2 states. Coloring as in Fig. 2. The right side shows individual close ups of the CDK2 T-loop to stress out structural changes upon cyclin binding (step 1) and T-loop phosphorylation (step 2). In the inactive, monomeric state, the ATP binding site (highlighted in green) is sterically blocked by the T-loop. The ATP molecule is shown in orange. Step 1: Cyclin binding releases the T-loop that leads to the formation of the activate site. However, the T-loop and the arginine triad are still misaligned to each other. Step 2: Phosphorylation of T160^{CDK2} within the CDK2 T-loop (phosT160) reorients the arginine triad and thereby positions the T-loop in its fully active conformation. Please note that the figure continuous on the following page.
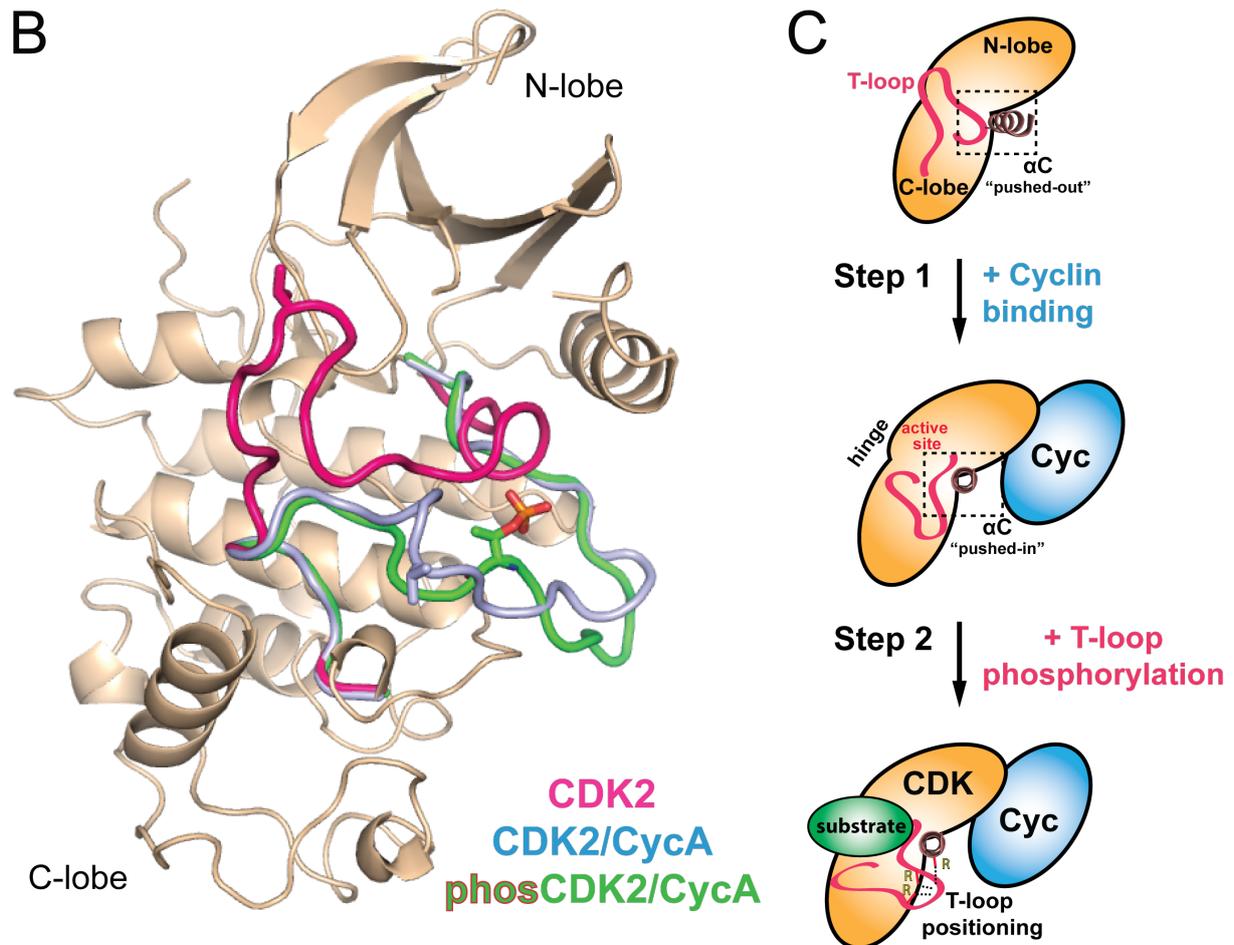
Figure 3 (continued): Canonical phosphorylation-dependent activation mechanism of the CDK/Cyclin family
(**B**) Superimposition of the different T-loop conformations that were shown in (A) on monomeric CDK2. The T-loop of the inactive, monomeric CDK2 is colored in pink, of the binary CDK2/CycA in blue and of phosphorylated, active CDK2/CycA complex in green. The activating phosphoresidue T160[CDK2] within each T-loop conformation is colored and illustrated in stick representation. (**C**) Schematic two-step activation mechanisms of the CDK/Cyclin family based on regulatory CDK2 states as shown in (A).

1.1.3 Non-canonical activation of Cyclin-dependent kinases

In addition to the canonical phosphorylation-dependent two-step activation mechanism, some mammalian CDKs have evolved deviating ways of kinase activation (Fig. 4). This is, for example, the case for the activation of CDK1 and CDK2 by Spy1/RINGO (Fig. 4A) (Cheng et al., 2005; McGrath et al., 2017). The structure of a CDK2/Spy1 complex revealed several interactions made by three consecutive acidic residues (E134[Spy1], E135[Spy1], and D136[Spy1]) which insert between the αC-helix and the T-loop of CDK2. Precisely, D136[Spy1] coordinates the arginine triad in CDK2 (R50[CDK2], R126[CDK2], and R150[CDK2]) (Jeffrey et al., 1995; McGrath et al., 2017). Moreover, the murine gammaherpesvirus 68 encodes a cyclin homologue (vCyc)
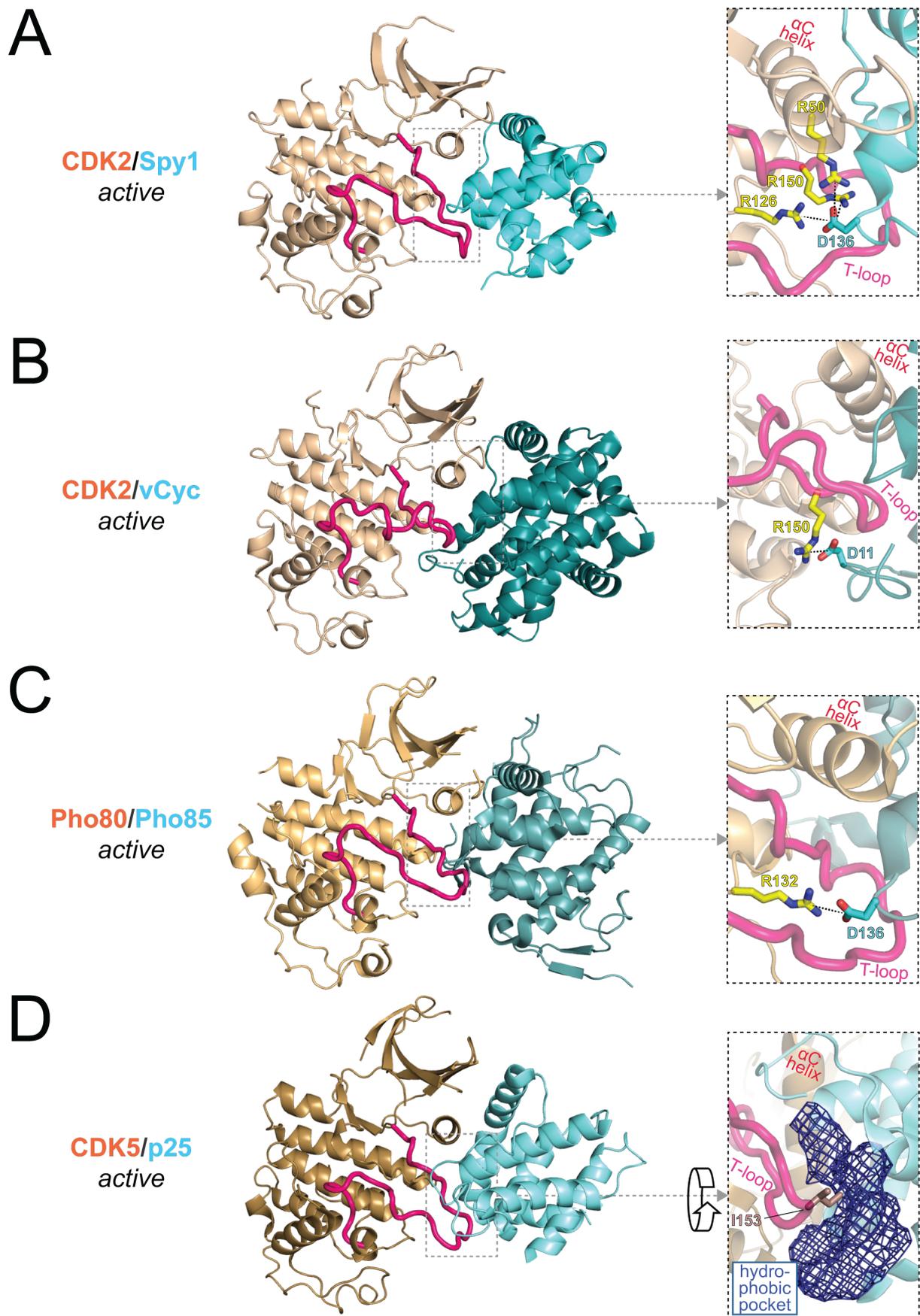
Figure 4: Mechanisms of non-canonical, phosphorylation-independent CDK activation.

For detailed description please see main text. PDB codes (**A**) CDK2/Spy1: 5UQ1, (**B**) CDK2/vCyc: 1F5Q, (**C**) Pho80/Pho85: 2PK9, (**D**) CDK5/p25: 1H4L.

that establishes a salt-bridge between R150^{CDK2} (part of the arginine triad) and D11^{vCyc} placing the T-loop in its active conformation (Fig. 4B) (Card et al., 2000). The mechanisms just described for the viral cyclin is also employed by the phosphate-dependent signaling complex Pho85/Pho80 that shows homology to CDK/cyclin complexes. Pho85 (the CDK) makes an ionic bond between R132^{Pho85}, again part of the arginine triad, and D136^{Pho80} on Pho80 (the cyclin) which locks the activation loop of Pho85, thereby circumventing the requirement for T-loop phosphorylation (Fig. 4C) (Huang et al., 2007). Last, p25 utilizes a non-ionic, phosphorylation-independent activation mechanism to activate CDK5. Specifically, p25 tethers the unphosphorylated T-loop of CDK5 in an active conformation. The side chain of I153^{CDK5}, located at the tip of the activation loop, is buried into a hydrophobic pocket (formed by the side chains of A199^{p25}, M237^{p25}, I275^{p25}, A277^{p25}, P279^{p25} and F282^{p25}) (Fig. 4D) (Tarricone et al., 2001).

Altogether, T-loop phosphorylation in CDK2/Spy1, CDK2/vCyc and Pho80/85 complexes is functionally replaced by a negatively charged side chain, whereas CDK5 activation by p25 relies on specific hydrophobic interactions that position the T-loop in its catalytically competent conformation. An additional phosphorylation-independent activation mechanism was reported for CDK6 in complex with a vCyc (PDB code 1JOW) (Schulze-Gahmen and Kim, 2002). The structure reveals that the vCyc folds around the T-loop of CDK6. In more detail, F172^{CDK6} located at the tip of the T-loop, is buried between hydrophobic residues from the vCyc, similar to the phosphorylation-independent activation mechanism of the CDK5/p25 complex (Fig. 4D). Intriguingly, CDK2/Spy1 and CDK/vCyc complexes show elevated kinase activity compared to natural CDK/cyclin complexes. Moreover, these complexes are resistant to endogenous Cyclin-dependent kinase inhibitors and thereby overcome cell cycle progression constrains (Cheng et al., 2005; Swanton et al., 1997).

1.1.4   CDK8 and CDK19 are specialized Cyclin-dependent kinases

The crystal structure of the binary CDK8/Cyclin C complex was solved almost a decade ago (Fig. 5) (Schneider et al., 2011). CDK8 is an atypical CDK for several reasons. First, CDK8 possesses an atypical DFG motif - instead of a phenylalanine it has a methionine (DMG) (Figs. 6 and 7). The CDK8 DMG motif undergoes a similar conformational change from DMG-out to DMG-in upon activation (Endicott and Noble, 2013). Second, CDK8 exclusively binds to Cyclin C. This can be seen by focusing on the αC-helix that displays a significantly altered amino acid composition in CDK8 (PSTAIRE$^{CDK1/CDK2}$ versus SMSACRE$^{CDK8/CDK19}$, please compare Figs. 2 and 7) (Xu and Ji, 2011). In addition, CDK8 possesses a unique N-terminal

helix, termed αB-helix, that makes extensive contacts to Cyclin C (Fig. 5) (Xu et al., 2014). A third specific feature of CDK8 is its extended C-terminal domain (residues 359-464) that most other CDKs lack and that might contribute to substrate recognition (Dixon-Clarke et al., 2015). The C-terminal domain could only be solved up to residue 359 by X-ray crystallography. As the utilized constructs comprise CDK8 residues 1-403, the CDK8 C-terminus is suggested to be flexible (Figs. 5 and 7). Last and most importantly, CDK8 lacks a phosphoresidue within its T-loop that could serve as activating organization center (Fig. 6). In aggregating all evidence, CDK8 must follow a currently unknown and distinct activation mechanism (Knuesel et al., 2009a; Schneider et al., 2011).
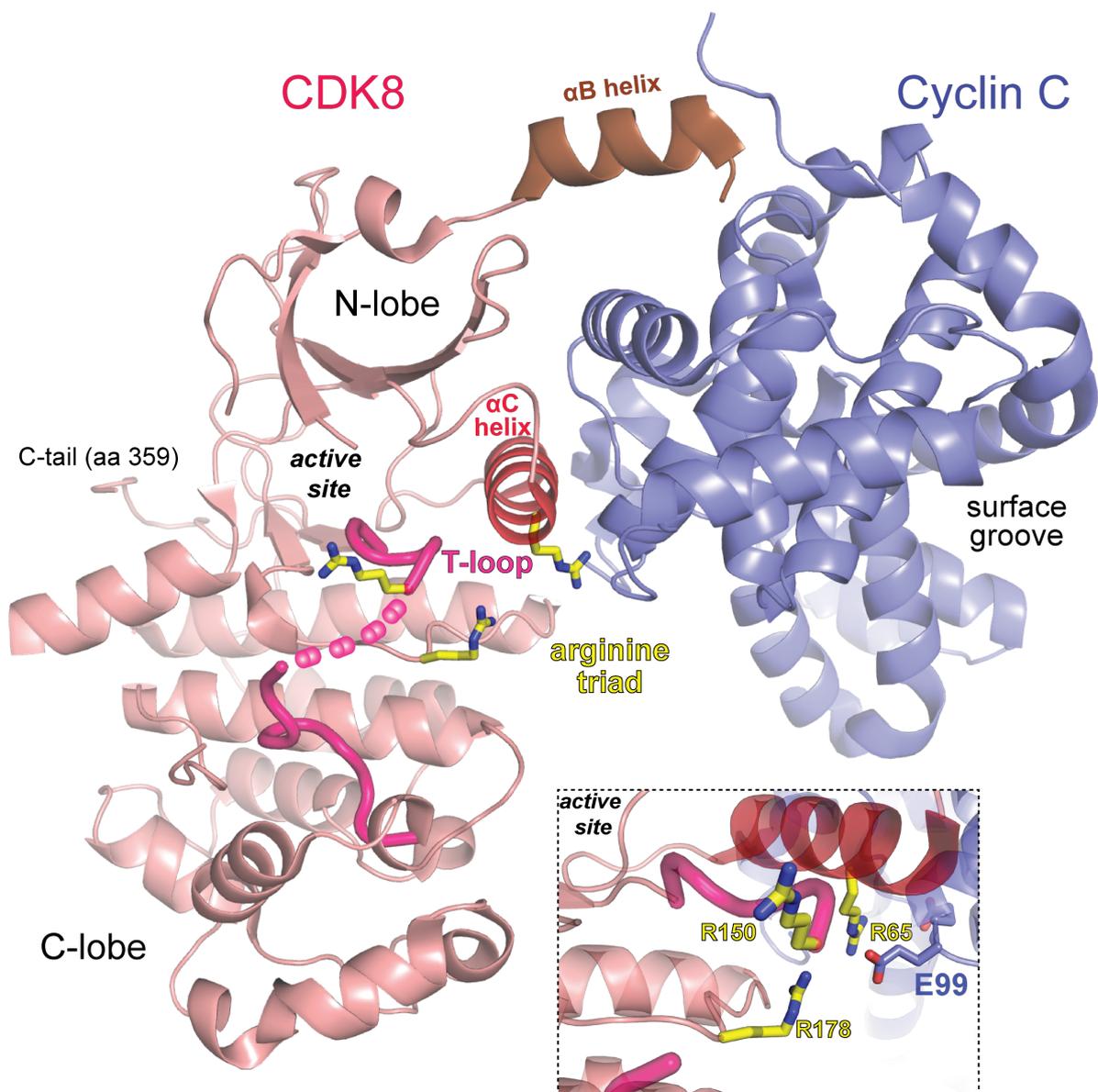
Figure 5: Crystal structure of the human CDK8/Cyclin C complex.

The CDK8/Cyclin C complex is shown in cartoon representation. The CDK8-specific αB helix is colored in brown. Please note that the arginine triad of CDK8 (shown as yellow sticks) is misaligned and the T-loop is partially disordered (the unresolved region is depicted as pink dashed line). The close up shows how E99 of Cyclin C points towards the disordered T-loop and the αC-helix of CDK8. PDB code 3RGF.

When comparing Cyclin C to other cyclins it also contains several unique features, like an extended hydrophobic surface groove, which is suggested for protein-protein interactions (Fig. 5). Notably, Cyclin C harbors two negatively charged residues ($E99^{CycC}$ and $E98^{CycC}$) in the vicinity of both the T-loop and the αC-helix of CDK8. Due to their proximity to the CDK8 active site, these residues were suggested to participate in CDK8 activation (Hoeppner et al., 2005; Schneider et al., 2011).

Figure 6: Sequence alignment of the T-loop in all human CDKs.

(**A**) The alignment was created as described in Fig. 3. Please note that the structure of the T-loop of CDK8 is only partially resolved (unresvoled residues are framed in pink) (**B**) The transitive consistency score (numbers to the right of each CDK) is an evaluation index, which indicates that CDK8 and CDK19 diverged significantly within the CDK family. The plot was generated using complete UniProt sequences (accession numbers are illustrated) (Chang et al., 2014; Madeira et al., 2019).

Currently, no structural information is available for CDK19. However, based on its high sequence identity to CDK8 (Fig. 7), CDK19 very likely shares most structural features of CDK8. The only region where both kinases differ significantly is their C-terminal domains, in which CDK19 carries two insertions with a length of roughly 40 residues (Fig. 7).

Figure 7: Sequence alignment of human CDK8 and CDK19.

Both Mediator kinases share CDK8 specific features. As the C-terminus of CDK8 is only resolved up to residue 359, it is believed that CDK8 has a flexible C-terminal domain. This also holds true for CDK19, however, CDK19 contains an even longer C-terminal domain due to two C-terminal CDK19-specific extensions.

1.2   Gene expression in eukaryotes

Eukaryotic organisms store their genetic information within the nucleus in the form of DNA (Crick and Watson, 1953; Oswald et al., 1944). In the nucleus, DNA is bound to proteins and organized in chromosomes. These proteins are called histones. The four different histones H2a, H2b, H3 and H4 build an octamer around which DNA is wound (Kornberg and Thomas, 1974). This complex associated with DNA is called nucleosome, which is the basic repeating structural and functional unit of chromatin.

The major difference to prokaryotes is the organization of DNA in nucleosomes. This leads to the requirement of numerous factors that make the DNA accessible for transcription. Therefore, many transcription factors are chromatin modifying proteins. The core of the eukaryotic transcription machinery is made by RNA polymerase II (Pol II). Pol II mediates the transcription of DNA into messenger RNA, which represents the majority of actively transcribed genes (Knorre, 1999; Orphanides et al., 1996). The process of transcription can be grossly divided into the three phases initiation, elongation and termination, that follow a cyclic mechanism (Fuda et al., 2009). The three phases of the Pol II transcription cycle are precisely orchestrated by the enzymatic activity of transcriptional CDKs, all of which cooperate to guide the Pol II through the nucleosome.

1.2.1   The Mediator complex and Pol II-dependent transcription

Transcription begins with the assembly of a macromolecular complex called the pre-initiation complex. The pre-initiation complex is dedicated to the regulation of Pol II activity and comprises apart from Pol II the general transcription factors TFIIA, TFIIB, TFIID, TFIIE, TFIIF and TFIIH (Cramer, 2019; Schilbach et al., 2017; Thomas and Chiang, 2006). This dynamic assembly is stabilized by the Mediator complex, which is globally required for transcription initiation (Kelleher et al., 1990; Malik and Roeder, 2005; Soutourina, 2018). When comparing Mediator with other components of the general transcription machinery, Mediator is the largest complex, in terms of its size and number of subunits (Allen and Taatjes, 2015; Kornberg, 2005; Malik and Roeder, 2010). Human Mediator comprises 30 protein subunits that are grouped into four modules: the head, the middle, the tail and the kinase module (Fig. 8). Whereas the first three modules form a stable complex, the kinase module reversibly associates with the three-module Mediator complex, building the CDK8-Mediator complex (Hengattner et al., 1995; Kim et al., 1994; Knuesel et al., 2009a). Although Mediator is conserved, its

sequences and subunit composition have diverged significantly in higher eukaryotes (Boube et al., 2002; Conaway et al., 2005). Nonetheless, structural and biochemical data indicate that the architectural framework of Mediator is conserved (Asturias et al., 1999; Tsai et al., 2014). As many structural models were obtained from yeast, this structural conservation allows the transfer of knowledge from yeast Mediator to its human counterpart.

The Mediator complex bridges between DNA bound transcription factors and the general transcription machinery at core promotors (Fig. 8). Transcription factors interact with the tail domain of the Mediator complex and bound regulatory information is transduced over the middle and head domain to Pol II (Larivière et al., 2012). Hence, Mediator can be considered as a universal signal processor by virtue of its ability to link activated transcription factors with Pol II. Moreover, Mediator is essential to connect distant regulatory elements like enhancers to the transcription machinery. Therefore, high transcription rates correlate with high Mediator densities on chromatin (Quevedo et al., 2019).
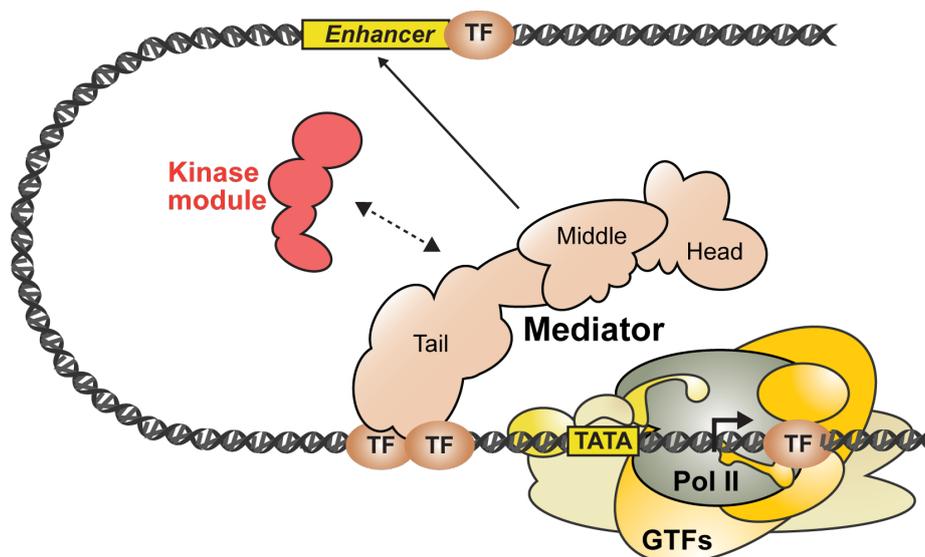
Figure 8: The Mediator complex and the general transcription machinery.
The three-module Mediator is colored in wheat, the reversibly binding kinase module is colored in red. DNA bound transcription factors (TF) are depicted in brown. Mediator-dependent chromatin looping brings the enhancer in proximity to its target gene. Adapted from Larivière et al., 2012.

1.2.2 The Pol II transcription cycle and the role of transcription-related CDKs

The transcriptional processivity of Pol II is finetuned by the phosphorylation status of its C-terminal domain (CTD). The Pol II CTD orchestrates the entire transcription cycle and acts as a dynamic command center (Eick and Geyer, 2013). Different sources of information are integrated to ensure that RNA synthesis is tailored precisely to the needs of the cell. The Pol II CTD is composed of 26 (in yeast) or 52 (in humans) heptad repeats of the seven amino acids

YSPTSPS (Di Giulio and Kreitman, 2009; Stiller and Hall, 2002). In contrast to other RNA polymerases, only Pol II possesses a CTD (Phatnani and Greenleaf, 2006; Sims et al., 2004). The three-dimensional structure of the CTD is modulated by phosphorylation, which provides a means to recruit transcription factors and chromatin modifiers (Spain and Govind, 2011).

The coevolutionary relationship between the Pol II CTD and transcription-related CDKs underscores the importance of transcriptional CDKs for Pol II regulation (Chapman et al., 2008; Guo and Stiller, 2004). Transcription-related CDKs regulate transcription by Pol II CTD phosphorylation and by phosphorylation of transcription factors (Allen and Taatjes, 2015; Pinhero et al., 2004; Poss et al., 2013). The phosphorylation of the three serine residues (Ser-2, Ser-5 and Ser-7) is linked to distinct stages of Pol II-dependent transcription and is mediated by CDK7, CDK9 and CDK8 (Fig. 9) (Adelman and Lis, 2012). Considering that these aforementioned transcription-related CDKs are part of large multiprotein complexes (TFIIH, p-TEFb, and Mediator, respectively), the enzymatic regulation of each respective kinase is apparently more complex (Lim and Kaldis, 2013; Malumbres, 2014).
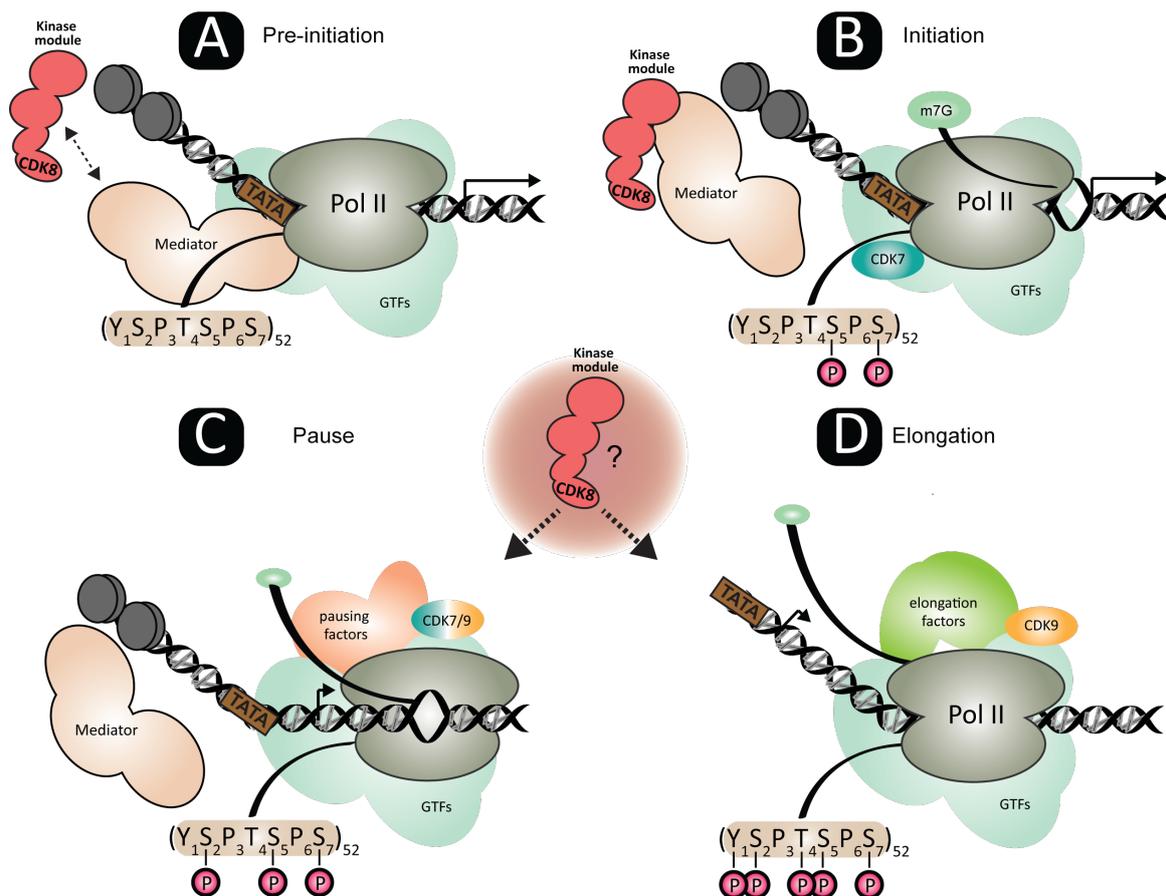
Figure 9: Simplified and shortened Pol II transcription cycle.

(**A**) The Mediator binds to the hypophosphorylated Pol II and ensures pre-initiation complex formation. (**B**) Prior to initiation, Ser-5 (and Ser-7) get phosphorylated by CDK7, which releases Mediator. (**C**) Pausing factors are recruited and activated by CDK7 and released by CDK9-dependent phosphorylation. In addition, CDK9 phosphorylates Ser-2. (**D**) Upon hyperphosphorylation of the Pol II CTD, Pol II is now allowed to proceed to productive elongation, which is stimulated by recruited elongation factors.

For transcription initiation, transcription factors within the pre-initiation complex bridge between the Pol II and core promotors. A key function of the pre-initiation complex is to open the DNA and thus to make it accessible for Pol II (Cramer, 2019). Mediator binds to the hypophosphorylated Pol II CTD and recruits TFIIH (Fig. 9A). CDK7, the kinase of TFIIH, phosphorylates Ser-5 (and Ser-7) within the pre-initiation complex (Fig. 9B) (Akhtar et al., 2009; Esnault et al., 2008; Glover-Cutter et al., 2009; Nair et al., 2005). This phosphorylation event releases Mediator from Pol II and creates a binding site for the capping enzyme that modifies the 5' end of the nascent RNA. At most core promoters, pausing factors are recruited and activated by CDK7, which holds the early Pol II elongating complex after synthesizing approximately 50-150 nucleotides (Fig. 9C) (Larochelle et al., 2012).

The transition from transcription initiation to productive elongation is associated with Ser-2 phosphorylation catalyzed by p-TEFb kinase CDK9. Upon inactivation of pausing factors, the paused polymerase proceeds to elongation (Fig. 9D) (Fuda et al., 2009; Larochelle et al., 2012). Further, Ser-2 phosphorylation promotes the recruitment of the RNA splicing machinery to the nascent transcript.

The Mediator kinase CDK8 phosphorylates Ser-2 and Ser-5 *in vitro,* independent of Mediator or the formation of the pre-initiation complex (Hengartner et al., 1999; Pinhero et al., 2004; Rickert et al., 1999; van Vuuren et al., 1995). However, as many studies have shown both positive and negative effects on transcriptional regulation upon CDK8 mediated CTD phosphorylation, the actual contribution of CDK8 kinase activity within the Pol II CTD cycle is not understood (Nemet et al., 2014).

1.3   The kinase module

The kinase module (also termed CDK8-module) is named after its catalytic core, cyclin-dependent kinase 8 (CDK8). Apart from CDK8 (56 kDa) the kinase module comprises the subunits Cyclin C (34 kDa) and the two large mediator subunits MED12 and MED13 (240 and 250 kDa, respectively). In mammals, the genes coding for CDK8, MED12, and MED13 are duplicated, giving rise to CDK19 (formerly termed CDK8-like), MED12-like (MED12L), and MED13-like (MED13L) (L. Daniels, 2013; Muncke et al., 2003). As all paralogs assemble into the kinase module in a mutually exclusive manner, at least eight different kinase module constellations can be assembled that possess specialized functions (L. Daniels, 2013).

In contrast to the head and middle module of Mediator, the structure of the entire kinase module is unknown and its role during the transcription cycle is unclear (Robinson et al., 2016; Schilbach et al., 2017; Tsai et al., 2013). As introduced before (Fig. 5), the crystal structure of the CDK8/Cyclin C complex is known (Schneider et al., 2011). However, no structural information on human MED12 and MED13 are available to date. Three-dimensional data on the yeast kinase module revealed that MED12 bridges between Cyclin C and MED13 (Fig. 10A) (Tsai et al., 2013; Wang et al., 2013b). This led to the suggestion that human MED12 binds Cyclin C via its surface groove (Fig. 5). The yeast kinase module was shown to adopt multiple conformations that differ in the orientation of CDK8 (Tsai et al., 2013; Wang et al., 2013b). One of these conformations proposes that, in addition to MED13, CDK8 forms extensive contacts to Mediator as well (Fig. 10B) (Taatjes et al., 2002; Tsai et al., 2013; Wang et al., 2013b). However, the functional implications of this binding event remain elusive (Elmlund et al., 2006; Tsai et al., 2013).
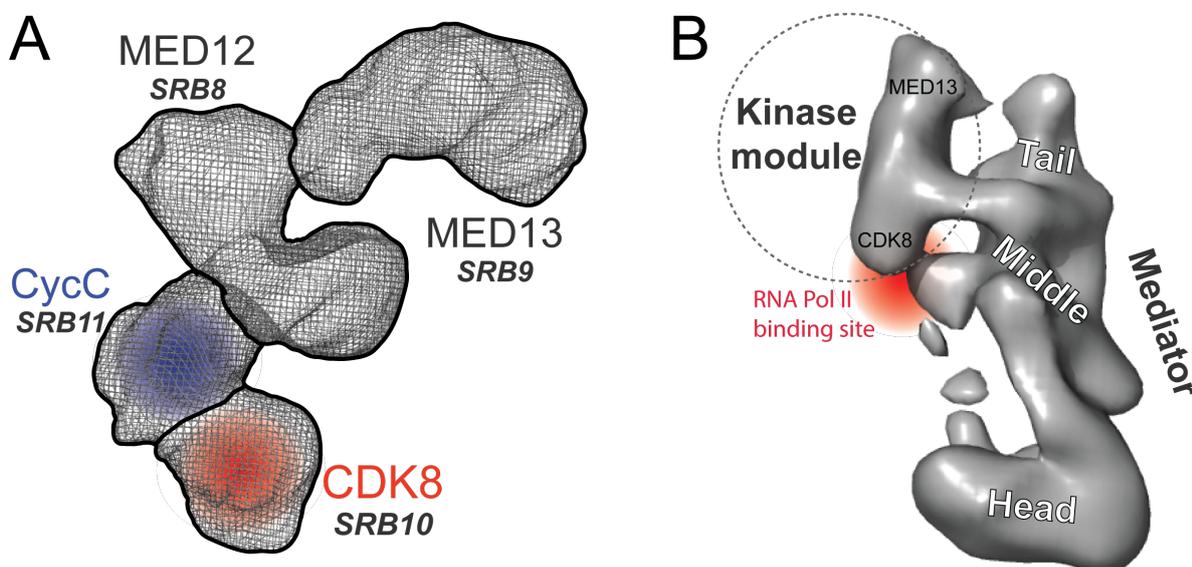
Figure 10: Cryo electron microscopy structures of the kinase module from yeast

(**A**) Structure of the yeast kinase module at 15 Å resolution. Yeast genes are in italic (EMDB code 5588) (Tsai et al., 2013). (**B**) Kinase module bound to Mediator at 35 Å. Please note that the structure has been solved in up to four different conformations, underlining structural flexibility. Please further note the large surface are due to channels and cavities in the structure. The illustrated EM structure shows a more extensive interface that involves besides MED13 in addition CDK8, making extensive contacts to Mediator, that excludes Pol II binding (EMDB code 5589)ˑ(Wang et al., 2013b).

The kinase module regulates Pol II-dependent transcription using two major mechanisms. First, binding of the kinase module to the Mediator complex induces structural changes within Mediator that physically disrupt the interaction between Pol II and Mediator. This disruption negatively affects transcription rates (Knuesel et al., 2009b; Myers et al., 1998; Taatjes et al., 2002). Whereas the yeast kinase module and the Mediator complex possess mutually exclusive binding interfaces on Pol II (Fig. 10B), the human kinase module traps Mediator in a conformation that is incompatible in Pol II binding (Bernecky et al., 2011; Elmlund et al., 2006; Tsai et al., 2013). Second and seemingly more complex, CDK8 phosphorylates multiple targets involved in transcription regulation (Poss et al., 2016). One of the first identified substrates besides the Pol II CTD was Cyclin H, which results in CDK7 inactivation (CDK7/Cyclin H are subunits of the TFIIH complex), which negatively regulates transcription (Akoulitchev et al., 2000)ˑ(Schneider et al., 2002). However, these early findings indicated that the kinase module is a global repressor of transcription and were inconsistent with later studies that implicated the kinase module in transcription activation (Knuesel et al., 2009a; Nemet et al., 2014).

1.3.1   CDK8 regulates transcription factors

Sequence-specific DNA-binding transcription factors are global drivers of cellular physiology and differentiation (Heinz et al., 2015; Lee and Young, 2013; Trompouki et al., 2012). The activity of transcription factors is regulated by phosphorylation, which affects their cellular localization, stability, and DNA binding (Tansey, 2001; Whitmarsh and Davis, 2000). CDK8 phosphorylates a large number of transcription-related targets, which implies CDK8 to be part of an elaborate regulatory network. Accordingly, CDK8 regulates transcription, chromatin state and metabolic processes (Fig. 11) (Poss et al., 2016).

CDK8 kinase targets

Biological processes &
signal transduction pathways
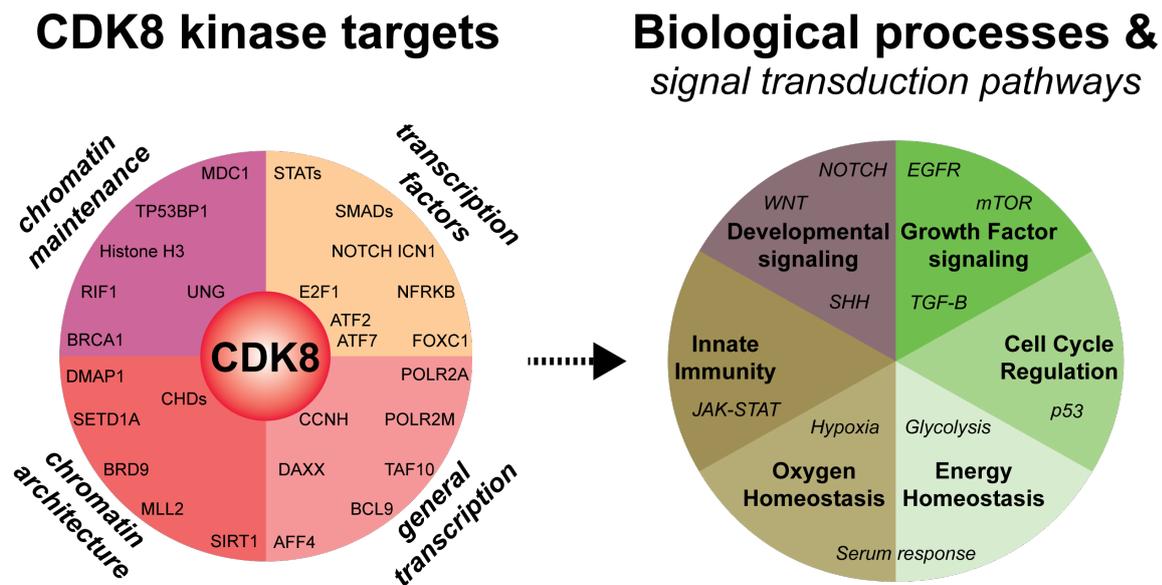
Figure 11: CDK8 kinase substrates and their associated biological processes.
The left pie chart shows CDK8 kinase target, which were grouped in four categories according to their biological function. The right pie chart illustrates biological processes together with associated signal transduction pathways, that are regulated by CDK8 kinase target phosphorylation. Adapted from Poss et al., 2016 and Clark et al., 2015.

Depending on stimulus and cell type, the kinase module regulates transcription factor function connected to the transcription apparatus (Bancerek et al., 2013). Several studies established roles for the kinase module in the NOTCH-, the TGF/ß-, and the JAK-STAT-signal transduction pathway (Alarcón et al., 2009; Bancerek et al., 2013; Fryer et al., 2004; Guo et al., 2019). There, CDK8 activates key transcription factors, which results in the expression of target genes. Interestingly, phosphorylation of the STAT1 transactivation domain on Ser-727 is unique to CDK8. CDK8-dependent STAT1-phosphorylation thereby solely occurs on promoter-bound STAT1 and it correlates with the presence of promoter-associated Pol II (Bancerek et al., 2013; Pelish et al., 2015; Sadzak et al., 2008).

Genes that are activated by internal or external stimuli are often part of signal-transduction pathways. These rapidly responding genes typically engage paused Pol II to facilitate short response times within a differentiation program or stimulus response (Adelman and Lis, 2012; Core and Lis, 2008; Gilmourt and Lis, 1986; Guenther et al., 2007). For these genes, CDK8 shows a positive influence during Pol II pause release within the serum response network, under hypoxia response and during p53-dependent stress response (Donner et al., 2007; Galbraith et al., 2010, 2013). This also holds true during the innate immune response (Bancerek et al., 2013; Steinparzer et al., 2019). Furthermore, CDK8 interacts with p-TEFb (and AFF4) at super elongation complexes (Galbraith et al., 2013). There, physical loss of

CDK8 abolishes the recruitment of CDK7, CDK9 and BRD4, which led to diminished Pol II CTD marks and decreased transcription rates (Galbraith et al., 2013).

The kinase module co-localizes with Mediator genome-wide, which suggests that a loss of CDK8 could impact gene expression globally (Kagey et al., 2010; Phillips-Cremins et al., 2013). Contrary to these assumptions, a CDK8 knockdown or the selective inhibition of CDK8 kinase activity affects only a subset of genes that vary in context (e.g. stimuli induced) or cell type. This is in agreement with the fact that the selective CDK8 inhibition or the loss of the protein is well-tolerated in cells under normal growth conditions (Johannessen et al., 2017; Nitulescu et al., 2017; Pelish et al., 2015). In stark contrast, the activation of genes in response to stress or developmental cues shows a strong dependence on CDK8. This supports the positive role that CDK8 plays in directing transcriptional programs through the phosphorylation of gene-specific transcription factors (Donner et al., 2007; Galbraith et al., 2010, 2013; Westerling et al., 2007). Moreover, CDK8 functions to maintain both tumors and embryonic stem cells in an undifferentiated state, whereas CDK8 knockout in flies or mice is embryonically lethal (Adler et al., 2012; Loncle et al., 2007; Westerling et al., 2007). These seemingly incompatible findings could be explained by emerging evidence that implies the kinase module (including CDK8 kinase activity) in regulating the communication between enhancers and promoters in dependence of chromatin structure and lineage-specific TFs (Heinz et al., 2015). Upon recruitment of the transcription machinery, enhancer-promotor loops are stabilized, thereby allowing high transcription rates (Deng et al., 2014; Dowen et al., 2014). Altogether, CDK8 kinase activity is an essential component to enable rapid gene expression responses based on its ability to modulate a large number of transcription-associated targets within signal-transduction pathways (Kuuluvainen et al., 2018; Pelish et al., 2015; Poss et al., 2016).

1.3.2   CDK8 and its implications in cancer

CDK8 phosphorylates transcription-related targets that regulate Pol II processivity. As most CDK8 targets are engaged in fundamental biological processes (Fig. 11), it is not surprising that deregulated CDK8 activity is associated with tumorigenesis (Poss et al., 2016; Vogelstein et al., 2013).

Initial evidence that CDK8 is a proto-oncogene derived from work on colorectal cancer. There, CDK8 was found to be amplified in almost every second patient sample (Firestein et al., 2008). Subsequent cohort studies revealed a negative correlation between CDK8 gene expression and the survival of colorectal cancer patients (Firestein et al., 2010; Seo et al., 2010).

Abnormal elevated CDK8 levels were additionally found in advanced stages of colorectal cancer, further supporting a role of CDK8 in promoting cancer progression (Seo et al., 2010). The oncogenic properties of CDK8 reside on its ability to modulate the Wnt/ß-catenin pathway by enhancing the transcriptional activity of ß-catenin due to its phosphorylation (Fig. 12) (Bienz and Clevers, 2000; Firestein et al., 2008; Kämpjärvi et al., 2012; Zhan et al., 2017).

Chromosom 13
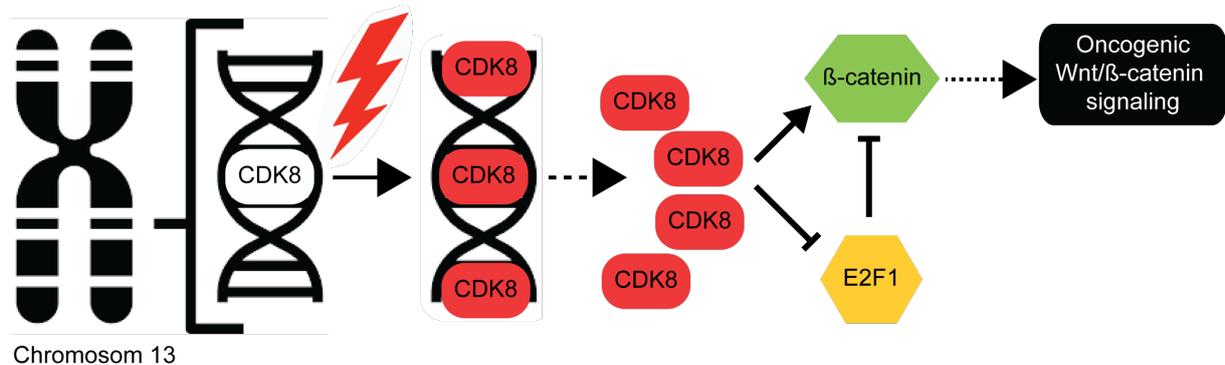
Figure 12: CDK8 regulates oncogenic Wnt/ß-catenin signaling through two different pathways.
13q12-encoded CDK8 is overexpressed through amplification-dependent means in a colorectal cancers. CDK8 controls Wnt/ß-catenin signaling by stimulating ß-catenin and by inhibiting the suppressive function of the ß-catenin inhibitor E2F1 in a kinase dependent manner. Both mechanisms promote oncogenic Wnt/ß-catenin signaling, which correlates with epithelial-mesenchymal transition. Adapted from Clark et al., 2015 (Clark et al., 2015).

Aberrant Wnt/ß-catenin signaling, in turn, stimulates epithelial-to-mesenchymal transition (Xu et al., 2015). Furthermore, CDK8 phosphorylates E2F1 and thereby abolishes its suppressive function on ß-catenin (Morris et al., 2008; Zhao et al., 2013). CDK8 knockdown in colorectal cancer cell lines reduces proliferation rates by cell cycle arrest (Firestein et al., 2008). In contrast, transient CDK8 knockdown in mouse promotes tumor development (McCleland et al., 2015). This apparent discrepancy in CDK8 function may reflect once again cell-type-specific and context-dependent roles for CDK8 in transcriptional regulation. Nonetheless, these findings highlight the role of CDK8 in colorectal cancer and identified it as both an oncogene and tumor suppressor. Furthermore, transcriptome analyses demonstrated that CDK8 stimulates the expression of glycolytic genes (Galbraith et al., 2017),(Vincent et al., 2001) and regulates lipogenesis (Zhao et al., 2012). Lastly, CDK8 reinforces the proliferation of melanomas (Kapoor et al., 2010), it is overexpressed in prostate cancer together with CDK19 (Brägelmann et al., 2017), and it mediates NF-κB induced transcription of tumor-promoting cytokines (Chen et al., 2017; Johannessen et al., 2017; Yamamoto et al., 2017).

1.3.3   MED12 is a cancer driver gene

The human *MED12* gene is located on the X-chromosome and consists of 45 exons that encode for 2177 amino acids (Fig. 13). The amino acid sequence of MED12 has no similarity to other protein sequences (El-Gebali et al., 2019) and is divided into four domains characterized by an enrichment of individual amino acids: a leucine-rich L-domain (aa 1-500), a leucine-serine-rich LS domain (aa 501-1650), a proline-glutamine-leucin-rich PQL domain (aa 1651-2086), and a glutamine-rich opposite paired (OPA) domain (aa 2087-2177) (Fig. 13A) (El-Gebali et al., 2019; Philibert et al., 1998, 1999).

MED12 can be considered as structural hub for the kinase module (Fig. 10A) and was identified as a so-called "cancer driver gene" (Lehner et al., 2006). MED12 is involved in many signaling pathways with an emphasis on developmental gene regulation (Keightley et al., 2017; Kim et al., 2016; Lawrence et al., 2014; Rocha et al., 2010; Shin et al., 2008; Vogelstein et al., 2013; Vogl et al., 2013). Although MED12 is ubiquitously expressed, its expression levels vary from tissue to tissue and are age-dependent (Philibert and Madan, 2007; Philibert et al., 1999). Alterations in both MED12 sequence and expression have been observed in many diseases. MED12 participates, for example, in the Sonic Hedgehog pathway by interacting with Sox9, Sox10 and Gli3 (Bien-Willner et al., 2007; Kamachi and Kondoh, 2013; Vogl et al., 2013; Zhou et al., 2002). MED12 further stimulates Wnt/ß-Catenin signaling by interacting with ß-Catenin (Fig. 13A) (Carrera et al., 2008; Kim et al., 2016). Deregulated MED12 expression and TGF/ß dysregulation has also been linked to drug resistance of tumor cells (Huang et al., 2012; Massagué, 2008; Shaikhibrahim et al., 2014; Shimada et al., 2016; Wang et al., 2015a) and abnormal TGF/ß-signaling affects the epidermal growth factor receptor-pathway (Keightley et al., 2017; Lawrence et al., 2014; Philibert and Madan, 2007; Shin et al., 2008; Zhou et al., 2002). Physical MED12 loss induces epithelial-mesenchymal transition in lung carcinoma (Huang et al., 2012; Shimada et al., 2016) and reduces CDK9 and Pol II occupancy at super elongation complexes (Bhagwat et al., 2016).
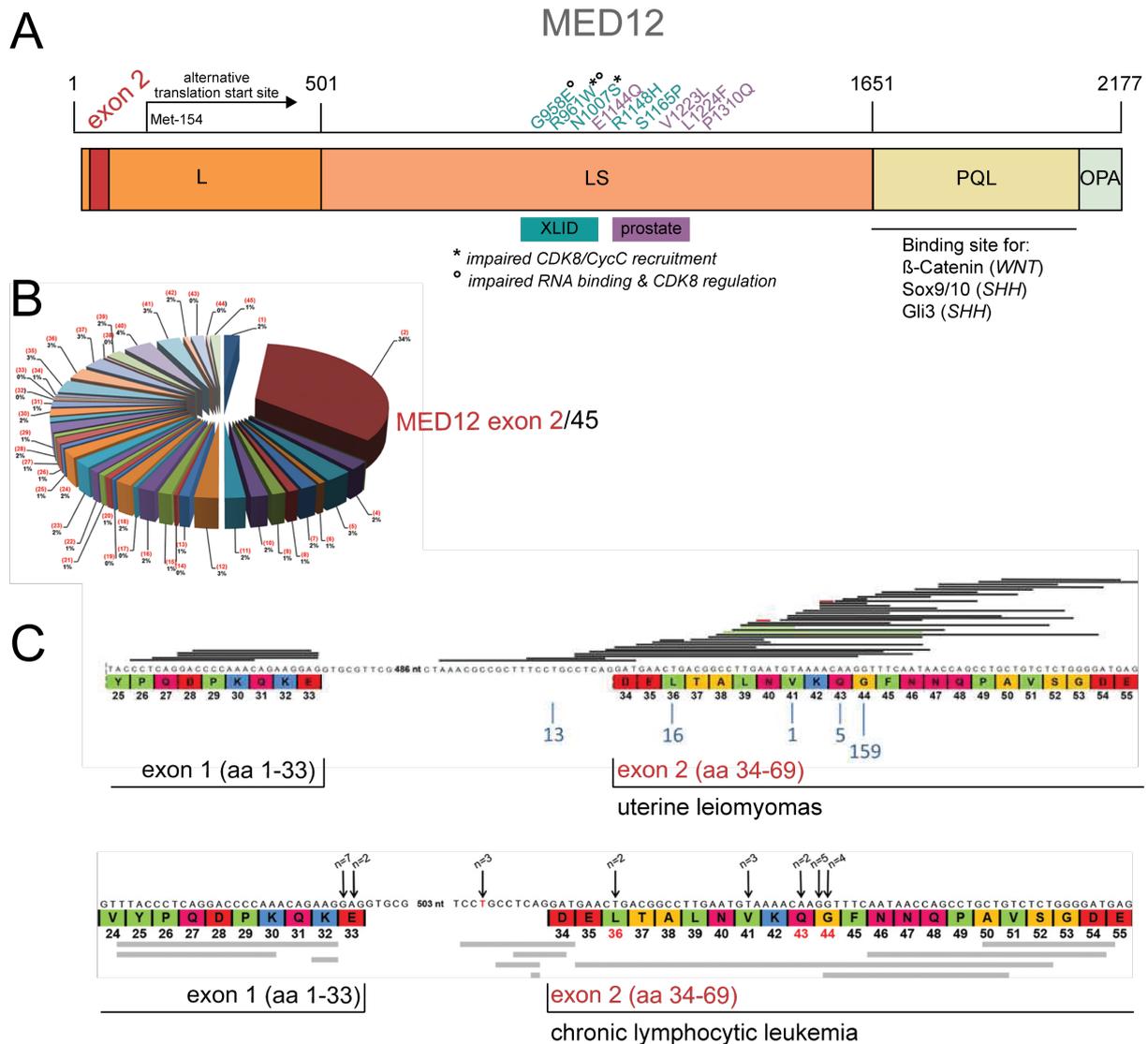
Figure 13: Domain architecture of MED12 and observed mutations in MED12.

(**A**) Schematic domain organization of MED12 including different functional characteristics. MED12 exon 2 is highlighted in red, XLID associated MED12 mutations were illustrated and colored in blue, prostate cancer associated mutations were colored in violet. (**B**) Total mutation spectrum of the *MED12* gene divided in 45 exons. Please note that over one third (34%) of all *MED12* mutations were found within the exon 2. Adapted from Banaganapalli et al., 2016. (**C**) The upper panel shows a schematic presentation of *MED12* exon 1 and exon 2 mutations found in one study that comprises 611 uterine leiomyomas-derived patient samples. The numbers below (upper panel) or above (lower panel) each residue indicate the number of missense mutations found in each study. The bars illustrate different insertions/deletions. Adapted from Kämpjärvi et al., 2014. The lower shows the same, just for a study that comprises 611 chronic lymphocytic leukemia-derived patient samples. Adapted from Kämpjärvi et al., 2015.

The distribution of cancer-associated mutations within the *MED12* gene is remarkable (Fig. 13B). Particularly evident in uterine leiomyomas and chronic lymphocytic leukemia, *MED12* mutations occur at high frequencies within the MED12 exon 2 (77% within uterine leiomyomas, Fig. 13C) (Kämpjärvi et al., 2014; Mäkinen et al., 2011; Pelish et al., 2015; Wu et al., 2017a). The majority of MED12 mutations observed in exon 2 are missense mutations

that affect three conserved amino acids: L36, Q43 and G44 (Fig. 13C). Other exon 2 mutations are frameshift mutations, that result in an N-terminally shortened MED12 protein due to an alternative translation start site at methionine 154 (Fig. 13A) (Heikkinen et al., 2017)·(Bazykin and Kochetov, 2011). Taken together, these findings suggest that the first two exons of the *MED12* gene encode for an important protein function (Turunen et al., 2014). Intriguingly, the N-terminal segment of MED12 encoded by these two exons was shown to be required for CDK8 kinase activity (Knuesel et al., 2009a; Park et al., 2018; Turunen et al., 2014).

Mutations outside *MED12* exon 1 and 2 were found in the LS-domain. Most of these mutations are associated with X-linked intellectual disabilities and prostate cancer (Barbieri et al., 2012; Ding et al., 2008; Graham and Schwartz, 2013; Srivastava et al., 2019; Wang et al., 2013a; Zhou et al., 2012) (Fig. 13A). As males carry one single X chromosome, these X-linked diseases predominantly affect males as the name indicates (Stevenson and Schwartz, 2009). Intriguingly, two juxtaposed mutations in the LS-domain (R961W and N1007S) showed impaired binding to CDK8/Cyclin C (Fig. 13A) (Zhou et al., 2012). Furthermore, MED12 interaction with long non-coding RNAs was abolished due MED12 G958E and R961W mutations, which resulted in deregulated CDK8 kinase activity (Lai et al., 2013). In summary, these findings highlight the oncogenic vulnerability of MED12.

1.4   Aims of this thesis

The oncogene CDK8 is of major interest to drug development. Therefore, significant efforts were made to develop CDK8-specific kinase inhibitors. Despite the availability of structural information on the binary CDK8/Cyclin C complex (Dale et al., 2015; Schneider et al., 2011), the development of CDK8-specific inhibitors is hindered by the currently unclear mechanism of CDK8 activation. In contrast to the common activation mechanism of cyclin-dependent kinases CDK8 does not require phosphorylation of its T-loop for full activity. Instead, MED12 binding to CDK8/Cyclin C seems to circumvent the missing phosphorylation event, which results in its activation. Based on available structural and functional information, the previous model for CDK8 activation hypothesized that the N-terminal portion of MED12 binds to the Cyclin C surface groove and thereby enhances CDK8 activity (Fig. 14) (Knuesel et al., 2009a; Park et al., 2018; Turunen et al., 2014). However, how MED12 binding to this distant surface groove is connected to CDK8 activation is ambiguous and the model therefore controversial. Using *in vitro* biochemistry in combination with structural- and system-biology techniques, I therefore aimed to elucidate the molecular mechanisms how MED12 activates CDK8.
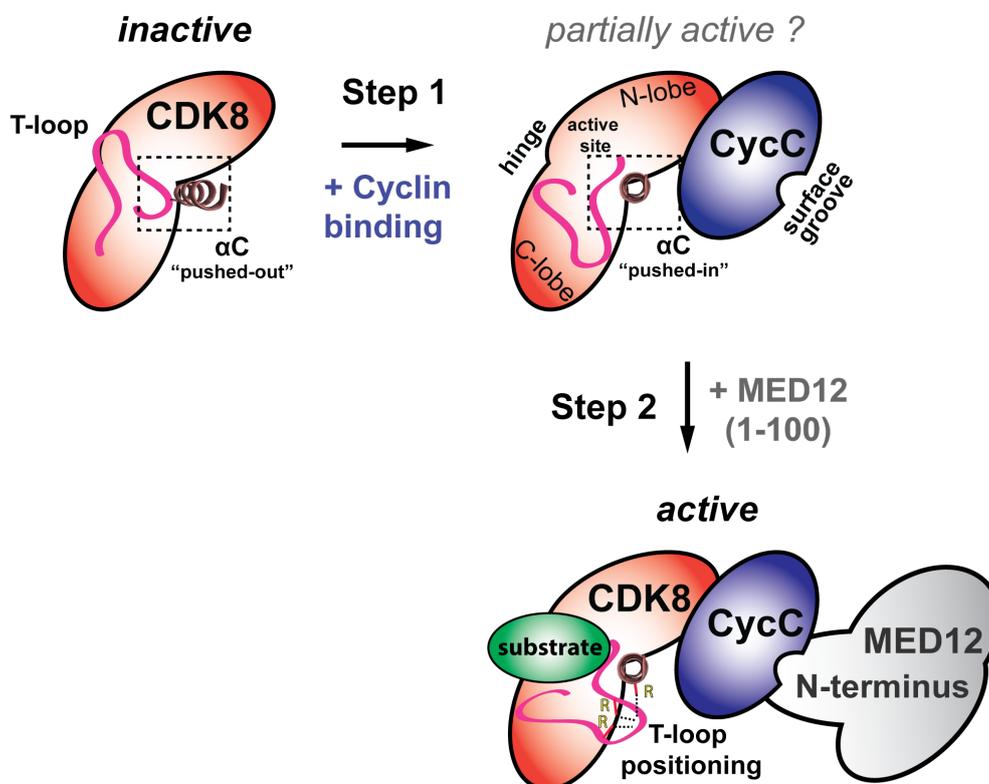
Figure 14: Possible mechanism for CDK8 activation by MED12

Step 1: Cyclin C binds to CDK8 and thereby positions the αC-helix of CDK8 into the "pushed-in" conformation. This binding event is crucial for the formation of the active site of CDK8. However, the kinase activity of the binary CDK8/Cyclin C complex is unknown. Step 2: MED12 binds to the CDK8/Cyclin C complex. In particular, it is suggested that the first 100 amino acids of MED12 bind to the Cyclin C surface groove and thereby activates the kinase. Adapted from Klatt et al., 2020.

Chapter 2: Results

2.1   Protein production of kinase module components in insect cells

To study how MED12 binding to CDK8 activates the kinase and thereby circumvents its necessity for T-loop phosphorylation, I established expression and purification strategies for a multitude of Mediator kinase module components in insect cells using MultiBac™ (Fig. 15) (Berger et al., 2004; Fitzgerald et al., 2006). For the expression of single proteins, individual genes encoded on pAceBac1 or pFL acceptor plasmids were transformed into DH10 MultiBac^Turbo cells. For multi-protein expression, desired acceptor-donor plasmids were first combined to obtain desired multi-gene assemblies and then transformed into DH10 MultiBac^Turbo cells.
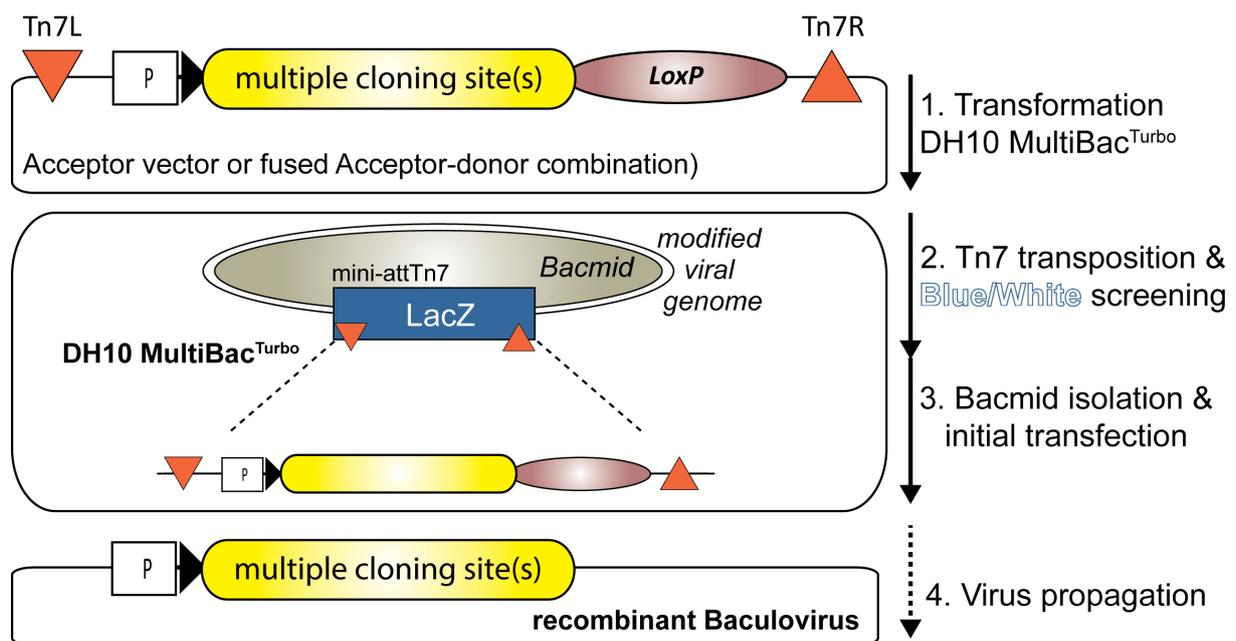
Figure 15: Schematic MultiBac workflow

Desired constructs were cloned (and, if needed single acceptor plasmids were combined with donor plasmids) and transformed into DH10 MultiBac^TURBO cells, which confines the baculoviral genome. After Tn7 transposition, positive clones that possesses the modified baculoviral genome were selected by blue/white screening. Bacmids were isolated and transfected into Sf21 insect cells to initiate viral proliferation.

2.1.1   Purification of the N-terminal segment of MED12

Baculovirus-infected High Five insect cells were lysed by sonication, cell debris was removed by centrifugation and the supernatant collected. Following Strep-affinity chromatography, MED12 was immobilized on a cation-exchange resin to recover the desired protein. Last, MED12 was isolated by size-exclusion chromatography. When used for MST measurements, the Strep-tag was removed prior to size-exclusion chromatography (Fig. 16C). As demonstrated on Fig. 16, the N-terminal fragment of MED12 comprising its first 100 amino acids could be purified to homogeneity.
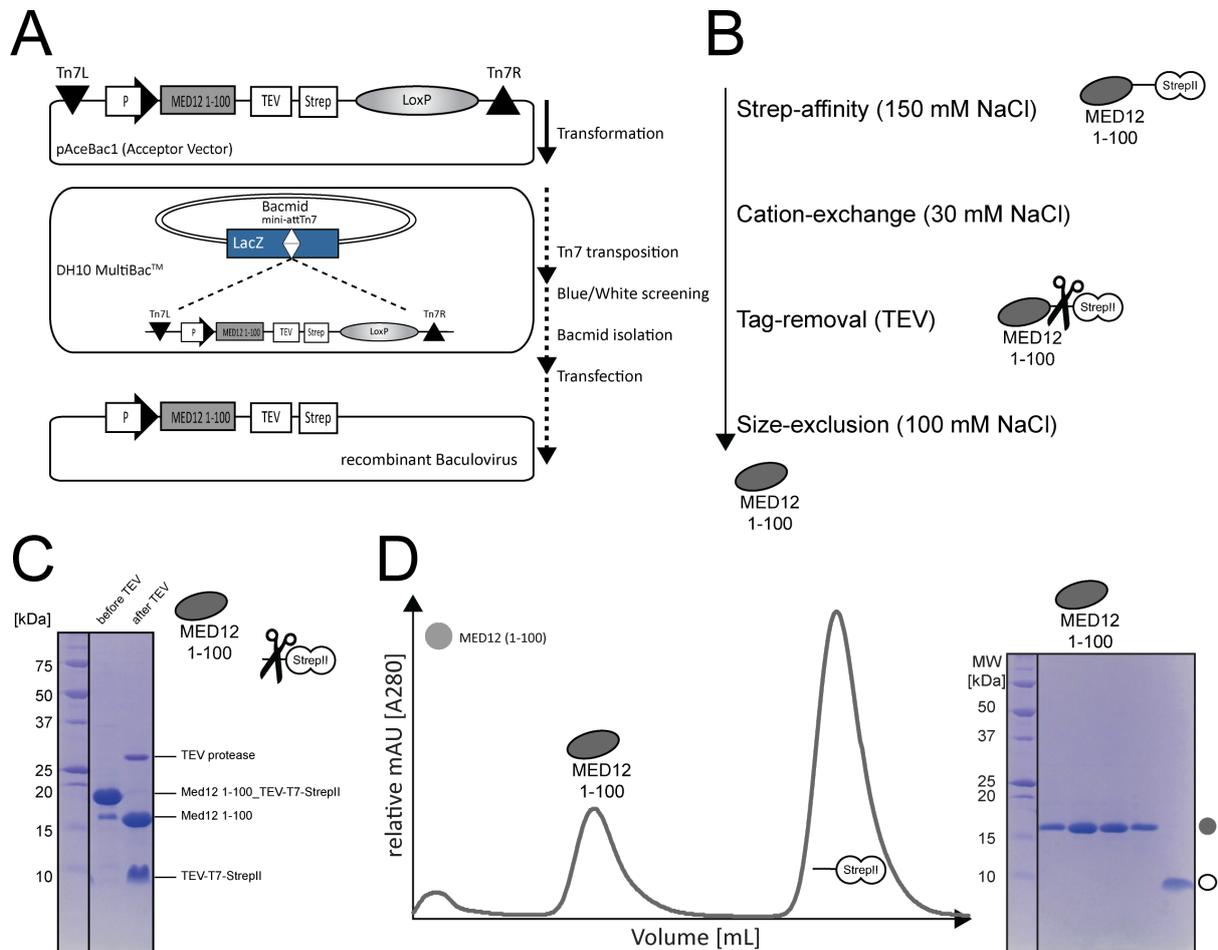
Figure 16: Expression and purification of the N-terminal segment of MED12

(**A**) Schematic MultiBac^{TM} workflow and expression cassette for the N-terminal fragment of MED12 (1-100). (**B**) Schematic purification scheme for MED12 (1-100). Salt-concentration of individual purification steps were illustrated. MED12 (1-100) is shown as a cartoon. (**C**) SDS-PAGE analysis of MED12 (1-100) before and after TEV treatment. (**D**) Size-exclusion chromatogram and SDS-PAGE analysis of MED12 (1-100) using a Superdex 75 (GE Healthcare). Please note that MED12 (1-100) is devoid of tryptophan and exhibits less A280 absorption as the TEV-T7-Strep-tag. MED12 (1-100) is shown as a cartoon above the gel and indicated next to the gel in grey, The cleaved TEV-T7-Strep-tag is in white. Please note that (D) is adapted from Klatt et al., 2020.

2.1.2   Purification of binary CDK8/Cyclin C and CDK19/Cyclin C complexes

To examine the affinity of MED12 (1-100) towards binary CDK8/Cyclin complexes, we co-expressed different binary CDK8/Cyclin C complexes and purified them to homogeneity (Fig. 17). Binary CDK8/Cyclin constructs were utilized tag-free for *in vitro* kinase assays, yet were kept tagged for MST-measurements.
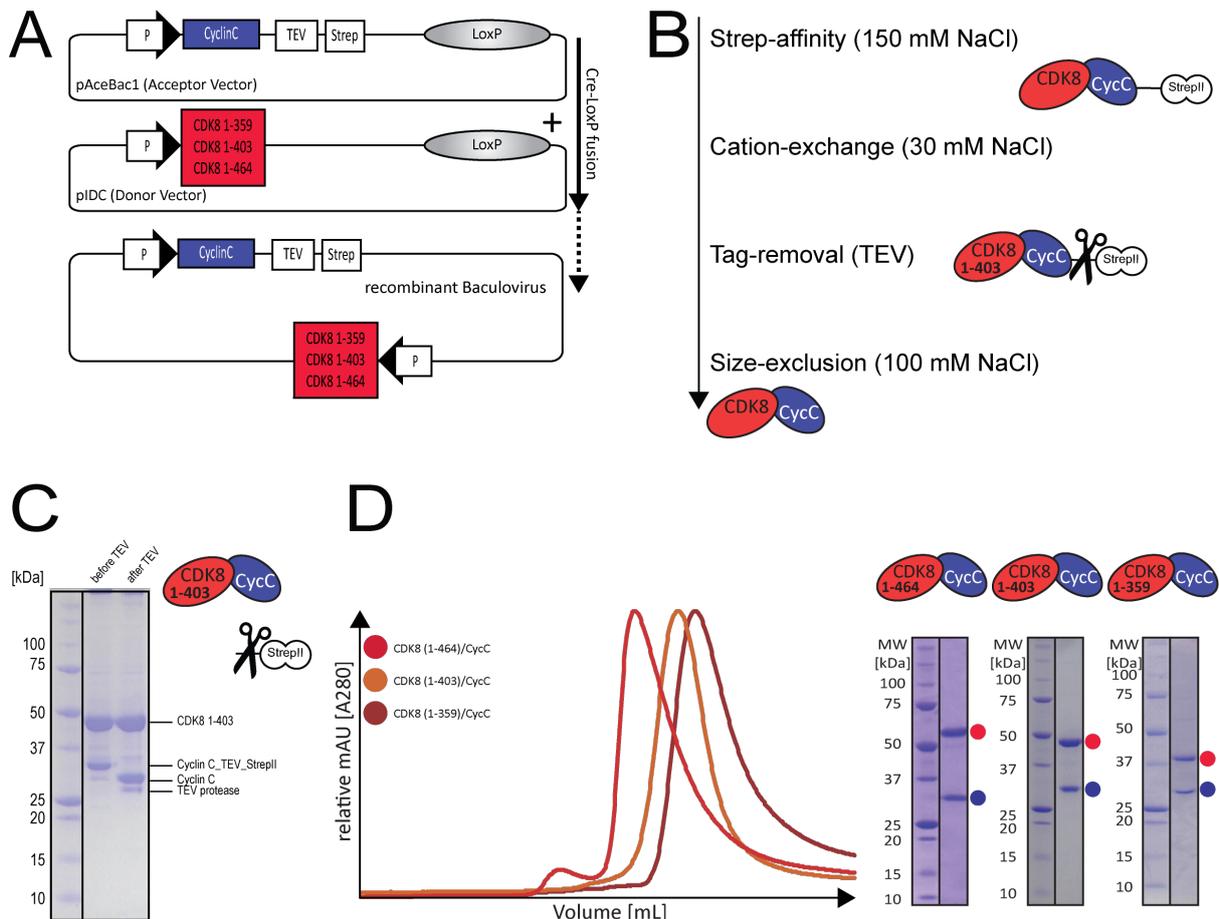
Figure 17: Co-expression and purification of binary CDK8/Cyclin C complexes

(**A**) Schematic fusion strategy and expression cassettes for binary CDK8/Cyclin C complexes using MultiBac^{Turbo}. (**B**) Schematic purification scheme for binary CDK8/Cyclin C. Salt-concentrations of individual purification steps were illustrated. CDK8/Cyclin C is shown as a cartoon. (**C**) SDS-PAGE analysis of CDK8 (1-403)/Cyclin C before and after TEV treatment. (**D**) Size-exclusion chromatograms and SDS-PAGE analysis of purified binary CDK8/Cyclin C complexes using a Superdex 200 (GE Healthcare). Protein complexes are shown as cartoons above each gel, individual proteins are indicated next to the gels. CDK8 variants (1-464 (full-length), 1-403 and 1-359) are shown in red, Cyclin C is in blue. Please note also that (D) is adopted from Klatt et al., 2020.

Binary CDK19/Cyclin C complexes were constructed in analogy to binary CDK8/Cyclin C complexes (Figs. 17A and 18A). Binary CDK19/Cyclin C complexes were co-expressed and purified to homogeneity using the established purification scheme employed for binary

CDK8/Cyclin C complexes (Figs. 17B and 18B). Also, binary CDK19/Cyclin complexes were utilized tag-free for *in vitro* kinase assays, yet were kept tagged for MST-measurements.
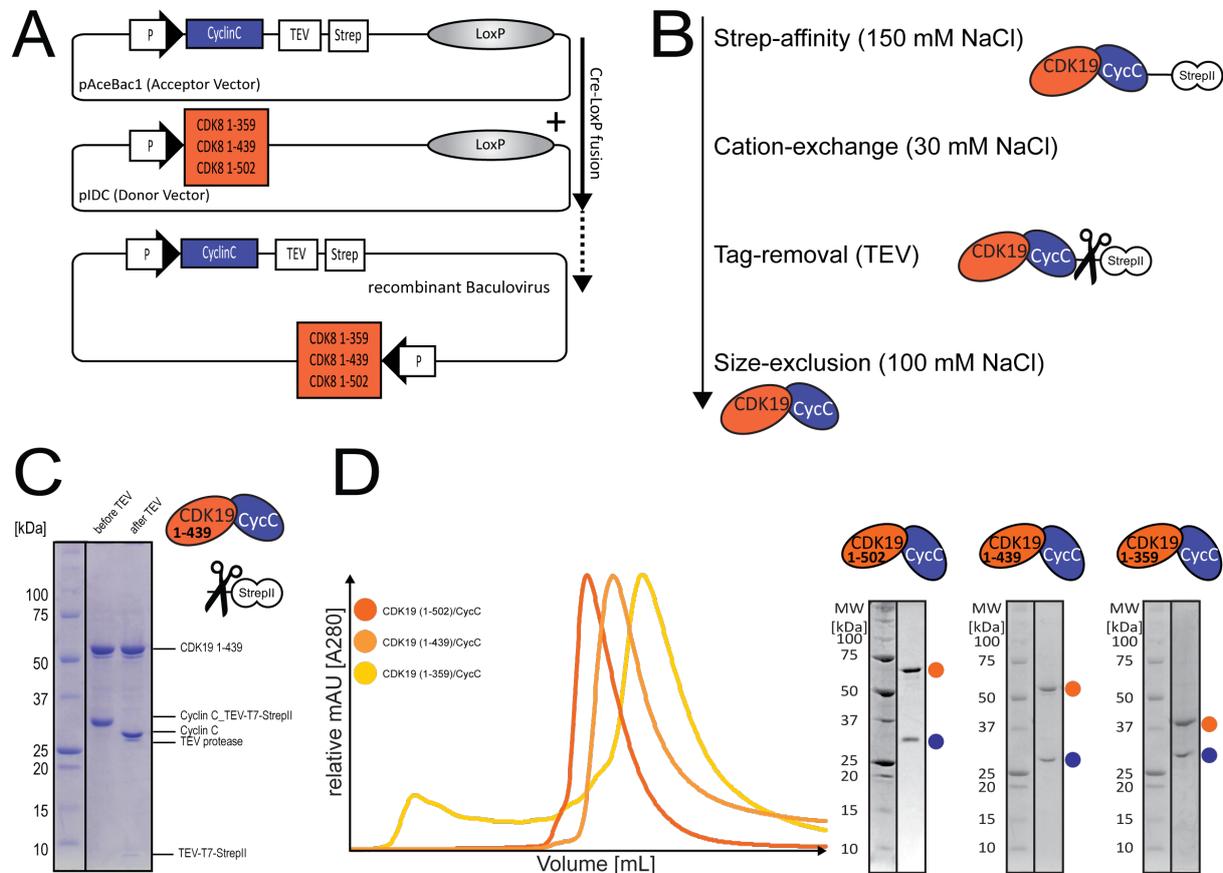
Figure 18: Co-expression and purification of binary CDK19/Cyclin C complexes

(**A**) Schematic fusion strategy and expression cassettes for binary CDK19/Cyclin C complexes using MultiBac[Turbo]. (**B**) Schematic purification scheme for binary CDK8/Cyclin C. Salt-concentrations of individual purification steps were illustrated. CDK19/Cyclin C is shown as a cartoon. (**C**) SDS-PAGE analysis of CDK19 (1-439)/Cyclin C before and after TEV treatment. (**D**) Size-exclusion chromatograms and SDS-PAGE analysis of purified binary CDK19/Cyclin C complexes using a Superdex 200 (GE Healthcare). Protein complexes are shown as cartoons above each gel, individual proteins are indicated next to the gels. CDK19 variants (1-502 (full-length), 1-439 and 1-359) are shown in orange, Cyclin C is in blue. Please note that the PAGE gel on (C) was taken by Melanie Müller.

Variants of binary CDK8/Cyclin C and CDK19/Cyclin C complexes possess an N-terminal Strep-SUMO-tag on the kinase to increase protein yield and stability (Peroutka et al., 2008). These binary complexes were utilized for ITC-measurements. As shown on Fig. 19, co-expressed SUMO-tagged binary CDK8 (1-403)/Cyclin C and CDK19 (1-439)/Cyclin C complexes were purified to homogeneity.
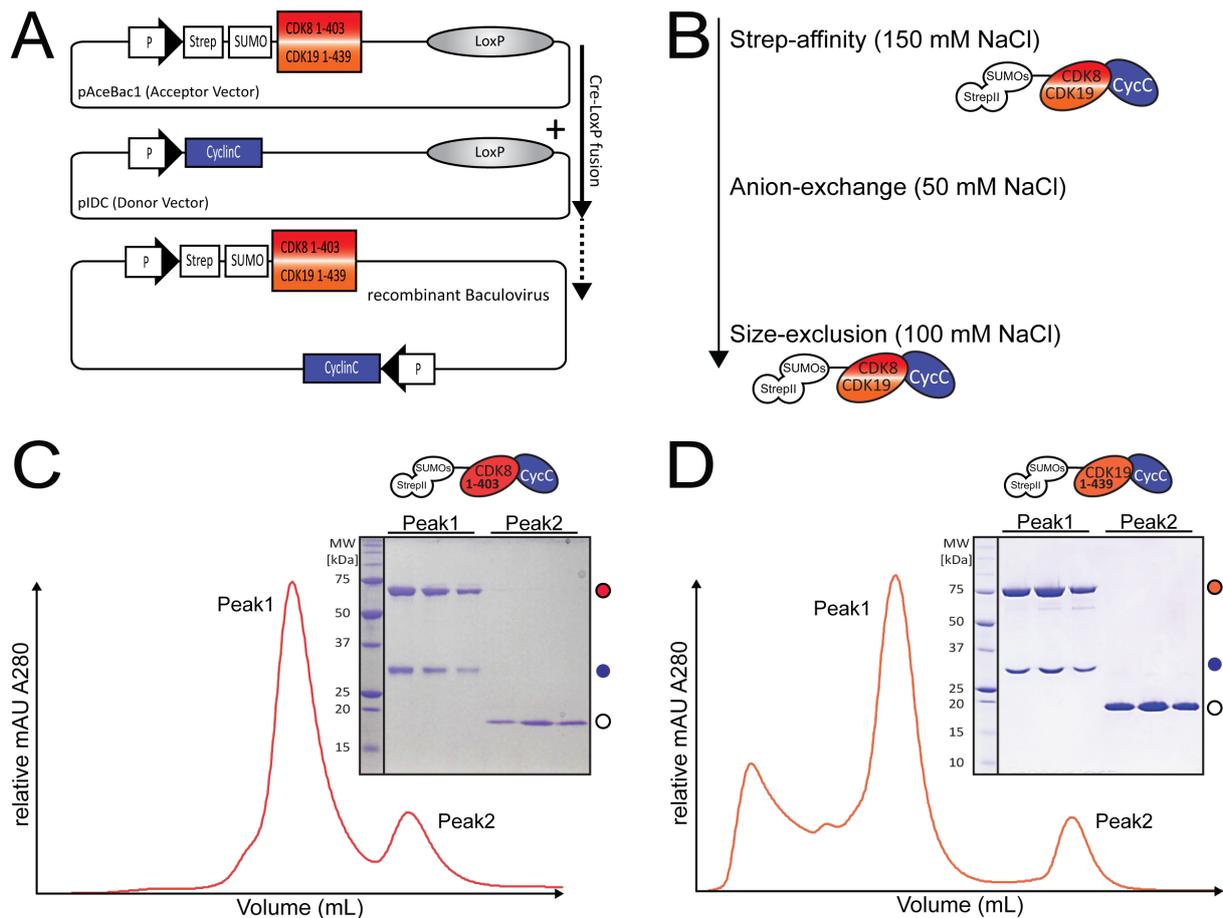
Figure 19: Co-expression and purification of SUMO-tagged CDK8/Cyclin C and CDK19/Cyclin C complexes
(**A**) Schematic fusion strategy and expression cassettes for SUMO-tagged CDK8 (1-403)/Cyclin C and CDK19 (1-439)/Cyclin C complexes using MultiBac[Turbo]. (**B**) Schematic purification scheme for SUMO-tagged CDK8/Cyclin C and CDK19/Cyclin C. Salt-concentrations of individual purification steps were illustrated. CDK8/Cyclin C and CDK19/Cyclin C are shown as a cartoon. (**C** and **D**) Size-exclusion chromatograms and SDS-PAGE analysis of purified SUMO-tagged binary CDK8/Cyclin C and CDK19/Cyclin C complexes using a Superdex 200 (GE Healthcare). Excessive amounts of SUMO could be efficiently separated (Peak 2). Protein complexes are shown as cartoons above each gel, individual proteins are indicated next to the gels. CDK8 (1-403) is shown in red, CDK19 (1-439) is shown in orange, Cyclin C is in blue, Strep-SUMO in white. CDK8 or CDK19 contain the Strep-SUMO tag (indicated by black circles) and run accordingly higher in the gel. Please note the protein purification shown on (D) was carried out by Melanie Müller.

Last, we established an additional co-expression strategy for binary CDK8 (1-403)/Cyclin C complexes. In contrast to our prior co-expression strategies (Fig. 17), both CDK8 and Cyclin C were cloned together into the pAceBac1 vector and co-expressed as a single gene expression cassette. This creates multi-gene expression plasmids without the necessity of acceptor-donor plasmid fusions (Fig. 20). The resulting bicistronic transcript encodes a polypeptide that is auto-cleaved by utilizing the 2A linker peptide (here P2A), which guarantees stoichiometric multi-protein expression (Liu et al., 2017; Wang et al., 2015b). Upon co-expression of CDK8 (1-403) and Cyclin C in insect cells, binary CDK8 (1-403)/Cyclin C complexes could be isolated and purified to homogeneity.
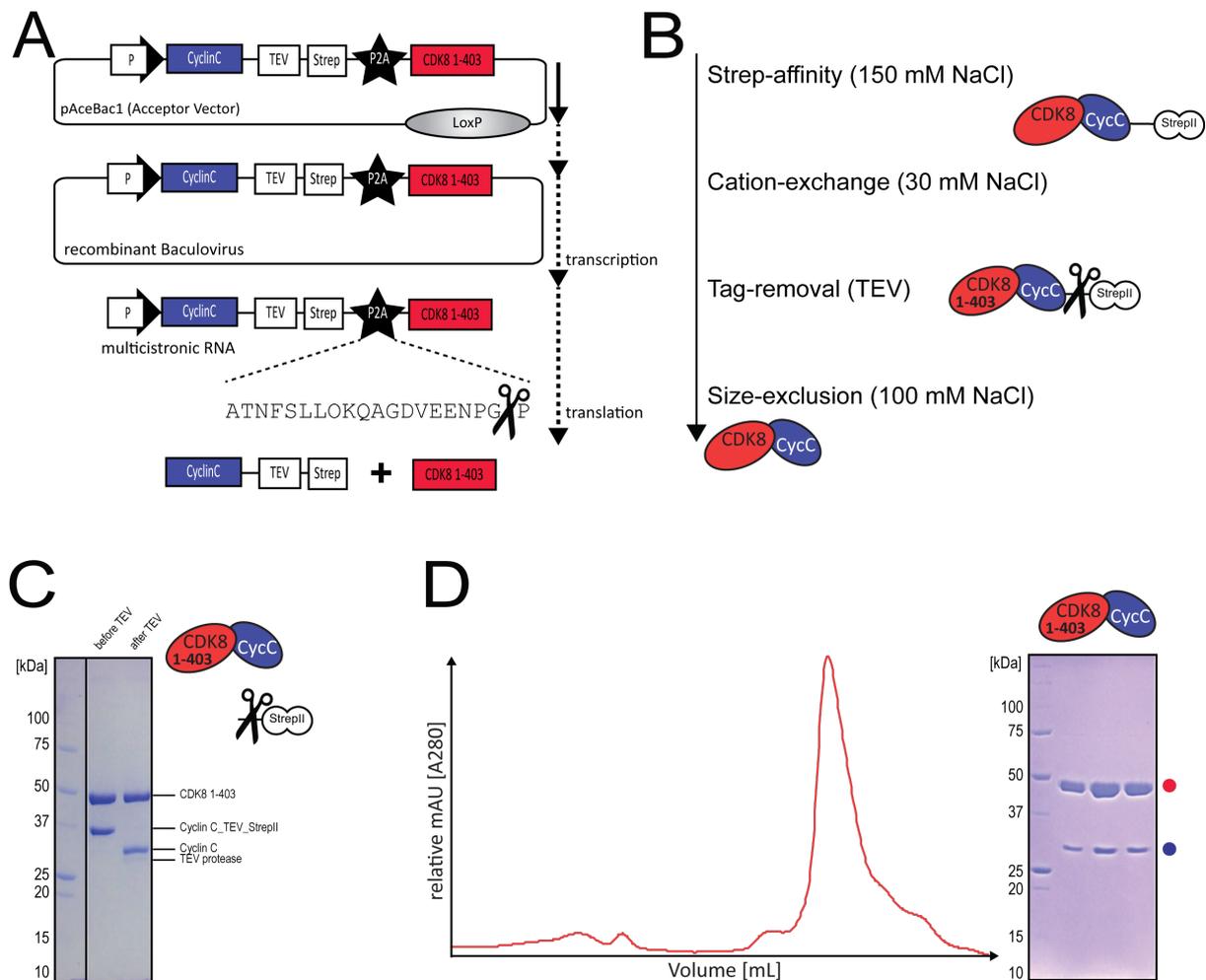
Figure 20: Co-expression and purification of CDK8 (1-403)/Cyclin C complexes utilized by a P2A linker
(**A**) Schematic expression cassette that results in a CDK8 (1-403) and Cyclin C polypeptide, which is self-cleaved by the usage of the P2A linker. (**B**) Schematic purification scheme for binary CDK8 (1-403)/Cyclin C complexes. Salt-concentrations of individual purification steps were illustrated. CDK8/Cyclin C is shown as a cartoon. (**C**) SDS-PAGE analysis of CDK8 (1-403)/Cyclin C before and after TEV treatment (**D**) Size-exclusion chromatogram and SDS-PAGE analysis of purified binary CDK8/Cyclin C complexes using a Superose 6 (GE Healthcare). The protein complex is shown as a cartoon above the gel, individual proteins are indicated next to the gels. CDK8 1-403 is shown in red, Cyclin C is in blue. Please note that protein purification was carried out by Silas Amarell.

2.1.3   Purification of ternary CDK8/CycC/MED12 and CDK19/CycC/MED12 complexes

To characterize CDK8/19 and Cyclin C in complex with the N-terminal part of MED12, three ternary complexes that comprises CDK8 (1-403)/Cyclin C and MED12 (1-100), (1-350) or (1-440), respectively, were cloned, co-expressed and purified to homogeneity (Fig. 21) (Klatt et al., 2020). As an additional purification step, ternary complexes were subjected to an anion-exchange column prior to cation-exchange chromatography (Fig. 21B). Whereas properly folded ternary complexes do not bind to the anion-exchange resin and, hence, reside in the flow-through, misfolded complexes that contain chaperones bind to the column and thus can be

removed. Subsequent cation-exchange- and size-exclusion chromatography were then used to recover the desired, highly pure ternary protein complexes (Fig. 21D).

To analyze the stoichiometry of the my ternary complexes, I subjected the CDK8 (1-403)/CycC/MED12 (1-100) complex as a representative to static light scattering. This technique revealed a monodisperse ternary complex with a 1:1:1 stoichiometry (Klatt et al., 2020).
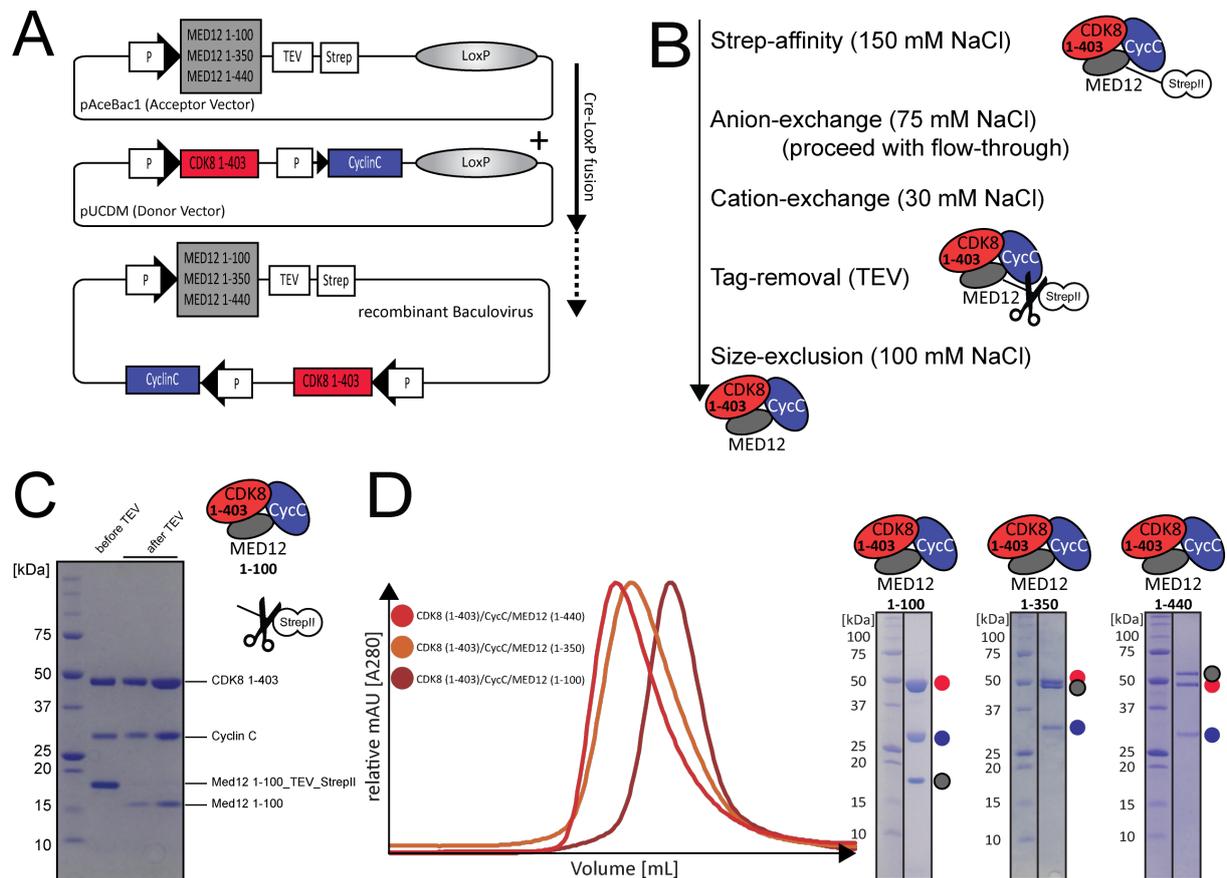
Figure 21: Co-expression and purification of ternary CDK8/CycC/MED12 complexes
(**A**) Schematic fusion strategy and expression cassettes for ternary CDK8/CycC/MED12 complexes using MultiBac[Turbo]. (**B**) Schematic purification scheme for ternary CDK8/CycC/MED12 complexes. Salt-concentrations of individual purification steps were illustrated. CDK8/CycC/MED12 is shown as a cartoon. (**C**) SDS-PAGE analysis of CDK8 (1-403)/CycC/MED12 (1-100) before and after TEV treatment. (**D**) Size-exclusion chromatograms and SDS-PAGE analysis of purified ternary CDK8/CycC/MED12 complexes using a Superose 6 10/300 GL (GE Healthcare). Protein complexes are shown as cartoons above each gel, individual proteins are indicated next to the gels. CDK8 (1-403) is shown in red, Cyclin C is in blue, MED12 is in grey. MED12 contains the Strep-tag (indicated by black circles) and runs accordingly higher in the gel as shown on (C). Please note that (D) is adopted from Klatt et al., 2020.

CDK19 containing ternary constructs were constructed as just described for CDK8/CycC/MED12 complexes (Fig 22). However, due to different acceptor-donor-plasmid combinations, some CDK19 containing ternary constructs harbor the C-terminal Strep-tag on Cyclin C instead of on MED12 (Figs. 22A and B). Please note here, that identical proteins and

protein-complexes can be co-expressed using multiple acceptor-donor combinations. The presented CDK19 containing ternary complexes on Fig. 22D were co-expressed and purified to homogeneity using the established purification scheme applied to CDK8-containing ternary complexes (Fig. 21B).
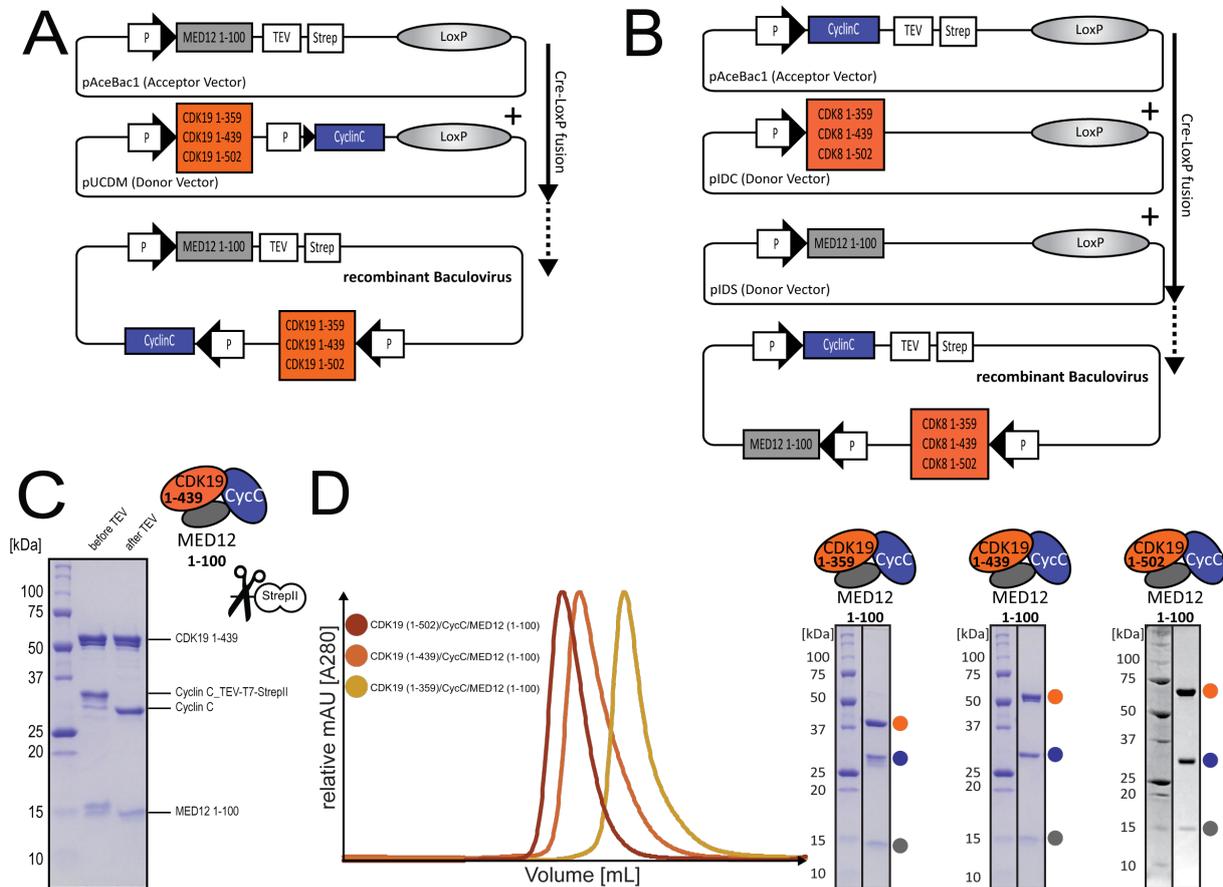
Figure 22: Co-expression and purification of ternary CDK19/CycC/MED12 complexes

(**A**) Schematic fusion strategy and expression cassettes for ternary CDK19/CycC/MED12 complexes that contain Strep-tagged MED12 (1-100). (**B**) Schematic fusion strategy and expression cassettes for ternary CDK19/CycC/MED12 complexes that contain C-terminally Strep-tagged Cyclin C (**C**) SDS-PAGE analysis of CDK19 (1-439)/CycC/MED12 (1-100) before and after TEV treatment. Please note that the Strep-tag is C-terminally located on Cyclin C. (**D**) Size-exclusion chromatograms and SDS-PAGE analysis of purified ternary CDK19/CycC/MED12 complexes using a Superdex 200 10/300 GL (GE Healthcare). Protein complexes are shown as cartoons above each gel, individual proteins are indicated next to the gels. CDK19 variants (1-502 (full-length), 1-439 and 1-359) are shown in orange, Cyclin C is in blue, MED12 is in grey. Please note that PAGE gels on (D) were partially taken by Bastian Jahreis.

2.1.4   Co-purification of binary and ternary complexes

In addition to the abovementioned co-expression strategies, we also established co-purification schemes for different binary and ternary complexes. To that end, we expressed individual subunits of the Mediator kinase module and co-purified them together. This co-purification strategy allows for enormous construct flexibility. As exemplified on Fig 23, binary CDK19

(1-359)/Cyclin C complexes and ternary CDK19/CycC/MED12 (1-100) complexes (as already shown on Figs. 18D and 22D) could be efficiently purified using our alternative co-purification technique.
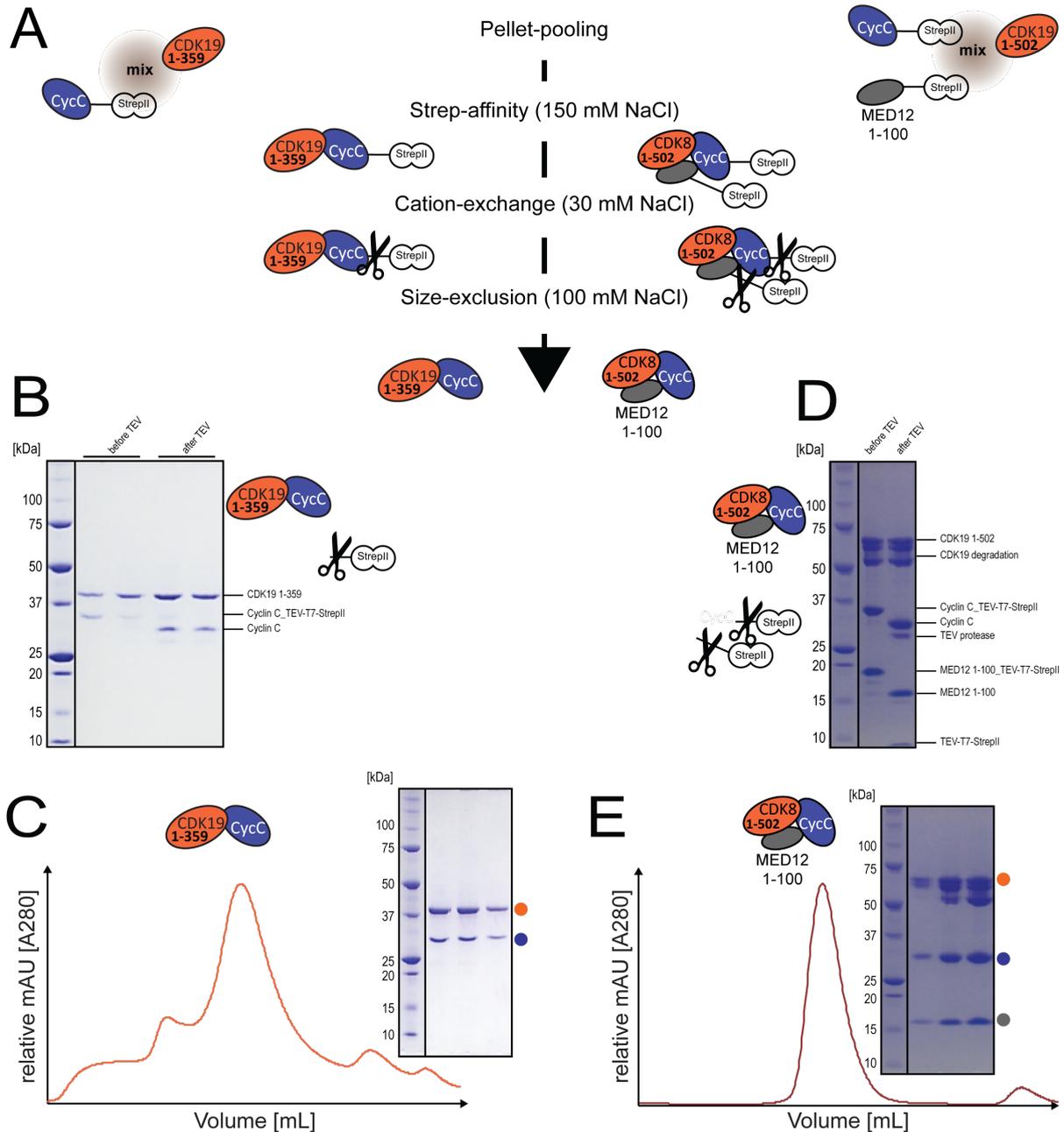
Figure 23: Expression and co-purification of binary CDK19/Cyclin C and ternary CDK19/CycC/MED12 complexes (**A**) Co-purification scheme for binary CDK19 (1-359)/Cyclin C and ternary CDK19 (1-502)/CycC/MED12 (1-100) complexes. Individual proteins were expressed, their cell pellets combined and purified together. Protein complexes are shown as cartoons. (**B**) SDS-PAGE analysis of binary CDK19 (1-359)/Cyclin C before and after TEV treatment. (**C**) Size-exclusion chromatogram and SDS-PAGE analysis of co-purified binary CDK19 (1-359)/Cyclin C complexes using a Superdex 200 (GE Healthcare). Protein complexes are shown as cartoons above the gel, individual proteins are indicated next to the gels. CDK19 (1-359) is shown in orange, Cyclin C is in blue. (**D**) Same as in (B), just for ternary CDK19 (1-502)/CycC/MED12 (1-100) complexes. (**E**) Same as in (C), just for ternary CDK19 (1-502)/CycC/MED12 (1-100) complexes. Protein complexes are shown as cartoons above the gel, individual proteins are indicated next to the gels. CDK19 (1-502) is shown in orange, Cyclin C is in blue, MED12 (1-100) is in grey. Please note that PAGE gels on (B) and (C) were taken by Melanie Müller.

2.1.5   Purification of the N-terminal segment of MED13

To gain insights into the structure and function of MED13, I first set out to express full-length MED13. To enhance protein expression, I therefore introduced an N-terminal Strep-SUMO tag on full-length MED13. Insect cell expression revealed, that MED13 is only marginally expressed and tends to degrade (data not shown). Electrospray ionization mass spectrometry of a degraded MED13 band suggested, that the N-terminal region comprising MED13 up to residue 496 is structured (see chapter 6.1, Fig. 64). In addition to electrospray ionization mass spectrometry, secondary structure predictions suggests that the MED13 N-terminal domain up to amino acid 545 is structured. These results guided me to clone MED13 (1-545) and to test its expression in High Five insect cells. Strikingly, after applying standard purification steps (Fig. 24A), the N-terminal portion of MED13 (1-545) could be purified to homogeneity (Fig. 24C). To unravel whether the N-terminal segment of MED13 is structured, we utilized circular dichroism (CD) spectroscopy. We expected this part of MED13 to be structured as we had identified this fragment as a stable degradation product of full-length MED13, which can be efficiently expressed. As predicted, using the aforementioned technique, we uncovered that MED13 (1-545) possesses α-helical properties that give rise to CD minima at 208 and 222 nm (Holzwarth and Doty, 1965) (Fig. 24D).
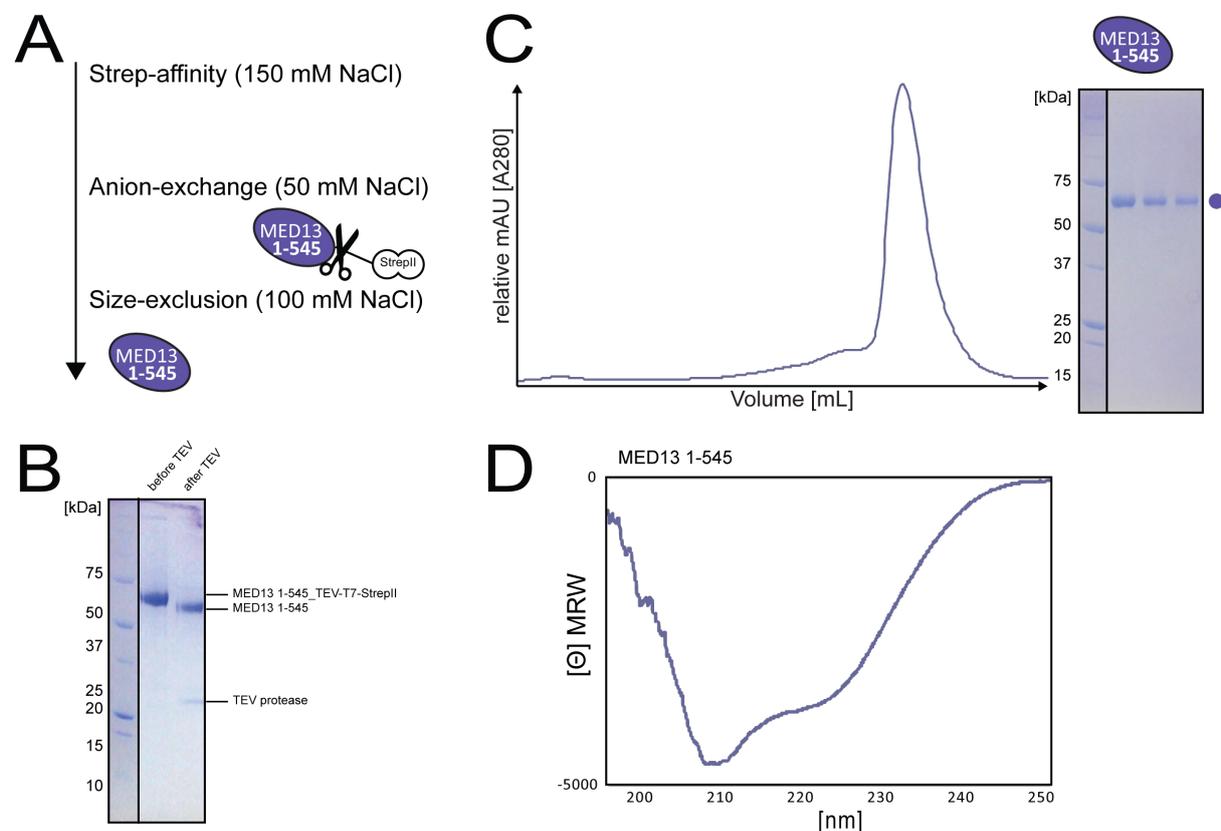
Figure 24: Purification and circular dichroism spectroscopy of N-terminal MED13

(**A**) Schematic purification scheme for single N-terminal MED13. Salt-concentrations of individual purification steps were illustrated. MED13 is shown as a cartoon. (**B**) SDS-PAGE analysis of MED13 (1-545) before and after TEV treatment. (**C**) Size-exclusion chromatogram and SDS-PAGE analysis of purified N-terminal MED13 using a Superose 6 10/300 GL (GE Healthcare). MED13 is shown as cartoons above each gel and indicated next to the gel in purple. (**D**) Far-UV CD-spectrum of MED13 (1-545). Please note that experiments were carried out by Silas Amarell.

2.1.6   Purification of quaternary CDK8/CycC/MED12/MED13 complexes

After I had tested numerous different constructs, I was finally able to establish a purification scheme that results in a protein complex that comprises all subunits of the human Mediator kinase module. To do so, I combined both my co-expression and co-purification strategies, which I had established together with my students for other kinase module components (see Figs. 17 and 23). The applied purification scheme confirms, that the kinase module can be reconstituted *in vitro* (Knuesel et al., 2009a) (Fig. 25). This leads me to suggest that even more kinase module combinations can be generated using a combination of co-expression and co-purification techniques. In more detail, to reconstitute the 4-subunit Mediator kinase module, I co-expressed CDK8 together with Cyclin C, however, MED12 and MED13 were expressed as proteins (Fig. 25A). In a first step, co-purification and a subsequent Strep-affinity chromatography captured all proteins simultaneously. However, the subsequent cation-exchange- and size-exclusion chromatography steps enabled me to isolate the 4-subunit Mediator kinase module. In summary, a highly pure Mediator kinase module comprising full-length CDK8, Cyclin C and C-terminally truncated MED12 (1-1227) and MED13 (1-947) could be expressed and co-purified. (Fig. 25C).
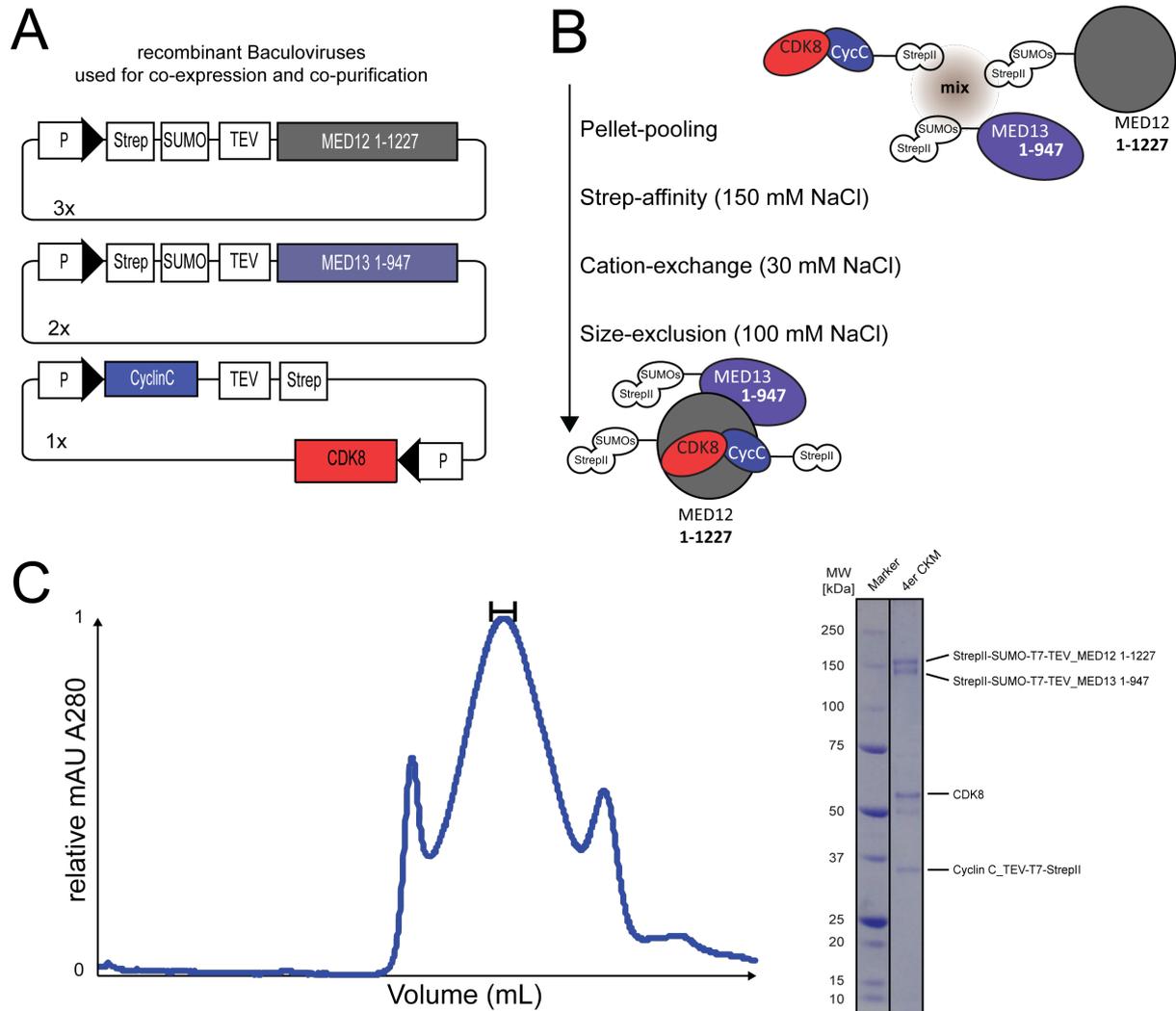
Figure 25: Expression and co-purification of quaternary CDK8/CycC/MED12/MED13 complexes
(**A**) Schematic expression cassettes utilized to express all four subunit of the mediator kinase module. Three individual constructs that encode for N-terminally Strep-SUMO-tagged MED12 (1-1227), MED13 (1-947), and CDK8 together with C-terminally Strep-tagged Cyclin C were used. Please note that the relative expression volumes for single MED12 were 3-times higher, for MED13 2-times higher compared to the binary CDK8/Cyclin C construct. (**B**) Schematic purification scheme for the recombinant mediator kinase module. Salt-concentrations of specific purification steps were illustrated. MED12, MED13 and CDK8/Cyclin C are shown as a cartoon. (**C**) Size-exclusion chromatogram and SDS-PAGE analysis of the co-purified and reconstituted kinase module using a Superose 6 Increase 3.2 (GE Healthcare).

2.2 Purification of kinase assay substrates

To test the enzymatic activity of the purified CDK complexes, I established a radioactive kinase assay together with Robin Weinmann (Klatt et al., 2020). Therefore, *bona fide* substrates of CDK8 (and CDK19) were cloned, (co-)expressed and purified.

2.2.1 Purification of STAT1, Sirtuin-1, Pol II and BRCA1

STAT1 is a known CDK8 target and phosphorylated by CDK8 at Ser-727 (Bancerek et al., 2013). Sirtuin-1 (phosphorylated at Thr-530) and BRCA1 (phosphorylated at Ser-1613), as well as Pol II, are additional substrates of CDK8 (Poss et al., 2016). STAT1, Sirtuin-1 and BRCA1 substrates were expressed in *E. coli* and purified to homogeneity (Fig. 26). Pol II was endogenously isolated from bovine thymus and purified as described (Bernecky et al., 2016).
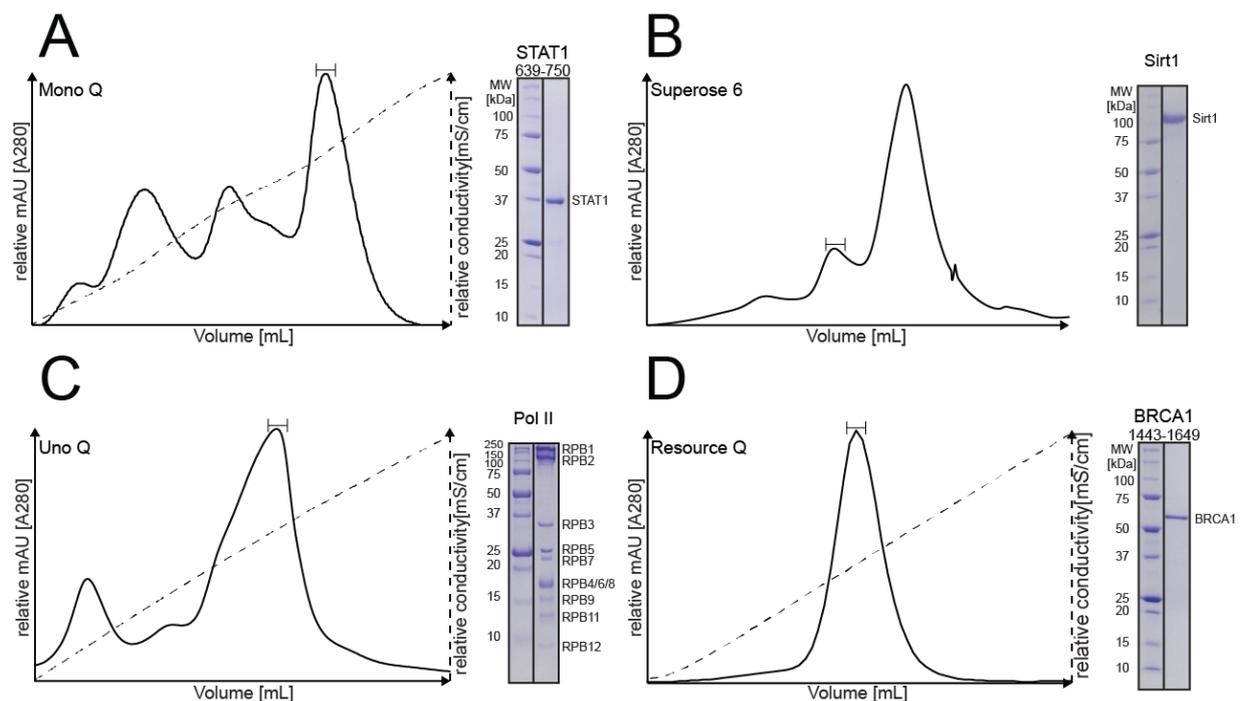
Figure 26: Purification of STAT1, Sirtuin-1, Pol II and BRCA1.

(**A**) Anion-exchange chromatogram of purified STAT1 TAD using a Mono Q (GE Healthcare) column and SDS-PAGE analysis. The analyzed fraction is depicted above the chromatogram. (**B**) Size-exclusion chromatogram of purified Sirtuin-1 using a Superose 6 10/300 GL (GE Healthcare) column and SDS-PAGE analyses. The analyzed fraction is depicted above the chromatogram. (**C**) Anion-exchange chromatogram of endogenously isolated Pol II using a Uno Q (Bio-Rad) column and SDS-PAGE analysis. The analyzed fraction is depicted above the chromatogram. (**D**) Anion-exchange chromatogram of purified BRCA1 using a Resource Q (GE Healthcare) column and SDS-PAGE analysis. The analyzed fraction is depicted above the chromatogram. Please note that (A) and (B) was carried out by myself, yet data were provided for Robin Weinmann; (C) was done by Robin Weinmann under supervision of Lisa-Marie Schneider, University of Bayreuth.

2.2.2 Purification of Cyclin H and binary CDK7/Cyclin H

Cyclin H is reported to be phosphorylated by CDK8 on its N- and C-terminal helices at Ser-5 and Ser-304 (Akoulitchev et al., 2000). Interestingly, this phosphorylation event was shown to inhibit CDK7 kinase activity. First, to validate Cyclin H as a target for CDK8, I expressed Cyclin H in *E. coli* and purified it to homogeneity (Fig. 27).
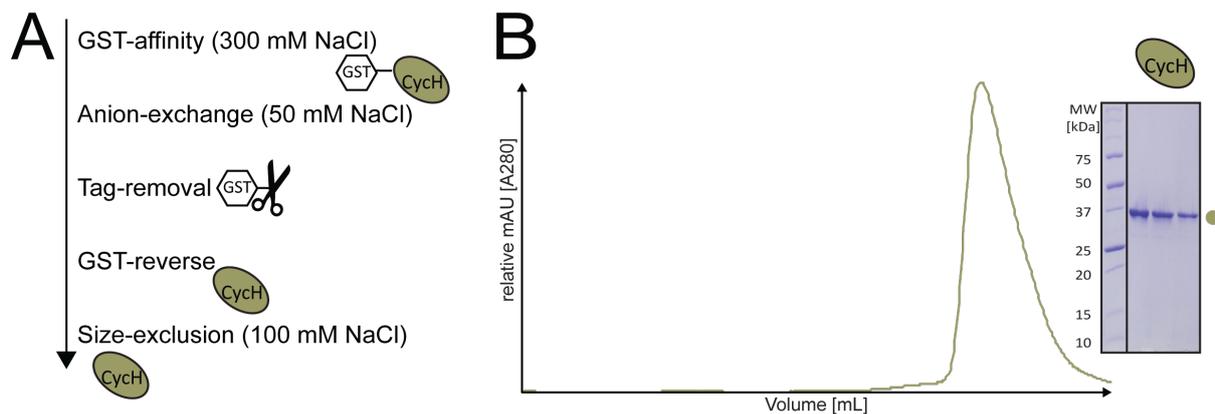
Figure 27: Purification of Cyclin H

(**A**) Schematic purification scheme for N-terminally GST-tagged Cyclin H from *E. coli*. Salt-concentrations of individual purification steps were illustrated. Cyclin H is shown as a cartoon. (**B**) Size-exclusion chromatogram and SDS-PAGE analysis of purified Cyclin H using a Superose 6 (GE Healthcare). Cyclin H is shown as a cartoon above the gel and indicated next to it in green.

In addition to purified Cyclin H from *E. coli* (Fig. 27), I co-expressed the binary CDK7/Cyclin H complex in insect cells (Fig. 28). The utilized construct was cloned and combined in analogy to my N-terminal Strep-SUMO tagged CDK8/Cyclin C and CDK19/Cyclin C complexes (Fig. 19). Baculovirus-infected High Five insect cells were lysed by sonication, cell debris was removed by centrifugation and the supernatant was collected. Following Strep-affinity chromatography, SUMO-tagged CDK7 bound to Cyclin H was immobilized on an anion-exchange resin to recover the desired proteins. In a final step, the binary CDK7/Cyclin H complex was isolated by size-exclusion chromatography resulting in highly pure CDK7/Cyclin H (Fig. 28C).
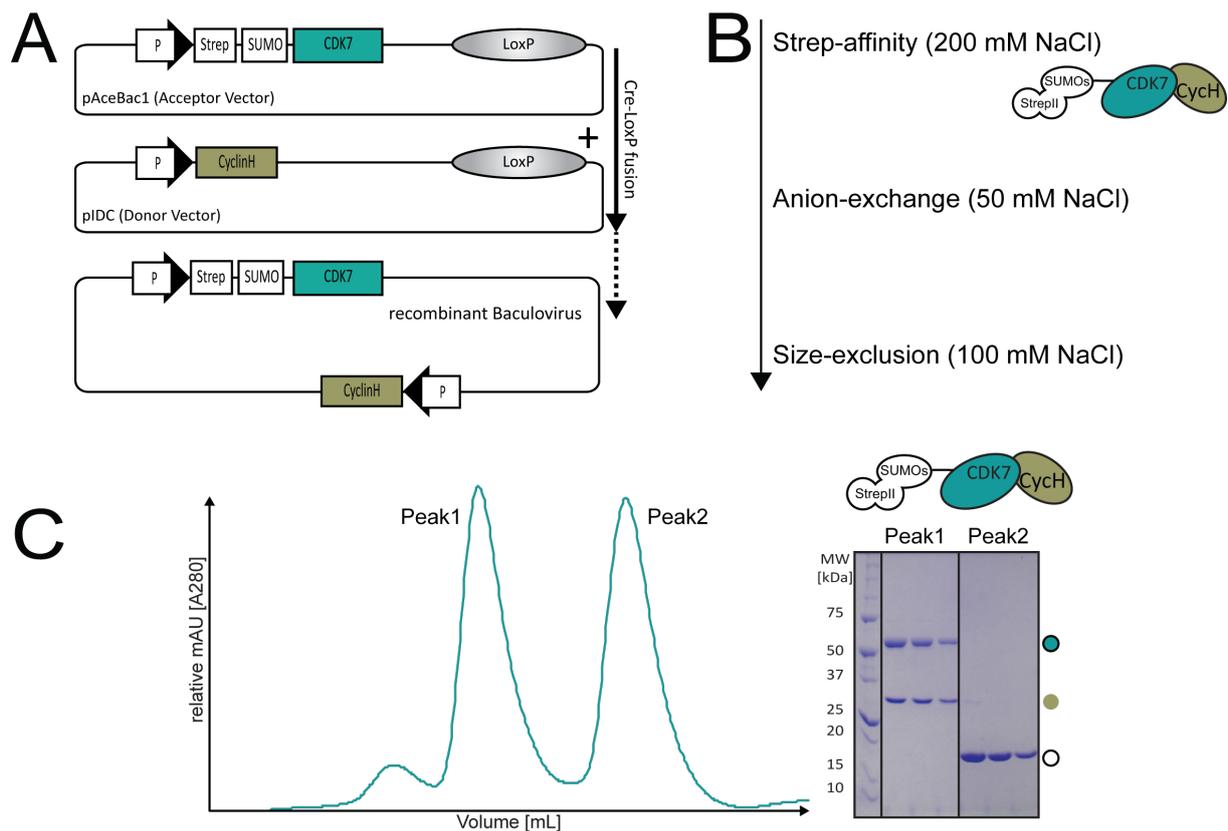
Figure 28: Expression and purification of binary CDK7/Cyclin H complexes

(**A**) Schematic fusion strategy and expression cassette for SUMO-tagged CDK7/Cyclin H using MultiBac^Turbo. (**B**) Schematic purification scheme for SUMO-tagged CDK7/Cyclin H. Salt-concentrations of individual purification steps were illustrated. CDK7/Cyclin H is shown as a cartoon. (**C**) Size-exclusion chromatogram and SDS-PAGE analysis of purified SUMO-tagged CDK7/Cyclin H complexes using a Superdex 200 (GE Healthcare). Excessive amounts of SUMO could be efficiently separated. The protein complex is shown as a cartoon above the gel, individual proteins are indicated next to the gel. CDK7 is shown in turquois, Cyclin H is in green, Strep-SUMO in white. CDK7 contains the Strep-SUMO tag (indicated by black circles) and runs accordingly higher in the gel.

2.2.3 Purification of NELF and DSIF

The negative elongation factor (NELF) is an additional target of CDK8 and was a gift of Prof. Dr. Patrick Cramer. In detail, the largest subunit NELF-A is phosphorylated on Ser-360 and Ser-363 (Poss et al., 2016). The quaternary NELF complex was co-expressed in High Five insect cells and purified as described (Vos et al., 2016). In brief, baculovirus-infected High Five insect cells were lysed by sonication, cell debris was removed by centrifugation and the supernatant was collected. Following Ni-NTA-affinity chromatography, NELF was immobilized on an anion-exchange resin to recover the desired complex. Last, NELF was subjected to size-exclusion chromatography (Fig. 29A).
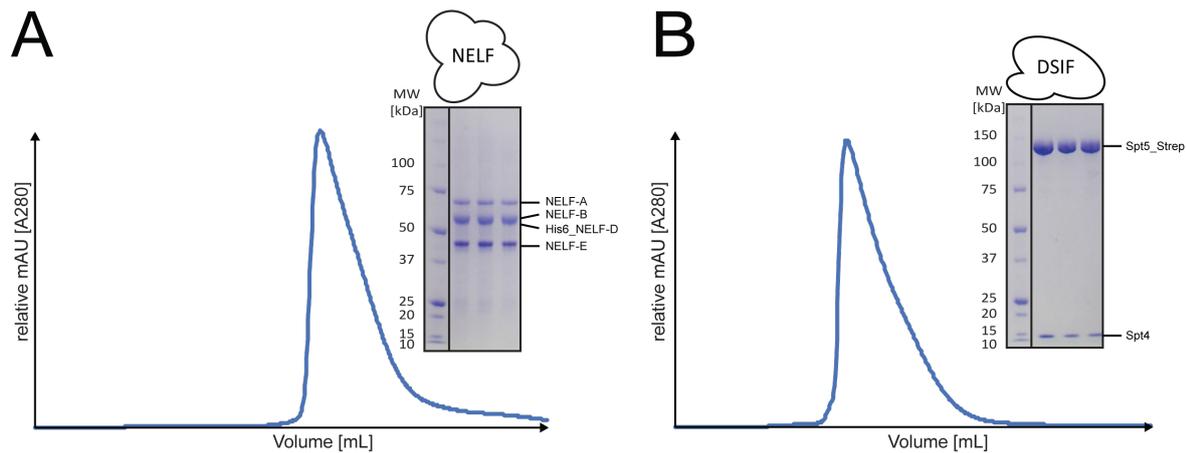
Figure 29: Purification of NELF and DSIF

(**A**) Size-exclusion chromatogram and SDS-PAGE analysis of His6-tagged NELF using a Superose 6 (GE Healthcare). Please note that NELF-B and His$_6$-NELF-D have a similar molecular weight and run on the same height. (**B**) Size-exclusion chromatogram and SDS-PAGE analysis of Strep-tagged DSIF using a Superdex 200 (GE Healthcare).

To assess how CDK8-mediated Cyclin H phosphorylation impacts CDK7 kinase activity, I sought to set up a kinase assay using the purified binary CDK7/Cyclin H complexes (see chapter 2.2.2). This would allow me to investigate the putative inhibitory effect on CDK7 kinase activity upon Cyclin H phosphorylation. Hence, I expressed the *bona fide* CDK7 substrate DRB sensitivity inducing factor (DSIF) in insect cells. More precisely, the larger subunit of the heterodimer DSIF Spt5 (the smaller being Spt4) is phosphorylated by CDK7 (Larochelle et al., 2006). Spt5 was cloned into a pAceBac1 acceptor-, Spt4 into a pIDK donor-vector. Both were combined to co-express the heterodimer DSIF. Human DSIF was a gift of Prof. Dr. Birgitta Wöhrl and was purified in analogy to NELF, yet harbored a Strep-tag instead of a hexahistidin-tag for affinity purification (Fig. 29B).

2.3   Biochemical characterization of the purified Mediator kinase module components

To study how MED12 binds and activates CDK8 and CDK19 and to characterize the highly pure Mediator kinase module components, that I and my supervised students had purified before (see chapter 2.1), we carried out *in vitro* biochemistry, cross-linking coupled to mass spectrometry, X-ray crystallography and *in vivo* experiments.

2.3.1   MED12 19-91 is a stable N-terminal fragment

To identify proteolytic resistant fragments of MED12 (1-100) when bound to CDK8 and Cyclin C, I carried out limited proteolysis using the CDK8 (1-403)/CycC/MED12 (1-100) ternary complex (Fig. 30). Electrospray ionization mass spectrometry of a proteolyzed MED12 fragment hints at the possibility that MED12 residues 19-91 form a stable N-terminal MED12 domain (see chapter 6.1, Fig. 63).
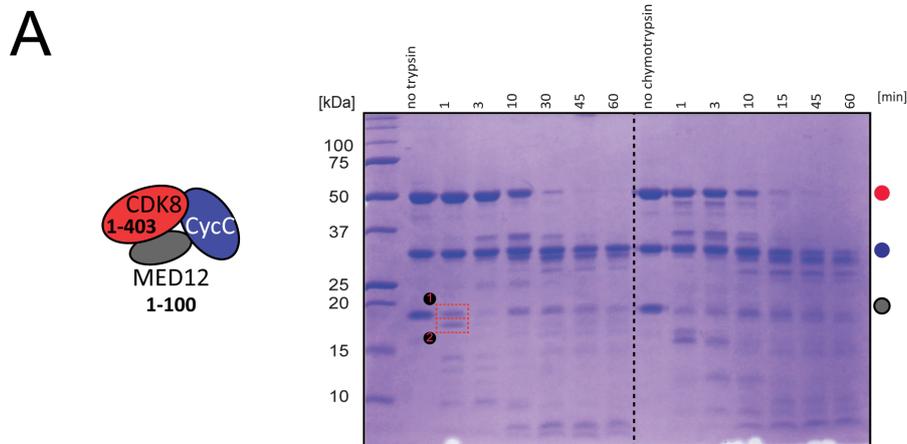
Figure 30: Limited proteolysis of the CDK8 (1-403)/CycC/MED12 (1-100) ternary complex
The CDK8 (1-403)/CycC/MED12 (1-100) ternary complex was treated with trypsin (left panel) or chymotrypsin (right panel). Samples were taken at indicated time points. MED12 (1-100) (1.) and the first trypsin-proteolyzed band MED12 (11-91) (2.) were prepared for electrospray ionization mass spectrometry and are boxed.

2.3.2   MED12 binds CDK8/Cyclin C and CDK19/Cyclin C complexes

To investigate the activation potential of the N-terminal segment of MED12 on CDK8 activity (Turunen et al., 2014), we measured the affinity of MED12 (1-100) to CDK8/Cyclin C complexes using both microscale thermophoresis (MST) and isothermal titration calorimetry (ITC). Using MST, we recorded a nanomolar affinity (K_d= 44 nM) of MED12 for full-length

CDK8 (Fig. 31A). Shortening of the CDK8 C-terminus reduced MED12 binding affinity by a factor of five for the shortest CDK8 variant (CDK8 (1-359), K_d= 220 nM). This suggests that the disordered C-terminus of CDK8 only marginally influences MED12 binding. To cross-validate my MST measurements I used ITC to confirm an affinity of 72 nM for MED12 (1-100) binding to CDK8 (1-403)/Cyclin C (The K_d using MST was 71 nM) (Fig. 31A and B) (Klatt et al., 2020).
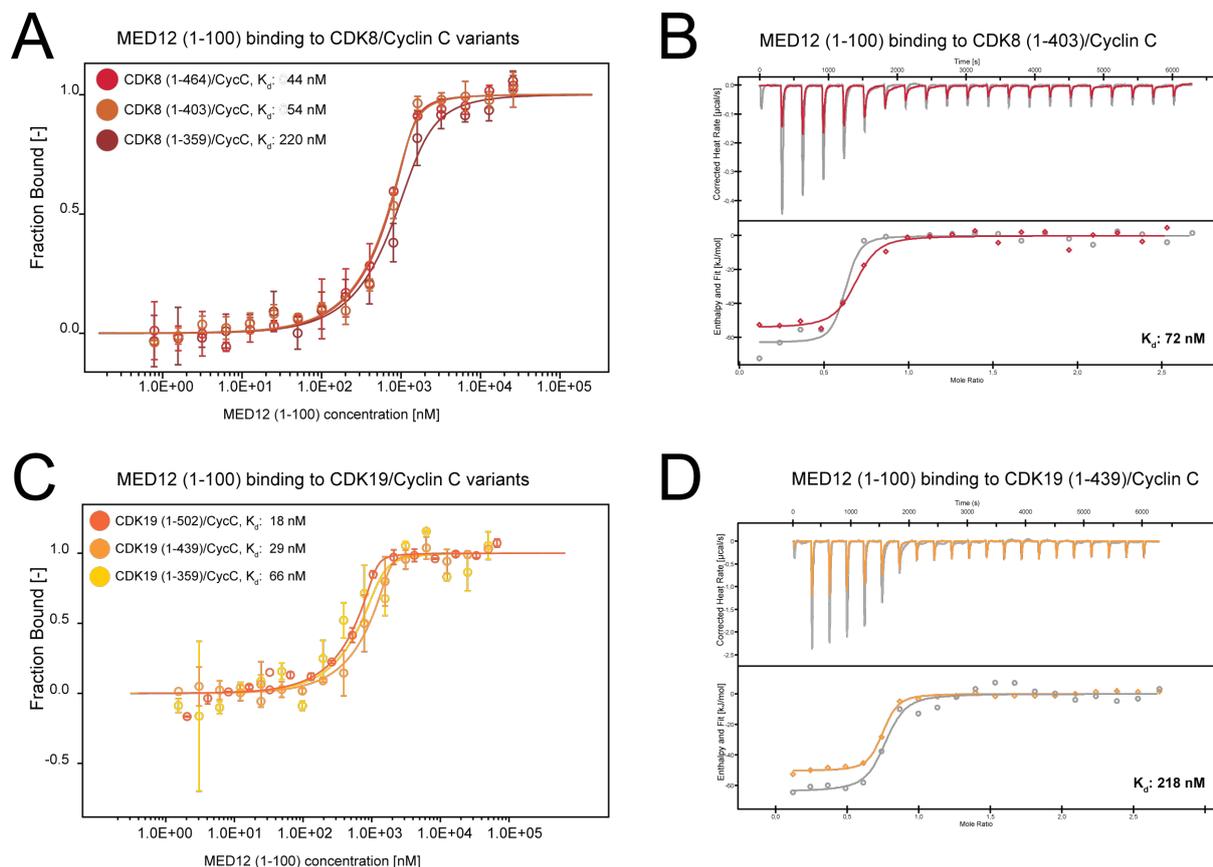
Figure 31: MED12 binds both CDK8/Cyclin C and CDK19/Cyclin C binary complexes

(**A**) Microscale thermophoresis (MST) binding experiments using of MED12 (1-100) and different binary CDK8/Cyclin C complexes. K_d values are indicated. Error bars reflect the standard deviation of four replicates. Please note that the K_d cannot be read off directly due to the experimental necessity to use high protein concentrations. (**B**) Same as in (A), just with binary CDK19/Cyclin C complexes. (**C**) Using isothermal titration calorimetry (ITC) with MED12 (1-100) and SUMO-tagged CDK8 (1-403)/Cyclin C we confirmed the K_d values that resulted from MST measurements. (**D**) Same as in (C), just with SUMO-tagged CDK19 (1-439)/Cyclin C. Please note that MST measurement were carried out by Franziska Langhammer, ITC measurements were carried out by Melanie Müller and myself, yet data were provided for Melanie Müller. Note further that (A) and (B) were adopted from Klatt et al., 2020.

Having determined nanomolar affinity for MED12 to the CDK8/Cyclin C complex, we next asked whether MED12 preferentially binds to binary CDK8/Cyclin C or binary CDK19/Cyclin C complexes. Therefore, we measured the affinity of MED12 (1-100) for our CDK19/Cyclin C complexes using again both MST and ITC (Figs. 31C and D). Utilizing MST, we detected a nanomolar affinity (K_d= 18 nM) of MED12 towards full-length CDK19.

Truncating the C-terminus of CDK19 reduced MED12 binding affinity by a factor of three for the shortest CDK19 variant (CDK19 (1-359), K_d= 66 nM) (Fig. 31C). This suggests that the also the C-terminus of CDK19 also only marginally affects MED12 binding, just as we found for CDK8. ITC measurements revealed a nanomolar affinity of 218 nM of MED12 (1-100) for CDK19 (1-439)/Cyclin C (The K_d using MST was 29 nM) (Figs. 31C and D). In consequence, the N-terminal portion of MED12 binds with nanomolar affinity to both CDK8/Cyclin C and CDK19/Cyclin C complexes and does not distinguish between CDK8/Cyclin C or CDK19/Cyclin C binding. Rather, MED12 seems to associate with both Mediator kinases equally well (Fig. 31).

2.3.3   MED12 stabilizes CDK8/Cyclin C complexes

To assess whether MED12 binding to different CDK8/Cyclin C complexes impacts protein stability, we recorded their thermal melting behavior using differential scanning fluorimetry (nanoDSF). We found a significantly increased melting temperature (+7°C) of ternary complexes, which demonstrates that MED12 has a major stabilizing effect on CDK8/Cyclin C complexes (Fig. 32A). Note here that the stability of CDK complexes was reported to correlate with their activity (Nolen et al., 2004). Moreover, our nanoDSF data uncover that the presence of CDK8's likely unstructured C-terminus destabilizes both binary and ternary complexes. Furthermore, we find that ternary complexes comprising a MED12 fragments 1-91 or 1-100 result in the most stable complexes. In contrast, MED12 constructs shorter than 70 residues significantly destabilize the ternary complex albeit still showing a stabilizing effect with respect to the binary complex (Fig. 32B) (Klatt et al., 2020).
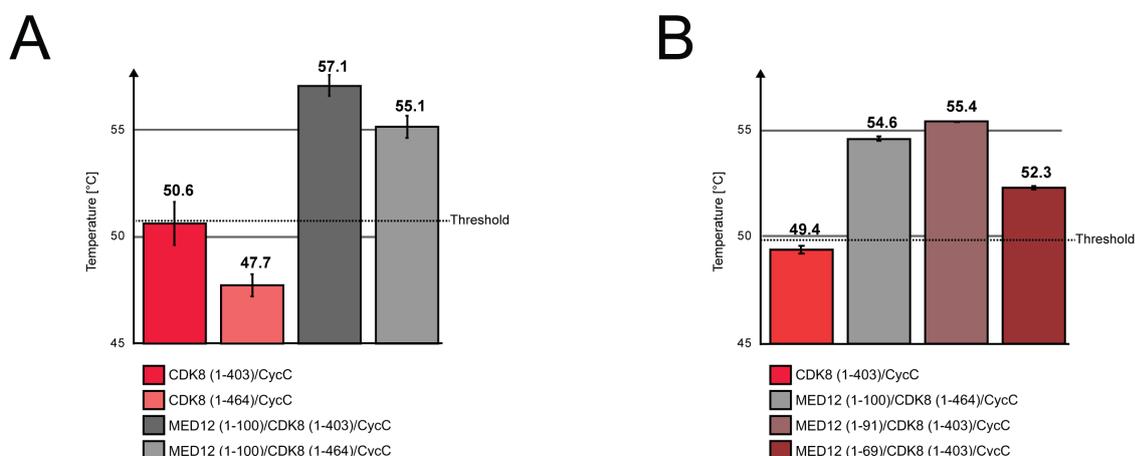
Figure 32: The N-terminal part of MED12 stabilizes CDK8/Cyclin C binary complexes.
Thermal stability of binary CDK8/Cyclin C complexes and ternary CDK8/CycC/MED12 complexes determined using differential scanning fluorimetry (nanoDSF). T_M values are indicated. The standard deviation of three experimental replicates

is shown as error bars. Please note that nanoDSF measurements were carried out by Franziska Langhammer at Proteros biostructures GmbH under supervision of Dr. Elisabeth Schneider from Proteros biostructures GmbH. I provided the protein complexes. Adopted from Klatt et al., 2020.

2.3.4 MED12 enhances CDK8 and CDK19 kinase activity

To measure CDK8 activity we utilized the tag-free binary CDK8/Cyclin C and ternary CDK8/CycC/MED12 complexes. In the presence of 50 pmol substrate (STAT1) and 7.5 pmol kinase (CDK8) we detected low kinase activity for binary CDK8/ Cyclin C complexes using an *in vitro* kinase assay system. The inclusion of MED12 in ternary CDK8 (1-403)/CycC/MED12 (1-100) complexes resulted in a pronounced stimulation of CDK8 kinase activity, confirming the activation potential of MED12 (Fig. 33A). Moreover, in addition to STAT1 phosphorylation (the substrate) we also observed signal for CDK8 phosphorylation (Fig. 33B) (Klatt et al., 2020). These results establish that CDK8 serves as a second substrate in the reaction (CDK8 phosphorylation will be presented in more detail in chapter 2.13) (Klatt et al., 2020).
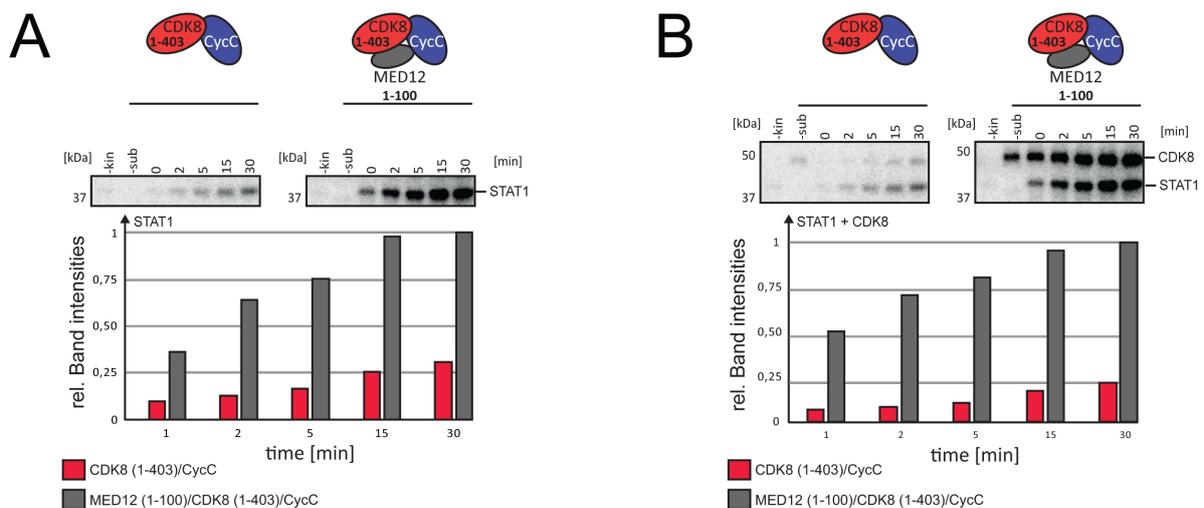
Figure 33: The N-terminal portion of MED12 enhances CDK8 kinase activity

In vitro kinase assays using purified binary CDK8 (1-403)/Cyclin C and ternary CDK8 (1-403)/CycC/MED12 (1-100) complexes. 7.5 pmol kinase complex was incubated with 50 pmol purified GST-tagged STAT1 transactivation domain (TAD) in presence of an excess of [γ-^{32}P]-ATP. Reactions were stopped at the indicated time points. The quantification of band intensities is shown below. (**B**) Same as in (A), yet CDK8 phosphorylation is plotted. The quantification of band intensities is shown below and incudes the CDK8 phosphorylation signal. Please note that kinase assays and band quantifications were carried out by Robin Weinmann. Kinases were purified and provided by Franziska Langhammer and myself. Adopted from Klatt et al., 2020.

We found that MED12 (1-100) has a profound stimulatory effect on CDK8 kinase activity (Fig. 33). Next, we asked whether the same holds true for the CDK8 paralog CDK19. Therefore, we

used our purified binary CDK19/Cyclin C and ternary CDK19/CycC/MED12 complexes. Due to the high sequence identity of both paralogs (97% conservation within their kinase domain, (see chapter 1.1, Figs. 1 and 7), we expected a similar MED12-dependent stimulation of CDK19 kinase activity, as we has established for CDK8. As hypothesized, this is exactly what we observed. The inclusion of MED12 (1-100) in CDK19 (1-439)/Cyclin C complexes resulted in a significant activation of CDK19 kinase activity (Fig. 34A). Moreover, we observed also a signal for CDK19, confirming that the kinase itself can also serve as a substrate (Fig. 34B).
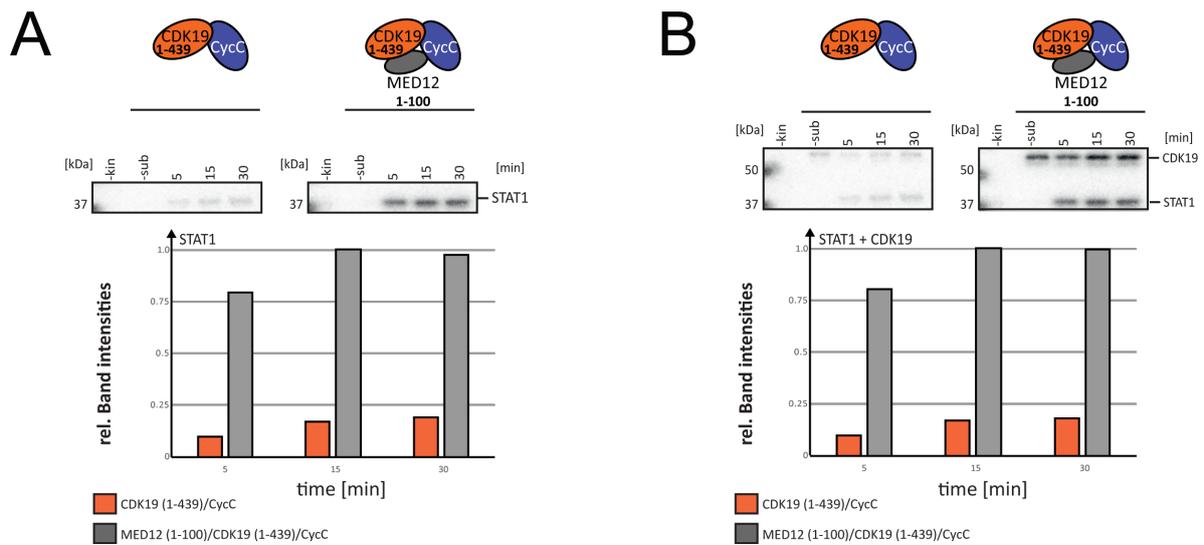
Figure 34: The N-terminal portion of MED12 enhances CDK19 kinase activity

In vitro kinase assays using purified binary CDK19 (1-439)/Cyclin C and ternary CDK19 (1-439)/CycC/MED12 (1-100) complexes. 7.5 pmol kinase complex was incubated with 50 pmol purified GST-tagged STAT1 transactivation domain (TAD) in presence of an excess of $[\gamma\text{-}^{32}P]$-ATP. Reactions were stopped at the indicated time points. The quantification of band intensities is shown below. (**B**) Same as in (A), yet CDK19 phosphorylation is plotted. The quantification of band intensities is shown below and incudes the CDK8 phosphorylation signal. Please note that kinase assays and band quantifications were carried out by Robin Weinmann. Kinases were provided by Melanie Müller and myself.

2.3.5 CDK8 and CDK19 phosphorylate transcription-related targets

To emphasize and extend these findings to more than a single substrate, we employed purified Sirtuin-1, BRCA1, NELF-A and Pol II as additional CDK8 targets in our *in vitro* assay system (see chapter 2.2). All of them were found to be phosphorylated by CDK8. Using these substrates, we observed similar MED12-dependent activation of CDK8 (Figs. 35A and B). This confirms earlier reports (Knuesel et al., 2009a)(Turunen et al., 2014), yet also demonstrates that the CDK8/Cyclin C complex possesses basal kinase activity whose extent varies with the ratio of kinase to substrate concentration (Figs. 33A and 35A). For CDK19, we utilized BRCA1 as additional substrate and observed, once again, a similar MED12-depedent activation of CDK19

kinase activity (Fig. 35C). Last, also the binary CDK19/Cyclin C complex shows basal kinase activity.
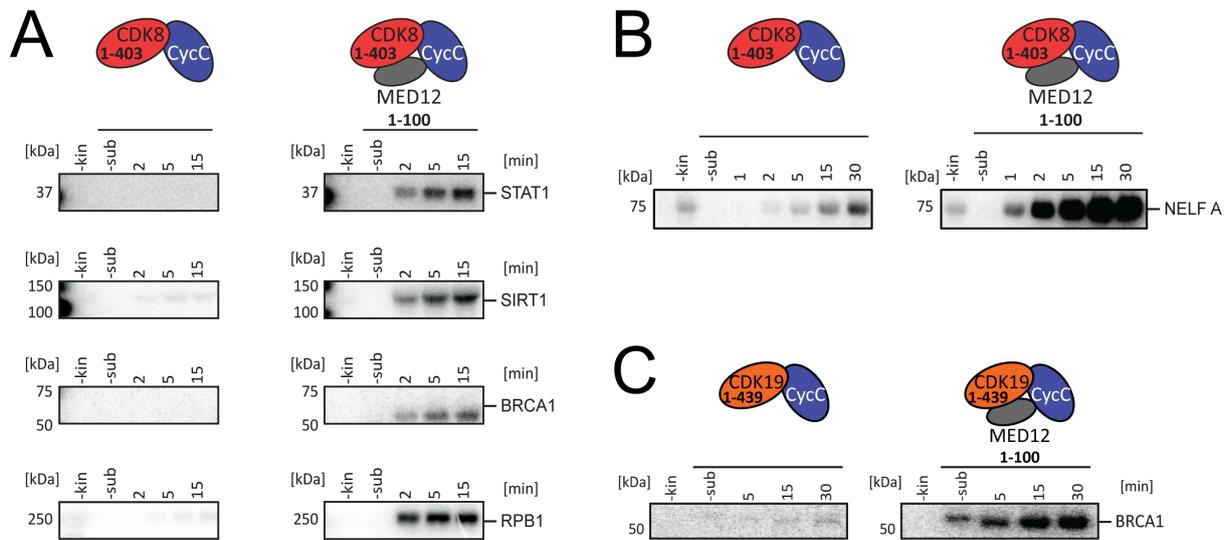
Figure 35: CDK8 and CDK19 phosphorylate transcription-related targets

(**A**) *In vitro* kinase assays using purified binary CDK8 (1-403)/Cyclin C and ternary CDK8 (1-403)/CycC/MED12 (1-100) complexes. Assays carried out as described in Figs. 33 and 34. A ratio of 0.25 pmol kinase complex and 75 pmol substrate was used for STAT1. For Sirt-1 and BRCA1, a ratio of 0.5 pmol kinase and 50 pmol Sirt-1 was used. For Pol II, 2 pmol of kinase complex was incubated in presence of 2 pmol Pol II. Please note that the Pol II CTD contains about 50 potential CDK8 phosphorylation sites, which made this 1:1 ratio necessary. (**B**) Same as in (A), just with A ratio of 7.5 pmol kinase complex with 50 pmol purified NELF. (**C**) Same as in (B), just with purified binary CDK19 (1-439)/Cyclin C and ternary CDK19 (1-439)/CycC/MED12 (1-100) complexes and BRCA1. Please note that BRCA1 and CDK19 (1-439) cannot be separated by SDS-PAGE. Please note further that (A), except for the BRCA1 assay, is adopted from Klatt et al., 2020. Kinase assays on (A) and (B) were carried out by Robin Weinmann and by myself.

2.3.6 CDK8 and CDK19 kinase activities are comparable

N-terminal portion of MED12 has a profound effect on both CDK8 and CDK19 kinase activity (Figs. 33, 34 and 35). To detect any differential kinase activity between CDK8 and CDK19 when stimulated by MED12, we used our established *in vitro* assay system with full-length CDK8 and CDK19 (Fig. 36). We note here, that CDK19 contains a larger C-terminal domain than CDK8 (see chapter 1.1, Fig. 7), that could be involved in substrate recognition (Dixon-Clarke et al., 2015). Therefore, in addition to STAT1, we tested Sirtuin-1 and Pol II as already established CDK8 targets.

However, we did not measure significant differences between MED12-stimulated CDK8 and CDK19 kinase activities (Fig. 36). Thus, and in conclusion, CDK8 and CDK19 show almost similar kinase activities without any apparent substrate preference in our *in vitro* system. Last,

we note that we cannot determine the exact phosphorylation sites within the Pol II CTD using our assay system (the CTD residues targeted by CDK19 are yet unknown).
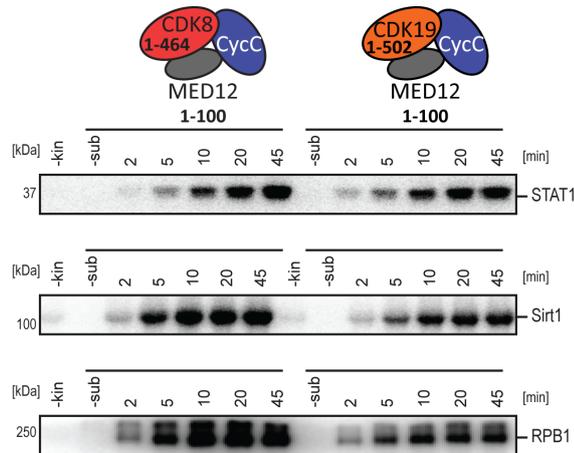
Figure 36: The kinase activities of CDK8 and CDK19 are highly comparable.

In vitro kinase assays using full-length CDK8/CycC/MED12 (1-100) and full-length CDK19/CycC/MED12 (1-100) ternary complexes. Kinase assays were carried out with STAT1 TAD, Sirt-1 and Pol II as substrates. Kinase assays were performed as described in Figs. 33 and 34. Please note that kinase assays were carried out by Bastian Jahreis.

2.3.7   The MED12 fragment 23-69 is both necessary and sufficient to stimulate CDK8

Having confirmed the CDK8-activation potential residing within the MED12 fragment 1-100, we next aimed to identify the minimal MED12 fragment sufficient to activate CDK8. Therefore, we systematically truncated the MED12 N- and C-terminus and utilized these variants in our kinase assay (Fig. 37). To that end, I was able to narrow down the minimal stable fragment sufficient for CDK8 activation to 46 amino acids at the N-terminus of MED12 (MED12 residues 23-69).
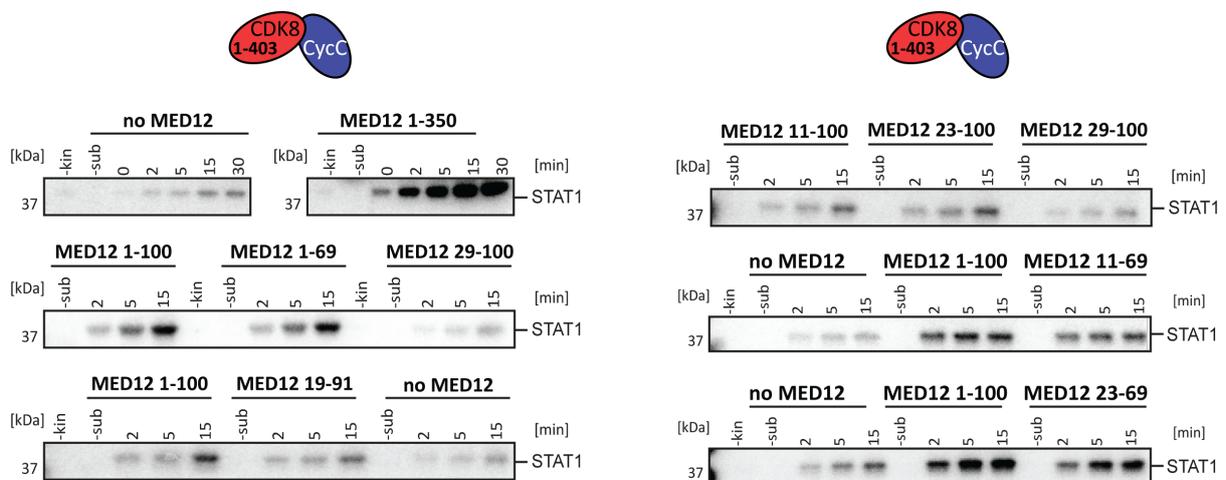
Figure 37: MED12 23-69 is both necessary and sufficient to enhance CDK8 activity.

(**A**) *In vitro* kinase assays using purified binary CDK8 (1-403)/Cyclin C and ternary CDK8 (1-403)/CycC/MED12 complexes encompassing different N- and C-terminal MED12 truncations. Kinase assays were carried out as described in Figs. 33 and 34.

2.3.8   MED12 harbors an activation helix that enhances CDK8 and CDK19 kinase activity

Interestingly, secondary structure prediction programs hinted at the formation of an α helix for MED12 residues 32 through 44. Moreover, crosslinking experiments coupled to mass spectrometry with my CDK8-containing ternary constructs uncovered that MED12 residues 30-42, which mostly encompass the predicted helix, are in proximity to the T-loop of CDK8 (see chapter 6.2, Figs. 65A and C) (Klatt et al., 2020). This suggests, that residues that are part of the predicted helix are crucial for CDK8 and CDK19 activation (Klatt et al., 2020).

To test this *in silico* analysis, I carried out circular dichroism spectroscopy with synthetic MED12 peptides that comprise the predicted α-helical sequence (Fig. 38A). I decided to measure peptides of two different length in presence of varying trifluoroethanol (TFE) concentrations to analyze their propensities to form helices (Fig. 38B) (Luo and Baldwin, 1997). In absence of TFE the far-UV CD spectra of both MED12 peptides show characteristics of disordered proteins. Strikingly, upon TFE titration, I observed spectral shifts to negative bands at 222 nm, 208 nm and positive bands at 193 nm, all of which are typical α-helical characteristics (Holzwarth and Doty, 1965). The shorter MED12 (29-40) peptide shows similar effects, yet the TFE-induced shifts were less marked (Fig. 38B). These measurements underscore secondary structure predictions, that suggested an α-helical fold within the N-terminal activation segment of MED12. Taken together, both peptides show α helical properties, that were especially profound for the longer MED12 (29-44) peptide. The results therefore confirm that MED12 residues 30-42 form an α-helix.

To elucidate the importance of this α-helix for CDK8 activation, I systematically mutated residues that are part of the helix. In particular, I was intrigued by a cluster of three acidic residues (E33, D34 and E35) at the predicted N-terminal tip of the helix that stabilize the positive helical dipole at this position (Fig. 39C) (Klatt et al., 2020). As some CDK homologs utilize a phosphorylation-independent activation mechanism, that relies on negatively charged residues (see chapter 1.1, Fig. 4), I asked whether one of the three acidic residues contributes to CDK8 activation. Much to our surprise, an E33Q mutation completely abolished CDK8 activation by MED12 (Fig. 39A). This was also the case for double-mutants involving E33. In contrast, neither the mutation of D34, nor of E35 had an effect on kinase activation. To exclude

a direct involvement of other charged residues in CDK8 activation we also measured the effect of K30A, Q31A and K32A mutations on kinase activity. However, we found none of them to influence CDK8 activation by MED12 (Fig. 39B). I thus conclude that MED12 E33 is essential to activate CDK8, a finding that prompted us to term the helix that harbors E33 at its tip "activation helix". Please note here that I was able to purify all ternary, mutation-containing complexes to homogeneity (data not shown). This clearly demonstrates that MED12 binding to CDK8/Cyclin C and CDK8 activation can be experimentally uncoupled (Klatt et al., 2020).
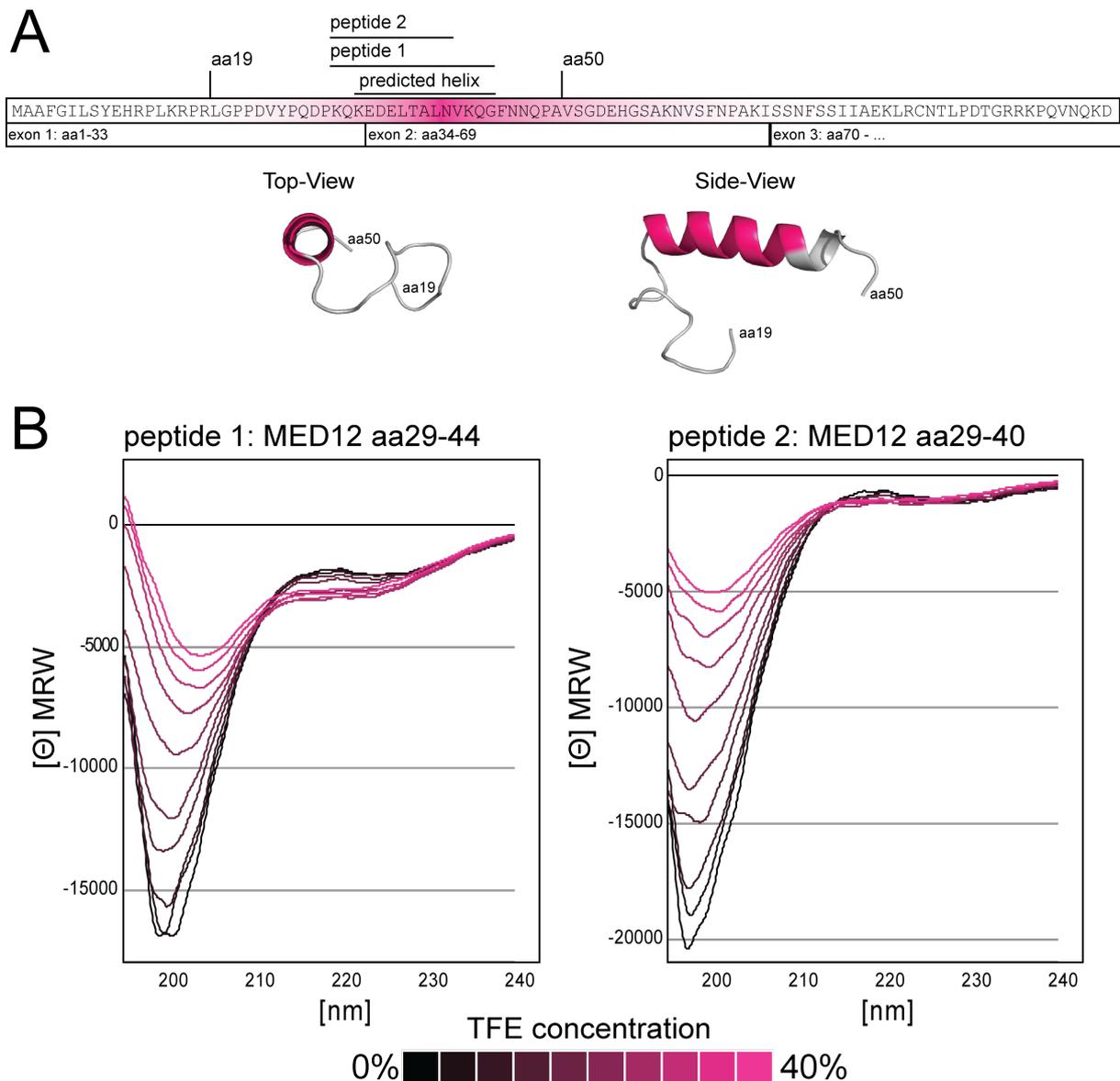
Figure 38: The N-terminal segment of MED12 possesses a helical topology

(**A**) Amino acid sequence of the N-terminal segment of MED12 encompassing its first 100 residues. The 3-dimensional structure prediction of the MED12 activation helix comprising MED12 residues 19-50, which was modeled using PEP-FOLD3 (Lamiable et al., 2016). Amino acids 32-44 of the secondary structure prediction are in pink. Adapted from Klatt et al., 2020. (**B**) Far-UV CD-spectra of two synthetic MED12 peptides under TFE titration. Utilized MED12 peptides and TFE concentrations were illustrated. Please note that MED12 peptides were a gift of Dr. Sascha Weidler, Dr. Marie Lott and Elisabeth Rozanski from Carlo Unverzagt's lab, University of Bayreuth.
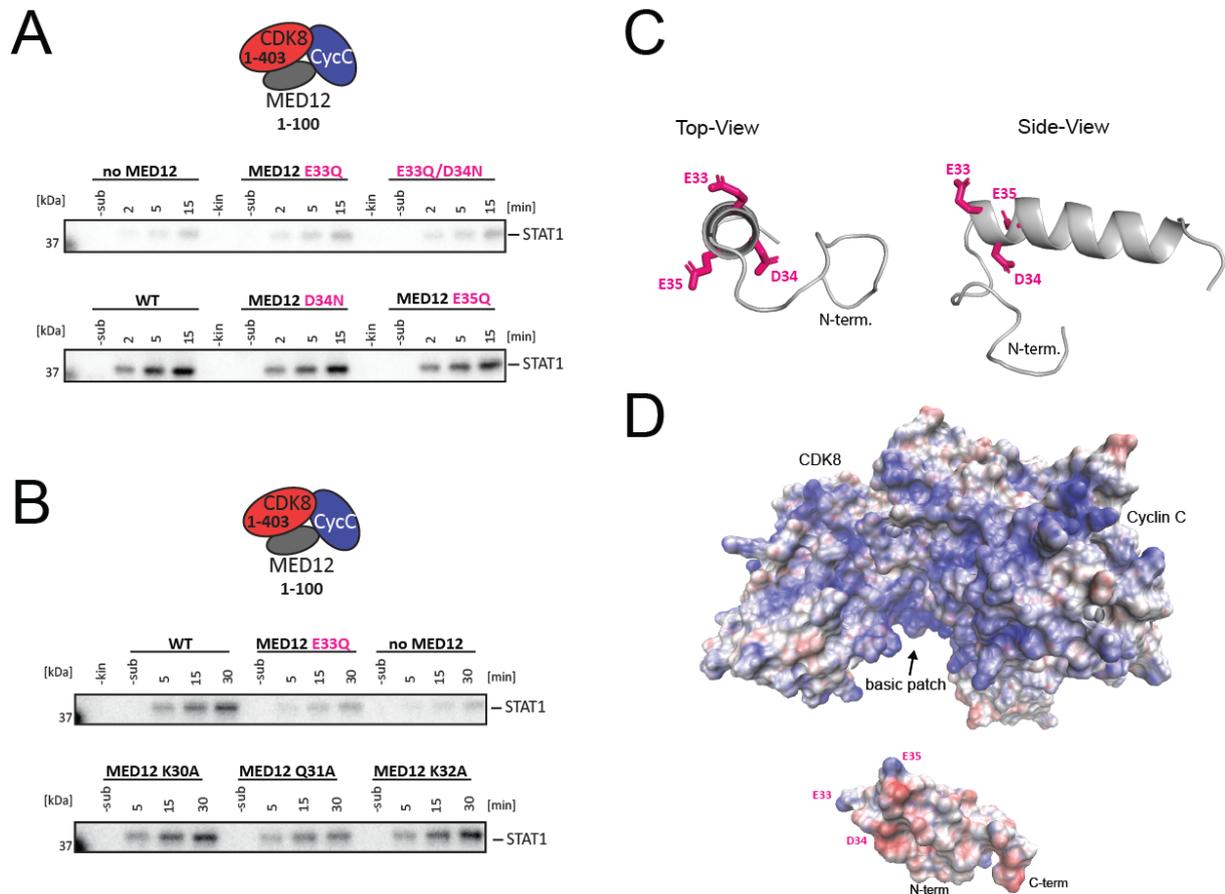
Figure 39: MED12 utilizes an activation helix with Glutamate-33 at its tip to stimulate CDK8 activity.
(**A**) *In vitro* kinase assays using purified ternary CDK8 (1-403)/CycC/MED12 (1-100) complexes that harbor point-mutations within MED12. Kinase assays were carried out with the STAT1 TAD as described in Fig. 33.. (**B**) Same as in (A), yet different point mutations within MED12 (1-100) were assayed (**C**) 3-dimensional model of the MED12 activation helix comprising MED12 residues 19-50. The model was calculated using PEP-FOLD3 (Lamiable et al., 2016). The negatively charged triad of amino acids at the N-terminal tip of the activation helix (E33, D34 and E35) is shown as sticks in pink. (**D**) Electrostatic surface potential of the 3D-model of MED12 (19-50) (see (C) and the binary CDK8 (1-403)/Cyclin C complex (PDB code 3RGF) were calculated using VMD (Humphrey et al., 1996). At the interface of CDK8 and Cyclin C there is a positively charged patch that could interact with the negatively charged N-terminus of the activation helix (MED12 E33-D34-E35). Please note that kinase assays were carried out by Robin Weinmann. Mutation-containing protein complexes were purified by myself. The electrostatic surface potential shown on (D) was modelled by Franziska Langhammer under supervision of Prof. Dr. Ullman, University of Bayreuth. Adapted from Klatt et al., 2020.

We next asked how the activation helix is able to bind in the interface of CDK8 and Cyclin C. To that end we calculated the electrostatic surface potential of the binary CDK8/Cyclin C complex and of a model of the MED12 activation helix (Fig. 39D). We noticed a basic patch at the interface of CDK8 and Cyclin C - in the same region where we had detected crosslinks of MED12 to CDK8. This warrants my speculation that the acidic triad E33-D34-E35 is responsible for positioning the MED12 activation helix properly for CDK8 activation (Klatt et al., 2020).

As the N-terminal segment of MED12 binds and activates both CDK8 and CDK19 (Figs. 31, 33 and 34), we asked next whether an E33Q mutation eliminates the stimulatory function of MED12 in activating CDK19 (Fig. 40). We expected this to be the case, as the catalytic domains of both CDK8 and CDK19 are highly conserved (97% conservation within their kinase domain, see chapter 1.1, Figs. 1 and 7). Just as expected, the mutation of MED12 E33Q led to a complete loss of the MED12-dependent activation of CDK19 (Fig. 40). In conclusion, the N-terminal portion of MED12, which carries the activation helix with E33 at its tip, binds and activates CDK19 in an analogous manner to CDK8.
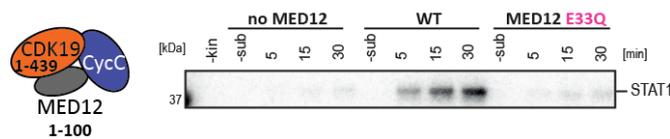
Figure 40: MED12 Glutamate-33 stimulates CDK19 activity

In vitro kinase assays using purified binary CDK19 (1-439)/Cyclin C and ternary CDK19 (1-439)/CycC/MED12 (1-100) complexes that harbor an E33Q mutation at the tip of the MED12 activation helix. Kinase assays were carried out with the STAT1 TAD as described in Fig. 34. The kinase assay was carried out by Robin Weinmann.

2.3.9   The MED12 activation helix with Glutamate-33 activates CDK8 also *in vivo*

Having discovered that a single residue within the MED12 activation helix, Glutamate-33, is both necessary and sufficient for MED12-dependent CDK8 activation, I next aimed to elucidate this finding *in vivo*. To that end I teamed up with Dr. Hung Ho-Xuan from Prof. Gunter Meister's lab at the University of Regensburg. Together, we generated a MED12 E33Q knock-in in HCT116 colon cancer cells by applying the CRISPR/Cas9 system (Fig. 41).
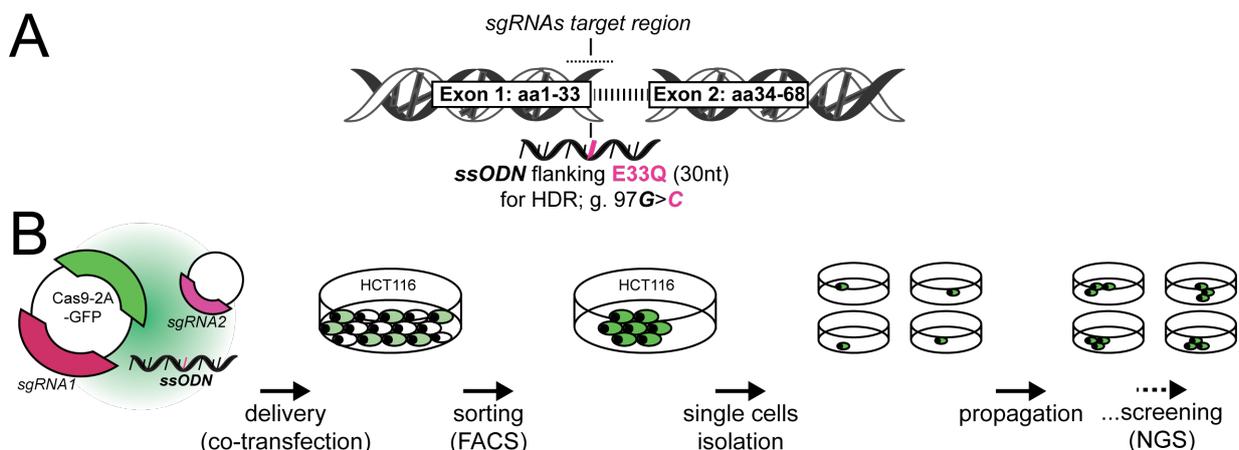
Figure 41: Schematic representation of the utilized CRISPR workflow.

(**A**) To generate an HCT116 cell line carrying a MED12 E33Q mutation, suited oligos were designed that target the genomic region of MED12 E33 for homology-directed repair (HDR). The Cas9-mediated nucleotide exchange, which results in a MED12 protein mutant carrying an E33Q mutation, is illustrated (**B**) Upon co-transfection of the two single guide RNAs (sgRNA) together with Cas9-2A-GFP, positive HCT116 cells were isolated by fluorescence-activated cell sorting (FACS) and

cultivated for RNA-Seq library preparation. Finally, RNA-Seq libraries were screened by next generation sequencing (NGS). Please note that the CRISPR workflow was carried out with help from Dr. Hung Ho-Xuan. Genotyping of more than 5,000 clones was done by myself. NGS libraries were prepared together with Dr. Xuan-Hung Ho, NGS screening was done by Dr. Hung Ho-Xuan and Norbert Eichner both from Prof. Gunter Meister's lab at the University of Regensburg. Adapted from Klatt et al., 2020.

After genotyping more than 5,000 clones we successfully obtained a stable HCT116 cell line that carries a MED12 E33Q mutation. Unfortunately, we additionally observed a K15N mutation in the generated cell line besides the desired E33Q mutation (Klatt et al., 2020). However, this mutation neither altered MED12 expression levels (Fig. 42A) nor its subcellular localization or its kinase activity (Fig. 42B) (Klatt et al., 2020). In order to further sensitize cells for MED12-dependent CDK8 activation, I decided to stimulate our HCT116 cells with interferon-γ (IFN-γ).
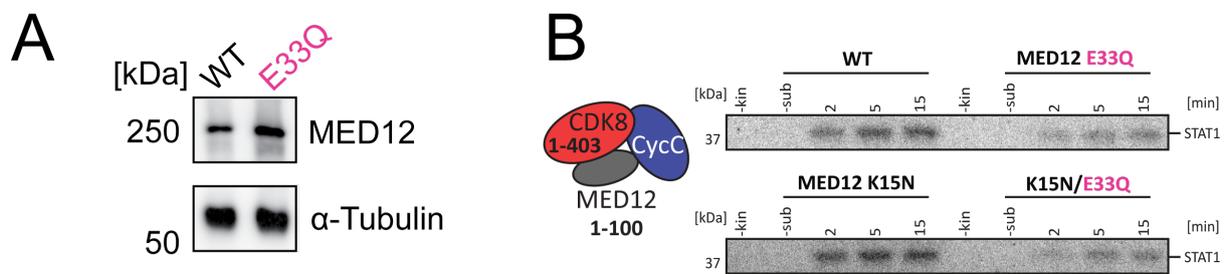
Figure 42: A MED12 K15N mutation has no profound effects on MED12 function.
(**A**) The presence of MED12 in the MED12 E33Q mutant cell line was verified by Western blotting. (**B**) *In vitro* kinase assays were performed using purified ternary CDK8 (1-403)/CycC/MED12 (1-100) complexes harboring individual mutations within MED12 (1-100). Mutations are indicated. Kinases assays were performed as described in Fig. 33 with the STAT1 TAD as a substrate. The results indicate the accidental K15N has no impact on CDK8 activity, in contrast to an E33Q mutation that is used as a control. Adapted from Klatt et al., 2020.

I chose IFN-γ stimulation as its rapid impact on interferon-response genes solely relies on STAT1 phosphorylation by CDK8 (Castro et al., 2018; Dannappel et al., 2019; Steinparzer et al., 2019). In perfect agreement with our *in vitro* data, upon IFN-γ stimulation I measured a significant reduction in STAT1 phosphorylation levels in the mutant (E33Q) cell lines as compared to HCT116 wild-type cells (Fig. 43). This clearly demonstrates that MED12 E33 on the activation helix enhances CDK8/19 kinase activity also *in vivo*.
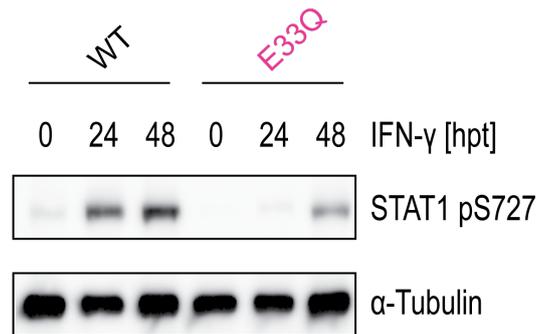
Figure 43: STAT1 phosphorylation is impaired in the CRISPRed HCT116 MED12 E33Q cells

The phosphorylation of Ser-727 in the STAT1 transactivation domain upon IFN-γ induction was analyzed by Western blotting. Adapted from Klatt et al., 2020.

Subsequently, I handed out the samples analyzed by Western blotting on Fig. 43 to my colleague Dr. Iana Kim to carry out differential gene expression analysis by RNA-seq as has been described (Klatt et al., 2020).

2.3.10 MED12 Glutamate-33 likely contacts the arginine triad of CDK8

Having discovered a helix in MED12 that is crucial for its CDK8 activation potential, I next asked which CDK8 residues contacts MED12 E33. As it is the case for all human CDKs, CDK8 possesses an arginine triad (R65, R150 and R178) (see chapter 1.1, Figs. 5 and 7). As some CDK homologs utilize a phosphorylation-independent activation mechanism, that involves amino acids of the arginine triad (see chapter 1.1, Fig. 4), I asked whether one of the arginine residues instead contacts E33 in MED12. To that end I prepared individual arginine mutants (R65Q, R150Q and R178Q) of CDK8 and tested those in complex with Cyclin C and in ternary MED12-containing complexes (Fig. 44A). If one of the three arginine residues indeed contacts E33 in MED12, I expected to see no effect of this mutation on the basal kinase activity of the binary CDK8/Cyclin C complex. In contrast, I expected the abrogation of MED12-dependent CDK8 activation by such mutation. This is exactly what we detected for all three arginine mutants (Fig. 44A). However, we were unable to detect significant and reproducible differences between the three arginine mutations, despite the fact that R65 is located in the αC helix of CDK8 and R150 and R178 are placed in its T-loop (see chapter 1.1, Fig. 5). To exclude that the individual arginine mutants impair MED12 binding to CDK8/Cyclin C, we measured the affinity of MED12 (1-100) for binary CDK8 (1-403)/ Cyclin C complexes carrying individual arginine mutations (R65Q, R150Q or R178Q) by MST without detecting significant changes in the affinity of MED12 for CDK8/Cyclin C (Fig. 44B) (Klatt et al., 2020).
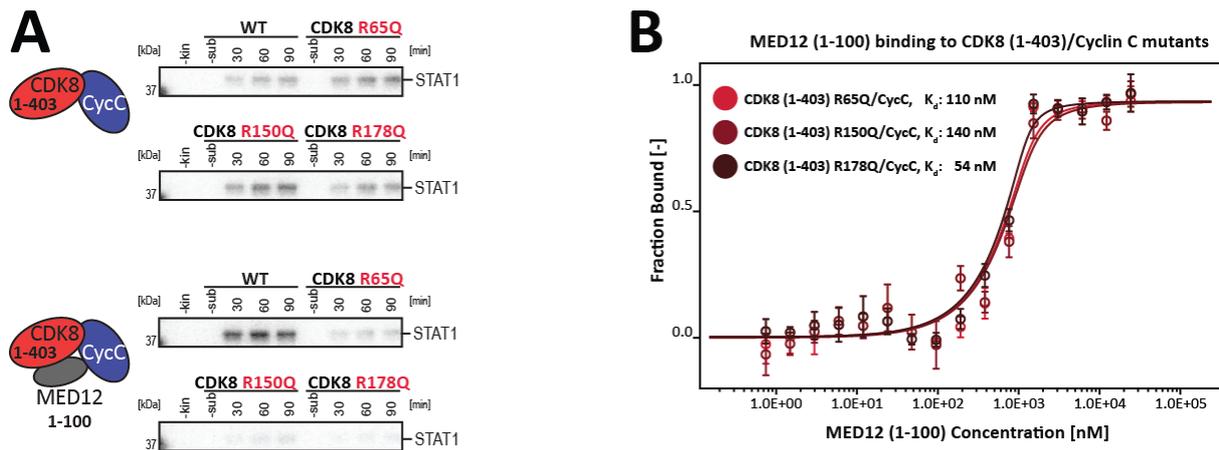
Figure 44: MED12-dependent CDK8 activation likely involves the arginine triad of CDK8.

(**A**) *In vitro* kinase assays using binary CDK8 (1-403)/Cyclin C and ternary CDK8 (1-403)/CycC/MED12 (1-100) complexes. Each complex harbor a mutation in the CDK8 arginine triad. Kinase assays were carried out with the STAT1 TAD as a substrate as in Fig. 33. (**B**) Microscale thermophoresis (MST) binding experiments using MED12 (1-100) and different binary CDK8 (1-403)/Cyclin C complexes that harbor individual mutations in their arginine triad (R65Q, R150Q and R178Q). K_d values are indicated. Error bars reflect the standard deviation of four experimental replicates. Please note that the K_d cannot be read off directly due to the experimental necessity to use high protein concentrations. Please note that kinase assays were carried out by Robin Weinmann, I purified and provided all kinases. Adopted from Klatt et al., 2020.

In summary, these data establish that both the CDK8 arginine triad and E33 of MED12 are essential for MED12-dependent CDK8 activation. Whether the active conformation of the CDK8 T-loop is induced by a direct salt bridge between E33 of MED12 and one of the members of the CDK8 arginine triad will require high-resolution structural information on a ternary CDK8/CycC/MED12 complex (Klatt et al., 2020).

2.3.10 MED12-dependent CDK8 activation is independent of Cyclin C

Cyclin binding triggers the repositioning of the αC-helix in cyclin-dependent kinases, thereby allowing for the formation of their active site (see chapter 1.1, Fig. 3) (Endicott and Noble, 2013; Lolli, 2010). This mechanism also applies to binding of Cyclin C to CDK8 (Schneider et al., 2011). In addition to this conserved role, residue E99 in Cyclin C and an unusually deep surface groove between its two cyclin boxes were also suggested to contribute to CDK8 activation (see chapter 1.1, Fig. 5) (Hoeppner et al., 2005; Nolen et al., 2004; Schneider et al., 2011; Turunen et al., 2014). We sought to confirm these results by using our *in vitro* kinase assay system. However, to my surprise neither a E98Q or E99Q mutation, nor the mutation of two surface groove residues (N181A, D182A) on Cyclin C that were suggest to bind MED12 (Park et al., 2018; Turunen et al., 2014) had an impact on MED12-driven CDK8 activation (Fig. 45A) (Klatt et al., 2020). Using nanoDSF measurements we could show that both Cyclin C

surface mutants (N181A, D182A) destabilize ternary MED12-containing complexes (Fig. 45B). Taken together, our functional and structural data therefore suggest that the Cyclin C surface groove is not directly involved in the MED12-dependent activation of CDK8. Rather, upon mutation of residues in the surface groove, the entire complex becomes destabilized and thereby leads to reduced kinase activity under specific experimental conditions (Klatt et al., 2020; Turunen et al., 2014). Alternatively, the surface groove might contribute to substrate recognition or serve as a protein interaction site, as is the case for CDK2/Cyclin A (Klatt et al., 2020; Russo et al., 1996; Schulman et al., 1998). In conclusion and despite the fact, that we detected crosslinks for Cyclin C E98 and E99 to the MED12 activation helix (see chapter 6.2, Figs. 65A and C), Cyclin C seems only of minor importance for the MED12-driven activation of CDK8 (Klatt et al., 2020).
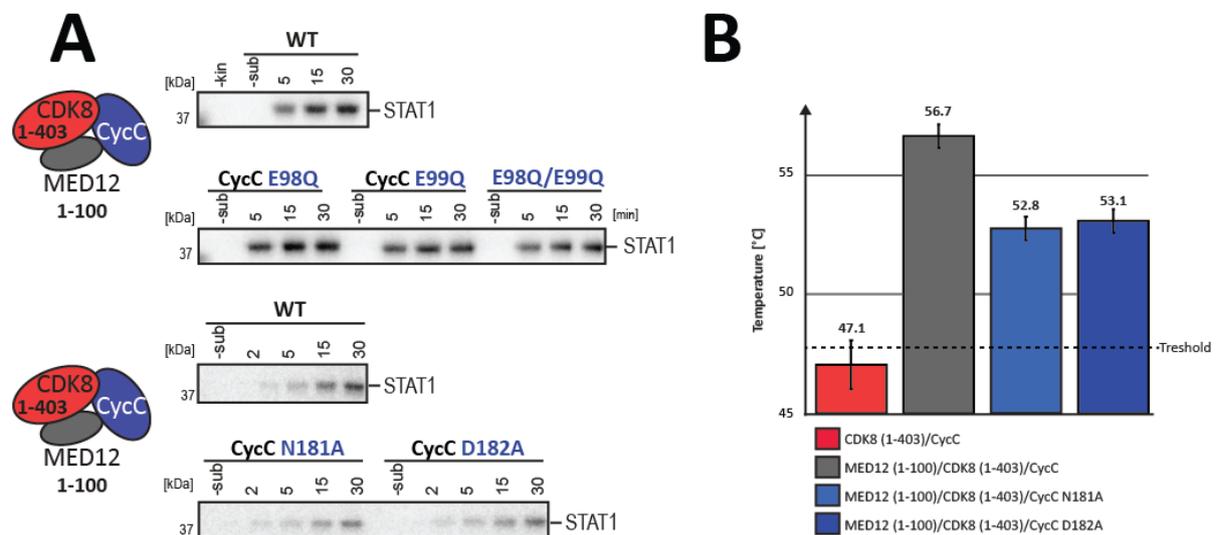
Figure 45: Cyclin C does not contribute to MED12-dependent CDK8 activation.
(**A**) *In vitro* kinase assays using purified ternary CDK8 (1-403)/CycC/MED12 (1-100) complexes that harbor point-mutations within Cyclin C. The activity of wild-type ternary CDK8 (1-403)/CycC/MED12 (1-100) is shown twice since the experiments were analyzed on separate gels. Kinase assays were carried out with the STAT1 TAD as a substrate as described in Fig. 33 (**B**) Thermal stability of ternary CDK8 (1-403)/CycC/MED12 (1-100) complexes that harbor point mutations within the Cyclin C surface groove, as determined by nanoDSF. T_M values are illustrated above each bar. Error bars indicate the standard deviation from three experimental replicates. Please note that kinase assays were carried out by Robin Weinmann. nanoDSF measurement were done by Franziska Langhammer at Proteros biostructures GmbH under supervision of Dr. Elisabeth Schneider from Proteros biostructures GmbH. I purified and provided the protein complexes. Adopted from Klatt et al., 2020.

2.3.11 Malignant MED12 mutations abrogate MED12-dependent CDK8 activation

Frequent somatic MED12 mutations are associated with, amongst others, uterine leiomyomas, tumors of both the breast and the prostate as well as chronic lymphocytic leukemia (see chapter 1.3, Fig. 13) (Kämpjärvi et al., 2015, 2016; Mäkinen et al., 2011; Wu et al., 2017b; Yoshida et

al., 2015). Despite the fact that MED12 consists of 45 exons, the overwhelming majority of these mutations are found in MED12 exon 2 (amino acids 34-68) and to a lesser extend in exon 1 (amino acids 1-33) (see chapter 1.3, Fig. 13B) (Darooei et al., 2019; Kämpjärvi et al., 2016). Strikingly, when I mapped the mutations occurring in the aforementioned malignancies onto the sequence of MED12 (Fig. 38A) (Heikkinen et al., 2017; Kämpjärvi et al., 2015; Mäkinen et al., 2011), I found that the patient-derived mutations perfectly match the activation helix that we unraveled to be essential for CDK8 activation by MED12 (Figs. 39C and 46C). As my mutational analysis of the activation helix uncovered only a single amino acid to be critical for the CDK8-stimulatory function of MED12, I next examined the functional consequences of recurring disease mutations in MED12 (Fig. 46). First, we measured the affinity of MED12 (1-100) fragments carrying L36R, Q43P or G44S mutations for binary CDK8 (1-403)/Cyclin C complexes. All three residues (L36, Q43 and G44) are mutational hotspots in uterine leiomyomas and were also found in chronic lymphocytic leukemia (see chapter 1.3, Fig. 13C) (Kämpjärvi et al., 2015; Mäkinen et al., 2011). In contrast to previously published results we did not detect significantly weakened binding of MED12 to binary CDK8/Cyclin C complexes when compared to wild type MED12 (1-100) (Fig. 46D) (Heikkinen et al., 2017; Park et al., 2018; Turunen et al., 2014). The same holds true for MED12 carrying the E33Q mutation. We note here that E33 is also found mutated in human cancers (Heikkinen et al., 2017). This raised the possibility that MED12 mutations that occur in different cancers might not influence MED12 binding to CDK8/Cyclin C, yet only its activation. To test this, we purified ternary complexes containing mutated MED12 variants (E33A, E33K, D34Y, L36R, Q43P, G44S) and measured their kinase activity (Fig. 46A and B). As expected, for all complexes the kinase activity was abolished or at least drastically reduced (Klatt et al., 2020). Interestingly, the nature of the mutation has a profound impact on the activation potential of MED12. Whereas the mutation of Asp-34 to Tyr (D34Y), which is found in uterine leiomyomas, reduces CDK8 kinase activity, a D34N mutation has no impact on kinase activity in our *in vitro* system (Figs. 39A and 46A). In contrast, all MED12 glutamate-33 mutants (E33Q, E33A, E33K) lead to a loss of CDK8 activation (Figs. 39A and 46B). Taken together, we find that MED12 mutations frequently found in cancer patients lead to an abrogation of CDK8 kinase activity without affecting the affinity of MED12 for CDK8/Cyclin C (Klatt et al., 2020).
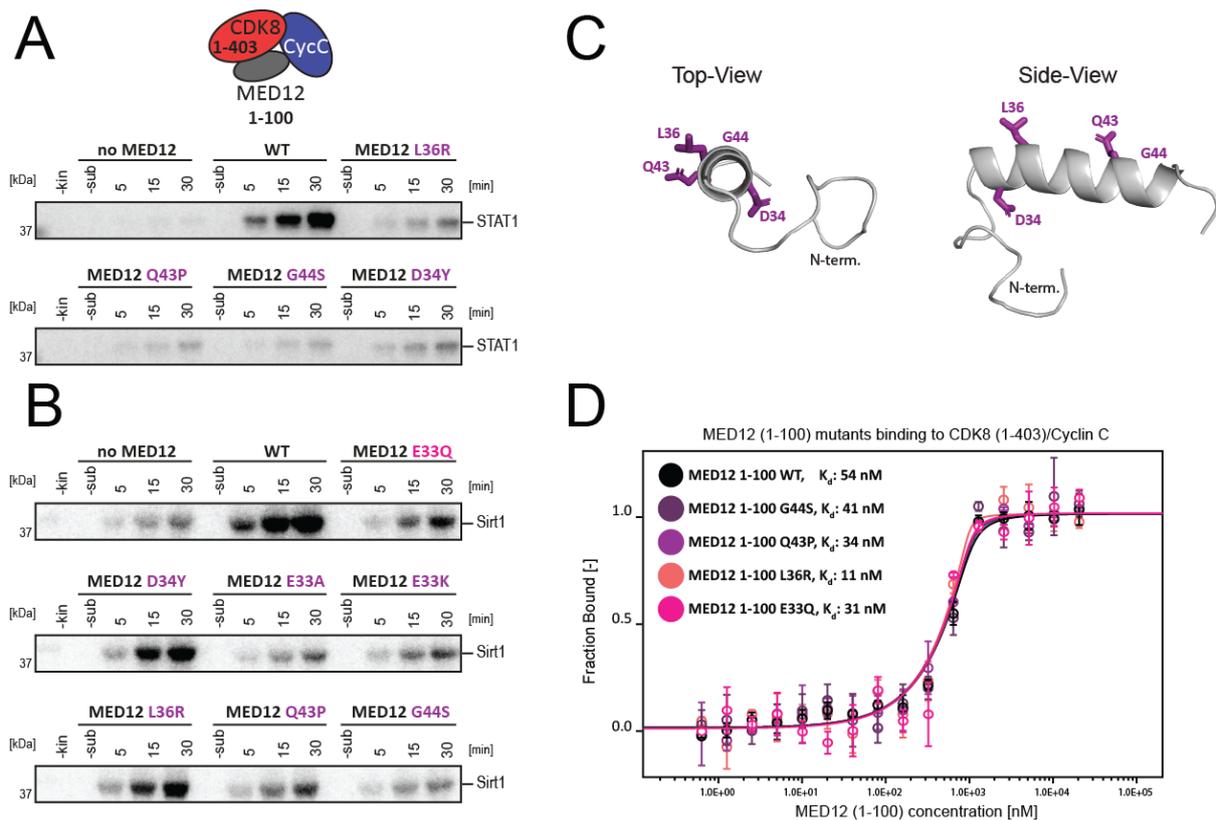
Figure 46: Cancer-associated MED12 mutations within its activation helix abolish CDK8 activation without altering MED12 affinity for CDK8/Cyclin C.

(**A**) *In vitro* kinase assays using ternary CDK8 (1-403)/CycC/MED12 (1-100) complexes harboring individual cancer-associated mutations within MED12. Assays carried out as described as in Fig. 21A. (**B**) Same as in (A), yet two additional cancer-associated mutations within MED12 (E33A and E33K) and the E33Q mutation were assayed using Sirt-1 as a substrate. 10 pmol kinase complex was incubated with 50 pmol purified Sirtuin-1 as a substrate. (**C**) 3-dimensional model of the MED12 activation helix comprising MED12 residues 19-50. The model was calculated using PEP-FOLD3 (Lamiable et al., 2016). MED12 residues frequently mutated in cancer are shown as violet sticks (D34Y, L36R, Q43P and G44S). (**D**) Microscale thermophoresis (MST) binding experiments using MED12 (1-100) variants carrying different cancer-associated mutations and binary CDK8/Cyclin C complexes. MED12 (1-100) E33Q serves as activation-dead control (see Fig. 24A). K_d values are indicated. Error bars reflect the standard deviation of four replicates. Please note that the K_d cannot be read off directly due to the experimental necessity to use high protein concentrations. Please note that kinase assays on (A) were carried out by Robin Weinmann. Kinase assays on (B) were set out by Bastian Jahreis, I purified and provided all kinases. (A, C, and D) were adopted from Klatt et al., 2020.

2.3.12 MED12 likely favors the CDK8 DMG-in conformation

Due to its prominent oncogenic role considerable efforts were made to develop CDK8-specific inhibitors (Bergeron et al., 2016; Dale et al., 2015; Mäkinen et al., 2011; Pelish et al., 2015). As I discovered that MED12 employs an activation helix to stimulate CDK8 activity, I asked whether the presence of MED12 alters the efficacy of commercially available inhibitors, all of which were developed against the <u>binary</u> CDK8/Cyclin C complex (Bergeron et al., 2016). I hypothesized that this might be the case because crosslinking coupled to mass spectrometry and

preliminary structure determination by X-ray crystallography suggested MED12 contacts the αC-helix of CDK8 (see chapter 6.2 and 6.3, Fig. 65C and 67, respectively). Moreover, MED12 likely positions the CDK8 T-loop in a catalytically competent conformation by contacting one or several members of its arginine triad (Fig. 39). In further support of a differential efficacy of commercial inhibitors against MED12-bound CDK8 complexes, I noticed that type II inhibitors, such as sorafenib, were previously reported not to translate their inhibitory efficacy into the cellular context (Dale et al., 2015; Klatt et al., 2020).

To test my hypothesis, we utilized two known type I inhibitors (CCT251545 (PDB code 5BNJ) and Compound A (PDB code 6T41) as well as two known type II inhibitors (Sorafenib (PDB code 3RGF) and BIRB976 (Pargellis et al., 2002) in our *in vitro* kinase assay and determined their IC_{50} values against the binary CDK8 (1-403)/Cyclin C and the ternary CDK8 (1-403)/CycC/MED12 (1-100) complex (Klatt et al., 2020). As expected, we found significantly higher IC_{50} concentrations for both type I and type II inhibitors towards MED12 bound ternary complexes as compared to binary ones. In more detail, we measured for the type II inhibitor Sorafenib an IC_{50} of 695 nM towards the binary complex compared to an IC_{50} of 2.8 μM towards MED12-bound ternary complexes, whereas the IC_{50} concentrations for the type I inhibitor CCT251545 were 155 nM and 85 nM, respectively. The same trend held true when assaying BIRB976 (type II) and Compound A (type I) (Fig. 47). These results indicate, that type II kinase inhibitors, which bind to the CDK8 hinge region and extend to the so-called deep pocket (Schneider et al., 2011), are hindered from binding to CDK8 when MED12 is part of the complex. The deep pocket is only accessible when CDK8 is in its inactive state (DMG-out conformation for CDK8), suggesting that MED12 binding to CDK8 induces a DMG-in-like conformation that renders type I kinase inhibitors more potent once CDK8 is part of the entire Mediator kinase module (Klatt et al., 2020).
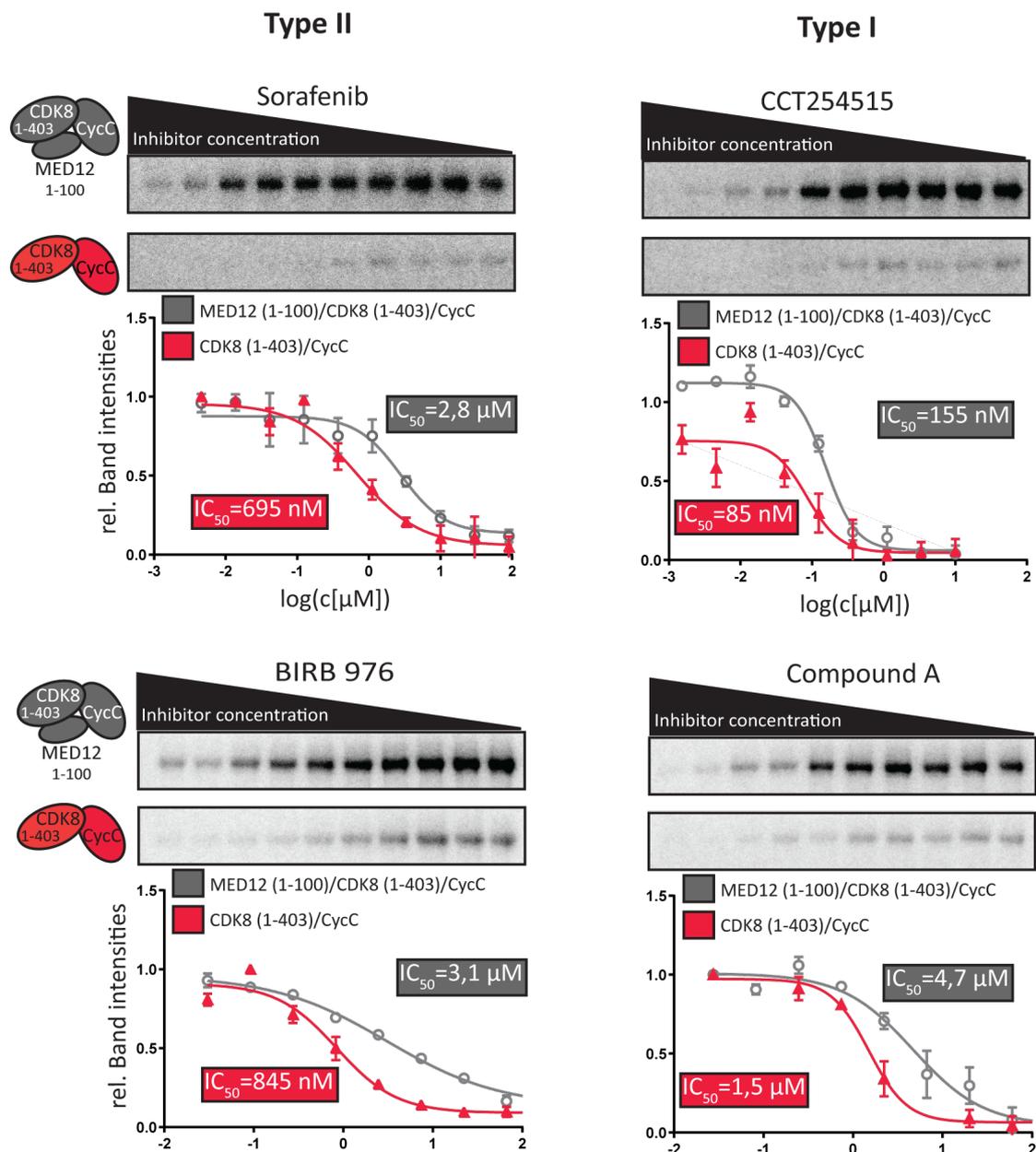
Figure 47: Type II kinase inhibitors loose part of their efficiency against MED12 bound CDK8/Cyclin C complexes
In vitro kinase assays with binary CDK8 (1-403)/Cyclin C and ternary CDK8 (1-403)/CycC/MED12 (1-100) complexes in presence of different concentrations of either a type II or a type I inhibitor using Sirtuin-1 as substrate. Reactions were pre-incubated with 3-fold dilution series of aforementioned inhibitors, started by addition of ATP and stopped after 30 min. Note here that 7.5 pmol ternary complexes were assayed, yet 15 pmol binary complexes to obtain significant band intensities. Please note that kinase assays were carried out by Franziska Langhammer.

To validate this conclusion, we used MST to measure the affinity of a MED12 (1-100) for binary CDK8 (1-403)/Cyclin C complexes in presence of saturating levels of a type I (CCT251545) or a type-II inhibitor (sorafenib) (Fig. 48). The affinity of MED12 (1-100) for CDK8 (1-403)/Cyclin C pre-bound to CCT251545 was about 21 nM, just like for the apo CDK8 (1-403)/Cyclin C control. In contrast, a binary complex pre-bound to the type II inhibitor sorafenib showed a fivefold reduced affinity for MED12 with a K_d of about 130 nM (Fig. 48A)

(Klatt et al., 2020). In further support of these results we used ITC to, once again, find a fivefold reduction in the affinity of MED12 (1-100) for CDK8 (1-403)/Cyclin C pre-bound to sorafenib as compared to pre-binding of CCT25155, which only showed a minor reduction of MED12 affinity for the binary CDK8 complex (Fig. 48B). We note here that a fivefold reduction in MED12 affinity for the binary CDK8 complex is highly significant, as we do not expect the inhibitors to interfere with MED12 interaction sites II+III (see chapter 6.2, Figs. 65A and C). Hence, we expected type II inhibitor pre-binding to only reduce MED12 affinity for CDK8 (1-403)/Cyclin C, which is precisely what we observed (Fig. 48) (Klatt et al., 2020).
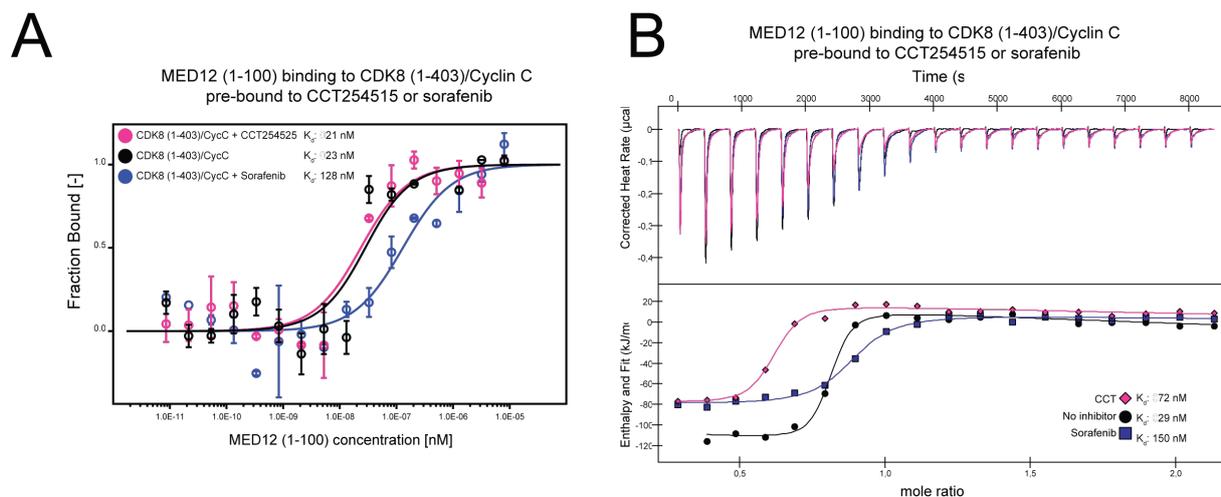
Figure 48: MED12 binding to CDK8/Cyclin C is hampered in presence of the type II kinase inhibitor sorafenib
(**A**) MST binding experiments using MED12 (1-100) and 2 nM binary CDK8 (1-403)/Cyclin C complexes that were either preloaded with 30 μM of the type I inhibitor CCT251545 or with 30 μM of the type II inhibitor sorafenib. Apo CDK8 (1-403)/Cyclin C was used as control. K_d values are indicated. Error bars reflect the SD of two replicates. Please note that MST measurements were carried out by Dr. Elisabeth Schneider from Proteros biostructures GmbH. I provided the proteins. (**B**) Using ITC, the MST measurements from (A) were confirmed. K_d values are indicated. (Upper) The corrected heat rates; (Lower) The calculated enthalpies per infection are plotted against the molar ratio of ligand and target. Please note that CCT251545 addition resulted in some protein precipitate, which altered the observed molar ratio. Adopted from Klatt et al., 2020.

Taken together, these data uncovered that type II kinase inhibitors show drastically reduced inhibitory potential towards ternary MED12-bound CDK8 complexes. Contrary, we did not observe this loss of efficacy for type I inhibitors, which prompts us to speculate that binding of MED12 induces a DMG-in conformation in the active site of CDK8. Thereby access to the deep pocket is blocked, precluding type II inhibitors from binding to CDK8 (Klatt et al., 2020).

2.3.13 CDK8 phosphorylation acts in an inhibitory manner

We established that CDK8 serves as a second substrate in our kinase assays (Fig. 33A and B), and took advantage of this finding when we utilized the ADP-Glo™ technology (Klatt et al., 2020; Schneider et al., 2011). These results motivated us to identify the exact CDK8 phosphosites in order to study their potential role in kinase regulation. CDK8 phosphorylation is reported to activate the kinase (Knuesel et al., 2009b). First, we sought to recapitulate these findings by incubating CDK8 in presence of ATP, prior to the addition of any *bona fide* substrate (Fig. 49). We expected to measure CDK8 phosphorylation and thereby higher kinase activities for the pre-phosphorylated CDK8 variant when compared to non-pre-phosphorylated CDK8. To validate this suggestion, we employed our binary CDK8/Cyclin C complexes in our kinase assay system in a direct comparison to ternary CDK8/CycC/MED12 (1-100) complexes using the aforementioned strategy (Fig. 49).
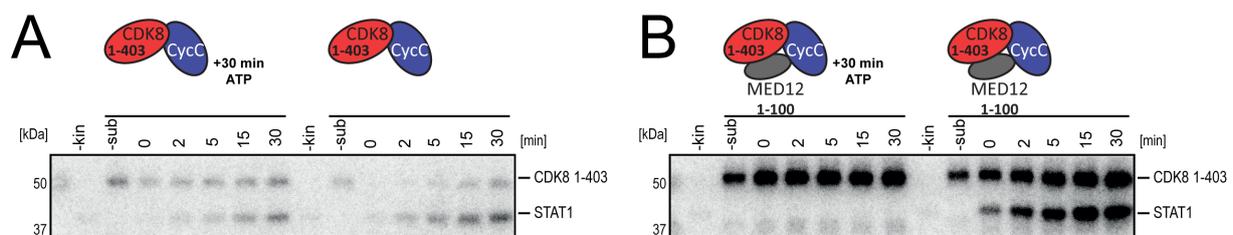
Figure 49: CDK8 phosphorylation acts inhibitory.
(**A**) *In vitro* kinase assays using binary CDK8 (1-403)/Cyclin C complexes. Kinases were pre-incubated for 30 min together with ATP prior STAT1 addition. Kinase assays were carried out as described in Fig. 33. (**B**) Same as in (A), just with ternary CDK8 (1-403)/CycC/MED12 (1-100) complexes. Please note that kinase assays were carried out by Robin Weinmann.

As proposed, the pre-incubation of CDK8 with ATP in absence of a *bona fide* substrate resulted in high CDK8 phosphorylation levels, which were especially pronounced in MED12-containing CDK8 complexes (Fig. 49). Interestingly, yet in contrast to published data (Knuesel et al., 2009b), the pre-phosphorylated CDK8 variant showed reduced substrate (STAT1) phosphorylation (Fig. 49A). Furthermore, and much to our surprise, the pre-phosphorylated MED12-stimulated CDK8 kinase lost its catalytic activity to phosphorylate STAT1 (Fig. 49B). These data reveal, at least in our assay system, that CDK8 phosphorylation has a negative impact on kinase activity, which is especially profound for MED12-stimulated CDK8 complexes.

2.3.14 CDK8 and CDK19 contain multiple phosphorylation sites

We established CDK8 phosphorylation to inhibit CDK8 kinase activity (Fig. 49) and inhibitory phosphorylation events are commonly found in CDKs (Atherton-Fessler et al., 1993; Hunter, 1995; Morgan, 1995). Despite the fact that MED12 functionally replaces CDK8/19 T-loop phosphorylation, CDK8 was reported to possess two T-loop distant phosphorylation sites on its C-terminal domain (T410 and S413) (Oppermann et al., 2009). However, whether these residues are phosphorylated by CDK8 itself or by a distinct kinase remains unknown. Moreover, we found CDK8 phosphorylation to be present in CDK8 (1-403), which indicates that CDK8 harbors (an) additional uncharacterized phosphorylation site(s). Alternatively, as we observed Cyclin C to be phosphorylated by CDK8 when it possesses a C-terminal Strep-tag (data not shown), we were aware of the possibility that the measured CDK8 phosphorylation signal might be an artifact which is caused by shortening of the CDK8 C-terminal domain up to residue 403. First, to validate that full-length CDK8 possesses additional unknown phosphorylation sites, we created CDK8 double mutants that lack the already known phosphorylation sites. In addition, to study a potential regulatory function, we also introduced aspartates as putative phosphomimetics (Chen and Cole, 2015; Hiscott et al., 1999) (Fig. 50). Intriguingly, both double mutants showed CDK8 phosphorylation (Fig. 50). This clearly demonstrates that full-length CDK8 contains unknown phosphorylation sites despite the previously observed T410 and S413. Moreover, these data also indicate that novel CDK8 phosphorylation sites can be found in the C-terminally truncated CDK8 (1-403) variant.
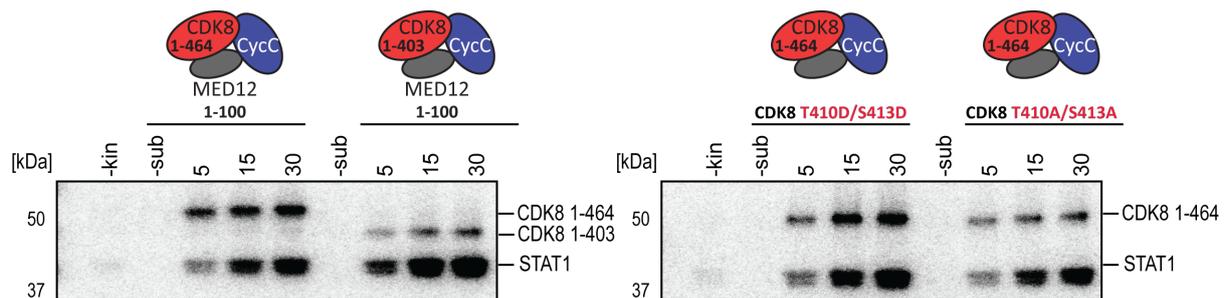
Figure 50: CDK8 possesses unknown phosphorylation sites

In vitro kinase assays using full-length CDK8/CycC/MED12 (1-100) ternary complexes that contain double-mutations on T410 and S413. Kinase assays were carried out with the STAT1 TAD as a substrate as described in Fig. 33. Please note that kinase assays were carried out by Bastian Jahreis.

The C-terminal domains of CDKs commonly participate in kinase phosphorylation (Smith et al., 1993). Out mutational profiling within the CDK8 C-terminal domain revealed that unknown phosphorylation sites exist in the shortened CDK8 (1-403) variant (Fig. 50). Next, I asked whether CDK8 phosphorylation only involves its unresolved C-terminal domain. Therefore, we

set out kinase assays using <u>both</u> of our C-terminally shortened CDK8 variants, CDK8 (1-403) and CDK8 (1-359) (Fig. 51).
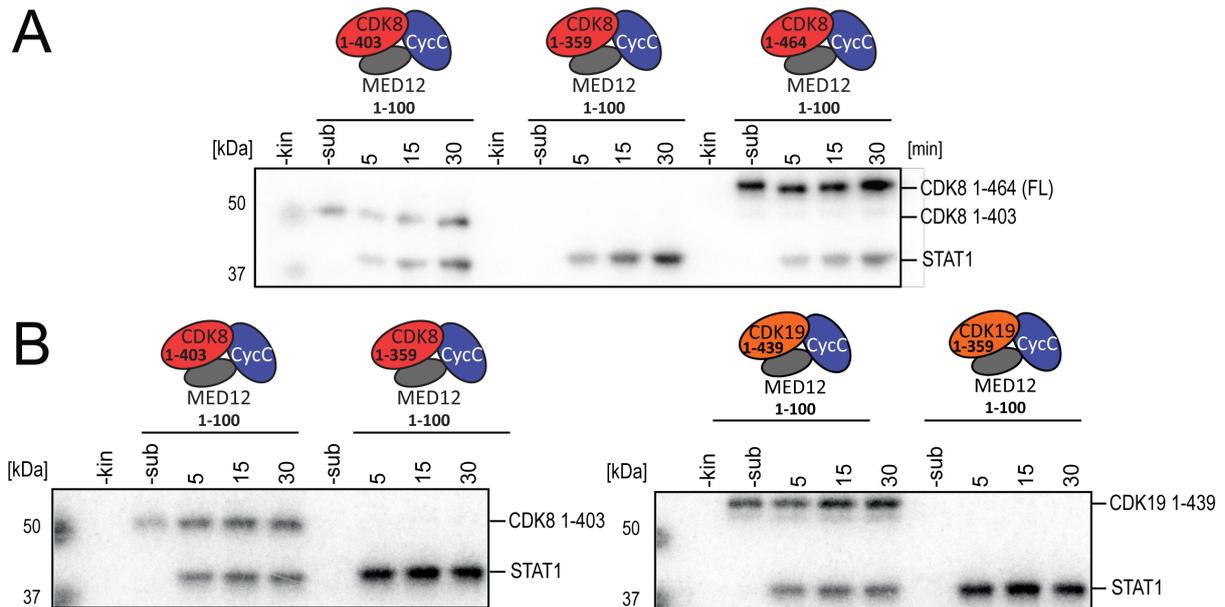
Figure 51: CDK8 and CDK19 harbor uncharacterized phosphorylation sites within the C-terminal domain
(**A**) *In vitro* kinase assays using wild-type full-length CDK8/CycC/MED12 (1-100) ternary complexes and both C-terminally shortened CDK8 (1-359) and CDK8 (1-403) variants. (**B**) Same as is (B) just with the two C-terminally shortened CDK8 variants including CDK19. Kinase assays were carried out as described in Figs. 33 and 34. Please note that kinase assays were carried out by Robin Weinmann.

Interestingly, we did not observe any CDK8 phosphorylation when we assayed the shortest CDK8 variant (1-359) (Fig 51A). This was also the case for CDK19 (1-359) (Fig. 51B). Moreover, both CDK8/19 (1-359) variants showed enhanced kinase activity (Figs. 51A and B), further supporting our hypothesis that CDK8/CDK19 phosphorylation acts inhibitory. The finding that the CDK8/CDK19 (1-359) variants lacks all phosphorylation signal strongly suggests that the CDK8/19 phosphorylation site(s) are located in the structurally unresolved C-terminal domain of CDK8/19 (residues 360-403/439, see chapter 1.1, Figs. 5 and 7). This flexible part of the kinase contains six potential phosphorylation sites (<u>T</u>EEEPDDKG DKKNQQQQQGNNH<u>T</u>NG<u>T</u>GHPGNQD<u>SS</u>H<u>T</u>QGPPLKK, potential phosphoresidues are underlined), all of which we mutated and tested their impact on CDK8 phosphorylation and kinase activity. Unfortunately, none of the phosphosite mutants showed altered CDK8 phosphorylation or kinase activity (Fig. 52). This suggests that CDK8 phosphorylation involves numerous phosphorylation sites.
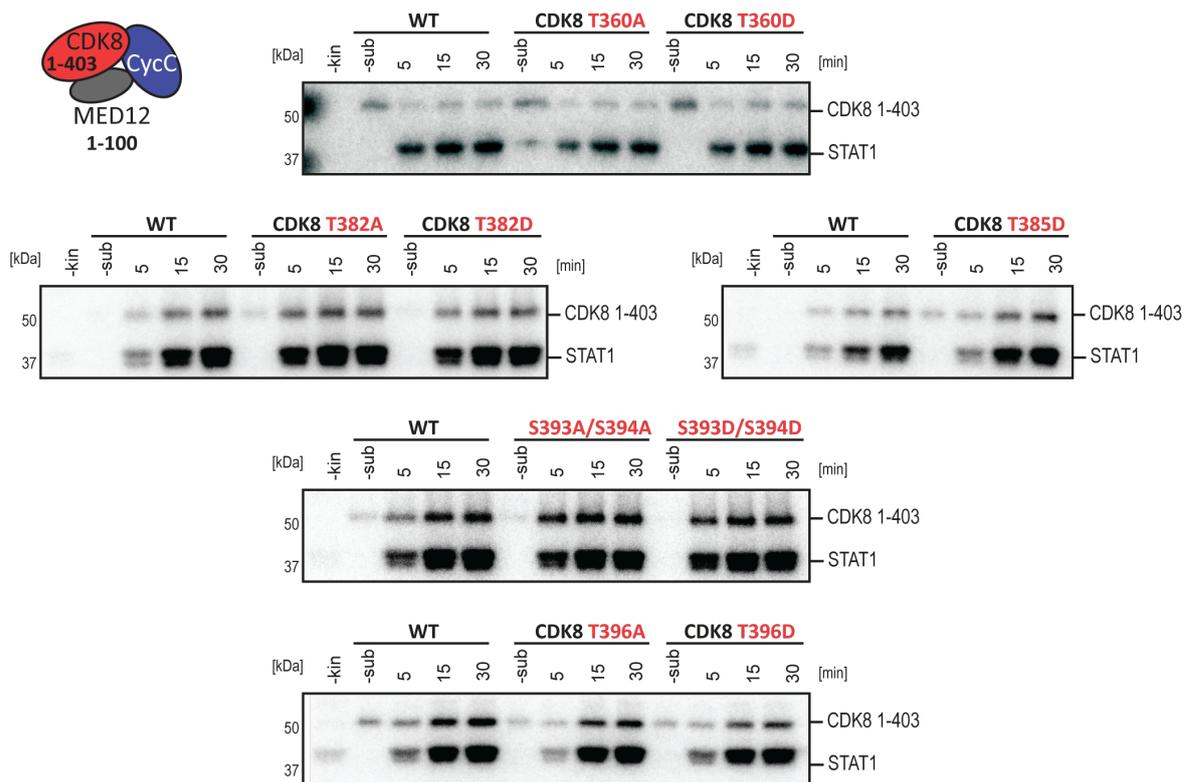
Figure 52: CDK8 (1-403) phosphorylation includes multiple phosphorylation sites.
In vitro kinase assay using ternary CDK8 (1-403)/CycC/MED12 (1-100) complexes. Each complex harbors mutations of serine and threonine residues in the C-terminal domain of CDK8, which spans from CDK8 residues 359-403. Kinase assays were carried out as described for Fig. 33. Please note that the kinase assay on top was carried out by Robin Weinmann, the other by Bastian Jahreis.

2.3.15 The C-terminal domain of CDK8 contacts its active site

We found that CDK8 phosphorylation has a negative effect on kinase activity (Fig. 49). The characteristic was especially pronounced in MED12-bound CDK8 complexes (Fig. 49). The systematic mutational profiling of putative CDK8 phosphorylation sites revealed unknown phosphorylation sites within the C-terminal domain of CDK8 (Figs. 50 and 51). As the CDK8 C-terminal part could not be solved by X-ray crystallography, yet might contribute to kinase regulation (Dixon-Clarke et al., 2015), I further analyzed the intra-subunit crosslinks obtained for CDK8-containing ternary complexes that involves residues of the C-terminal domain (Fig. 53). Intriguingly, all intra-subunit crosslinks that comprise residues of the unresolved C-terminal domain of CDK8 cluster between residues 361 and 370 (Fig. 53A). In more detail, I identified this segment to interact with three residues that are part of the CDK8 T-loop (K153, K170 and D173) and with three residues that are in direct vicinity to its ATP binding site (K26, K37 and E55) (Figs. 53A and B). Furthermore, this stretch significantly overlaps with the MED12 interaction site II (K115, K118, K119), a finding that further supports our hypothesis

that MED12 binds adjacent to the disordered C-terminus of CDK8 (see chapter 6.2, Figs. 65A and C) (Klatt et al., 2020). In summary, intra-subunit crosslinks demonstrate that the unresolved C-terminal domain contacts the CDK8 active site. There, it is able to contact the T-loop, the ATP binding site and it overlaps with the MED12 interaction site II on CDK8 (Fig. 53B) (Klatt et al., 2020)
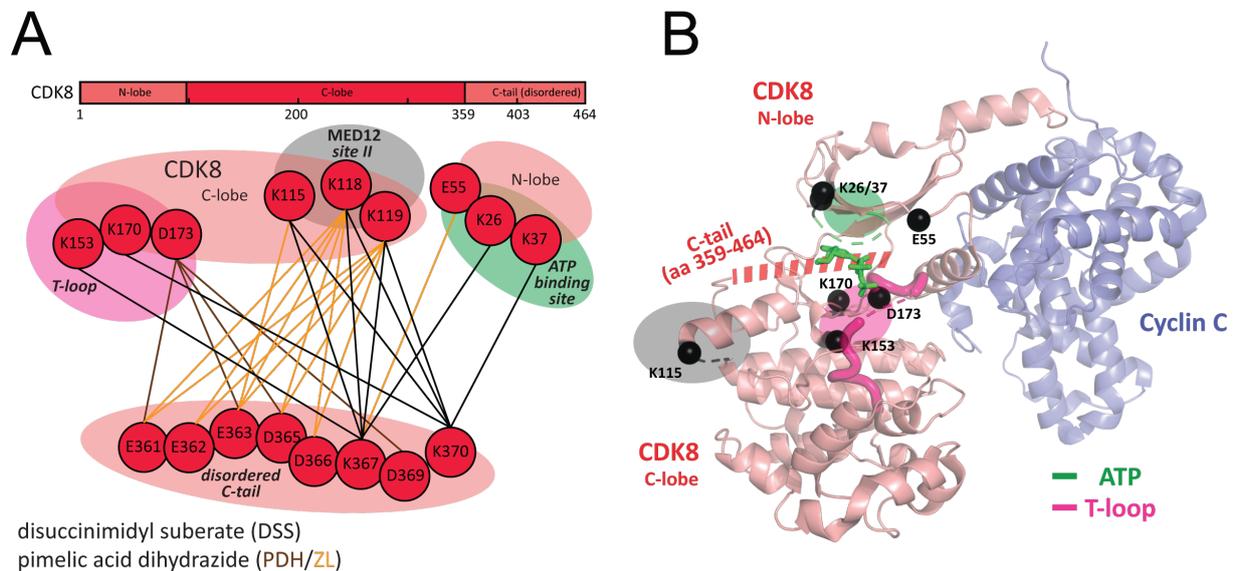
Figure 53: The unresolved C-terminus of CDK8 contacts its active site.
(**A**) The upper panel shows full-length CDK8 (1-464) with different protein domains highlighted. The lower panel shows a cartoon depiction of all intra-subunit crosslinks involving the unresolved C-terminus of CDK8. The intra-subunit crosslinks were grouped in three interaction sites (T-loop, MED12 interaction site II and ATP binding site) according to their localization on the surface of the binary CDK8/Cyclin C complex. (**B**) 3-dimensional arrangement of the three major sites of intra-subunit crosslinks between the C-terminal domain of CDK8 and CDK8 (1-403)/Cyclin C. Lysine and glutamate residues that were found crosslinked are represented as black spheres and plotted onto the structure of the CDK8 (1-403)/Cyclin C complex (PDB code 3RGF (Schneider et al., 2011). The ATP-molecule in the active site (colored in green) was superimposed from CDK9 (PDB code 3BLQ) (Baumli et al., 2008). Please note that only K115 is shown instead of the structurally unresolved, cross-linked residues K118 and K119. Please note that crosslinking experiments were carried out by Dr. Alexander Leitner. Raw data analysis and visualization was done by myself.

CDK1 and CDK2 are negatively regulated by phosphorylation within their ATP binding site (Nakanishi et al., 2000; Pomerening et al., 2003). Despite the fact that crosslinking data that result from binary and ternary CDK8 (1-403) and CDK8 (1-464) complexes showed unchanged crosslinking patterns (Klatt et al., 2020), we found the C-terminal domain of CDK8 to contact its ATP binding site and T-loop (Fig. 53). This suggests that CDK8 can only be phosphorylated in its full-length form with its disordered C-terminal domain present. To substantiate this conclusion and to exclude phosphorylation sites within the ATP binding site and the T-loop, we finally mutated T31 and F32 within the CDK8 ATP binding pocket and T196 within the CDK8 T-loop (Fig. 54). CDK8 T31 and F32 align with the aforementioned conserved CDK1

and CDK2 phosphorylation sites, whereas CDK8 T196 has been hypothesized to be phosphorylated based on its sequence conservation to CDK7 T170 (which represents the activating phosphoresidue within the T-loop of CDK7, see chapter 1.1, Fig. 2) (Lolli et al., 2004; Xu and Ji, 2011). The CDK8 T-loop mutations (T196D and T196A) showed drastically reduced enzymatic activity, yet CDK8 phosphorylation persisted. The reduced kinase activity is likely a result of the lost structural integrity of the T-loop introduced by such a mutation (Xu et al., 2014). However, the mutation in the CDK8 ATP binding pocket T31D, but not the T31A and Y32F, led to a loss of CDK8 phosphorylation and, concomitantly, to a loss in substrate kinase activity. The introduced aspartate therefore likely functions as a phosphomimic that excludes ATP binding, as has been observed for CDK1 and CDK2 (Nakanishi et al., 2000; Pomerening et al., 2003). Altogether, none of the substituted putative phosphorylation sites led to a loss of CDK8 phosphorylation and all mutations negatively affected kinase activity. However, I established that the CDK8 T31D mutant is a catalytically incompetent kinase. Thus, I denoted CDK8 (1-403) carrying an T31D mutation the "kinase-dead" mutant.
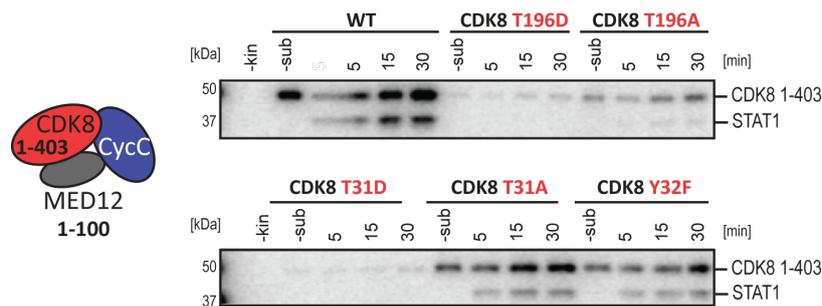
Figure 54: CDK8 ATP binding site and T-loop mutations abrogate substrate kinase activity
In vitro kinase assays using ternary CDK8 (1-403)/CycC/MED12 (1-100) complexes. Each complex harbor either a mutation in the ATP bind site or a mutation within the T-loop of CDK8. Kinase assays were carried out with STAT1 TAD as a substrate as described in Fig. 33.

2.3.16 CDK8 phosphorylation occurs in *cis*

We found that CDK8 phosphorylation has an inhibitory impact on kinase activity (Fig. 49). However, we did not know whether this phosphorylation event takes place in *cis* or in *trans*. Therefore, I replaced the *bona fide* substrate in our assay with the aforementioned CDK8 "kinase-dead" mutant T31D (Fig. 54). I expected to only measure CDK8 phosphorylation of the "kinase-dead" mutant in case wild-type CDK8 was able to phosphorylate the aforementioned mutant. This, in turn, would strongly suggest that CDK8 phosphorylation occurs in *trans*, meaning that one CDK8 molecule phosphorylates another one. In contrast, no phosphorylation signal would indicate that CDK8 phosphorylation takes place in *cis*, which is

known as autophosphorylation (Smith et al., 1993). As shown on Fig. 55, I did not observe any phosphorylation of the "kinase-dead" mutant upon incubation with wild-type CDK8. This leads me to conclude that CDK8 phosphorylation takes place in *cis*, meaning that CDK8 phosphorylates itself.
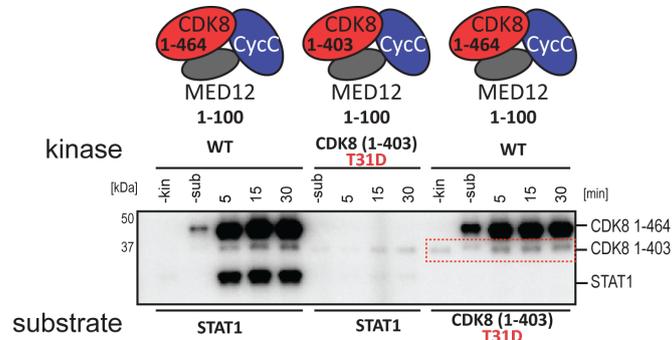
Figure 55: CDK8 phosphorylation occurs in *cis*

In vitro kinase assays using different CDK8-containing ternary complexes. The left shows kinase activity of natural full-length CDK8 towards STAT1 TAD, whereas the "kinase-dead" mutant (right next) shows no kinase activity. Both assays serve as controls. Kinase assays were carried out as described in Fig. 33. The right assay demonstrates, that the "kinase-dead" CDK8 (1-403) T31D mutant is not phosphorylated by full-length and wild type CDK8 (7.5 pmol), even when utilized in high substrate (50 pmol) concentrations.

2.3.17 CDK8 auto- and substrate-phosphorylation are coupled

Having shown that CDK8 phosphorylation is a *cis*-regulatory event, we lastly suspected that CDK8 autophosphorylation and substrate phosphorylation are mechanistically coupled (Smith et al., 1993). To investigate a potential interdependence between CDK8 autophosphorylation and substrate phosphorylation, we titrated the *bona fide* substrate STAT1 against wild type CDK8 (Fig. 56). Interestingly, we find the signal intensity of CDK8 phosphorylation to correlate with increasing STAT1 concentrations and phosphorylation levels. This demonstrates, that CDK8 auto- and substrate-phosphorylation are mechanistically coupled, at least in our *in vitro* assay system.
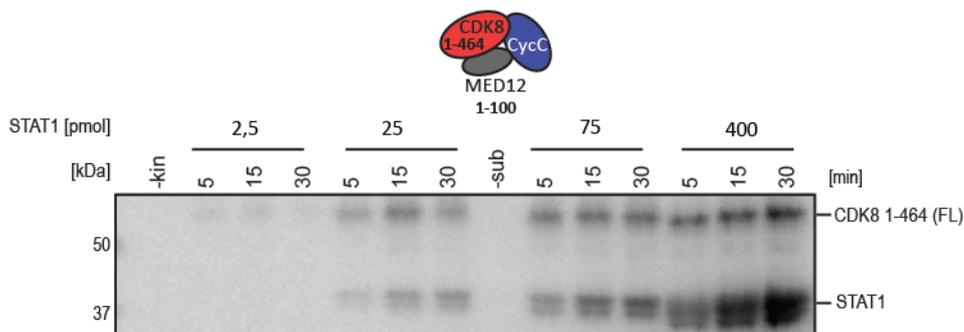
Figure 56: CDK8 and substrate phosphorylation are mechanistically coupled.

In vitro kinase assays using wild type CDK8/CycC/MED12 (1-100) ternary complexes. 2,5 pmol kinase was utilized against different STAT1 TAD substrate concentrations. Individual substrate concentrations within each assay is shown on top. The

four choosen kinase to substrate ratios are 1:1, 1:10, 1:30 and 1:160, respectively. Please note that kinase assays were carried out by Bastian Jahreis.

2.3.18 Does Cyclin H phosphorylation by CDK8 regulate CDK7 kinase activity?

Cyclin H possesses two phosphorylation sites on its N- and C-terminal helices (Ser-5 and Ser-304) (Akoulitchev et al., 2000). To test whether CDK8-mediated Cyclin H phosphorylation negatively impacts CDK7 kinase activity, I first established a kinase assay for our purified binary CDK7/Cyclin H complex with DSIF and Pol II as known substrates (Glover-Cutter et al., 2009) (Fig. 57). As demonstrated on Fig 57A, the purified binary CDK7/Cyclin H complex is active and phosphorylates both Spt5 and Pol II. Moreover, as it was the case for CDK8/19, in addition to substrate phosphorylation (here DSIF or Pol II), I observed CDK7 autophosphorylation (Garrett et al., 2001). Having established a functional assay to measure CDK7 kinase activity, we finally utilized purified Cyclin H as a substrate for CDK8. We expected Cyclin H to be phosphorylated by CDK8, as we had been able to validate several CDK8 targets, such as Sirtuin-1, BRCA1 and NELF-A (Klatt et al., 2020; Poss et al., 2016). To my disappointment, however, we did not observe any phosphorylation of Cyclin H (data not shown) and therefore decided to utilize our purified and active binary CDK7/Cyclin H complex as a substrate of CDK8. However, yet again, we did not detect Cyclin H phosphorylation by CDK8 (Fig. 57B). This strongly suggests that other subunits of the TFIIH complex - like MAT1 - are required for the CDK7/Cyclin H complex to serve as a *bona fide* CDK8 substrate (Akoulitchev et al., 2000; Greber et al., 2020). Altogether, the binary CDK7/Cyclin H complex is active and shows CDK7 autophosphorylation. However, Cyclin H, both as a single protein or bound to CDK7, is not subject to phosphorylation by CDK8 under the tested conditions.
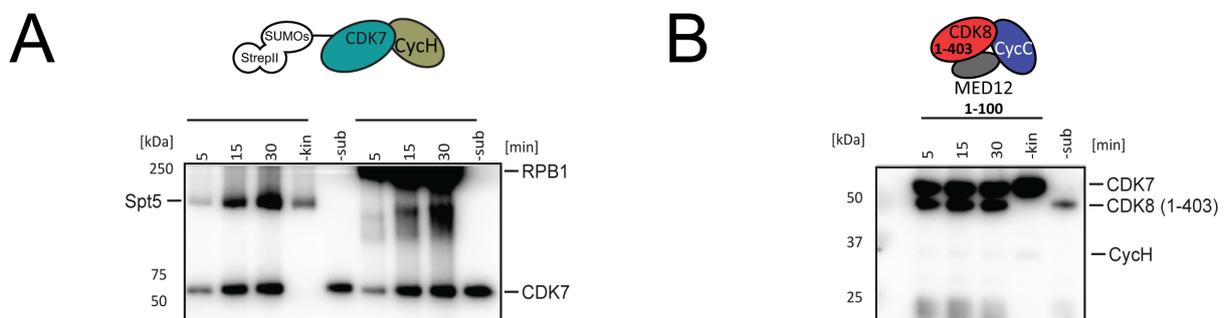
Figure 57: The binary CDK7/Cyclin H complex is highly active, yet Cyclin H does not get phosphorylated by CDK8
(**A**) *In vitro* kinase assays with N-terminally GST-tagged CDK7/Cyclin H binary complexes. 10 pmol kinase was utilized against 50 pmol DSIF or 10 pmol Pol II. Kinase assays carried out as decribed in Fig 33. (**B**) Same as in (A), just using 7.5 pmol ternary CDK8 (1-403)/CycC/MED12 (1-100) complexes as kinase and 50 pmol binary CDK7/Cyclin H complex as potential CDK8 substrate.

2.4   MED12 forms an active ternary complex with CDK3 and Cyclin C

The role of CDK3 is poorly understood. The reason therefore is likely due to its low expression levels and based on the fact that CDK3 is inactive in most strains of inbred mice (Malumbres and Barbacid, 2001; Ye, 2001). Hence, it is conceivable that CDK3 is dispensable for the cell cycle as its role can be compensated by CDK1 and CDK2 (Ye, 2001). In contrast, CDK3 from wild-type mice species express full-length CDK3. This is also the case in humans. CDK3 has originally been classified as a cell cycle-related CDK, because of its high sequence identity with CDK1/2 (see chapter 1.1, Fig. 1) and its ability to complement CDK2 mutations in yeast (Meyerson et al., 1992). Moreover, CDK3 is known to bind Cyclin C and is involved in G_0-G_1 and G_1-S cell cycle transitions by phosphorylating the retinoblastoma protein at Ser-807/811 (Hofmann and Livingston, 1996; Ren and Rollins, 2004). Interestingly, high p21 levels were reported to inhibit the aforementioned kinase activity (Harper et al., 1995). Furthermore, the activity of the transcription factors E2F and ATF1 are dependent on CDK3 (Zheng et al., 2008). Interestingly, viruses encode a Cyclin C homologue that competes with Cyclin C in binding to both CDK3 and CDK8 and thereby modulates the cell cycle (Brewster et al., 2011). Last and probably most importantly, aberrant CDK3 expression levels were observed in human cancer cells and linked to abnormal Wnt-signaling, indicating a functional role for CDK3 (Zheng et al., 2008). Despite these studies, our understanding of human CDK3 and its biological role is limited. To that end, I got interested into CDK3 and started to investigate this cell-cycle related CDK.

During my protein purifications, I observed that N-terminal MED12 forms distinct binary complexes with Cyclin C devoid of CDK8/19 (data not shown). This finding prompted me to examine a potential interaction between the N-terminal part of MED12 and the binary CDK3/Cyclin C complex. Indeed, our results demonstrate that a ternary complex comprising MED12 (1-100), CDK3 and Cyclin C can be co-expressed and purified close to homogeneity (Fig. 58A). Next, to validate CDK3 kinase activity and to examine whether the N-terminal part of MED12 stimulates CDK3 kinase activity as we confirmed for CDK8/19, we carried out kinase assays with Pol II as a substrate. Therefore, we co-expressed the binary CDK3/Cyclin C complex and measured its kinase activity against the ternary CDK3/CycC/MED12 (1-100) complex (Fig. 58B). I note here, that the binary CDK3/Cyclin C complex was only marginally co-expressed (data not shown), which hindered standard protein purification. Much to my surprise, the inclusion of MED12 (1-100) not only enhances CDK3/Cyclin C co-expression, furthermore, it also shows a profound stimulatory effect on CDK3 kinase activity. The MED12-

stimulated CDK3 phosphorylates the Pol II CTD in a comparable dynamic range as MED12-stimulated CDK8 and we did not detect any phosphorylation of CDK3 (Fig. 58B).
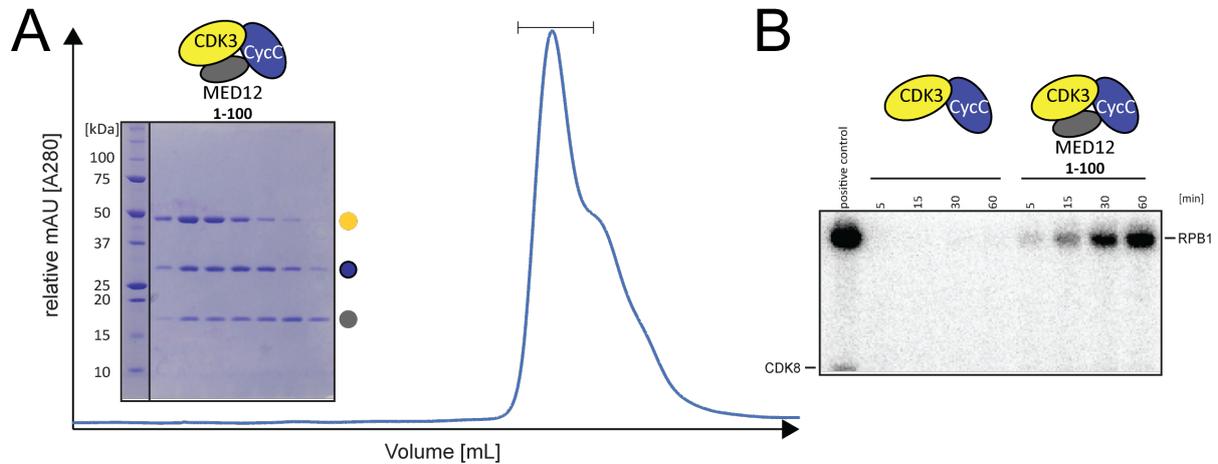
Figure 58: Purification of an active ternary CDK3/CycC/MED12 complex

(**A**) Size-exclusion chromatogram of a purified ternary CDK3/CycC/MED12 (1-100) complex using a Superdex 200 (GE Healthcare). The peak shoulder shows an excess of Cyclin C and MED12, which can be separated as demonstrated by SDS-PAGE. The protein complex is shown as a cartoon above the gel, individual proteins are indicated next to the gels. CDK3 is depicted in yellow, Cyclin C in blue and MED12 in grey. Cyclin C in encircled in black as it contains a C-terminal Strep-tag. Please note that protein purification was carried out by Amelie Lindner. (**B**) *In vitro* kinase assays with CDK3/Cyclin C binary and CDK3/CycC/MED12 (1-100) ternary complexes using Pol II as substrate. 5 pmol kinase was utilized against 5 pmol Pol II. Kinase assays were carried by Amelie Lindner as described in Fig 33. MED12-stimulated CDK8 was used as control (left lane). Please note that the binary CDK3/Cyclin C complex was poorly expressed and therefore only affinity-purified.

Chapter 3: Discussion

3.1   A revised model of how MED12 activates CDK8

In summarizing our *in vitro* and *in vivo* data, we propose a new model of how MED12 activates CDK8 (Fig. 59) (Klatt et al., 2020). In a first step, CDK8 is bound by Cyclin C, which leads to a "pushed-in" conformation of the αC-helix of CDK8, generating the kinase active site (Schneider et al., 2011). At this step CDK8 inhibitors were shown to trap the kinase in both a DFG-in conformation (type I) as required for catalysis (PDB code 5BNJ) (Dale et al., 2015) or in a DFG-out conformation (type II) that impedes catalysis and engages the deep pocket of the kinase (Fig. 60) (PDB code 3RGF) (Schneider et al., 2011). Binding of ATP-competitive type
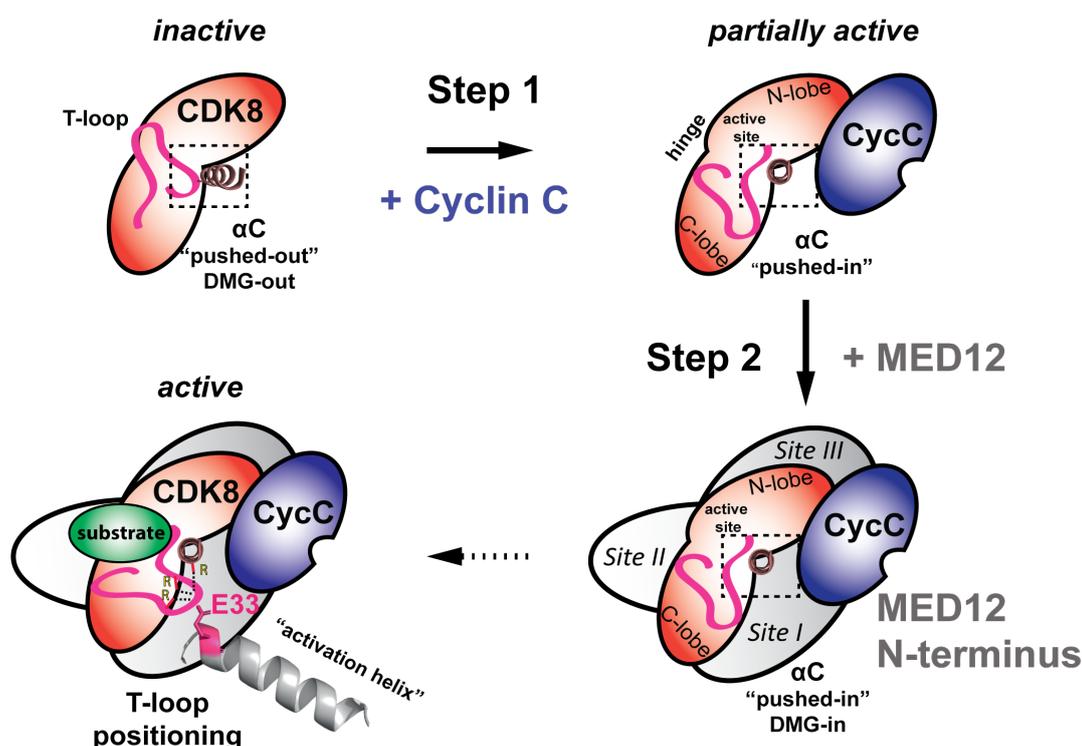
Figure 59: A revised model of how MED12 activates CDK8 and remodels the active site of CDK8.

(**A**) Step 1: Cyclin C binds to CDK8 and pushed the αC-helix of CDK8 into the "pushed-in" conformation. This binding event is crucial for the formation of the active site of CDK8 and results in basal kinase activity as demonstrated in Fig. 21. Step 2: MED12 binding to CDK8/Cyclin C stabilizes and activates the entire ternary complex. In particular, an activation helix in MED12 contacts and stabilizes the T-loop of CDK8, thereby activating the kinase. Likely, this contact is established through an interaction of an acidic residue at the N-terminal tip of the MED12 activation helix (E33) and the CDK8 arginine triad (R65, R150 and R178). Moreover, MED12 binding favors the active site of CDK8 to adopt a DMG-in conformation of the active site and disfavors type II kinase inhibitors from binding and inhibiting CDK8 in ternary CDK8/CycC/MED12 complexes. Please note that this model includes data that were not generated by myself. Adapted from Klatt et al., 2020.

I inhibitors is promiscuous due to the well conserved ATP binding site within the CDK family, increasing the potential for off-target side effects (Echalier et al., 2010; Force and Kolaja, 2011; Kufareva and Abagyan, 2008). CDK8 was found to be the only known CDK that provides access to its deep pocket, enabling selective type II inhibitor binding (Schneider et al., 2013).
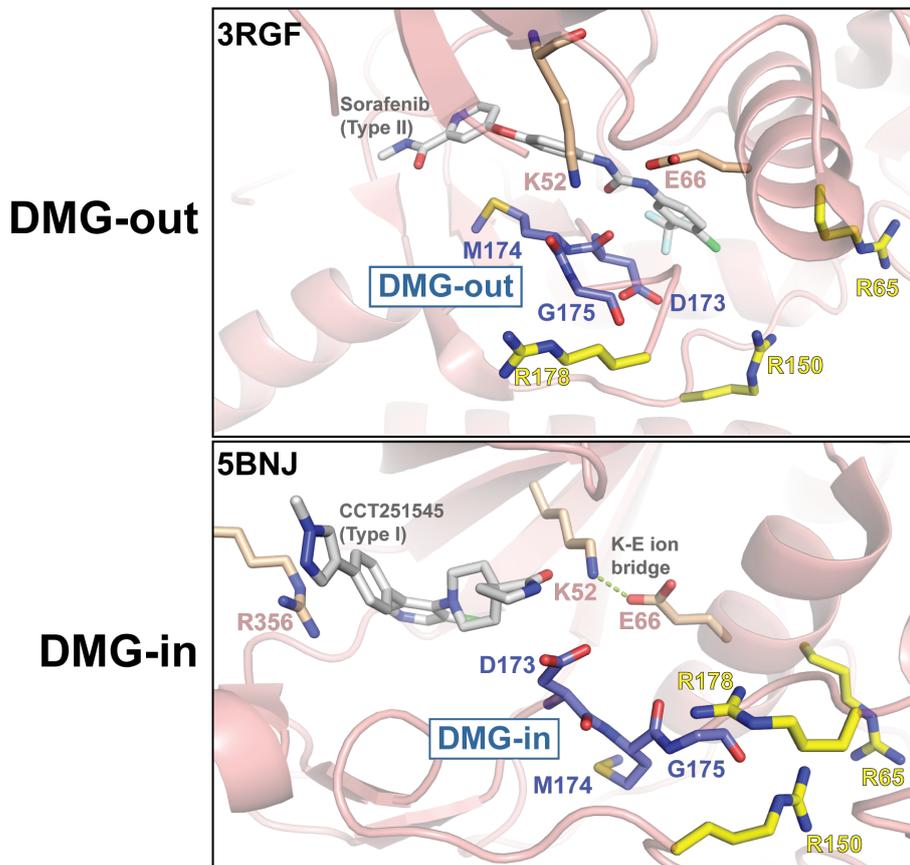
Figure 60: Views of the CDK8 active site in DMG-out and DMG-in conformation
Views of the CDK8 active site in DMG-out and DMG-in conformation (PDB codes 3RGF and 5BNJ, respectively). The CDK8 residues that are part of the arginine triad are shown as yellow sticks. The residues making up the DMG motif in CDK8 (D173-M174-G175) are shown in blue color. K52 and E66, two residues that are part of the catalytic triad of CDK8 (together with D173) and form a salt bridge once type I inhibitors bind to CDK8 in a DMG-in conformation, are shown in wheat color. The salt bridge is depicted as a dashed line- We note here that we found E66 to be crosslinked to MED12 K32 (Fig. 65A) and that we measured difference (fofc) density for the αC-helix by X-ray crystallography (Fig. 67). Adapted from Klatt et al., 2020.

We envision that the active site of the basal active CDK8/Cyclin C binary complex can exhibit both a DFG-in, as well as a DFG-out conformation. Next, the N-terminal segment of MED12 wraps around CDK8, thereby placing its "activation helix" right next to the T-loop of CDK8 (Klatt et al., 2020). Our mutational data indicate that the exact placement of this helix is crucial for activation of CDK8 by MED12. Binding alone is insufficient (Figs. 44 and 46). Moreover, our data indicate that the fact that MED12 wraps around CDK8 is important for its activity. A minimal fragment of MED12, for which we were able to isolate a stable, active ternary complex, comprised MED12 residues 23 to 69 (Fig. 61) (Klatt et al., 2020). This correlates well with

sites I and II (see chapter 6.2, Figs. 65A and C) and suggests that MED12 has to at least bind to these two sites for any stable association with CDK8. In more detail, our data suggest a direct contact between the arginine triad of CDK8 and E33 in MED12 (Figs. 39A and 44A). In support
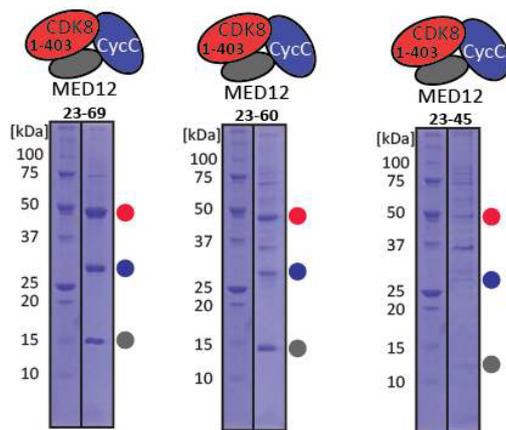
Figure 61: Purification of ternary CDK8 (1-403)/CycC/MED12 complexes comprising numerous MED12 truncations The minimal stable truncation is MED12 (23-69), comprising the MED12 interaction site I and II. Shortening or eliminating the MED12 interaction II leads to hindered complex expression and thereby formation. Please note that ternary complexes were only affinity-purified and therefore MED12 still carries the Strep-tag.

of this contact, we also detected a zero-length crosslink between K32 in MED12 and E66 in the αC-helix of CDK8 (see chapter 6.2, Figs. 65A and C). K32 is situated right next to E33, the residue critical for MED12 function, and E66 is close to R65, one of the three members of the CDK8 arginine triad. As E66 is pointing towards the interior of the CDK8 molecule in binary CDK8/Cyclin C complexes, a further rearrangement of the αC-helix upon MED12 binding to CDK8 is likely (Fig. 60). We note here that E66 is part of the CDK8 catalytic triad. In addition to our crosslinking data, we detected negative fofc difference density in proximity of the αC-helix in a preliminary structure solution of a ternary CDK8/CycC/MED12 complex (see chapter 6.3, Fig. 67), which further supports a MED12-dependent rearrangement of the CDK8 active site. Finally, we hypothesize that the contact between the arginine triad and the activation helix of MED12 leads to a stably "folded-away" conformation of the CDK8 T-loop, allowing unobstructed substrate binding to the active site (Klatt et al., 2020). We note here, that the CAK assembly factor MAT1 was recently shown to utilize an extended helix that positions the T-loop of CDK7 in a comparable stably "folded-away" and fully active conformation (Greber et al., 2020).

The low-resolution cryo-EM map of the entire kinase module from *Saccharomyces cerevisiae* (Tsai et al., 2013) was interpreted to show that MED12 contacts Cyclin C only (see chapter 1.3, Fig. 10A). In contrast, our structural, functional and mutational data indicate the essential role of the MED12 N-terminal segment and the CDK8 αC-helix for contact formation.

This apparent discrepancy may be due to the limited resolution (15 Å) of the cryo-electron microscopy map that cannot resolve the extended shape of the MED12 N-terminal segment and its detailed interactions with the kinase (Klatt et al., 2020).

3.2   Future CDK8 inhibitors need to be developed against MED12-bound CDK8 complexes

Whereas class I kinase inhibitors inhibit both binary CDK8/Cyclin C and ternary CDK8/CycC/MED12 complexes equally well, class II inhibitors lose a significant fraction of their inhibitory potential when utilized against the ternary CDK8/CycC/MED12 complex (Fig. 47). This finding highlights a common problem in drug development: Whereas atomic resolution structures are needed for rational structure-based drug design, most drug targets are part of larger complexes, whose structures are unknown. Our study suggests that future drug development aimed at CDK8-specific drugs needs to focus on ternary, MED12-containing complexes. This is the case as our data suggest that MED12 induces - or at least favors - a DFG-in conformation of the active site of CDK8 (Figs. 47 and 60), thereby essentially precluding efficient binding of class II inhibitors. The fact that we found CCT251545 to be equally effective against both binary and ternary complexes is likely due to its discovery in cell-based SILAC (stable isotope labeling by/with amino acids in cell culture) pulldown assays (Dale et al., 2015). There, CDK8 is predominantly present in complex with MED12, which enabled the discovery of CCT251545 as potent inhibitor of ternary CDK8 complexes. Lastly, novel drugs intended at reducing CDK8 activity may also be developed by using small molecules that disrupt the interface between the MED12 activation helix and CDK8 (Jin et al., 2014). Such approach would likely not impair the structural integrity of the Mediator kinase module and may only specifically target MED12's role in activating CDK8 (Klatt et al., 2020).

Furthermore, our data demonstrate that reducing CDK8 activity can have both positive and negative effects on target gene expression (Klatt et al., 2020). This is likely the result of the multitude of CDK8 targets and the differential functional outcome of target phosphorylation by CDK8 (Poss et al., 2016). For future drug development efforts it is therefore imperative to first decipher the exact role of CDK8 in the particular cancer under investigation and then to decide whether reducing CDK8 activity is the right route to take to impact the disease. This caution is warranted since MED12 was found to be involved in chemotherapy resistance without this finding having anything to do with its nuclear function as a CDK8 activator and part of the Mediator kinase module (Huang et al., 2012; Klatt et al., 2020)

3.3 MED12 stimulates the activity of CDK19 in analogous ways to CDK8

In focusing on our *in vitro* data, the N-terminal portion of MED12 binds CDK8/Cyclin C and CDK19/Cyclin C equally well (Fig. 31), leading in both cases to their activation (Figs. 33 and 34). However, arguing against our findings, CDK19 was recently reported to act in a kinase-independent manner (Steinparzer et al., 2019). However, based on our results, we suggest that CDK19 kinase activity is relevant as we found MED12 to bind and to activate the kinase in analogous ways to CDK8. Moreover, nanomolar affinities of MED12 (1-100) towards binary CDK8/ Cyclin C and CDK19/Cyclin C complexes reveal that the assembly of CDK8- or CDK19-containing kinase modules that lack MED13 is determined by the physical presence of individual mediator kinases and not dependent on different binding affinities between the mediator kinase paralogs (Fig. 31). Further, the structural and functional data for CDK19 indicate a similar binding and activation mode as shown for CDK8. In detail, the MED12 interaction site I (see chapter 6.2, Figs. 65A and C), which harbors the activation helix (Figs. 38 and 39), seems to bind in an analogous manner to CDK19 as we showed for CDK8 (see chapter 6.2, Figs. 65A and B). Additionally, the number of intra-subunit crosslinks is reduced in all MED12-containing ternary complexes compared to their respective binary complexes (Klatt et al., 2020) and we demonstrated that MED12 (1-100) significantly stabilizes CDK8/Cyclin C complexes (Fig. 32). As activation correlates with complex stabilization (Nolen et al., 2004), we expect an increase in thermal stability for CDK19/Cyclin C complexes upon MED12 binding. Moreover, a MED12 E33 mutation also eliminated the stimulatory function of MED12 to activate CDK19 (Fig. 40). Thus, we propose that the MED12 activation helix similarly contacts the arginine triad in CDK19 – just as we found to be the case for CDK8. In consequence, cancer-associated MED12 exon 2 mutations located on the activation helix would also impair CDK19 kinase activity. Based on the obtained *in vitro* data for CDK8/19 and their high sequence conservation (see chapter 1.1, Fig. 7), we further propose that binding of type II inhibitors to MED12-bound CDK19 complexes might be drastically reduced - as we showed for CDK8 (Fig. 47). Last and in conclusion, our generated HCT116 MED12 E33Q knock-in cell line (Klatt et al., 2020) not only lacks to activate CDK8, it further is unable to stimulate CDK19 kinase activity, resulting in diminished STAT1 phosphorylation levels (Fig. 43). However, despite the fact that CDK8 and CDK19 apparently harbor comparable activities and substrate preferences in our assay system (Fig. 36), CDK8- and CDK19-specific functions are likely to exist *in vivo*, which can explain the differential output upon individual Mediator kinase knockdown (Steinparzer et al., 2019; Tsutsui et al., 2011).

3.4   CDK8 autophosphorylation participates in a negative feedback loop

We demonstrated that CDK8 autophosphorylation acts inhibitory (Fig. 49) and uncovered uncharacterized phosphorylation sites within CDK8 (Figs. 50 and 51). As we found our C-terminally shortened CDK8/CDK19 (1-359) variants to lack CDK8 autophosphorylation (Fig. 51), we propose that CDK8 autophosphorylation involves the structurally unresolved C-terminal domain of the kinase. The elevated kinase activity for both CDK8/CDK19 (1-359) variants compared to CDK8 (1-403) and CDK19 (1-439) could be rationalized due to the missing second alternative substrate in the reaction together with the lacking inhibitory effect of CDK8 autophosphorylation (Fig. 51). Crosslinking data obtained for CDK8-containing ternary complexes showed that the C-terminal domain of CDK8 contacts the active site (Fig. 53). Following systematic profiling of potential phosphorylation sites we concluded that CDK8 neither carries phosphorylation sites within its ATP binding site, nor within its T-loop (Fig. 54). Instead, any additional regulatory phosphorylation sites in CDK8 are very likely located in its unresolved C-terminal domain.

However, as the individual knockout of all potential phosphorylation sites within the shortened CDK8 (1-403) C-terminal domain had no impact on CDK8 autophosphorylation (Fig. 52), we hypothesize that CDK8 autophosphorylation involves multiple phosphorylation sites (Johnson et al., 1996)·(Osusky et al., 1995). In support of this hypothesis, we find the signal intensities of CDK8 autophosphorylation to correlate with signal intensities obtained from *bona fide* kinase substrates (Figs. 33 and 34), all of which we utilized in six-fold higher concentrations. Even titrating the *bona fide* substrate up to one hundred-fold higher against CDK8 resulted in comparable CDK8 and STAT1 signal intensities (Fig. 56), further strengthening our idea that CDK8 autophosphorylation comprises numerous phosphorylation sites. This could also be the reason, why the individual knockout of the six potential CDK8 phosphorylation sites did not significantly alter CDK8 phosphorylation (Fig. 52). In summary, however, these data confirm, that CDK8 by itself serves as a substrate, which we measured in our ADP-Glo assays (Klatt et al., 2020).

We found CDK8 autophosphorylation significantly enhanced in MED12-stimulated CDK8/Cyclin C complexes, yet not in basal active CDK8/Cyclin C complexes (Fig. 49). Strikingly, the MED12 interaction site II, which we identified to be critical to activate the kinase (Klatt et al., 2020), overlaps with the localization of the unresolved C-terminus of CDK8 (please compare Figs. 53A and B with 65A and C). These findings allow me to speculate, that first, MED12 binding involves the CDK8 C-terminal domain, and second, MED12 binding to CDK8

positions the C-terminal domain of CDK8 in a conformation favored to autophosphorylation. In support of a contact between N-terminal MED12 and the CDK8/19 C-terminal domain, we observed slightly higher affinities of MED12 for both full-length CDK8/CDK19 variants when compared to their C-terminally shortened variants (Figs. 31A and C). Last, CDK8 autophosphorylation seems to be mechanistically coupled to substrate phosphorylation (Fig. 56).

In aggregating all evidence, I ascribe a functional role of CDK8 autophosphorylation only for MED12-stimulated CDK8 complexes. In detail, I envision that negatively charged phosphate groups on the flexible CDK8 C-terminal domain can impede with ATP binding thereby negatively regulating kinase activity as shown for the transcription-related CDK12/Cyclin K complex (Dixon-Clarke et al., 2015). Finally, I propose a model for CDK8 autophosphorylation that participates in a negative feedback loop (Fig. 62). In support of my model, the dephosphorylation of CDK8 exerted by the protein phosphatase 2 (PP2A) was shown to elevate CDK8 kinase activity (Rovnak et al., 2012).
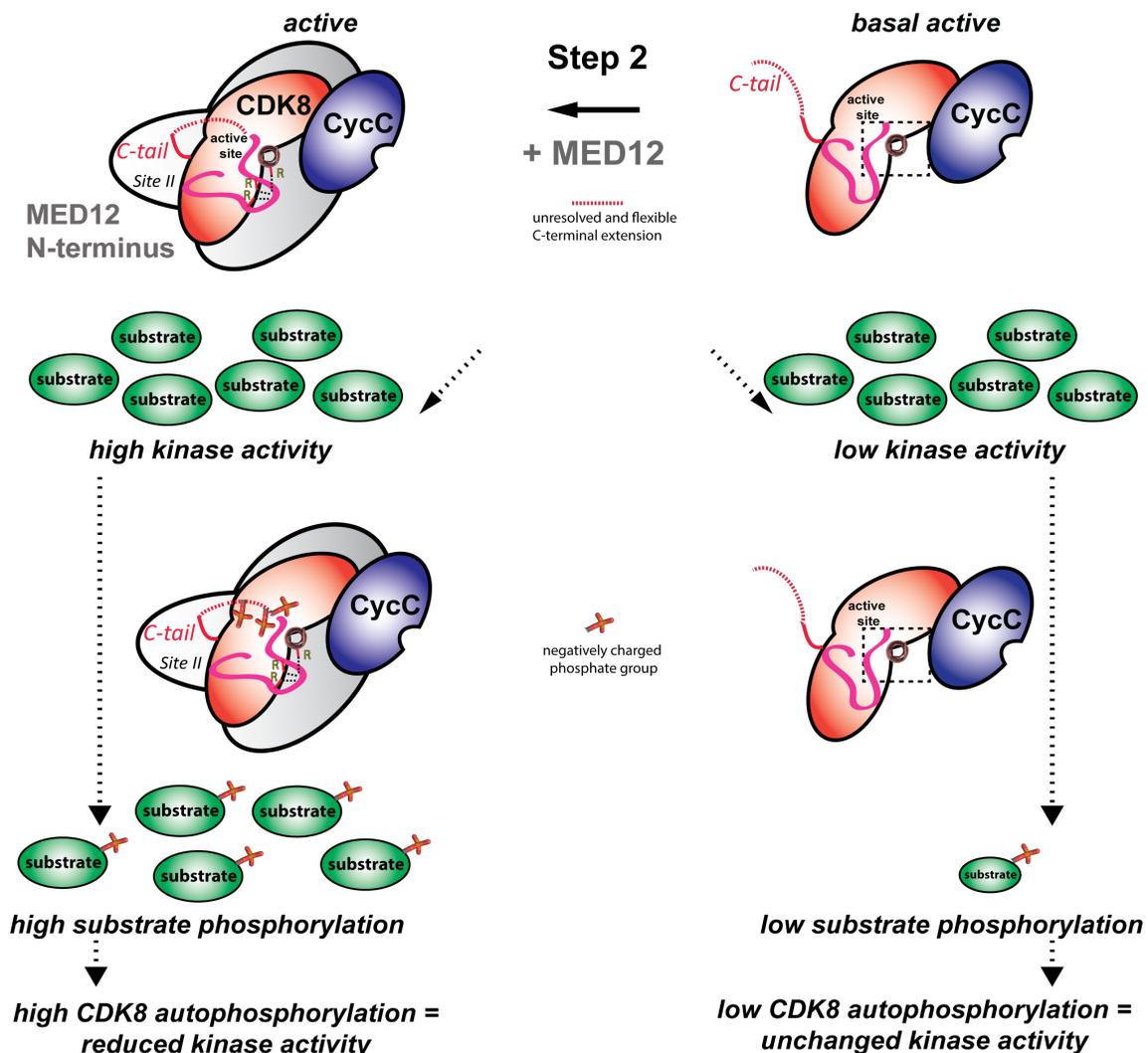
Figure 62: CDK8 autophosphorylation might contribute in a negative feed-back loop

CDK8 autophosphorylation is especially significant in MED12-stimulated CDK8 complexes (Fig. 49). Upon MED12 binding (Step: 2), the CDK8 C-terminus adopts a conformation that is favored to autophosphorylation. High *bona fide* substrate concentrations trigger CDK8 autophosphorylation (Fig. 56), thereby impeding with ATP binding. This finally decreases CDK8 kinase activity in a substrate- and MED12-dependent manner. Please note that this model includes data that were not generated by myself.

3.5   A novel and functional ternary CDK3/CycC/MED12 complex

First and foremost, an interaction between MED12 and CDK3 has never been reported. My discovery that MED12 (1-100) associates with Cyclin C is in line with our described overall architecture of our CDK8/CycC/MED12 ternary complexes, in which we found MED12 primarily to contact the CDK. In support of a direct contact between MED12 and Cyclin C, we detected highly significant intra-subunit crosslinks from MED12 K32 and D34 to Cyclin C E99 and E98 (please see 6.2, Fig. 61A and C), both of which we found not to be involved in the MED12-dependent CDK8 activation mechanism (Fig. 45).

Cyclin C binding pushes the αC-helix in the so called "pushed-in conformation" (see chapter 1.1, Fig. 3; and Fig. 59) and we established MED12 to contact the αC-helix of CDK8 (see chapter 6.2 and 6.3, Fig. 65 and 67, respectively). Therefore, we envision that MED12 binding to the CDK is dependent on a "pushed-in" conformation of the αC-helix. This leads me to speculate, that both Cyclin C and the binary Cyclin C/MED12 complex, yet not MED12 alone, can bind to the monomeric CDK (which comprises the αC-helix in the "pushed-out" conformation), resulting in a partially or fully active CDK. However, to gain more insights how MED12 binds to Cyclin C and to binary CDK3/Cyclin C, it will be exciting to measure the affinity of MED12 for Cyclin C and to compare obtained results to binary CDK3/Cyclin C complexes. I note here, that the cell cycle-related CDK3 binds also A- and E-type cyclins (Connell-Crowley et al., 1997). Whether MED12 would still bind to these resulting CDK3 binary complexes remains elusive. However, currently, neither the *in vivo* cyclin partner(s) of CDK3 nor the *in vivo* substrates of this kinase are known (Braun et al., 1998).

Intriguingly, MED12 has a profound effect on CDK3 kinase activity (Fig. 58B). I did not expect such a stimulatory function of MED12 for the CDK3/Cyclin C complex as the T-loop of CDK3 possesses the canonical activating T-loop phosphorylation site (see chapter 1.1, Fig. 6). However, CDK3 T-loop phosphorylation by CAK or another kinase has not been reported yet. Whether the MED12 activation helix, which we describe to be essential to activate CDK8/19, positions the T-loop of CDK3 in analogous ways as we found for CDK8/19 will

require more detailed biochemical data. Lastly, as the binary CDK3/Cyclin C complex is only poorly co-expressed, we propose that the N-terminal part of MED12 helps to fold the binary CDK3/Cyclin C complex, leading to its activation and therefore complex stabilization (Nolen et al., 2004). This matches our previous observations, in which we found the N-terminal portion of MED12 to enhance protein co-expression of all the CDK8/19-containing ternary complexes. Finally, based on these preliminary results, I propose that CDK3 might be able to assemble into a novel Mediator kinase module with the N-terminal segment of MED12 functioning as universal co-activator of all Cyclin C-associated kinases.

Chapter 4: Conclusions

CDK8, the catalytic core of the Mediator kinase module, is activated by MED12. A prior model proposed that MED12 binds to a surface groove on Cyclin C and thereby activates CDK8 (see chapter 1.4, Fig. 14). However, how MED12 binding to the distant surface on Cyclin C is coupled to CDK8 activation remained elusive and the model was therefore controversial. The presented data within this thesis advance our understanding of how CDK8 kinase activity is stimulated by MED12.

The main findings of this thesis, which are also based on data by other scientists, are summarized below (Klatt et al., 2020):

- MED12 binding to CDK8/Cyclin C stabilizes the complex and activates the kinase
- MED12 binding likely induces a DMG-in conformation in the active site of CDK8
- The N-terminal segment of MED12 wraps around CDK8 without contacting Cyclin C
- A newly identified MED12 activation helix functionally replaces CDK8 T-loop phosphorylation and likely contacts the arginine triad of CDK8
- A misplaced MED12 activation helix likely contributes to human oncogenesis

Based on obtained structural and functional data, we propose a new model for MED12-dependent CDK8 activation (Fig. 59). In addition, this study invigorates that future drug development should be aimed at ternary MED12-bound CDK8/Cyclin C complexes, as we find type II inhibitors to lose their efficiency when utilized against MED12-bound CDK8 complexes (Klatt et al., 2020).

Chapter 5: Materials and Methods

5.1 Material

5.1.1 Chemicals

1,4-Dithiothreitol (DTT)	Carl Roth GmbH + Co.KG, Karlsruhe
Agarose	GERBU Biotchnik GmbH, Heidelberg
Dimethyl sulfoxide (DMSO)	Carl Roth GmbH + Co.KG, Karlsruhe
Desthiobiotin	Sigma-Aldrich, St. Louis, MO, USA
Ethylendiaminetetraacetic acid (EDTA)	Carl Roth GmbH + Co.KG, Karlsruhe
Ethanol (EtOH), absolute	VWR International, Radnor, PA, USA
Fetal bovine serum (FBS)	PAA Laboraties, Pasching, Österreich
Isopropanol, absolute	VWR International, Radnor, PA, USA
Isopropyl-β-D-thiogalactoside (IPTG)	Carl Roth GmbH + Co.KG, Karlsruhe
Polyacrylamide 40% (PAA), 29:1	Carl Roth GmbH + Co.KG, Karlsruhe
Powdered milk, blotting grade	Carl Roth GmbH + Co.KG, Karlsruhe
Prestained Protein Ladder	Bio-Rad Laboratories, München
Sodium dodecyl sulfate (SDS)	Carl Roth GmbH + Co.KG, Karlsruhe
Tetramethylethylenediamine (TEMED)	Carl Roth GmbH + Co.KG, Karlsruhe
Tris(2-carboxyethyl)phosphine (TCEP)	Carl Roth GmbH + Co.KG, Karlsruhe
TRIzol (peqGOLD TriFast FL)	Peqlab Biotechnologie GmbH, Erlangen

Common chemicals not listed like antibiotics, protease inhibitors or buffering agents were obtained from Carl Roth GmbH + Co. KG.

5.1.2 Consumables

1 kb DNA ladder	New England Biolabs, Ipswich, MA, USA
ATP, [y-^{32}P]-3000 Ci/mmol	PerkinElmer, Waltham, MA, USA
Benzonase®Endonuclease	*Selfmade*
Centrifugal Filter Units Amicon® Ultra-4/15	Merck Millipore, Burlington, MA, USA
Cre-recombinase	New England Biolabs, Ipswich, MA, USA
ECL^{TM} detection reagent	GE Healthcare, Chicago, IL, USA
EZ Vision DNA loading dye	Amresco LLC, Solon, OH, USA
QIAquick Gel Extraction Kit	Qiagen GmbH, Hilden
QIAprep Spin Miniprep Kit	Qiagen GmbH, Hilden
Taq DNA polymerase	*Selfmade*
TEV Protease	*Selfmade*
Phusion DNA polymerase	New England Biolabs, Ipswich, MA, USA
Strep-Tactin® Superflow	IBA Lifesciences, Göttingen
XtremeGENE™ HP	Roche, Mannheim, DE

General and standard plastic consumables not listed were obtained from Greiner Bio-One, Sarstedt GmbH, or Brand GmbH.

5.1.3 Technical Instruments

-80°C freezer	Thermo Fischer Scientific, Waltham, MA, USA
ÄKTA™ pure	GE Healthcare, Chicago, IL, USA
New Brunswick™ Innova 42 (throw 25 mm)	Eppendorf Deutschland, Wesseling-Berzdorf
Electrophoresis equipment (proteins)	Bio-Rad Laboratories, München
Electrophoresis equipment (DNA)	Peqlab Biotechnologie GmbH, Erlangen
Eppendorf Centrifuge 5417R	Eppendorf Deutschland, Wesseling-Berzdorf
Eppendorf Thermomixer C	Eppendorf Deutschland, Wesseling-Berzdorf
Eppendorf Biospectrometer basic	Eppendorf Deutschland, Wesseling-Berzdorf
Insect cell shaker, Multitron Pro (throw 50 mm)	Infors HT, Bottmingen, CH
Monolith NT.LabelFree	TA Instruments, New Castle, DE, USA
Nano ITC Low Volume	TA Instruments, New Castle, DE, USA
Sonifier	Branson Ultrasonics, Danbury, CT, USA
Sterile Bench, HERAsafe® KS18 1/PE AC	Thermo Fischer Scientific, Waltham, MA, USA
Thermocycler peqSTAR	Peqlab Biotechnologie GmbH, Erlangen
Ultracentrifuge Optima XPN and Ti-45 Rotor	Beckman Coulter, Brea, CA, USA

5.1.4 Software

AIDA Image Analysis software	Elysia-Raytest GmbH, Straubenhardt
Adobe Illustrator CS6	San Jose, CA, USA
CLC workbench	QIAGEN, Hilden
CR-Reader	Elysia-Raytest GmbH, Straubenhardt
Image J	NIH, Bethesda, MD, USA
ITC run	TA Instruments, New Castle, DE, USA
Microsoft Office 2011	Microsoft Corporation, Redmond, WA, USA
PMi-Byonic™	Protein Metrics, Cupertino, CA, USA
PyMOL 2.0.6	Schrodinger LLC, New York, NY, USA
VMD	University of Illinois, IL, USA
NanoAnalyze 3.7.5	TA Instruments, New Castle, DE, USA

5.1.5 Buffers and Solutions

50x TAE	50 mM	EDTA
	2 M	Tris
	1 M	Acetic acid
6x SDS-dye	300 mM	Tris (pH 6.8)
	600 mM	DTT
	60%	Glycerol
	12%	SDS
	0.6%	Bromophenol Blue
Lysis-buffer A	150 mM	NaCl
	50 mM	Hepes (pH 7.4)
	2 mM	DTT
High-salt-buffer A	2 M	NaCl
	50 mM	Hepes (pH 7.4)
	2 mM	DTT
Low-salt buffer A	50 mM	Hepes (pH 7.4)
	2 mM	DTT
Low-salt buffer B	50 mM	Tris (pH 8.0)
	2 mM	DTT
Gelfiltration-buffer A	100 mM	NaCl
	50 mM	Hepes (pH 7.4)
	2/1 mM	DTT/TCEP
5x SDS-PAGE running buffer	250 mM	Tris
	250 mM	MOPS
	5 mM	Na_2EDTA
	0.5%	SDS
Coomassie	40%	MeOH
	10%	Acetic acid
	0.1%	Comassie Brilliant Blue R250
Destaining solution	12%	MeOH
	9%	Acetic acid
5x Western-transfer buffer	120 mM	Tris
(1x contained 20% MeOH)	960 mM	Glycine
	0.15%	SDS
10x TBS	250 mM	Tris
(1x contained 0.1% Tween-20)	1.4 M	NaCl
	20 mM	KCl
Blocking buffer	5%	Milkpowder
	or 3%	BSA in 1x TBS-T
LB-media	1%	Tryptone
(LB-agar contained 1.5% Bacto Agar)	1%	NaCl
	0.5%	Yeast extract

5.1.7   Oligos

All Oligos used for Gibson cloning were designed following certain criteria. The hybridization temperature of all oligos was calculated *in silico* (Kibbe, 2007). A hybridization temperature of 60-63°C for standard PCRs and 57-60°C for colony PCRs was chosen. Oligos for colony PCRs were additionally used for Sanger sequencing. The complementary overhangs for sequence and ligation independent cloning had a variable length between 22 and 28 nts and were always located on the gene-specific insert. Oligos with overhangs were designed to be in total shorter than 50 nt when possible. Oligos used to modify plasmids had a maximal length of 100 nt. Oligos for nested PCRs hybridize for about 80 - 120 nts and encompass the coding sequence within the 5' and 3' UTRs of individual mRNA sequences. Oligos used in this study are listed in Appendix A.

5.1.8   Peptides

Synthesized MED12 peptides covering residues 29-44 and 29-40, which were used for CD spectroscopy, were a gift of the Unverzagt lab. Peptides were received as lyophilized powder.

5.1.8   Cells

Abbreviation	Species	Usage	Reference
BW23474	*Escherichia coli*	MultiBac™; Cloning of donor-plasmids	Geneva Biotech
DH5a	*Escherichia coli*	Cloning	Prof. Dr. Stemmann (University of Bayreuth)
Top10	*Escherichia coli*	Cloning	Prof. Dr. Stemmann (University of Bayreuth)
BL21 (DE3) CodonPlus	*Escherichia coli*	Protein expression	Stratagene
DH10B MultiBac™	*Escherichia coli*	Bacmid generation	Geneva Biotech
Sf21	*Spodoptera frugiperda*	MultiBac™; Virus generation	
High Five	*Trichoplusia ni*	MultiBac™ Protein expression	

5.2   Methods

5.2.1   Gibson Cloning

Total RNA was isolated from human A549 cells using TRIfast^{TM} according to the manufacturer's protocol. PolyA-selected RNA was used for first-strand cDNA synthesis mediated by Superscript II RT according manufactures protocol. The cDNA was further handed out to Lisa-Marie Schneider for cloning approaches. PCR products for cloning were amplified by nested PCR (Hill and Stewart, 1992).

All construct were generated using the Gibson variant of sequence and ligation independent cloning (SLIC) (Gibson et al., 2009). Please note that multiple fragments were ligated in one reaction to change affinity-tags and/or protease-cleavage sites. Positive clones were identified by colony PCR prior to Sanger sequencing. Point-mutations were introduced by primers. All affinity tags contain a TEV cleavage site prior to the coding sequence or directly after the coding sequence, respectively. All plasmid constructs used in this study are listed. Please note, that many constructs seemingly exists twice. This is the case as we also utilized codon-optimized sequences for expression in insect cells (to distinguish both possibilities codon-optimized sequences are underlined).

Backbone	Insert*[1]	Amino acids/ mutation	5' modification	3' modification	Internal ID
pAceBac1	CDK8	1-403/wt	T7-TEV		7
pAceBac1	CDK8	1-403/wt	Strep-SUMO-T7-TEV		8
pAceBac1	CDK8	1-403/wt	Strep-SUMO-T7-TEV		68
pAceBac1	CDK19	1-439/wt	Strep-SUMO-T7-TEV		96b
pAceBac1	CDK7	1-346/wt	Strep-SUMO-T7-TEV		150
pAceBac1	Cyclin C	1-283/wt	T7-TEV		10
pIDK	Cyclin C	1-283/wt	T7-TEV		12
pIDK	CDK8	1-464/wt	T7-TEV		13
pIDK	Cyclin C	1-283/wt			28
pIDC	Cyclin H	1-323/wt			151
pAceBac1	MED12	1-2177/wt	Strep-SUMO-T7-TEV		1

Backbone	Insert	Amino acids/ mutation	5' modification	3' modification	Internal ID
pAceBac1	MED13	1-2174/wt	Strep-SUMO-T7-TEV		5
pAceBac1	<u>MED13</u>	1-2174/wt	Strep-SUMO-T7-TEV		72
pFL	<u>MED13</u>	1-2174/wt	Strep-SUMO-T7-TEV		71
pAceBac1	MED12	1-69/wt		TEV-T7-Strep	125
pAceBac1	MED12	1-91/wt		TEV-T7-Strep	119
pAceBac1	MED12	6-100/wt		TEV-T7-Strep	126
pAceBac1	MED12	11-100/wt		TEV-T7-Strep	127
pAceBac1	MED12	23-100/wt		TEV-T7-Strep	128
pAceBac1	MED12	29-100/wt		TEV-T7-Strep	129
pAceBac1	MED12	19-91/wt		TEV-T7-Strep	103
pAceBac1	MED12	11-69/wt		TEV-T7-Strep	132
pAceBac1	MED12	11-91/wt		TEV-T7-Strep	131
pAceBac1	MED12	23-69/wt		TEV-T7-Strep	134
pFL	<u>MED12</u>	1-100/wt		TEV-T7-Strep	92
pAceBac1	MED12	1-100/wt		TEV-T7-Strep	41
	MED12	1-100/E33Q		TEV-T7-Strep	41M1
	MED12	1-100/E33Q/D34N		TEV-T7-Strep	41M2
	MED12	1-100/D34N		TEV-T7-Strep	41M3
	MED12	1-100/D34N/E35Q		TEV-T7-Strep	41M4
	MED12	1-100/E35Q		TEV-T7-Strep	41M5
	MED12	1-100/E33A		TEV-T7-Strep	41M6
	MED12	1-100/E33L		TEV-T7-Strep	41M7
	MED12	1-100/K30A		TEV-T7-Strep	41M8
	MED12	1-100/Q31A		TEV-T7-Strep	41M9
	MED12	1-100/K32A		TEV-T7-Strep	41M10
	MED12	1-100/L36R		TEV-T7-Strep	41M11
	MED12	1-100/Q43P		TEV-T7-Strep	41M12
	MED12	1-100/G44S		TEV-T7-Strep	41M13
	MED12	1-100/D34Y		TEV-T7-Strep	41M14

Backbone	Insert	Amino acids/ mutation	5' modification	3' modification	Internal ID
pAceBac1	MED12	1-100/K15N		TEV-T7-Strep	41M15
	MED12	1-100/K15N/E33Q		TEV-T7-Strep	41M16
	MED12	1-100/E33K		TEV-T7-Strep	41M17
pAceBac1	MED12	1-350/wt		TEV-T7-Strep	43
pAceBac1	MED12	1-440/wt		TEV-T7-Strep	80
pAceBac1	MED12	1-1227/wt	Strep-SUMO-T7-TEV		3
pAceBac1	MED12	1-1227/wt	Strep-SUMO-T7-TEV		66
pFL	MED12	1-1227/wt	Strep-SUMO-T7-TEV		47
pFL	MED12	1-1227/wt	Strep-SUMO-T7-TEV		65
pFL	MED13	1-947/wt	Strep-SUMO-T7-TEV		141
pAceBac1	Cyclin C	1-283/wt		TEV-T7-Strep	108
pIDC	CDK8	1-359/wt			122
pIDC	CDK8	1-403/wt			118
	CDK8	1-403/R65Q			118M2
	CDK8	1-403/R150Q			118M3
	CDK8	1-403/R178Q			118M4
pIDC	CDK8	1-464/wt			123
pIDC	CDK19	1-359/wt			116
pIDC	CDK19	1-439/wt			115
pIDC	CDK19	1-502/wt			137
pIDC	CDK3	1-305/wt			143
pIDS	MED12	1-100/wt			117
pUCDM	Cyclin C CDK8	1-283/wt 1-359/wt			79c
pUCDM	Cyclin C CDK8	1-283/wt 1-403/wt			79a
	CDK8	1-403/R65Q			79aM7
	CDK8	1-403/R150Q			79aM8
	CDK8	1-403/R178Q			79aM9
	CDK8	1-403/T196D			79aM10
	CDK8	1-403/T196A			79aM11

Backbone	Insert	Amino acids/ mutation	5' modification	3' modification	Internal ID
pUCDM	Cyclin C	1-283/wt			79a
	CDK8	1-403/wt			
	CDK8	1-403/T31D			79aM12
	CDK8	1-403/T31A			79aM13
	CDK8	1-403/Y32F			79aM14
	CDK8	1-403/T360A			79aM15
	CDK8	1-403/T360D			79aM16
	CDK8	1-403/M174F			79aM19
	CDK8	1-403/S393A/S394A			79aM20
	CDK8	1-403/S393D/S394D			79aM21
	CDK8	1-403/T396A			79aM22
	CDK8	1-403/T396D			79aM23
	CDK8	1-403/T382A			79aM24
	CDK8	1-403/T382D			79aM25
	CDK8	1-403/T385A			79aM26
	CDK8	1-403/T385D			79aM27
	CDK8	1-403/D173A			79aM28
pUCDM	CDK8	1-403/wt			79a
	Cyclin C	1-283/wt			
	Cyclin C	1-283/E98Q			79aM4
	Cyclin C	1-283/E99Q			79aM5
	Cyclin C	1-283/E98Q/E99Q			79aM6
	Cyclin C	1-283/N181A			79aM17
	Cyclin C	1-283/D182A			79aM18
pUCDM	Cyclin C	1-283/wt			79d
	CDK8	1-464/wt			
	CDK8	1-464/T410D			79dM1
	CDK8	1-464/T410A			79dM2
	CDK8	1-464/T413D			79dM3
	CDK8	1-464/T413A			79dM4
	CDK8	1-464/T410D/S413D			79dM5
	CDK8	1-464/T410A/T413A			79dM6

Backbone	Insert	Amino acids/ mutation	5' modification	3' modification	Internal ID
pSPL	Cyclin C	1-283/wt	T7		98a
	CDK19	1-359/wt	T7		
pSPL	Cyclin C	1-283/wt	T7		96a
	CDK19	1-439/wt	T7		
pUCDM	Cyclin C	1-283/wt			98d
	CDK19	1-502/wt			
pAceBac1	CDK19	1-502/wt			111
pAceBac1	Cyclin C P2A	1-283		TEV-T7-Strep	130
	CDK8	1-403			
pGEX-4T1	STAT1	639-750/wt	GST-Thrombin		EC6
pGEX-4T1	STAT1	639-750/wt	GST-TEV		EC7
pGEX-4T1	Cyclin H	1-323/wt	GST-TEV		EC8
pGEX-4T1	BRCA1	1443-1649/wt	GST-TEV		EC9

5.2.2 Polymerase Chain Reaction

Polymerase chain reaction (PCR) was used to linearize plasmids and to generate amplicons carrying desired overhangs suited for subsequent ligation. PCRs were performed using Phusion DNA polymerase. Amplification was carried out in a Thermocycler (peqSTAR, Peqlab) using the listed reaction mix. Nested PCRs were carried in presence of 5% DMSO using cDNA as template.

PCR program for standard DNA amplification

Reaction mix	[µL]	Thermal profile		
ddH2O	32,5	98°C	30 s	
5x Phusion buffer	10,0	98°C	15 s	
dNTPs	0,5	60°C	10 s	35x
10 µM Primer forward	2,5	72°C	15s/kb	
10 µM Primer reverse	2,5	72°C	10 min	
Template DNA 1ng/µL	1,0	4°C	∞	
Phusion DNA polymerase (NEB)	1,0			

5.2.3 Agarose Gel Electrophoresis and Gel Extraction

PCR products were separated on 0.5-2% agarose gels. DNA fragments were mixed 1:6 using EZ Vision DNA loading dye (Amresco) and run at 130V in 1x TAE-buffer (40 mM Tris pH 8.0, 20 mM acetic acid, 1 mM EDTA). 1 kb DNA ladder (NEB) was loaded as marker. Desired bands were cut out under UV-light for gel extraction using QIAquick® Gel Extraction kit (QIAGEN) and protocol. The DNA concentration was determined via absorbance at 260 nm (Eppendorf Biospectrometer basic).

5.2.4 Gibson Assembly and Colony PCR

Linearized, purified vectors and one or several inserts were ligated via the Gibson assembly method. For this, 0,03 - 0,20 pmol of total DNA (vector to insert ratio 1:2) was added to 7.5 µL Gibson Master Mix (10 µL total reaction volume) and incubated at 50°C for 30 min. The reaction mix was transformed in competent Top10 or BW23473 *E. coli* cells.

PCR program for colony PCR

Reaction mix	[µL]	Thermal profile		
ddH2O	20,75	98°C	5 min	
10x TaqPol buffer	2,5	98°C	15 s	
10 mM dNTP mix	0,5	57°C	10 s	25x
10 µM Primer forward	0,5	68°C	1 min/kb	
10 µM Primer reverse	0,5	68°C	10 min	
Taq DNA polymerase (selfmade)	1,0	4°C	∞	

5.2.5 Cre-LoxP Recombination

Desired acceptor-donor-plasmid combinations for protein expression in insect cells were combined via Cre-*LoxP*-mediated recombination. Therefore, 200-400 ng acceptor-plasmid was incubated with 300-750 ng donor-plasmid. The reaction was mediated by Cre Recombinase (NEB). Upon ligation, the fused constructs were named after their acceptor-donor-plasmid combination giving rise to the order of ligation reactions. For example, the fusion of the acceptor plasmid ID 41 with the donor plasmid ID 79a results in the fused construct 41.79a. The first plasmid ID always represent an acceptor plasmid constructs, whereas the following plasmid IDs are donor plasmids. Please note that due to systematic fusion of different acceptor-donor plasmid combinations more than a single construct can be generated that encodes for the same protein or protein complex. For example, the fused construct 41.79a encodes the identical proteins like 108.118.117. Therefore, for some, yet not for all, multiple acceptor-donor combinations were produced that encode for the same proteins. However, the order and localization of the protein tags might differ as well as the coding sequence as we ordered codon optimized sequences for insect cells.

5.2.6 Bacterial Transformation

Chemically competent *E. coli* cells were incubated on ice for 5 min in the presence of DNA. After heat shock (42°C for 42 s) and subsequent recovery (1h), cells were plated out on LB agar plates in presence of appropriate antibiotics. Plates were incubated at 37° overnight.

5.2.7   Isolation of Plasmid DNA

Plasmid DNA isolation using QIAprep Spin Miniprep Kit (QIAGEN) was done according to manufactures protocol. Plasmid-DNA was eluted using 50 µL ddH$_2$O. DNA-Concentration was determined via absorbance at 260 nm (Eppendorf Biospectrometer basic).

5.2.8   Protein Expression in *E. coli*

For all recombinant protein expression in *E. coli*, transformed RosettaBL21-CodonPlus (DE3) were inoculated and grown overnight in LB media supplemented with the appropriate antibiotics. To produce STAT1, 1-4 L *E. coli* cells were cultivated (37°C, 160 rpm) and protein expression induced by the addition of 1 mM IPTG (OD$_{600}$ 0.6). Cells were cultivated at 18°C overnight and harvested by centrifugation (6000g, 15 min). To produce Sirtuin-1, 1-6 L *E. coli* cells were cultivated (37°C, 160 rpm) and protein expression induced by the addition of 0.5 mM IPTG (OD$_{600}$ 0.6). All used media was supplemented with 25 µM ZnOAc. Cells were cultivated at 18°C overnight and harvested by centrifugation (6000g, 15 min). To generate BRCA1, 1-2 L *E. coli* cells were cultivated (37°C, 160 rpm) and protein expression induced by the addition of 1 mM IPTG (OD$_{600}$ 0.8). Cells were cultivated at 37°C for 4 h and harvested by centrifugation (6000g, 15 min). To express Cyclin H, 1-2 L *E. coli* cells were cultivated (37°C, 160 rpm) and protein expression induced by the addition of 1 mM IPTG (OD$_{600}$ 0.6). Cells were cultivated at 18°C overnight and harvested by centrifugation (6000g, 15 min).
All cell pellets were either processed directly or stored at -80°C.

5.2.9   Protein Expression in Insect Cells

Insect cells derived from *Spodoptera frugiperda* (SF21) were used for virus generation and amplification, whereas cells from *Trichoplusia ni* were utilized for protein production. SF-4 Baculo Express ICM ready-to-use media complemented with 200 mM L-Glutamin (Bio Concept AG) was used for both insect cell lines. Cells were incubated at 27°C in a rotary shaker (100 rpm, shaking throw 50 mm). Protein expression in insect cells was done using Multibac^{Turbo} according to the manufacturer's protocol (Berger et al., 2004; Fitzgerald et al., 2006). As we did not determine viral titers to obtain their multiplicity of infections (MOI), we utilized so-called "titerless" protocols (Berger et al., 2013; Scholz and Suppmann, 2017; Wasilko et al., 2009).

Bacmid-isolation

Desired constructs were transformed into DH10MultiBac *E. coli* cells (75 ng in total) and incubated on LB plates. Successful bacmid integration upon Tn7 transposition was controlled by blue-white screening. Bacmid-DNA isolation was carried out using QIAprep Spin Mini Kit according to the manufacturer's instructions up to the addition of N3 and subsequent centrifugation. Cleared supernatants were then transferred into fresh reaction tubes and DNA was precipitated by adding Isopropanol 1:1 (v/v) followed by centrifugation (20,000g, 15 min, 4°C). The pellet was washed twice with 70% EtOH and Bacmid-DNA solubilized in 50 µL sterile ddH$_2$O.

Virus-generation V0 and V1

For production of recombinant baculovirus, the composite bacmid was transfected (200 µL Media, 20 µg Bacmid-DNA, 16 µL X-tremeGENE HP DNA Transfection Reagent) into freshly diluted SF21 cells (0.8 x 10^6 cells/mL, 25 mL). 3 days post transfection, SF21 cells were diluted to the initial density and viruses harvested after 1-3 additional days. To produce large amounts of viruses, needed volumes of SF21 cells (0.8 x 10^6 cells/mL) were infected with V0 viruses using a titerless protocol 1:50 - 1:100 (v/v) and harvested 3 days post infection.

Protein-production

1 – 5 L High Five insect cells were seeded (1.2 – 1.4 x 10^6 cells/mL) in Fernbach flasks and V0/V1 viruses added at a ratio between 1:10 – 1:50. Flasks were incubated for 2-3 days and cells harvested by centrifugation (700g, 10 min). The pellet was subsequently resuspended in lysis buffer supplemented with protease inhibitors and Benzonase® and stored at -80°C.

5.2.10 Protein Purification

For 1 L expression volume, insect cells were consequently resuspended in 50-70 mL lysis buffer. For 1 L expression volume, 1 mL slurry (GST-, Ni-NTA- or StrepTactin beads) in differently shaped gravity-flow columns was used. Protein tags were removed by TEV-protease (self-made), which was added in a ratio of 1:10 – 1:40, depending on the enzymatic activity of the purified TEV batch. The cleavage reaction was incubated for 16 h at 4°C. Tag-removal was carried out either after affinity- or prior size-exclusion chromatography in varying buffers. Reaction volumes varied ranging from less than 50 µL up to 50 mL.

5.2.10.1   Purification of MED12 1-100

To generate MED12 1-100 alone, MED12 1-100 was cloned into pAceBac1 vector (plasmid IDs 41 and 92). A C-terminal Strep-Tag preceded by a TEV cleavage site on MED12 1-100 allowed affinity purification and tag-removal. Single MED12 1-100 was expressed in High5 insect cells by recombinant baculovirus infection. For one liter culture volume, cells were resuspended in 50-70 mL Lysis buffer A and lysed by sonication. Cell debris was removed by centrifugation at 35,000 rpm for 90 min in a Beckmann Ti-45 rotor. Either StrepTactin beads (IBA Lifesciences) in a gravity flow column (selfmade) or a StrepTrap HP column (GE healthcare) was equilibrated with 10-20 CV buffer A. Supernatants were collected and bound to the Strep resin. The resin was washed with 5-10 CV buffer A prior elution with buffer A supplemented with 2.5 mM desthiobiotin. Cleavage of Strep-tag fusions was performed when needed for MST measurements. MED12 1-100 was diluted to 30 mM NaCl (with Low-Salt buffer A) and loaded onto a cation-exchange column (Resource S, GE Healthcare) to recover the desired protein. In a final step MED12 1-100 was polished by size-exclusion chromatography using a Superdex 75 10/300 GL (GE Healthcare) column in gel filtration buffer A.

5.2.10.2   Purification of binary CDK8/Cyclin C and CDK19/Cyclin C complexes

To obtain binary CDK8/Cyclin C complexes, full-length Cyclin C (1-283) and different CDK8/CDK19 variants, *e.g.* full-length (1-464/1-502) and C-terminally truncated CDK8 (1-403/1-439 and 1-359/1-359) were cloned into pAceBac1 and pIDC vectors, respectively (construct IDs 108.123/108.137; 108.118/108.116 and 108.122/108.115). To enable affinity purification Cyclin C carried a C-terminal Strep-Tag and a Tobacco Etch Virus (TEV) cleavage site. Binary CDK8/Cyclin C (construct IDs 8.28, 68.28, 8.22 and 68.22) and CDK19/Cyclin C (construct ID 96b.28 and 96b.22) complexes used for ITC measurements, harbor an N-terminal Strep-SUMO-tag on the kinase. Binary CDK8/Cyclin C and CDK19/Cyclin C complexes were co-expressed in High Five insect cells by recombinant baculovirus infection via a titerless protocol. Cells were lysed by sonication and cell debris was removed by centrifugation at 35,000 rpm for 90 min in a Beckmann Ti-45 rotor. Either StrepTactin beads (IBA Lifesciences) or StrepTrap HP (GE healthcare) were equilibrated with 10-20 CV lysis buffer A. Supernatants were collected and bound to the Strep resin. The resin was washed with 10-20 CV lysis buffer A prior elution with lysis buffer A supplemented with 2.5 mM desthiobiotin. Cleavage of Strep-

tag fusions was performed overnight with TEV protease when utilized for *in vitro* kinase assays. This was necessary as the C-terminal Strep-tag on Cyclin C is being phosphorylated by CDK8 and CDK19 in our assays. After cleavage, tag-free protein complexes were diluted to 30 mM NaCl and loaded onto a cation-exchange column (Resource S, GE Healthcare) to recover the desired protein. Binary constructs that possess an N-terminal Strep-SUMO tag were kept uncleaved, diluted to 50 mM NaCl (with low-salt buffer A) and loaded onto an anion-exchange column (Resource Q, GE Healthcare). In a final step all binary CDK8/Cyclin C and CDK19/Cyclin C were polished by size-exclusion chromatography using a Superdex 200 10/300 GL (GE Healthcare) column in gel filtration buffer A.

Binary CDK8 (1-403)/Cyclin C complexes both encoded on the pAceBac-vector with the P2A linker (plasmid ID 130) were co-expressed and purified in analogy to aforementioned, not SUMO-tagged CDK8/Cyclin C complex variants.

5.2.10.3   Purification of ternary CDK8/CycC/MED12 and CDK19/CycC/MED12 complexes

Ternary complexes were constructed using several acceptor-donor plasmid combinations. However, the majority of our ternary constructs contained a C-terminal Strep-tag on multiple N- (6-100, 11-100, 19-100, 23-100, 29-100; construct IDs 126.79a, 127.79a, 128.79a, 129.79a) or C-terminally truncated MED12 variants (1-69, 1-91, 1-100, 1-350, 1-440; construct IDs 125.79a, 119.79a, 41.79a, 43.79a, 80.79a). For ternary constructs that contain MED12 1-100, the Strep-tag can also be located C-terminally on Cyclin C. Ternary constructs, that possess the C-terminal Strep-tag on MED12, CDK8 and Cyclin C were both encoded on pUCDM vector, yet CDK19 and Cyclin C were both encoded on pSPL vector. All ternary complexes were co-expressed in High Five insect cells by recombinant baculovirus infection. Cells were lysed by sonication and cell debris was removed by centrifugation at 35,000 rpm for 90 min in a Beckmann Ti-45 rotor. StrepTactin beads (IBA Lifesciences) or StrepTrap HP (GE healthcare) was equilibrated with 10-20 CV buffer A. Supernatants were collected and bound to the Strep resin, the resin washed with 10-20 CV lysis buffer A followed by their elution with lysis buffer A supplemented with 2.5 mM desthiobiotin. Cleavage of Strep-tag fusions was performed overnight with TEV protease when needed. After cleavage, tag-free protein complexes were diluted to 75 mM NaCl (with low-salt buffer A) and subjected to an anion-exchange column (ResourceQ, GE Healthcare). The flow-through after anion-exchange chromatography was again diluted to 30 mM NaCl (with low-salt buffer A) and subsequently loaded onto a cation-

exchange column (Resource S, HE Healthcare) to recover the desired protein complexes. In a final step the protein complexes were polished by size-exclusion chromatography (SEC) using a Superdex 200 10/300 GL (GE Healthcare) or Superose6 10/300 GL (GE Healthcare) column in gel filtration buffer A. Ternary constructs for kinase assays were kept uncleaved, except for acceptor-donor combinations that possess the Strep-tag C-terminally on Cyclin C.

5.2.10.4   Co-purification of binary and ternary complexes

Co-purification of binary and ternary complexes was carried out using multiple acceptor plasmids. Please note that acceptor plasmids used for our co-purification method were also utilized for acceptor-donor combinations for co-expression. Co-purified complexes were purified and utilized just as the co-expressed complexes, as they result in identical protein complexes. The binary CDK 19 (1-359)/Cyclin C complexes shown on Fig. 23B and C were co-purified using the plasmid IDs 108 together with plasmid 111, the ternary CDK19/CycC/MED12 (1-100) complex on Fig. 23D and E using the plasmid IDs 41 together with plasmid 108 and 112, respectively. All used (acceptor-) plasmids are listed in chapter 5.2.1.

5.2.10.5   Purification of MED13 1-545

MED13 (1-545) was cloned into a pAceBac1 vector (plasmid ID 88). A C-terminal Strep-Tag preceded by a TEV cleavage site on MED13 1-545 allowed affinity purification and tag-removal. Single MED13 1-545 was expressed in High Five insect cells by recombinant baculovirus infection. Cells were resuspended in lysis buffer A and lysed by sonication. Cell debris was removed by centrifugation at 35,000 rpm for 90 min in a Beckmann Ti-45 rotor. Either StrepTactin beads in a gravity flow column (IBA Lifesciences) or a StrepTrap HP column (GE healthcare) was equilibrated with 10-20 CV buffer A. Supernatants were collected and bound to the Strep resin. The resin was washed with 5-10 CV buffer A prior elution with buffer A supplemented with 2.5 mM desthiobiotin. MED13 1-545 was diluted to 50 mM NaCl with Low-Salt buffer A and loaded onto a anion-exchange column (Resource Q, GE Healthcare) to recover the desired protein. In a final step MED13 1-545 was polished by size-exclusion chromatography using a Superdex 200 10/300 GL (GE Healthcare) column in gel filtration buffer A.

5.2.10.6   Purification of a quaternary CDK8/CycC/MED12/MED13 complex

For the production of a recombinant 4-subunit kinase module, N-terminally tagged MED12 (1-1227) was cloned into the pAceBac1 and pFL vector (plasmid IDs 3, 47, 65 and 66), N-terminally tagged MED13 (1-947) was cloned into the pFL vector (plasmid ID 141). Both, MED12 and MED13 contained a SUMO-tag to enhance protein yield and stability. Binary full-length CDK8/Cyclin C (construct ID 108.123) were cloned and expressed as described before. Single MED12, MED13 and binary CDK8/Cyclin C complexes were separately (co-)expressed in High Five insect cells. Cells from 12 liter culture volume were resuspended in 600 mL lysis buffer A. Cells were lysed by sonication and cell debris was removed by centrifugation at 35,000 rpm for 4 h in a Beckmann Ti-45 rotor. Supernatants were collected, filtrated (0,8 μm) and bound to a StrepTrap HP 5 mL column (GE Healthcare) followed by their elution with buffer A supplemented with 2.5 mM desthiobiotin. Note that the usage of the StrepTrap column instead of StrepTactin Superflow (IBA Lifesciences) resin was crucial to concentrate large sample volumes (approx. 550 mL supernatant loaded and all bound proteins eluted in less than 5 mL) for *in vitro* complex reconstitution. The complex was diluted to 30 mM NaCl (with low salt buffer A). Subsequent cation-exchange chromatography (Resource S, HE Healthcare) recovered the desired protein complex. In a final step the recombinant kinase module was polished by size-exclusion chromatography (SEC) using a Superose 6 3.2 Increase (GE Healthcare) in gel filtration buffer A.

5.2.10.8   Purification of kinase assay substrates

The STAT1 transactivation domain (639-750) was cloned into a pGEX-4T1 plasmid and contained an N-terminal GST-tag allowing GST-affinity chromatography (plasmid IDs EC6 and 7). The STAT1 transactivation domain was then purified as described (Pelish et al., 2015). In brief, *E. coli* cells were resuspended in lysis buffer (500 mM NaCl, 50 mM Tris/HCl, pH 8.0, 0.5 mM EDTA, 1 mM DTT or 5 mM BME), lysed by sonication and cell debris removed by centrifugation at 25,000 rpm for 60 min in a SS-34 rotor. Supernatants were collected and bound to the GST resin, the resin washed with 10-20 CV lysis buffer followed by their elution with elution buffer (150 mM KCl, 50 mM Tris/HCl, pH 7.9, 2 mM DTT, 0.1 mM EDTA and 30 mM reduced GSH). After GST affinity chromatography STAT1 elution fraction were diluted to 50 mM KCl with low-salt buffer B and subjected to anion-exchange chromatography (MonoQ, GE Healthcare).

Full-length Sirtuin-1 was a gift of Prof. Dr. Steegborn, University of Bayreuth, Germany. Sirtuin-1 was cloned into a pET28a plasmid and bore an N-terminal hexahistidin-tag for purification. Cells were resuspended in lysis buffer (300 mM NaCl, 50 mM Tris/HCl, pH 8.0, 20 mM Imidazol, 1 mM DTT or 5 mM BME, protease inhibitor cocktail) and lysed by sonication. Cell debris was removed by centrifugation at 25,000 rpm for 60 min in a SS-34 rotor. Ni-NTA beads (Qiagen) or HisTrap FF (GE Healthcare) was equilibrated with 10-20 CV lysis buffer. Supernatants were collected and bound to the Ni-NTA resin, the resin washed with 10-20 CV lysis buffer followed by their elution with lysis buffer supplemented with 150 mM Imidazol. After Ni-NTA affinity chromatography Sirt-1 elution fraction were diluted to 50 mM NaCl (with low salt buffer B) and subjected to anion-exchange chromatography (Resource Q, GE Healthcare) and finally isolated by size-exclusion chromatography in gelfiltration buffer A using a Superose6 10/300 GL column (GE Healthcare).

BRCA1 (1443-1649) was identified by limited proteolysis as a stable and soluble fragment (Mark et al., 2005) and cloned likewise STAT1 TAD (plasmid ID EC9). Cells were resuspended in lysis buffer (300 mM NaCl, 50 mM Tris/HCl, pH 8.0, 1 mM DTT or 5 mM BME, protease inhibitor cocktail) and lysed by sonication. Cell debris was removed by centrifugation at 25,000 rpm for 60 min in a SS-34 rotor. GST beads (Glutathion Sepharose® 4B, GE Healthcare or Pierce™ Glutathion Agarose) were equilibrated with 10-20 CV lysis buffer. Supernatants were collected and bound to the GST resin, the resin washed with 10-20 CV lysis buffer followed by their elution with lysis buffer supplemented with 30 mM reduced L-Glutathion. After GST-affinity chromatography, BRCA1 elution fractions were diluted to 50 mM NaCl with low salt buffer B and loaded on an anion-exchange column (Resource Q, GE Healthcare).

Bovine RNA Polymerase II was endogenously isolated by Robin Weinmann under supervision of Lisa-Marie Schneider, University of Bayreuth, Germany. Typically, 0.5 kg bovine thymus was used and purified as described (Bernecky et al., 2016).

Cyclin H was cloned as described for the STAT1 TAD (plasmid ID EC8). Cells were resuspended in lysis buffer (300 mM NaCl, 50 mM Tris/HCl, pH 8.0, 1 mM DTT or 5 mM BME, protease inhibitor cocktail) and lysed by sonication. Cell debris was removed by centrifugation at 25,000 rpm for 60 min in a SS-34 rotor. GST beads (Glutathion Sepharose® 4B, GE Healthcare or Pierce™ Glutathion Agarose) were equilibrated with 10-20 CV lysis buffer. Supernatants were collected and bound to the GST resin, the resin washed with 10-20 CV lysis buffer followed by their elution with lysis buffer supplemented with 30 mM reduced L-glutathione. After GST-affinity chromatography, Cyclin H elution fractions were diluted to

50 mM NaCl with low salt buffer B and loaded on an anion-exchange column (Resource Q, GE Healthcare). Cleavage of GST-tag fusions was performed overnight with TEV-protease. After cleavage, GST-reverse chromatography resulted in tag-free protein fractions (flow-through), that were finally isolated by size-exclusion chromatography using a Superdex200 (GE Healthcare).

To co-express binary CDK7/Cyclin H complexes, CDK7 and Cyclin H were cloned into pAceBac1 vector, and pIDC vector, respectively (construct ID 150.151). An N-terminal Strep-SUMO tag on CDK7 enabled affinity purification. The binary CDK7/Cyclin H complex was co-expressed in High5 insect cells by recombinant baculovirus infection. Cells were resuspended in lysis buffer (200 mM NaCl, 50 mM Tris/HCl, pH 8.0, 2 mM DTT), lysed by sonication and cell debris was removed by centrifugation at 35,000 rpm for 90 min in a Beckmann Ti-45 rotor. StrepTactin beads (IBA Lifesciences) or StrepTrap HP (GE healthcare) were equilibrated with 10-20 CV buffer A. Supernatants were collected and bound to the Strep resin, the resin washed with 10-20 CV buffer A followed by their elution with buffer A supplemented with 2.5 mM desthiobiotin. CDK7/Cyclin H elution fractions were diluted to 50 mM NaCl with low salt buffer B and loaded onto a anion-exchange column (Resource Q, HE Healthcare) to recover the desired protein complexes. In a final step the protein complexes were isolated by size-exclusion chromatography using a Superdex 200 10/300 GL (GE Healthcare) in gelfiltration buffer A.

NELF was a gift of Dr. Seychelle Vos/ Prof. Dr. Patrick Cramer, co-expressed in High Five insect cells and purified as described (Vos et al., 2016).

The human heterodimer DSIF was a gift of Prof. Dr. Wöhrl, University of Bayreuth, Germany. In brief, hSpt5 was cloned into pAceBac1 acceptor vector and possess a C-terminal Strep-tag for affinity purification. hSpt4 was cloned into pIDK donor vector. DSIF was captured by Strep-affinity chromatography, subjected to an anion-exchange column (Resource Q, GE Healthcare) and finally recovered by size-exclusion chromatography using a Superdex 200 (GE Healthcare).

5.2.11 SDS-PAGE

Protein purification steps were analyzed by SDS-PAGE. Depending on the molecular mass of the protein of interest, different concentration of PAA were used (8-12%). Polymerization was induced by the addition of APS and TEMED. 0.75 mm thick gels and a separating gel (4%

PAA) were utilized. Proteins were separated in SDS-PAGE running buffer at 150V for 40-60 minutes.

5.2.12 Limited Proteolysis

Purified ternary CDK8 (1-403)/CycC/MED12 (1-100) complexes (0.5 mg/mL in Gelfiltration buffer A) that possesses a C-terminal Strep-tag on MED12 were incubated at 37°C and proteolyzed with sequencing grade trypsin (Promega), which was dissolved in 1 mM HCl at 1 mg/mL. Samples were taken after 1, 2, 5, 15, 30 and 60 minutes after the addition of trypsin. Reactions were subsequently stopped by the addition of 6x SDS loading dye and analyzed by SDS-PAGE.

5.2.13 Sample Preparation for Electrospray Ionization Mass Spectrometry

Coomassie stained gel bands were cut out and incubated with 50% MeOH (v/v) for 1 min. To destain the gel pieces, 100 µL of 50 mM NH_4HCO_3, pH 8.0 with 50% acetonitrile (ACN) were added and incubated for 15 min at 37°C. Gel pieces were dried using a SpeedVac^{TM} at 55°C for 15 – 60 min. Gel pieces were rehydrated in 50 µL of 25 mM DTT (in 25 mM NH_4HCO_3) und reduced for 20 min at 56°C. To alkylate the proteins, residual liquids were discarded and 55 mM iodoacete acid (IAA, in 25 mM NH_4HCO_3) added for 20 minutes in the dark. Residual IAA solution was taken off and the gel pieces washed 3-5 times using H_2O. Gel pieces were dehydrated for 5 min with 200 µL 25 mM NH_4HCO_3/50% ACN (v/v) and once more for 5 minutes in 100 µL 100% ACN. Gel pieces were dried in a SpeedVac^{TM} and 10-25 µL Trypsin (12.5 ng/µL in 25 mM NH_4HCO_3) added to cover the gel pieces. In gel digestion was carried out over night at 37°C. Next day, the supernatant was collected and stored. 10 µL of 50% ACN and 0.5 % TFA were added to the gel pieces, mixed and sonicated for 20 min. The supernatant was once again collected and pooled with the first collected supernatant. The supernatant mixture was dried in a SpeecVac^{TM}, 20 µL 0.1% formic acid added and incubated with the gel pieces for 10 min. Samples were stored at -20 or subsequently analyzed by mass spectrometry.

5.2.12 Differential Scanning Fluorimetry

Thermal stabilities of kinase complexes were recorded as published in Klatt et al. (Klatt et al., 2020). Measurements were carried out by Franziska Langhammer at Proteros biostructures under supervision of Dr. Elisabeth Schneider. I provided the protein complexes.

5.2.13 Microscale Thermophoresis

Microscale Thermophoresis (MST) measurements were recorded as published in Klatt et al. (Klatt et al., 2020). Please note that MED12 (1-100) was consistently used tag-free. MST-measurements were carried by Franziska Langhammer and myself. I provided the proteins.

5.2.14 Isothermal Titration Calorimetry

Isothermal titration calorimetry (ITC) measurements were recorded as published in Klatt et al. (Klatt et al., 2020). Please note that binary CDK8 (1-403)/Cyclin C and CDK19 (1-439)/Cyclin C complexes were co-expressed and/or co-purified. Cyclin C can possess an N-terminal T7-TEV-tag, depending on the used construct. ITC measurements were performed by Melanie Müller and myself. I provided the proteins.

5.2.15 Circular Dichroism Spectroscopy

Far UV Circular dichroism (CD) spectroscopy using untagged MED13 1-545 was performed on a Jasco J-710 spectropolarimeter using purified MED13 (10 μM) in 20 mM Tris pH 7.6 and 20 mM NaCl in a 0.1 mL cuvette. Polarized light was measured from 195 to 250 nm.
Far UV CD spectra of synthetic MED12 peptides were recorded on a Jasco J-1100 spectropolarimeter (Jasco) with peptide concentrations between 300-200 μM in 10 mM potassium phosphate buffer, pH 7.5. Two synthetic MED12 peptides (amino acids 29-44 and 29-40) were measured and TFE stepwise titrated (up to 40% v/v) in a 0.1 mL cuvette. Spectra were accumulated five times at 20°C with an increment of 0.1 nm. Polarized light was measured from 195 to 240 nm.

Measured ellipticity [theta] was normalized against the protein concentration c in mM, the path length d in cm and the number of amino acids N according the following equation:

$$[\boldsymbol{\theta}]_{MRW} = \frac{\mathbf{100} \times [\boldsymbol{\theta}]}{(\boldsymbol{c} \times \boldsymbol{d} \times \boldsymbol{N})}$$

5.2.16 *In Vitro* Kinase Assays

In vitro kinase assays were carried out with purified binary or ternary complexes as published in Klatt et al. (Klatt et al., 2020). Kinase assays in presence of type I or type II inhibitors were carried out using 15 pmol binary CDK8 (1-403)/Cyclin C and 7.5 pmol ternary CDK8 (1-403)/CycC/MED12 (1-100) complexes. The concentration of utilized binary complexes was doubled to obtain significant band intensities for IC_{50} calculations. All kinases were incubated with a 3-fold serial dilution of Sorafenib, CCT251545, Compound A and BIRB976, final starting concentrations were 270 µM, 10 µM, 180 µM abd 200 µM, respectively. IC_{50} was calculated based on the relative band intensities (including both substrate and CDK8 phosphorylation signal) and the inhibitor concentration. Inhibitors were pre-incubated for 15 min together with the kinase, reactions started by the addition of ATP and stopped after 30 min.

5.2.17 Human Cell Culture

HCT116 cells were a gift of Dr. Martin Ehrenschwender, University of Regensburg, Germany. A549 cells were cultured in DMEM (Gibco), HCT116 cells in McCoy's 5A (Modified, Gibco) medium both supplemented with 10% FBS at 37°C, 5% CO_2. Cells were trypsinated and passaged every 2-3 days. For human IFN-γ treatment cells were seeded in 10 cm plates at a confluency of 70%. IFN-γ was added to final concentration of 0.5 ng/mL. For RNA isolation cells (500.000 cells total) were harvested 24 h post IFN-γ treatment in TRIfast (Peqlab). Samples were handed out to Dr. Iana Kim for RNA-seq library preparation. For Western-Blot analysis in total 1,000,000 cells were harvested in 150 µL NETN buffer supplemented with protease inhibitors.

5.2.18 Generation of a MED12 E33Q Knockin Mutant in HCT116 Cells

The MED12 E33Q knock-in in HCT116 cells was generated as published in Klatt et al. (Klatt et al., 2020). Please note that both guide RNAs as well as the ssODN was designed by Dr. Hung Ho-Xuan and myself. Dr. Hung Ho-Xuan performed co-transfections, I carried out genotyping

and prepared partially NGS libraries together with Dr. Hung Ho-Xuan. NGS data analysis was carried out Dr. Hung Ho-Xuan and Norbert Eichner.

5.2.19 Western Blotting

For Western blot analysis, proteins were prior separated by SDS-PAGE and then transferred to polyvinylidene fluoride (PVDF) membranes. The wet tank blotting apparatus was filled with transfer buffer and the protein transfer was performed at 100 V for 1 h. Primary antibodies were incubated for 1 h (room temperature) or overnight (4°C).

Anti-MED12 (Cell Signaling Technology) was utilized together with anti-α-tubulin (Sigma Aldrich) (1:1,000 and 1:50,000, respectively). Anti-phosSer-727-STAT1 (Cell Signaling Technology) was utilized together with anti-α-tubulin (1:1,000 and 1:8,000, respectively). All secondary antibodies were utilized 1:20,000 and incubated for 1 h.

Chapter 6: Data by other scientists

Please note that this chapter contains exclusively experimental data that were not generated by myself or my supervised students. However, all proteins analyzed in this chapter were cloned, (co-)expressed and purified by myself. Received data were then also analyzed and visualized by myself.

6.1 Peptide identification by electrospray ionization mass spectrometry

Proteolyzed MED12 (please see 2.3.1, Fig 30) was analyzed by electrospray ionization mass spectrometry.
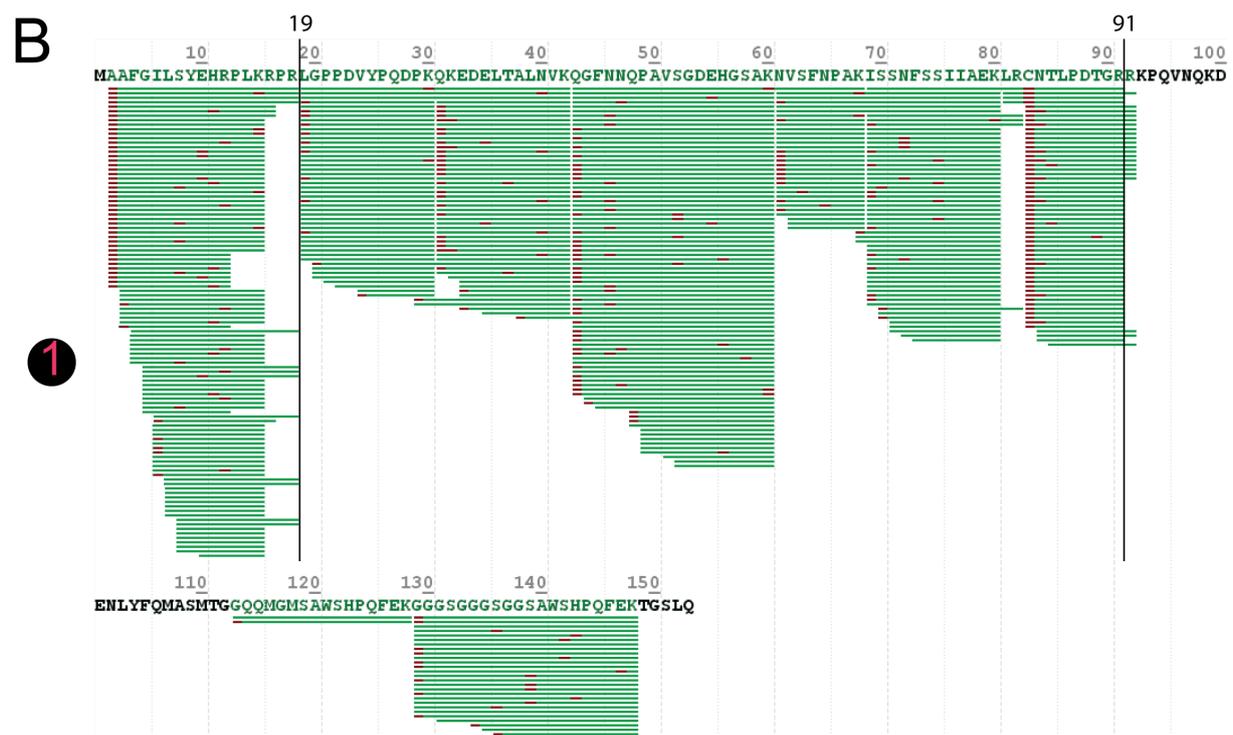
Figure 63: MED12 (1-100) peptide identification of a proteolyzed MED12 band after SDS PAGE

Sequence coverage that result from proteolyzed MED12 peptides. Analyzed bands (1 and 2) are shown on Fig. 30. Each green line represent an identified MED12 peptide, the smaller red bars within the green bars illustrate peptide modifications. MED12 (19-91) is highlighted. Views were created using Byonic™ by myself(Bern et al., 2012). Please note that electrospray ionization mass spectrometry run was conducted by Dr. Matt Fuszard.
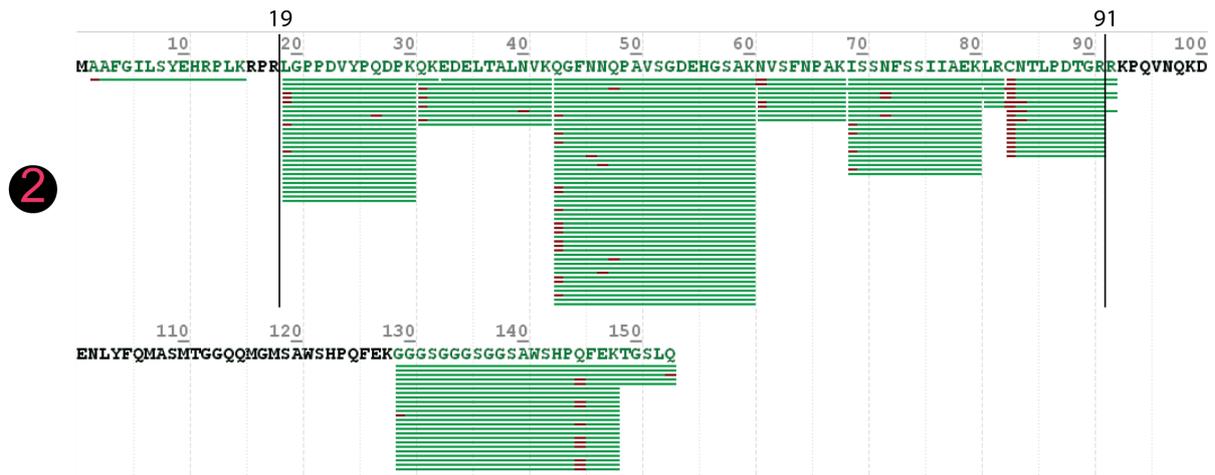
Figure 63 (continued): MED12 (1-100) peptide identification of a proteolyzed MED12 band after SDS PAGE

Sequence coverage that result from proteolyzed MED12 peptides. Analyzed bands (1 and 2) are shown on Fig. 30. Each green line represent an identified MED12 peptide, the smaller red bars within the green bars illustrate peptide modifications. MED12 (19-91) is highlighted. Views were created using Byonic™ by myself (Bern et al., 2012). Please note that electrospray ionization mass spectrometry run was conducted by Dr. Matt Fuszard.
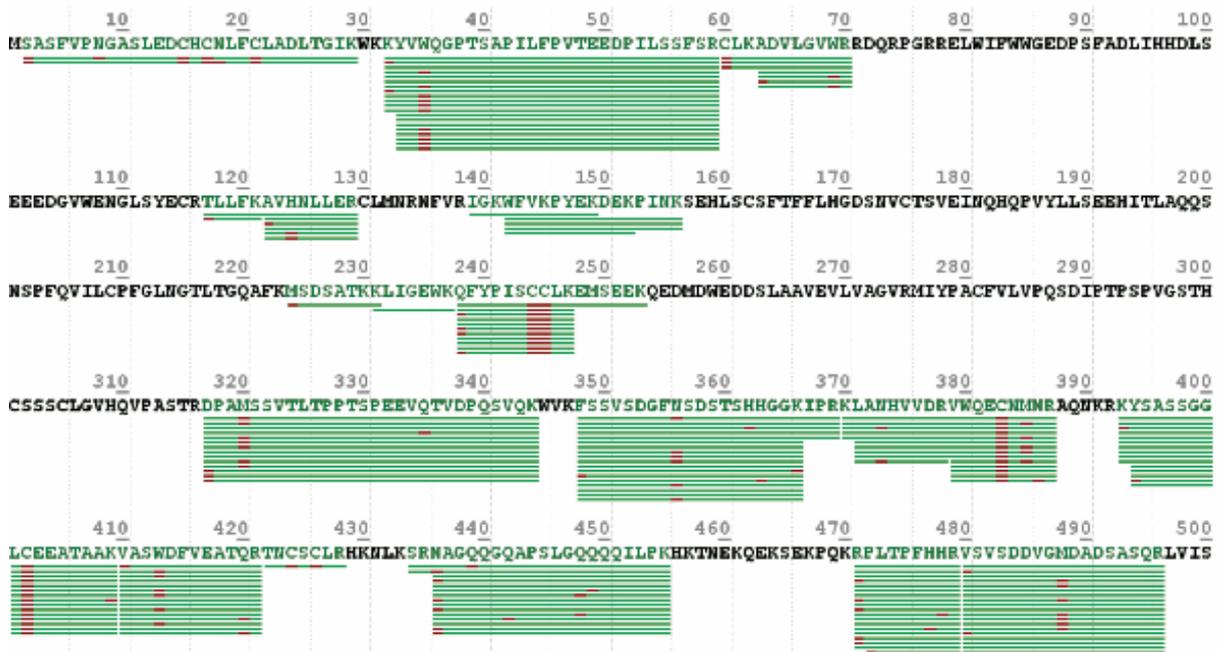
Figure 64: MED13 peptide identification of a degraded and stable MED13 band after SDS PAGE

Sequence coverage of a degraded MED13 band. Each green line represent an identified MED12 peptide, the smaller red bars within the green bars illustrate peptide modifications. Views were created using Byonic™ by myself (Bern et al., 2012). Please note that the electrospray ionization mass spectrometry run was carried out by Dr. Andrea di Fonzo.

6.2 Crosslinking coupled to mass spectrometry of CDK8/19 ternary complexes

The three CDK8-containing ternary complexes comprising MED12 of length (Fig. 21D) were analyzed by crosslinking coupled to mass spectrometry (Klatt et al., 2020). The same applies to the CDK19/CycC/MED12 (1-100) complex (Fig. 22D). Experiments were carried out by Dr. Alexander Leitner, ETH Zürich, Switzerland. I provided the purified protein complexes and performed raw data analysis. Raw data visualization was done with xiVIEW by myself (Graham et al., 2019). Mass spectrometry data involving CDK19 were deposited to the ProteomeXchange Consortium via the PRIDE partner repository by Dr. Alexander Leitner (dataset identifier PXD019251; Supplemental Data table S3) (Perez-Riverol et al., 2019).
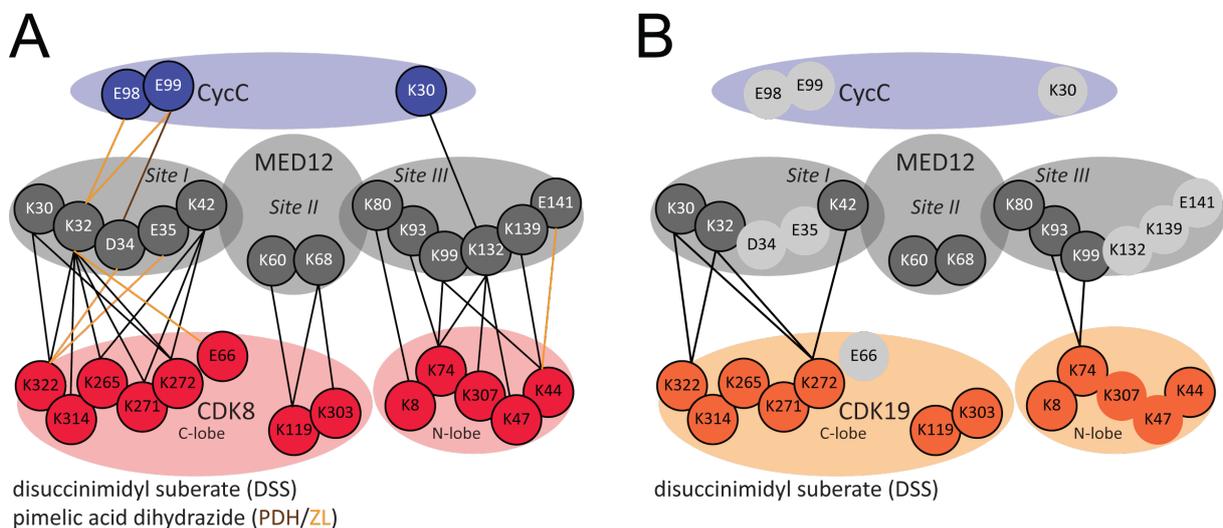
Figure 65: Crosslinking coupled to mass spectrometry of CDK8 and CDK19 ternary complexes
(**A**) Cartoon depiction of all inter-subunit crosslinks involving MED12 that resulted from crosslinking coupled to mass spectrometry analysis utilizing our CDK8 ternary complexes with varying MED12 length. The inter-subunit crosslinks were grouped in three interaction sites (Sites I - III) according to their localization on the surface of the binary CDK8/Cyclin C complex. (**B**) Cartoon depiction of all inter-subunit crosslinks involving obtained from the CDK19/CycC/MED12 (1-100) ternary complex. The inter-subunit crosslinks were colored in black and grouped in three interaction sites (Sites I - III) according to according to their presumable localization on the surface of the binary CDK19/Cyclin C complex. DSS-mediated intersubunit cross-links obtained from ternary CDK8 complexes, which are covered in ternary CDK19 complexes were shown in black. Involved amino acids of intersubunit crosslinks obtained from CDK8-containing ternary complex with varying MED12-length, which cannot be resolved within CDK19-containing ternary complexes, are not encircled. Please note that only 2 datasets for CDK19-containing ternary constructs were analyzed compared to 8 datasets for CDK8-containing ternary complexes. Please note that the figure continuous on the next page.
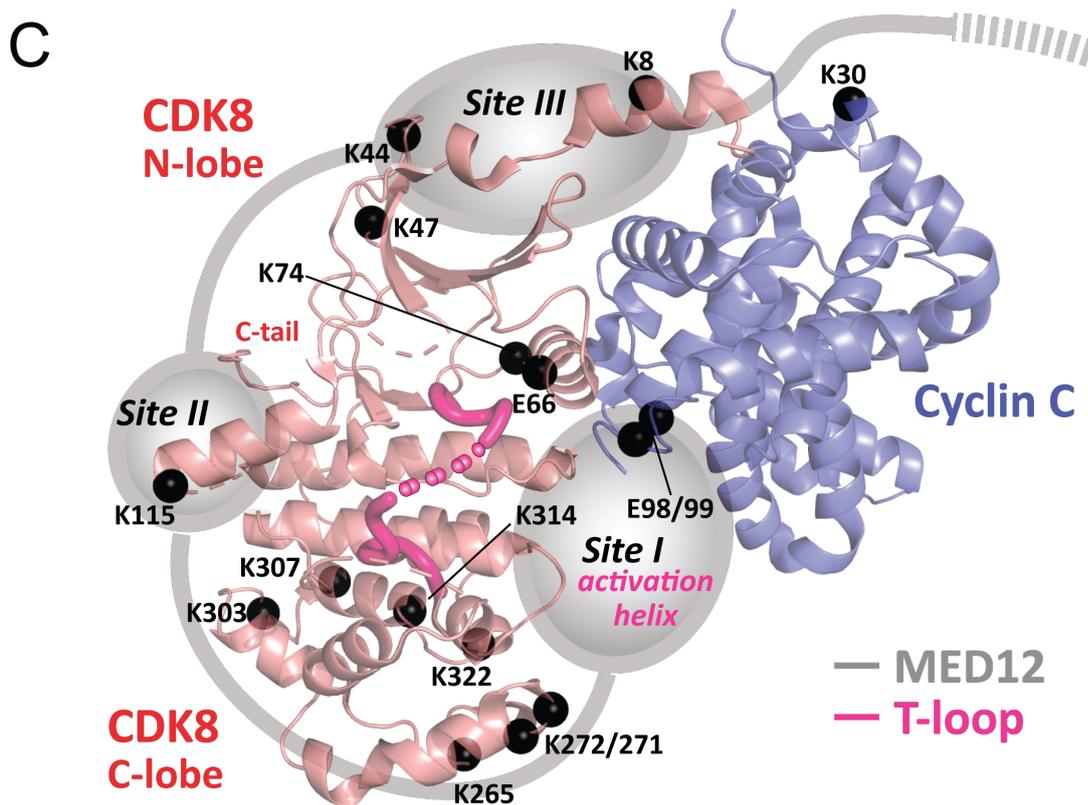
Figure 65 (continued): Crosslinking coupled to mass spectrometry of CDK8 and CDK19 ternary complexes
(**C**) 3-dimensional arrangement of the three major crosslink sites between MED12 and CDK8 (1-403)/Cyclin C. Lysine and glutamate residues that were found crosslinked are represented as black spheres and plotted onto the structure of the CDK8 (1-403)/Cyclin C complex (PDB code 3RGF) (Schneider et al., 2011). Please note that K115 is shown instead of the structurally unresolved, cross-linked residue K119. The figure was prepared by myself using PYMOL (Schroeding_LLC, 2015). Please note also that crosslinking coupled to mass spectrometry experiments were carried out by Dr. Alexander Leitner. Note further that (**A**) and (**C**) were adopted from Klatt et al., 2020.

6.3 Crystallization and preliminary structure determination of ternary CDK8 (1-403)/CycC/MED12 (11-91) complexes

For the crystallization of the CDK8 (1-403)/CycC/MED12 (11-91) ternary complex, Meret Kuck and I concentrated the protein complex to 40 mg/mL and subsequently sent the protein complex on ice to Dr. Elisabeth Schneider from Proteros biostructures GmbH.
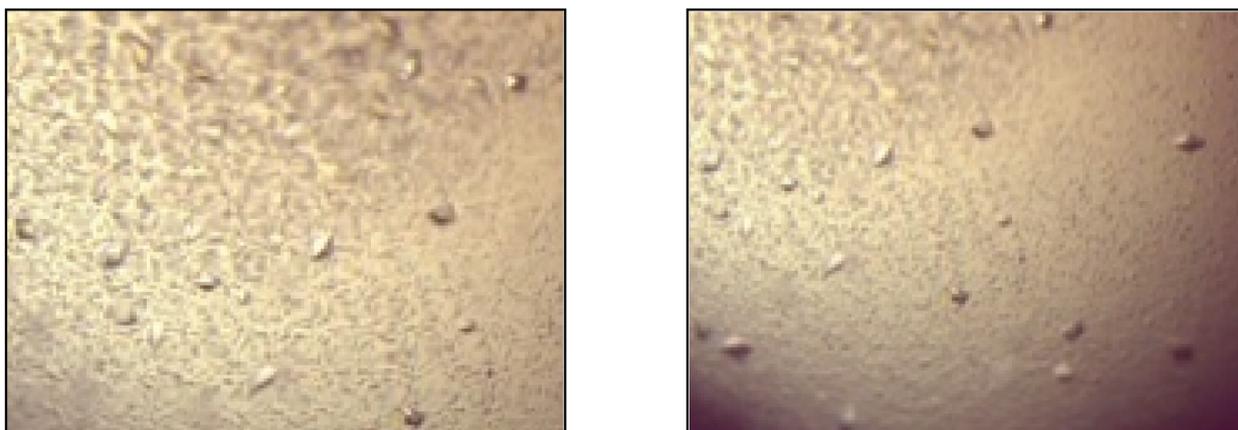
Figure 66: Crystals of the CDK8 (1-403)/CycC/MED12 (11-91) ternary complex

Crystals obtained utilizing the CDK8 (1-403)/CycC/MED12 (11-91) ternary complex at 40 mg/mL with 0.2 M sodium format (left panel) or 0.2 M lithium chloride (right panel), 20% PEG 3350 and 20 mM HEPES/NaOH pH 6.9 at 20 C. Please note that crystallization trials were carried out by Dr. Elisabeth Schneider. Meret Kuck and I provided proteins.
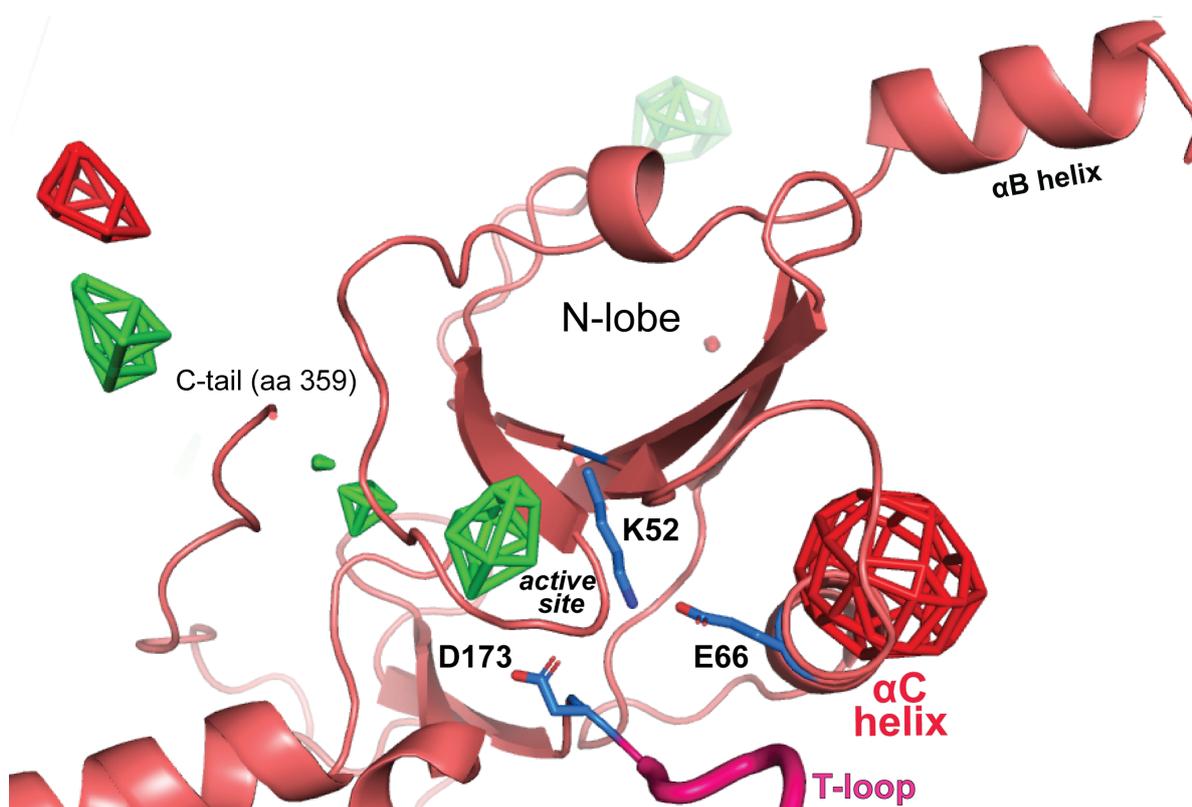
Figure 67: Preliminary structure determination of the CDK8 (1-403)/CycC/MED12 (11-91) ternary complex

Difference density (fofc) of data recorded from crystals grown of the ternary CDK8 (1-403)/CycC/MED12 (11-91) complex, as shown in Fig. 66. Data were processed in space group P4$_3$2$_1$2 to 8.6 Å using XDS (Kabsch, 2010). The structure was solved by molecular replacement using PHENIX (Adams et al., 2010) and the binary CDK8/Cyclin C complex as a reference (PDB code 3RGF). The limited resolution only allowed for a single round of rigid body refinement with PHENIX (see fofc density above). All further attepts at refinement failed due to the limited number of only 987 reflections. Please note that crystallization trials were carried out by Dr. Elisabeth Schneider. Crystals were measured at Swiss Light Source, Paul Scherer Institute (beamline X06SA) by Robin Weinmann, Franziska Langhammer and myself. Data processing and structure solution was carried out by Dr. Claus-D. Kuhn. The figure was prepared by myself using PYMOL (Schroeding_LLC, 2015).

Chapter 7: References

Adams, P.D., Afonine, P. V., Bunkóczi, G., Chen, V.B., Davis, I.W., Echols, N., Headd, J.J., Hung, L.W., Kapral, G.J., Grosse-Kunstleve, R.W., et al. (2010). PHENIX: A comprehensive Python-based system for macromolecular structure solution. Acta Crystallogr. Sect. D Biol. Crystallogr. *66*, 213–221.

Adelman, K., and Lis, J.T. (2012). Promoter-proximal pausing of RNA polymerase II: emerging roles in metazoans. Nat. Rev. Genet. *13*, 720–731.

Adler, A.S., McCleland, M.L., Truong, T., Lau, S., Modrusan, Z., Soukup, T.M., Roose-Girma, M., Blackwood, E.M., and Firestein, R. (2012). CDK8 maintains tumor dedifferentiation and embryonic stem cell pluripotency. Cancer Res. *72*, 2129–2139.

Akhtar, M.S., Heidemann, M., Tietjen, J.R., Zhang, D.W., Chapman, R.D., Eick, D., and Ansari, A.Z. (2009). TFIIH Kinase Places Bivalent Marks on the Carboxy-Terminal Domain of RNA Polymerase II. Mol. Cell *34*, 387–393.

Akoulitchev, S., Chuikov, S., and Reinberg, D. (2000). TFIIH is negatively regulated by cdk8-containing mediator complexes. Nature *407*, 102–106.

Alarcón, C., Zaromytidou, A.I., Xi, Q., Gao, S., Yu, J., Fujisawa, S., Barlas, A., Miller, A.N., Manova-Todorova, K., Macias, M.J., et al. (2009). Nuclear CDKs Drive Smad Transcriptional Activation and Turnover in BMP and TGF-β Pathways. Cell *139*, 757–769.

Allen, B.L., and Taatjes, D.J. (2015). The Mediator complex: A central integrator of transcription. Nat. Rev. Mol. Cell Biol. *16*, 155–166.

Asturias, F.J., Jiang, W.J., Myers, L.C., Gustafsson, C.M., and Kornberg, R.D. (1999). Conserved structures of Mediator and RNA polymerase holoenzyme. Science (80-.). *283*, 985–987.

Atherton-Fessler, S., Hannig, G., and Piwnica-Worms, H. (1993). Reversible tyrosine phosphorylation and cell cycle control. Semin. Cell Dev. Biol. *4*, 433–442.

Bancerek, J., Poss, Z.C., Steinparzer, I., Sedlyarov, V., Pfaffenwimmer, T., Mikulic, I., Dölken, L., Strobl, B., Müller, M., Taatjes, D.J., et al. (2013). CDK8 Kinase Phosphorylates Transcription Factor STAT1 to Selectively Regulate the Interferon Response. Immunity *38*, 250–262.

Barbieri, C.E., Baca, S.C., Lawrence, M.S., Demichelis, F., Blattner, M., Theurillat, J.P., White, T.A., Stojanov, P., Van Allen, E., Stransky, N., et al. (2012). Exome sequencing identifies recurrent SPOP, FOXA1 and MED12 mutations in prostate cancer. Nat. Genet. *44*, 685–689.

Baumli, S., Lolli, G., Lowe, E.D., Troiani, S., Rusconi, L., Bullock, A.N., Debreczeni, J.É., Knapp, S., and Johnson, L.N. (2008). The structure of P-TEFb (CDK9/cyclin T1), its complex with flavopiridol and regulation by phosphorylation. EMBO J. *27*, 1907–1918.

Bazykin, G.A., and Kochetov, A. V. (2011). Alternative translation start sites are conserved in eukaryotic genomes. Nucleic Acids Res. *39*, 567–577.

Berger, I., Fitzgerald, D.J., and Richmond, T.J. (2004). Baculovirus expression system for heterologous multiprotein complexes. Nat. Biotechnol. *22*, 1583–1587.

Berger, I., Garzoni, F., Chaillet, M., Haffke, M., Gupta, K., and Aubert, A. (2013). The MultiBac protein complex production platform at the EMBL. J. Vis. Exp. 1–8.

Bergeron, P., Koehler, M.F.T., Blackwood, E.M., Bowman, K., Clark, K., Firestein, R., Kiefer, J.R., Maskos, K., McCleland, M.L., Orren, L., et al. (2016). Design and Development of a Series of Potent and Selective Type II Inhibitors of CDK8. ACS Med. Chem. Lett. *7*, 595–600.

Bern, M., Kil, Y.J., and Becker, C. (2012). Byonic: Advanced peptide and protein

identification software. Curr. Protoc. Bioinforma. 1–14.

Bernecky, C., Grob, P., Ebmeier, C.C., Nogales, E., and Taatjes, D.J. (2011). Molecular architecture of the human Mediator-RNA polymerase II-TFIIF assembly. PLoS Biol. *9*.

Bernecky, C., Herzog, F., Baumeister, W., Plitzko, J.M., and Cramer, P. (2016). Structure of transcribing mammalian RNA polymerase II. Nature *529*, 551–554.

Bhagwat, A.S., Roe, J.S., Mok, B.Y.L., Hohmann, A.F., Shi, J., and Vakoc, C.R. (2016). BET Bromodomain Inhibition Releases the Mediator Complex from Select cis-Regulatory Elements. Cell Rep. *15*, 519–530.

Bien-Willner, G.A., Stankiewicz, P., and Lupski, J.R. (2007). SOX9cre1, a cis-acting regulatory element located 1.1 Mb upstream of SOX9, mediates its enhancement through the SHH pathway. Hum. Mol. Genet. *16*, 1143–1156.

Bienz, M., and Clevers, H. (2000). Linking colorectal cancer to Wnt signaling. Cell *103*, 311–320.

Blume-Jensen, P., and Hunter, T. (2001). Oncogenic kinase signalling. Nature *411*, 355–365.

De Bondt, H.L., Rosenblatt, J., Jancarik, J., Jones, H.D., Morgant, D.O., and Kim, S.H. (1993). Crystal structure of cyclin-dependent kinase 2. Nature *363*, 595–602.

Boube, M., Joulia, L., Cribbs, D.L., Sabatier, P., and Cedex, T. (2002). Evidence for a Mediator of RNA Polymerase II Transcriptional Regulation Conserved from Yeast to Man. Cell *110*, 143–151.

Brägelmann, J., Klümper, N., Offermann, A., and Mässenhausen, A. Von (2017). Pan-cancer analysis of the Mediator complex transcriptome identifies CDK19 and CDK8 as therapeutic targets in advanced prostate cancer. Clincal Cancer Res. *23*, 1829–1840.

Braun, K., Hölzl, G., Soucek, T., Geisen, C., Möröy, T., and Hengstschläger, M. (1998). Investigation of the cell cycle regulation of cdk3-associated kinase activity and the role of cdk3 in proliferation and transformation. Oncogene *17*, 2259–2269.

Brewster, C.D., Birkenheuer, C.H., Vogt, M.B., Quackenbush, S.L., and Rovnak, J. (2011). The retroviral cyclin of walleye dermal sarcoma virus binds cyclin-dependent kinases 3 and 8. Virology *409*, 299–307.

Card, G.L., Knowles, P., Laman, H., Jones, N., and Mcdonald, N.Q. (2000). Crystal structure of a g -herpesvirus cyclin ± cdk complex. *19*, 2877–2888.

Carrera, I., Janody, F., Leeds, N., Duveau, F., and Treisman, J.E. (2008). Pygopus activates Wingless target gene transcription through the mediator complex subunits Med12 and Med13. Proc. Natl. Acad. Sci. U. S. A. *105*, 6644–6649.

Castro, F., Cardoso, A.P., Gonçalves, R.M., Serre, K., and Oliveira, M.J. (2018). Interferon-gamma at the crossroads of tumor immune surveillance or evasion. Front. Immunol. *9*, 1–19.

Chang, J.M., Di Tommaso, P., and Notredame, C. (2014). TCS: A new multiple sequence alignment reliability measure to estimate alignment accuracy and improve phylogenetic tree reconstruction. Mol. Biol. Evol. *31*, 1625–1637.

Chapman, R.D., Heidemann, M., Hintermair, C., and Eick, D. (2008). Molecular evolution of the RNA polymerase II CTD. Trends Genet. *24*, 289–296.

Chen, Z., and Cole, P.A. (2015). Synthetic approaches to protein phosphorylation. Curr. Opin. Chem. Biol. *28*, 115–122.

Chen, M., Liang, J., Ji, H., Yang, Z., Altilia, S., Hu, B., Schronce, A., McDermott, M.S.J., Schools, G.P., Lim, C.U., et al. (2017). CDK8/19 Mediator kinases potentiate induction of transcription by NFκB. Proc. Natl. Acad. Sci. U. S. A. *114*, 10208–10213.

Cheng, A., Gerry, S., Kaldis, P., and Solomon, M.J. (2005). Biochemical characterization of Cdk2-Speedy/Ringo A2. BMC Biochem. *6*, 1–17.

Clark, A.D., Oldenbroek, M., and Boyer, T.G. (2015). Mediator kinase module and human tumorigenesis. Crit. Rev. Biochem. Mol. Biol. *50*, 393–426.

Conaway, R.C., Sato, S., Tomomori-Sato, C., Yao, T., and Conaway, J.W. (2005). The mammalian Mediator complex and its role in transcriptional regulation. Trends Biochem. Sci.

30, 250–255.

Connell-Crowley, L., Harper, J.W., and Goodrich, D.W. (1997). Cyclin D1/Cdk4 regulates retinoblastoma protein-mediated cell cycle arrest by site-specific phosphorylation. Mol. Biol. Cell *8*, 287–301.

Core, L.J., and Lis, J.T. (2008). Transcription regulation through promoter-proximal pausing of RNA polymerase II. Science (80-.). *319*, 1791–1792.

Cramer, P. (2019). Organization and regulation of gene transcription. Nature *573*, 45–54.

Crick, F., and Watson, J. (1953). Molecular Structure of Nucleic Acids: A Structure for Deoxyribose Nucleic Acid. Nature *171*, 737–738.

Dale, T., Clarke, P.A., Esdar, C., Waalboer, D., Adeniji-Popoola, O., Ortiz-Ruiz, M.J., Mallinger, A., Samant, R.S., Czodrowski, P., Musil, D., et al. (2015). A selective chemical probe for exploring the role of CDK8 and CDK19 in human disease. Nat. Chem. Biol. *11*, 973–980.

Dannappel, M.V., Sooraj, D., Loh, J.J., and Firestein, R. (2019). Molecular and in vivo Functions of the CDK8 and CDK19 Kinase Modules. Front. Cell Dev. Biol. *6*, 1–9.

Darooei, M., Khan, F., Rehan, M., Zubeda, S., Jeyashanker, E., Annapurna, S., Shah, A., Maddali, S., and Hasan, Q. (2019). MED12 somatic mutations encompassing exon 2 associated with benign breast fibroadenomas and not breast carcinoma in Indian women. J. Cell. Biochem. *120*, 182–191.

Deng, W., Rupon, J.W., Krivega, I., Breda, L., Motta, I., Jahn, K.S., Reik, A., Gregory, P.D., Rivella, S., Dean, A., et al. (2014). Reactivation of developmentally silenced globin genes by forced chromatin looping. Cell *158*, 849–860.

Denicourt, C., and Dowdy, S.F. (2004). Cip/Kip proteins: More than just CDKs inhibitors. Genes Dev. *18*, 851–855.

Diehl, J.A. (2002). Cycling to cancer with cyclin D1. Cancer Biol. Ther. *1*, 226–231.

Ding, N., Zhou, H., Esteve, P.O., Chin, H.G., Kim, S., Xu, X., Joseph, S.M., Friez, M.J., Schwartz, C.E., Pradhan, S., et al. (2008). Mediator Links Epigenetic Silencing of Neuronal Gene Expression with X-Linked Mental Retardation. Mol. Cell *31*, 347–359.

Dixon-Clarke, S.E., Elkins, J.M., Cheng, S.W.G., Morin, G.B., and Bullock, A.N. (2015). Structures of the CDK12/CycK complex with AMP-PNP reveal a flexible C-terminal kinase extension important for ATP binding. Sci. Rep. *5*, 1–13.

Donner, A.J., Szostek, S., Hoover, J.M., and Espinosa, J.M. (2007). CDK8 Is a Stimulus-Specific Positive Coregulator of p53 Target Genes. Mol. Cell *27*, 121–133.

Dowen, J.M., Fan, Z.P., Hnisz, D., Ren, G., Abraham, B.J., Zhang, L.N., Weintraub, A.S., Schuijers, J., Lee, T.I., Zhao, K., et al. (2014). Control of cell identity genes occurs in insulated neighborhoods in mammalian chromosomes. Cell *159*, 374–387.

Echalier, A., Endicott, J.A., and Noble, M.E.M. (2010). Recent developments in cyclin-dependent kinase biochemical and structural studies. Biochim. Biophys. Acta - Proteins Proteomics *1804*, 511–519.

Eick, D., and Geyer, M. (2013). The RNA polymerase II carboxy-terminal domain (CTD) code. Chem. Rev. *113*, 8456–8490.

El-Gebali, S., Mistry, J., Bateman, A., Eddy, S.R., Luciani, A., Potter, S.C., Qureshi, M., Richardson, L.J., Salazar, G.A., Smart, A., et al. (2019). The Pfam protein families database in 2019. Nucleic Acids Res. *47*, D427–D432.

Elmlund, H., Baraznenok, V., Lindahl, M., Samuelsen, C.O., Koeck, P.J.B., Holmberg, S., Hebert, H., and Gustafsson, C.M. (2006). The cyclin-dependent kinase 8 module sterically blocks Mediator interactions with RNA polymerase II. Proc. Natl. Acad. Sci. U. S. A. *103*, 15788–15793.

Endicott, J.A., and Noble, M.E.M. (2013). Structural characterization of the cyclin-dependent protein kinase family. Biochem. Soc. Trans. *41*, 1008–1016.

Esnault, C., Ghavi-Helm, Y., Brun, S., Soutourina, J., Van Berkum, N., Boschiero, C.,

Holstege, F., and Werner, M. (2008). Mediator-Dependent Recruitment of TFIIH Modules in Preinitiation Complex. Mol. Cell *31*, 337–346.

Espinosa, J.M. (2019). Transcriptional CDKs in the spotlight. Transcription *10*, 45–46.

Firestein, R., Bass, A.J., Kim, S.Y., Dunn, I.F., Silver, S.J., Guney, I., Freed, E., Ligon, A.H., Vena, N., Ogino, S., et al. (2008). CDK8 is a colorectal cancer oncogene that regulates β-catenin activity. Nature *455*, 547–551.

Firestein, R., Shima, K., Nosho, K., Irahara, N., Baba, Y., Bojarski, E., Giovannucci, E.L., Hahn, W.C., Fuchs, C.S., and Ogino, S. (2010). CDK8 expression in 470 colorectal cancers in relation to β-catenin activation, other molecular alterations and patient survival. Int. J. Cancer *126*, 2863–2873.

Fisher, R.P. (2005). Secrets of a double agent: CDK7 in cell-cycle control and transcription. J. Cell Sci. *118*, 5171–5180.

Fitzgerald, D.J., Berger, P., Schaffitzel, C., Yamada, K., Richmond, T.J., and Berger, I. (2006). Protein complex expression by using multigene baculoviral vectors. Nat. Methods *3*, 1021–1032.

Force, T., and Kolaja, K.L. (2011). Cardiotoxicity of kinase inhibitors: The prediction and translation of preclinical models to clinical outcomes. Nat. Rev. Drug Discov. *10*, 111–126.

Fryer, C.J., White, J.B., Jones, K.A., and Jolla, L. (2004). Mastermind Recruits CycC:CDK8 to Phosphorylate the NOTCH ICD and Coordinate Activation with Turnover. Mol. Cell *16*, 1–12.

Fuda, N.J., Ardehali, M.B., and Lis, J.T. (2009). Defining mechanisms that regulate RNA polymerase II transcription in vivo. Nature *461*, 186–192.

Galbraith, M.D., Donner, A.J., and Espinosa, J.M. (2010). CDK8: A positive regulator of transcription elongation within the serum response network. Transcription *1*, 4–12.

Galbraith, M.D., Allen, M.A., Bensard, C.L., Wang, X., Schwinn, M.K., Qin, B., Long, H.W., Daniels, D.L., Hahn, W.C., Dowell, R.D., et al. (2013). HIF1A employs CDK8-mediator to stimulate RNAPII elongation in response to hypoxia. Cell *153*, 1327.

Galbraith, M.D., Andrysik, Z., Pandey, A., Hoh, M., Bonner, E.A., Hill, A.A., Sullivan, K.D., and Espinosa, J.M. (2017). CDK8 Kinase Activity Promotes Glycolysis. Cell Rep. *21*, 1495–1506.

Garrett, S., Barton, W.A., Knights, R., Jin, P., Morgan, D.O., and Fisher, R.P. (2001). Reciprocal Activation by Cyclin-Dependent Kinases 2 and 7 Is Directed by Substrate Specificity Determinants outside the T Loop. Mol. Cell. Biol. *21*, 88–99.

Gibson, D.G., Young, L., Chuang, R.Y., Venter, J.C., Hutchison, C.A., and Smith, H.O. (2009). Enzymatic assembly of DNA molecules up to several hundred kilobases. Nat. Methods *6*, 343–345.

Gilmourt, D.S., and Lis, J.T. (1986). RNA Polymerase II interacts with the Promotor Region of the Noninduced hsp70 Gene in Drosophila melanogaster Cells. Mol. Cell. Biol. *6*, 3984–3989.

Di Giulio, M., and Kreitman, M. (2009). Journal of Molecular Evolution: Introduction. J. Mol. Evol. *69*, 405.

Glover-Cutter, K., Larochelle, S., Erickson, B., Zhang, C., Shokat, K., Fisher, R.P., and Bentley, D.L. (2009). TFIIH-Associated Cdk7 Kinase Functions in Phosphorylation of C-Terminal Domain Ser7 Residues, Promoter-Proximal Pausing, and Termination by RNA Polymerase II. Mol. Cell. Biol. *29*, 5455–5464.

Graham, J.M., and Schwartz, C.E. (2013). MED12 related disorders. Am. J. Med. Genet. Part A *161*, 2734–2740.

Graham, M.J., Combe, C., Kolbowski, L., and Rappsilber, J. (2019). xiView: A common platform for the downstream analysis of Crosslinking Mass Spectrometry data. BioRxiv 1–5.

Greber, B.J., Nguyen, T.H.D., Fang, J., Afonine, P. V., Adams, P.D., and Nogales, E. (2020). The cryo-electron microscopy structure of human CDK-activating kinase. Proc. Natl. Acad.

Sci. *549*, 414–417.

Guenther, M.G., Levine, S.S., Boyer, L.A., Jaenisch, R., and Young, R.A. (2007). A Chromatin Landmark and Transcription Initiation at Most Promoters in Human Cells. Cell *130*, 77–88.

Guo, Z., and Stiller, J.W. (2004). Comparative genomics of cyclin-dependent kinases suggest co-evolution of the RNAP II C-terminal domain and CTD-directed CDKs. BMC Genomics *5*, 1–13.

Guo, Z., Wang, G., Lv, Y., Wan, Y.Y., and Zheng, J. (2019). Inhibition of Cdk8/Cdk19 activity promotes treg cell differentiation and suppresses autoimmune diseases. Front. Immunol. *10*, 1–10.

Hanahan, D., and Weinberg, R.A. (2011). Hallmarks of cancer: The next generation. Cell *144*, 646–674.

Harper, J.W., Elledge, S.J., Keyomarsi, K., Dynlacht, B., Tsai, L.H., Zhang, P., Dobrowolski, S., Bai, C., Connell-Crowley, L., Swindell, E., et al. (1995). Inhibition of cyclin-dependent kinases by p21. Mol. Biol. Cell *6*, 387–400.

Hartwell, L.H., Culotti, J., Pringle, J.R., and Reid, B.J. (1974). Genetic Control of the Cell Division Cycle in Yeast: A model to account for the order of cell cycle events is deduced from the phenotypes of yeast mutants. Science (80-.). *183*, 46–51.

Heikkinen, T., Kämpjärvi, K., Keskitalo, S., von Nandelstadh, P., Liu, X., Rantanen, V., Pitkänen, E., Kinnunen, M., Kuusanmäki, H., Kontro, M., et al. (2017). Somatic MED12 Nonsense Mutation Escapes mRNA Decay and Reveals a Motif Required for Nuclear Entry. Hum. Mutat. *38*, 269–274.

Heinz, S., Romanoski, C.E., Benner, C., and Glass, C.K. (2015). The selection and function of cell type-specific enhancers. Nat. Rev. Mol. Cell Biol. *16*, 144–154.

Hengartner, C.J., Myer, V.E., Liao, S.M., Wilson, C.J., Koh, S.S., and Young, R.A. (1999). Temporal regulation of RNA polymerase II by Srbl0 and Kin28 cyclin-dependent kinases. Chemtracts *12*, 933–937.

Hengattner, C.J., Thompson, C.M., Zhang, J., Chao, D.M., Liao, S.M., Koleske, A.J., Okamura, S., and Young, R.A. (1995). Association of an activator with an RNA polymerase II holoenzyme. Genes Dev. *9*, 897–910.

Hill, P.J., and Stewart, G.S.A.B. (1992). The polymerase chain reaction in molecular and micro-biology. Biotechnol. Genet. Eng. Rev. *10*, 343–377.

Hiscott, J., Pitha, P., Genin, P., Nguyen, H., Heylbroeck, C., Mamane, Y., Algarte, M., and Lin, R. (1999). Triggering the interferon response: The role of IRF-3 transcription factor. J. Interf. Cytokine Res. *19*, 1–13.

Hoeppner, S., Baumli, S., and Cramer, P. (2005). Structure of the mediator subunit cyclin C and its implications for CDK8 function. J. Mol. Biol. *350*, 833–842.

Hofmann, F., and Livingston, D.M. (1996). Differential effects of cdk2 and cdk3 on the control of pRb and E2F function during G1 exit. Genes Dev. *10*, 851–861.

Holzwarth, G., and Doty, P. (1965). The Ultraviolet Circular Dichroism of Polypeptides. J. Am. Chem. Soc. *87*, 218–228.

Huang, K., Ferrin-O'Connell, I., Zhang, W., Leonard, G.A., O'Shea, E.K., and Quiocho, F.A.A. (2007). Structure of the Pho85-Pho80 CDK-Cyclin Complex of the Phosphate-Responsive Signal Transduction Pathway. Mol. Cell *28*, 614–623.

Huang, S., Hölzel, M., Knijnenburg, T., Schlicker, A., Roepman, P., McDermott, U., Garnett, M., Grernrum, W., Sun, C., Prahallad, A., et al. (2012). MED12 controls the response to multiple cancer drugs through regulation of TGF-β receptor signaling. Cell *151*, 937–950.

Hunter, T. (1995). Protein kinases and phosphatases: The Yin and Yang of protein phosphorylation and signaling. Cell *80*, 225–236.

Huse, M., and Kuriyan, J. (2002). The conformational plasticity of protein kinases. Cell *109*, 275–282.

Jeffrey, P.D., Russo, A.A., Polyak, K., Gibbs, E., Hurwitz, J., Massagué, J., and Pavletich, N.P. (1995). Mechanism of CDK activation revealed by the structure of a cyclinA-CDK2 complex. Nature *376*, 313–320.

Jin, L., Wang, W., and Fang, G. (2014). Targeting Protein-Protein Interaction by Small Molecules. Annu. Rev. Pharmacol. Toxicol. *54*, 435–456.

Johannessen, L., Sundberg, T.B., O'Connell, D.J., Kolde, R., Berstler, J., Billings, K.J., Khor, B., Seashore-Ludlow, B., Fassl, A., Russell, C.N., et al. (2017). Small-molecule studies identify CDK8 as a regulator of IL-10 in myeloid cells. Nat. Chem. Biol. *13*, 1102–1108.

Johnson, L.N., Noble, M.E.M., and Owen, D.J. (1996). Active and inactive protein kinases: Structural basis for regulation. Cell *85*, 149–158.

Kabsch, W. (2010). Integration, scaling, space-group assignment and post-refinement. Acta Crystallogr. Sect. D Biol. Crystallogr. *66*, 133–144.

Kagey, M.H., Newman, J.J., Bilodeau, S., Zhan, Y., Orlando, D.A., Van Berkum, N.L., Ebmeier, C.C., Goossens, J., Rahl, P.B., Levine, S.S., et al. (2010). Mediator and cohesin connect gene expression and chromatin architecture. Nature *467*, 430–435.

Kamachi, Y., and Kondoh, H. (2013). Sox proteins: Regulators of cell fate specification and differentiation. Dev. *140*, 4129–4144.

Kämpjärvi, K., Mäkinen, N., Kilpivaara, O., Arola, J., Heinonen, H.R., Böhm, J., Abdel-Wahab, O., Lehtonen, H.J., Pelttari, L.M., Mehine, M., et al. (2012). Somatic MED12 mutations in uterine leiomyosarcoma and colorectal cancer. Br. J. Cancer *107*, 1761–1765.

Kämpjärvi, K., Park, M.J., Mehine, M., Kim, N.H., Clark, A.D., Bützow, R., Böhling, T., Böhm, J., Mecklin, J.P., Järvinen, H., et al. (2014). Mutations in exon 1 highlight the role of MED12 in uterine leiomyomas. Hum. Mutat. *35*, 1136–1141.

Kämpjärvi, K., Järvinen, T.M., Heikkinen, T., Ruppert, A.S., Senter, L., Hoag, K.W., Dufva, O., Kontro, M., Rassenti, L., Hertlein, E., et al. (2015). Somatic MED12 mutations are associated with poor prognosis markers in chronic lymphocytic leukemia. Oncotarget *6*, 1884–1888.

Kämpjärvi, K., Kim, N.H., Keskitalo, S., Clark, A.D., Von Nandelstadh, P., Turunen, M., Heikkinen, T., Park, M.J., Mäkinen, N., Kivinummi, K., et al. (2016). Somatic MED12 mutations in prostate cancer and uterine leiomyomas promote tumorigenesis through distinct mechanisms. Prostate *76*, 22–31.

Kanamori, Y., and Nakashima, N. (2001). A tertiary structure model of the internal ribosome entry site (IRES) for methionine-independent initiation of translation. Rna *7*, 266–274.

Kapoor, A., Goldberg, M.S., Cumberland, L.K., Ratnakumar, K., Segura, M.F., Emanuel, P.O., Menendez, S., Vardabasso, C., LeRoy, G., Vidal, C.I., et al. (2010). The histone variant macroH2A suppresses melanoma progression through regulation of CDK8. Nature *468*, 1105–1111.

Keightley, M.C., Nilsson, S.K., and Lieschke, G.J. (2017). MED12 in hematopoietic stem cells - Cell specific function despite ubiquitous expression. Stem Cell Investig. *2017*, 2–6.

Kelleher, R.J., Flanagan, P.M., and Kornberg, R.D. (1990). A novel mediator between activator proteins and the RNA polymerase II transcription apparatus. Cell *61*, 1209–1215.

Kibbe, W.A. (2007). OligoCalc: An online oligonucleotide properties calculator. Nucleic Acids Res. *35*, 43–46.

Kim, N.H., Livi, C.B., Yew, P.R., and Boyer, T.G. (2016). Mediator subunit Med12 contributes to the maintenance of neural stem cell identity. BMC Dev. Biol. *16*, 1–15.

Kim, Y.J., Björklund, S., Li, Y., Sayre, M.H., and Kornberg, R.D. (1994). A multiprotein mediator of transcriptional activation and its interaction with the C-terminal repeat domain of RNA polymerase II. Cell *77*, 599–608.

Klatt, F., Leitner, A., Kim, I. V., Ho-Xuan, H., Schneider, E. V., Langhammer, F., Weinmann, R., Müller, M.R., Huber, R., Meister, G., et al. (2020). A precisely positioned MED12 activation helix stimulates CDK8 kinase activity. Proc. Natl. Acad. Sci. U. S. A. *117*,

2894–2905.

Knorre, D.G. (1999). RNA polymerase II. Mol. Biol. *33*, 129–134.

Knuesel, M.T., Meyer, K.D., Donner, A.J., Espinosa, J.M., and Taatjes, D.J. (2009a). The Human CDK8 Subcomplex Is a Histone Kinase That Requires Med12 for Activity and Can Function Independently of Mediator. Mol. Cell. Biol. *29*, 650–661.

Knuesel, M.T., Meyer, K.D., Bernecky, C., and Taatjes, D.J. (2009b). The human CDK8 subcomplex is a molecular switch that controls Mediator coactivator function. Genes Dev. *23*, 439–451.

Kornberg, R.D. (2005). Mediator and the mechanism of transcriptional activation. Trends Biochem. Sci. *30*, 235–239.

Kornberg, R., and Thomas, J. (1974). Oligomers of the Histones. Science (80-.). *184*, 865–868.

Kufareva, I., and Abagyan, R. (2008). Type-II kinase inhibitor docking, screening, and profiling using modified structures of active kinase states. J. Med. Chem. *51*, 7921–7932.

Kuuluvainen, E., Domènech-Moreno, E., Niemelä, E.H., and Mäkelä, T.P. (2018). Depletion of Mediator Kinase Module Subunits Represses Superenhancer-Associated Genes in Colon Cancer Cells. Mol. Cell. Biol. *38*.

L. Daniels, D. (2013). Mutual Exclusivity of MED12/MED12L, MED13/13L, and CDK8/19 Paralogs Revealed within the CDK-Mediator Kinase Module. J. Proteomics Bioinform. *01*.

Lai, F., Orom, U.A., Cesaroni, M., Beringer, M., Taatjes, D.J., Blobel, G.A., and Shiekhattar, R. (2013). Activating RNAs associate with Mediator to enhance chromatin architecture and transcription. Nature *494*, 497–501.

Lamiable, A., Thévenet, P., Rey, J., Vavrusa, M., Derreumaux, P., and Tufféry, P. (2016). PEP-FOLD3: faster de novo structure prediction for linear peptides in solution and in complex. Nucleic Acids Res. *44*, W449–W454.

Larivière, L., Seizl, M., and Cramer, P. (2012). A structural perspective on Mediator function. Curr. Opin. Cell Biol. *24*, 305–313.

Larochelle, S., Amat, R., Glover-Cutter, K., Sansó, M., Zhang, C., Allen, J.J., Shokat, K.M., Bentley, D.L., and Fisher, R.P. (2012). Cyclin-dependent kinase control of the initiation-to-elongation switch of RNA polymerase II. Nat. Struct. Mol. Biol. *19*, 1108–1115.

Lawrence, M.S., Stojanov, P., Mermel, C.H., Robinson, J.T., Garraway, L.A., Golub, T.R., Meyerson, M., Gabriel, S.B., Lander, E.S., and Getz, G. (2014). Discovery and saturation analysis of cancer genes across 21 tumour types. Nature *505*, 495–501.

Lee, T.I., and Young, R.A. (2013). Transcriptional regulation and its misregulation in disease. Cell *152*, 1237–1251.

Lehner, B., Crombie, C., Tischler, J., Fortunato, A., and Fraser, A.G. (2006). Systematic mapping of genetic interactions in Caenorhabditis elegans identifies common modifiers of diverse signaling pathways. Nat. Genet. *38*, 896–903.

Lim, S., and Kaldis, P. (2013). Cdks, cyclins and CKIs: Roles beyond cell cycle regulation. Dev. *140*, 3079–3093.

Liu, J., and Kipreos, E.T. (2000). Evolution of cyclin-dependent kinases (CDKs) and CDK-activating kinases (CAKs): Differential conservation of CAKs in yeast and metazoa. Mol. Biol. Evol. *17*, 1061–1074.

Liu, L., Spurrier, J., Butt, T.R., and Strickler, J.E. (2008). Enhanced protein expression in the baculovirus/insect cell system using engineered SUMO fusions. Protein Expr. Purif. *62*, 21–28.

Liu, Z., Chen, O., Wall, J.B.J., Zheng, M., Zhou, Y., Wang, L., Ruth Vaseghi, H., Qian, L., and Liu, J. (2017). Systematic comparison of 2A peptides for cloning multi-genes in a polycistronic vector. Sci. Rep. *7*, 1–9.

Lolli, G. (2010). Structural dissection of cyclin dependent kinases regulation and protein recognition properties. Cell Cycle *9*, 1551–1561.

Lolli, G., Lowe, E.D., Brown, N.R., and Johnson, L.N. (2004). The crystal structure of human CDK7 and its protein recognition properties. Structure *12*, 2067–2079.

Loncle, N., Boube, M., Joulia, L., Boschiero, C., Werner, M., Cribbs, D.L., and Bourbon, H.M. (2007). Distinct roles for Mediator Cdk8 module subunits in Drosophila development. EMBO J. *26*, 1045–1054.

Luo, P., and Baldwin, R.L. (1997). Mechanism of helix induction by trifluoroethanol: A framework for extrapolating the helix-forming properties of peptides from trifluoroethanol/water mixtures back to water. Biochemistry *36*, 8413–8421.

Madeira, F., Park, Y.M., Lee, J., Buso, N., Gur, T., Madhusoodanan, N., Basutkar, P., Tivey, A.R.N., Potter, S.C., Finn, R.D., et al. (2019). The EMBL-EBI search and sequence analysis tools APIs in 2019. Nucleic Acids Res. *47*, W636–W641.

Mäkinen, N., Mehine, M., Tolvanen, J., Kaasinen, E., Li, Y., Lehtonen, H.J., Gentile, M., Yan, J., Enge, M., Taipale, M., et al. (2011). MED12, the mediator complex subunit 12 gene, is mutated at high frequency in uterine leiomyomas. Science (80-.). *334*, 252–255.

Malik, S., and Roeder, R.G. (2005). Dynamic regulation of pol II transcription by the mammalian Mediator complex. Trends Biochem. Sci. *30*, 256–263.

Malik, S., and Roeder, R.G. (2010). The metazoan Mediator co-activator complex as an integrative hub for transcriptional regulation. Nat. Rev. Genet. *11*, 761–772.

Malumbres, M. (2014). Cyclin-dependent kinases. Genome Biol. *15*, 1–10.

Malumbres, M., and Barbacid, M. (2001). To Cycle Or Not To Cycle: A Critical Decision in Cancer. Nat. Rev. Cancer *1*, 222–231.

Manning, G., Whyte, D.B., Martinez, R., Hunter, T., and Sudarsanam, S. (2002). The protein kinase complement of the human genome. Science (80-.). *298*, 1912–1934.

Mark, W.Y., Liao, J.C.C., Lu, Y., Ayed, A., Laister, R., Szymczyna, B., Chakrabartty, A., and Arrowsmith, C.H. (2005). Characterization of segments from the central region of BRCA1: An intrinsically disordered scaffold for multiple protein-protein and protein-DNA interactions? J. Mol. Biol. *345*, 275–287.

Massagué, J. (2008). TGFβ in Cancer. Cell *134*, 215–230.

McCleland, M.L., Soukup, T.M., Liu, S.D., Esensten, J.H., De Sousa E Melo, F., Yaylaoglu, M., Warming, S., Roose-Girma, M., and Firestein, R. (2015). Cdk8 deletion in the ApcMin murine tumour model represses EZH2 activity and accelerates tumourigenesis. J. Pathol. *237*, 508–519.

McGrath, D.A., Fifield, B., Marceau, A.H., Tripathi, S., Porter, L.A., and Rubin, S.M. (2017). Structural basis of divergent cyclin-dependent kinase activation by Spy1/ RINGO proteins . EMBO J. *36*, 2251–2262.

Meyerson, M., Enders, G.H., Wu, C.L., Su, L.K., Gorka, C., Nelson, C., Harlow, E., and Tsai, L.H. (1992). A family of human cdc2-related protein kinases. EMBO J. *11*, 2909–2917.

Morgan, D.O. (1995). Principles of CDK regulation. Nature *374*, 131–134.

Morgan, D.O. (1997). Cyclin-dependent Kinases: Engines, Clocks, and Microprocessors. Annu. Rev. Cell Dev. Biol. *13*, 261–291.

Morris, E.J., Ji, J.Y., Yang, F., Di Stefano, L., Herr, A., Moon, N.S., Kwon, E.J., Haigis, K.M., Näär, A.M., and Dyson, N.J. (2008). E2F1 represses β-catenin transcription and is antagonized by both pRB and CDK8. Nature *455*, 552–556.

Muncke, N., Jung, C., Rüdiger, H., Ulmer, H., Roeth, R., Hubert, A., Goldmuntz, E., Driscoll, D., Goodship, J., Schön, K., et al. (2003). Missense Mutations and Gene Interruption in PROSIT240, a Novel TRAP240-Like Gene, in Patients with Congenital Heart Defect (Transposition of the Great Arteries). Circulation *108*, 2843–2850.

Myers, L.C., Gustafsson, C.M., Bushnell, D.A., Lui, M., Erdjument-Bromage, H., Tempst, P., and Kornberg, R.D. (1998). The Med proteins of yeast and their function through the RNA polymerase II carboxy-terminal domain. Genes Dev. *12*, 45–54.

Nair, D., Kim, Y., and Myers, L.C. (2005). Mediator and TFIIH govern carboxyl-terminal

domain-dependent transcription in yeast extracts. J. Biol. Chem. *280*, 33739–33748.

Nakanishi, M., Ando, H., Watanabe, N., Kitamura, K., Ito, K., Okayama, H., Miyamoto, T., Agui, T., and Sasaki, M. (2000). Identification and characterization of human Wee1B, a new member of the Wee1 family of Cdk-inhibitory kinases. Genes to Cells *5*, 839–847.

Nemet, J., Jelicic, B., Rubelj, I., and Sopta, M. (2014). The two faces of Cdk8, a positive/negative regulator of transcription. Biochimie *97*, 22–27.

Nitulescu, I.I., Meyer, S.C., Wen, Q.J., Crispino, J.D., Lemieux, M.E., Levine, R.L., Pelish, H.E., and Shair, M.D. (2017). Mediator Kinase Phosphorylation of STAT1 S727 Promotes Growth of Neoplasms With JAK-STAT Activation. EBioMedicine *26*, 112–125.

Nolen, B., Taylor, S., and Ghosh, G. (2004). Regulation of protein kinases: Controlling activity through activation segment conformation. Mol. Cell *15*, 661–675.

Oppermann, F.S., Gnad, F., Olsen, J. V., Hornberger, R., Greff, Z., Kéri, G., Mann, M., and Daub, H. (2009). Large-scale proteomics analysis of the human kinome. Mol. Cell. Proteomics *8*, 1751–1764.

Orphanides, G., Lagrange, T., and Reinberg, D. (1996). The general transcription factors of RNA polymerase II. Genes Dev. *10*, 2657–2683.

Osusky, M., Taylor, S.J., and Shalloway, D. (1995). Autophosphorylation of purified c-Src at its primary negative regulation site. J. Biol. Chem. *270*, 25729–25732.

Oswald, T., Avery, M., Colin, M., and MacLeod, MD and Maclyn McCarty, M. (1944). Studies on the chemical nature of the substrate inducing transformation of pneumococcal types. J. Exp. Med. *79*, 137–158.

Pargellis, C., Tong, L., Churchill, L., Cirillo, P.F., Gilmore, T., Graham, A.G., Grob, P.M., Hickey, E.R., Moss, N., Pav, S., et al. (2002). Inhibition of p38 MAP kinase by utilizing a novel allosteric binding site. Nat. Struct. Biol. *9*, 268–272.

Park, M.J., Shen, H., Spaeth, J.M., Tolvanen, J.H., Failor, C., Knudtson, J.F., McLaughlin, J., Halder, S.K., Yang, Q., Bulun, S.E., et al. (2018). Oncogenic exon 2 mutations in Mediator subunit MED12 disrupt allosteric activation of cyclin C-CDK8/19. J. Biol. Chem. *293*, 4870–4882.

Pavletich, N.P. (1999). Mechanisms of cyclin-dependent kinase regulation: Structures of Cdks, their cyclin activators, and Cip and INK4 inhibitors. J. Mol. Biol. *287*, 821–828.

Pelish, H.E., Liau, B.B., Nitulescu, I.I., Tangpeerachaikul, A., Poss, Z.C., Da Silva, D.H., Caruso, B.T., Arefolov, A., Fadeyi, O., Christie, A.L., et al. (2015). Mediator kinase inhibition further activates super-enhancer-associated genes in AML. Nature *526*, 273–276.

Perez-Riverol, Y., Csordas, A., Bai, J., Bernal-Llinares, M., Hewapathirana, S., Kundu, D.J., Inuganti, A., Griss, J., Mayer, G., Eisenacher, M., et al. (2019). The PRIDE database and related tools and resources in 2019: Improving support for quantification data. Nucleic Acids Res. *47*, D442–D450.

Peroutka, R.J., Elshourbagy, N., Piech, T., and Butt, T.R. (2008). Enhanced protein expression in mammalian cells using engineered SUMO fusions: Secreted phospholipase A 2 . Protein Sci. *17*, 1586–1595.

Phatnani, H.P., and Greenleaf, A.L. (2006). Phosphorylation and functions of the RNA polymerase II CTD. Genes Dev. *20*, 2922–2936.

Philibert, R.A., and Madan, A. (2007). Role of MED12 in transcription and human behavior. Pharmacogenomics *8*, 909–916.

Philibert, R.A., King, B.H., Winfield, S., Cook, E.H., Lee, Y.H., Stubblefield, B., Damschroder-Williams, P., Dea, C., Palotie, A., Tengstrom, C., et al. (1998). Association of an X-chromosome dodecamer insertional variant allele with mental retardation. Mol. Psychiatry *3*, 303–309.

Philibert, R.A., Winfield, S.L., Damschroder-Williams, P., Tengstrom, C., Martin, B.M., and Ginns, E.I. (1999). The genomic structure and developmental expression patterns of the human OPA-containing gene (HOPA). Hum. Genet. *105*, 174–178.

Phillips-Cremins, J.E., Sauria, M.E.G., Sanyal, A., Gerasimova, T.I., Lajoie, B.R., Bell, J.S.K., Ong, C.T., Hookway, T.A., Guo, C., Sun, Y., et al. (2013). Architectural protein subclasses shape 3D organization of genomes during lineage commitment. Cell *153*, 1281–1295.

Pines, J. (1999). Four-Dimensional control of the cell cycle. Nat. Cell Biol. *1*, E73–E79.

Pinhero, R., Liaw, P., Bertens, K., and Yankulov, K. (2004). Three cyclin-dependent kinases preferentially phosphorylate different parts of the C-terminal domain of the large subunit of RNA polymerase II. Eur. J. Biochem. *271*, 1004–1014.

Pomerening, J.R., Sontag, E.D., and Ferrell, J.E. (2003). Building a cell cycle oscillator: Hysteresis and bistability in the activation of Cdc2. Nat. Cell Biol. *5*, 346–351.

Poss, Z.C., Ebmeier, C.C., and Taatjes, D.J. (2013). The Mediator complex and transcription regulation. Crit. Rev. Biochem. Mol. Biol. *48*, 575–608.

Poss, Z.C., Ebmeier, C.C., Odell, A.T., Tangpeerachaikul, A., Lee, T., Pelish, H.E., Shair, M.D., Dowell, R.D., Old, W.M., and Taatjes, D.J. (2016). Identification of Mediator Kinase Substrates in Human Cells using Cortistatin A and Quantitative Phosphoproteomics. Cell Rep. *15*, 436–450.

Quevedo, M., Meert, L., Dekker, M.R., Dekkers, D.H.W., Brandsma, J.H., van den Berg, D.L.C., Ozgür, Z., IJcken, W.F.J. va., Demmers, J., Fornerod, M., et al. (2019). Mediator complex interaction partners organize the transcriptional network that defines neural stem cells. Nat. Commun. *10*.

Ren, S., and Rollins, B.J. (2004). Cyclin C/Cdk3 promotes Rb-dependent G0 exit. Cell *117*, 239–251.

Rickert, P., Corden, J.L., and Lees, E. (1999). Cyclin C/CDK8 and cyclin H/CDK7/p36 are biochemically distinct CTD kinases. Oncogene *18*, 1093–1102.

Robinson, P.J., Trnka, M.J., Bushnell, D.A., Davis, R.E., Mattei, P.J., Burlingame, A.L., and Kornberg, R.D. (2016). Structure of a Complete Mediator-RNA Polymerase II Pre-Initiation Complex. Cell *166*, 1411-1422.e16.

Rocha, P.P., Scholze, M., Bleiß, W., and Schrewe, H. (2010). Med12 is essential for early mouse development and for canonical Wnt and Wnt/PCP signaling. Development *137*, 2723–2731.

Rovnak, J., Brewster, C.D., and Quackenbush, S.L. (2012). Retroviral Cyclin Enhances Cyclin-Dependent Kinase-8 Activity. J. Virol. *86*, 5742–5751.

Russo, A.A., Jeffrey, P.D., Patten, A.K., Massagué, J., and Pavletich, N.P. (1996). Crystal structure of the p27(Kip1) cyclin-dependent-kinase inhibitor bound to the cyclin A-Cdk2 complex. Nature *382*, 325–331.

Rzymski, T., Mikula, M., Wiklik, K., and Brzózka, K. (2015). CDK8 kinase - An emerging target in targeted cancer therapy. Biochim. Biophys. Acta - Proteins Proteomics *1854*, 1617–1629.

Sadzak, I., Schiff, M., Gattermeier, I., Glinitzer, R., Sauer, I., Saalmüller, A., Yang, E., Schaljo, B., and Kovarik, P. (2008). Recruitment of Stat1 to chromatin is required for interferon-induced serine phosphorylation of Stat1 transactivation domain. Proc. Natl. Acad. Sci. U. S. A. *105*, 8944–8949.

Schilbach, S., Hantsche, M., Tegunov, D., Dienemann, C., Wigge, C., Urlaub, H., and Cramer, P. (2017). Structures of transcription pre-initiation complex with TFIIH and Mediator. Nature *551*, 204–209.

Schneider, E., Kartarius, S., Schuster, N., and Montenarh, M. (2002). The cyclin h/cdk7/mat1 kinase activity is regulated by CK2 phosphorylation of cyclin H. Oncogene *21*, 5031–5037.

Schneider, E. V., Böttcher, J., Blaesse, M., Neumann, L., Huber, R., and Maskos, K. (2011). The structure of CDK8/CycC implicates specificity in the CDK/cyclin family and reveals interaction with a deep pocket binder. J. Mol. Biol. *412*, 251–266.

Schneider, E. V., Böttcher, J., Huber, R., Maskos, K., and Neumann, L. (2013). Structure-

kinetic relationship study of CDK8/CycC specific compounds. Proc. Natl. Acad. Sci. U. S. A. *110*, 8081–8086.

Scholz, J., and Suppmann, S. (2017). A new single-step protocol for rapid baculovirus-driven protein production in insect cells. BMC Biotechnol. *17*, 1–9.

Schroeding_LLC (2015). The PyMOL Molecular Graphics System, Version 1.8.

Schulman, B.A., Lindstrom, D.L., and Harlow, E. (1998). Substrate recruitment to cyclin-dependent kinase 2 by a multipurpose docking site on cyclin A. Proc. Natl. Acad. Sci. U. S. A. *95*, 10453–10458.

Schulze-Gahmen, U., and Kim, S.H. (2002). Structural basis for CDK6 activation by a virus-encoded cyclin. Nat. Struct. Biol. *9*, 177–181.

Seo, J.O., Iy, H.S., and Lim, S.C. (2010). Role of CDK8 and B-catenin in colorectal adenocarcinoma. Oncol. Rep. *24*, 285–291.

Shaikhibrahim, Z., Offermann, A., Braun, M., Menon, R., Syring, I., Nowak, M., Halbach, R., Vogel, W., Ruiz, C., Zellweger, T., et al. (2014). MED12 overexpression is a frequent event in castration-resistant prostate cancer. Endocr. Relat. Cancer *21*, 663–675.

Shimada, Y., Tajima, Y., Kameyama, H., Yagi, R., Okamura, T., Hirose, Y., Sakata, J., Kobayashi, T., Matsuda, Y., Ajioka, Y., et al. (2016). Clinical significance of MED12 expression in colorectal cancer. Int. J. Clin. Exp. Pathol. *9*, 6937–6944.

Shin, C.H., Chung, W.S., Hong, S.K., Ober, E.A., Verkade, H., Field, H.A., Huisken, J., and Y. R. Stainier, D. (2008). Multiple roles for Med12 in vertebrate endoderm development. Dev. Biol. *317*, 467–479.

Sims, R.J., Belotserkovskaya, R., and Reinberg, D. (2004). Elongation by RNA polymerase II: The short and long of it. Genes Dev. *18*, 2437–2468.

Smith, J.A., Francis, S.H., and Corbin, J.D. (1993). Autophosphorylation: a salient feature of protein kinases. Mol. Cell. Biochem. *127–128*, 51–70.

Soutourina, J. (2018). Transcription regulation by the Mediator complex. Nat. Rev. Mol. Cell Biol. *19*, 262–274.

Spain, M.M., and Govind, C.K. (2011). A role for phosphorylated Pol II CTD in modulating transcription coupled histone dynamics. Transcription *2*, 78–81.

Srivastava, S., Niranjan, T., May, M.M., Tarpey, P., Allen, W., Hackett, A., Jouk, P.S., Raymond, L., Briault, S., Skinner, C., et al. (2019). Dysregulations of sonic hedgehog signaling in MED12-related X-linked intellectual disability disorders. Mol. Genet. Genomic Med. *7*, 1–10.

Steinparzer, I., Sedlyarov, V., Rubin, J.D., Dowell, R.D., Taatjes, D.J., and Kovarik, P. (2019). Transcriptional Responses to IFN- g Require Mediator Kinase-Dependent Pause Release and Article Transcriptional Responses to IFN- g Require Mediator Kinase-Dependent Pause Release and Mechanistically Distinct CDK8 and CDK19 Functions. Mol. Cell 1–15.

Stevenson, R.E., and Schwartz, C.E. (2009). X-linked intellectual disability: Unique vulnerability of the male genome. Dev. Disabil. Res. Rev. *15*, 361–368.

Stiller, J.W., and Hall, B.D. (2002). Evolution of the RNA polymerase II C-terminal domain. Proc. Natl. Acad. Sci. U. S. A. *99*, 6091–6096.

Swanton, C., Mann, D.J., Fleckenstein, B., Neipel, F., Peters, G., and Jones, N. (1997). Herpes viral cyclin/Cdk6 complexes evade inhibition by CDK inhibitor proteins. Nature *390*, 184–187.

Taatjes, D.J., Näär, A.M., Andel, F., Nogales, E., and Tjian, R. (2002). Structure, function, and activator-induced conformations of the CRSP coactivator. Science (80-.). *295*, 1058–1062.

Tansey, W.P. (2001). Transcriptional activation: Risky business. Genes Dev. *15*, 1045–1050.

Tarricone, C., Dhavan, R., Peng, J., Areces, L.B., Tsai, L.H., and Musacchio, A. (2001). Structure and regulation of the CDK5-p25nck5a complex. Mol. Cell *8*, 657–669.

Thomas, M.C., and Chiang, C.M. (2006). The general transcription machinery and general

cofactors. Crit. Rev. Biochem. Mol. Biol. *41*, 105–178.

Trembley, J.H., Hu, D., Hsu, L.C., Yeung, C.Y., Slaughter, C., Lahti, J.M., and Kidd, V.J. (2002). PITSLRE p110 protein kinases associate with transcription complexes and affect their activity. J. Biol. Chem. *277*, 2589–2596.

Trompouki, E., Bowman, T. V, Lawton, L.N., Fan, Z.P., Wu, D., Dibiase, A., Martin, C.S., Cech, J.N., Sessa, A.K., Jocelyn, L., et al. (2012). Lineage regulators direct BMP and Wnt pathways to cell-specific programs during differentiation and regeneration. Cell *147*, 577–589.

Tsai, K.L., Sato, S., Tomomori-Sato, C., Conaway, R.C., Conaway, J.W., and Asturias, F.J. (2013). A conserved Mediator-CDK8 kinase module association regulates Mediator-RNA polymerase II interaction. Nat. Struct. Mol. Biol. *20*, 611–619.

Tsai, K.L., Tomomori-Sato, C., Sato, S., Conaway, R.C., Conaway, J.W., and Asturias, F.J. (2014). Subunit architecture and functional modular rearrangements of the transcriptional mediator complex. Cell *157*, 1430–1444.

Tsutsui, T., Fukasawa, R., Tanaka, A., Hirose, Y., and Ohkuma, Y. (2011). Identification of target genes for the CDK subunits of the Mediator complex. Genes to Cells *16*, 1208–1218.

Turunen, M., Spaeth, J.M., Keskitalo, S., Park, M.J., Kivioja, T., Clark, A.D., Mäkinen, N., Gao, F., Palin, K., Nurkkala, H., et al. (2014). Uterine Leiomyoma-Linked MED12 Mutations Disrupt Mediator-Associated CDK Activity. Cell Rep. *7*, 654–660.

Ubersax, J.A., and Ferrell, J.E. (2007). Mechanisms of specificity in protein phosphorylation. Nat. Rev. Mol. Cell Biol. *8*, 530–541.

Varjosalo, M., Keskitalo, S., VanDrogen, A., Nurkkala, H., Vichalkovski, A., Aebersold, R., and Gstaiger, M. (2013). The Protein Interaction Landscape of the Human CMGC Kinase Group. Cell Rep. *3*, 1306–1320.

Vincent, O., Kuchin, S., Hong, S.-P., Townley, R., Vyas, V.K., and Carlson, M. (2001). Interaction of the Srb10 Kinase with Sip4, a Transcriptional Activator of Gluconeogenic Genes in Saccharomyces cerevisiae. Mol. Cell. Biol. *21*, 5790–5796.

Vogelstein, B., Papadopoulos, N., Velculescu, V.E., Zhou, S., Diaz, L.A., and Kinzler, K.W. (2013). Cancer genome landscapes. Science (80-.). *340*, 1546–1558.

Vogl, M.R., Reiprich, S., Küspert, M., Kosian, T., Schrewe, H., Nave, K.A., and Wegner, M. (2013). Sox10 cooperates with the mediator subunit 12 during terminal differentiation of myelinating glia. J. Neurosci. *33*, 6679–6690.

Vos, S.M., Pöllmann, D., Caizzi, L., Hofmann, K.B., Rombaut, P., Zimniak, T., Herzog, F., and Cramer, P. (2016). Architecture and RNA binding of the human negative elongation factor. Elife *5*, 1–27.

van Vuuren et al., V. (1995). 374193a0.Pdf.

Wang, H., Shen, Q., Ye, L. hua, and Ye, J. (2013a). MED12 mutations in human diseases. Protein Cell *4*, 643–646.

Wang, L., Zeng, H., Wang, Q., Zhao, Z., Boyer, T.G., Bian, X., and Xu, W. (2015a). MED12 methylation by CARM1 sensitizes human breast cancer cells to chemotherapy drugs. Sci. Adv. *1*, 1–12.

Wang, X., Wang, J., Ding, Z., Ji, J., Sun, Q., and Cai, G. (2013b). Structural flexibility and functional interaction of mediator Cdk8 module. Protein Cell *4*, 911–920.

Wang, Y., Wang, F., Wang, R., Zhao, P., and Xia, Q. (2015b). 2A self-cleaving peptide-based multi-gene expression system in the silkworm Bombyx mori. Sci. Rep. *5*, 1–10.

Wasilko, D.J., Edward Lee, S., Stutzman-Engwall, K.J., Reitz, B.A., Emmons, T.L., Mathis, K.J., Bienkowski, M.J., Tomasselli, A.G., and David Fischer, H. (2009). The titerless infected-cells preservation and scale-up (TIPS) method for large-scale production of NO-sensitive human soluble guanylate cyclase (sGC) from insect cells infected with recombinant baculovirus. Protein Expr. Purif. *65*, 122–132.

Westerling, T., Kuuluvainen, E., and Makela, T.P. (2007). Cdk8 Is Essential for

Preimplantation Mouse Development. Mol. Cell. Biol. *27*, 6177–6182.

Whitmarsh, A.J., and Davis, R.J. (2000). Regulation of transcription factor function by phosphorylation. Cell. Mol. Life Sci. *57*, 1172–1183.

Wu, B., Słabicki, M., Sellner, L., Dietrich, S., Liu, X., Jethwa, A., Hüllein, J., Walther, T., Wagner, L., Huang, Z., et al. (2017a). MED12 mutations and NOTCH signalling in chronic lymphocytic leukaemia. Br. J. Haematol. *179*, 421–429.

Wu, J., Zou, Y., Luo, Y., Guo, J.B., Liu, F.Y., Zhou, J.Y., Zhang, Z.Y., Wan, L., and Huang, O.P. (2017b). Prevalence and clinical significance of mediator complex subunit 12 mutations in 362 Han Chinese samples with uterine leiomyoma. Oncol. Lett. *14*, 47–54.

Xu, W., and Ji, J.Y. (2011). Dysregulation of CDK8 and Cyclin C in tumorigenesis. J. Genet. Genomics *38*, 439–452.

Xu, W., Amire-Brahimi, B., Xie, X.J., Huang, L., and Ji, J.Y. (2014). All-atomic molecular dynamic studies of human CDK8: Insight into the A-loop, point mutations and binding with its partner CycC. Comput. Biol. Chem. *51*, 1–11.

Xu, W., Wang, Z., Zhang, W., Qian, K., Li, H., Kong, D., Li, Y., and Tang, Y. (2015). Mutated K-ras activates CDK8 to stimulate the epithelial-to-mesenchymal transition in pancreatic cancer in part via the Wnt/β-catenin signaling pathway. Cancer Lett. *356*, 613–627.

Yamamoto, S., Hagihara, T., Horiuchi, Y., Okui, A., Wani, S., Yoshida, T., Inoue, T., Tanaka, A., Ito, T., Hirose, Y., et al. (2017). Mediator cyclin-dependent kinases upregulate transcription of inflammatory genes in cooperation with NF-κB and C/EBPβ on stimulation of Toll-like receptor 9. Genes to Cells *22*, 265–276.

Ye, X. (2001). A premature-termination mutation in the Mus musculus cyclin-dependent kinase 3 gene. Proc. Natl. Acad. Sci. *98*, 1682–1686.

Yoshida, M., Sekine, S., Ogawa, R., Yoshida, H., Maeshima, A., Kanai, Y., Kinoshita, T., and Ochiai, A. (2015). Frequent MED12 mutations in phyllodes tumours of the breast. Br. J. Cancer *112*, 1703–1708.

Zhan, T., Rindtorff, N., and Boutros, M. (2017). Wnt signaling in cancer. Oncogene *36*, 1461–1473.

Zhao, J., Ramos, R., and Demma, M. (2013). CDK8 regulates E2F1 transcriptional activity through S375 phosphorylation. Oncogene *32*, 3520–3530.

Zhao, X., Feng, D., Wang, Q., Abdulla, A., Xie, X.J., Zhou, J., Sun, Y., Yang, E.S., Liu, L.P., Vaitheesvaran, B., et al. (2012). Regulation of lipogenesis by cyclin-dependent kinase 8 - Mediated control of SREBP-1. J. Clin. Invest. *122*, 2417–2427.

Zheng, D., Cho, Y.Y., Lau, A.T.Y., Zhang, J., Ma, W.Y., Bode, A.M., and Dong, Z. (2008). Cyclin-dependent kinase 3-mediated activating transcription factor 1 phosphorylation enhances cell transformation. Cancer Res. *68*, 7650–7660.

Zhou, H., Spaeth, J.M., Kim, N.H., Xu, A., Friez, M.J., Schwartz, C.E., and Boyer, T.G. (2012). MED12 mutations link intellectual disability syndromes with dysregulated GLI3-dependent Sonic Hedgehog signaling. Proc. Natl. Acad. Sci. U. S. A. *109*, 19763–19768.

Zhou, R., Roeder, R., Francis, P., and Berta, P. (2002). SOX9 interacts with a component of the human thyroid hormone receptor-associated protein complex. Nucleic Acids Res. *30*, 3245–3252.

Appendix A: Oligos

cDNA synthesis was performed using poly(A)+-selected RNA from A549 cells. Novel gene amplifications were cloned using nested PCR. Oligos used to introduce or delete affinity-tags and/or protease-cleavage sites are not listed. Please note that several plasmids encode for the identical protein. However, these plasmids can differ in their coding sequence (codon optimized genes are underlined) and/or tags and backbone. Please note that the applied Strep-tag is the twin StrepII-tag. As eukaryotic expression systems encode endogenous deSUMOylases, the genetically engineered SUMOstar was used throughout this study (Liu et al., 2008).

Please note that MultiBac™ vectors of the second generation (pAceBac1, pIDK, pIDC and pIDK) and first generation (pFL, pUCDM and pSPL) contain partially identical multiple cloning sites and are compatible. Therefore, oligos that hybridize at conserved regions like for example promotor and/or terminator regions, can be used to linearize several plasmids. This accounts for all oligos that target conserved genetic sites, which typically encompass the multiple-cloning site. This fact also allows for the usage of gene-specific oligos (which carry the complementary overhang) for several assemblies. Please further note that donor plasmids from the first MultiBac™ generation (pUCDM and pSPL) possess two expression cassettes. Taken together, based on the usage of varying PCR templates (already cloned plasmids), multiple oligos can be used to clone a myriad of plasmids.

The plasmid pIRESneo contains an internal ribosome entry site (IRES), which forms strong tertiary structures (Kanamori and Nakashima, 2001) that hinders plasmid linearization by PCR. To remedy this issue, pIRESneo was linearized using EcoRI (NEB) according to the manufacturer's protocol.

ID	Description	Overhang	Usage	Sequence 5' – 3'
FK001 FK079	pAceBac1, pFL linearization (targets TEV)	-	multiple	CTGGAAGTACAGGTTCTC GC
FK003	pAceBac1 linearization (targets SV40)	-	multiple	TGATAGGATCGAATCGGA CTT
FK011	5' MED12 aa1	pAceBac1 pFL	multiple	CAGCAGATGGGCGAGAAC CTGTACTTCCAGATGGCG GCCTTCGGGATC
FK012	3' MED12 aa2177	pAceBac1	multiple	TAGATTCGAAAGTCCGAT TCGATCCTATCAGTAGCG TCCAAATATGTTGGTAC

ID	Description	Overhang	Usage	Sequence 5' – 3'
FK013	5' MED13 aa1	pAceBac1	multiple	CAGCAGATGGGCGAGAAC CTGTACTTCCAGATGAGT GCCTCCTTCGTGC
FK014	3' MED13 aa2174	pAceBac1	5	TAGATTCGAAAGTCCGAT TCGATCCTATCACAGCAT ATTCATAATAAAGTTATA TAACT
FK015	5' Cyclin C aa1	pAceBac1	multiple	CAGCAGATGGGCGAGAAC CTGTACTTCCAGATGGCA GGGAACTTTTGGCAGAG
FK016	3' Cyclin C aa283	pAceBac1	10	TAGATTCGAAAGTCCGAT TCGATCCTATCAAGATTG GCTGTAGCTAGAGTTCT
FK017	5' CDK8 aa1	pAceBac1	8	CAGCAGATGGGCGAGAAC CTGTACTTCCAGATGGAC TATGACTTTAAAGTGAAG C
FK018	3' CDK8 aa464	pAceBac1	multiple	TAGATTCGAAAGTCCGAT TCGATCCTATCAGTACCG ATGTGTCTGATGTGA
FK019	½ MED12	FK20	1	AGAGCTGACCGGCTATTG C
FK020	½ MED12	FK19	1	CTCAGTGACTTGCAATAG CCG
FK021	½ MED13	FK22	5	TGTTGCATCTGTGTTTGC AACAT
FK022	½ MED13	FK21	5	TTGATGTTCATGTTGCAA ACACAGA
FK025	pIDK, pIDS, pUCDM pSPL linearization (targets T7)		multiple	GCCCATCTGCTGGCCAC
FK026	pIDK, pIDS, pUCDM pSPL linearization (targets polh)		multiple	TAGGATCGAATCGGACTT CTG
FK027	5' MED13 aa1	pIDS	multiple	CTTCCATGACCGGTGGCC AGCAGATGGGCATGAGTG CCTCCTTCGTGC
FK028	3' MED13 aa2174	pIDS	multiple	CAGAAGTCCGATTCGATC CTATCACAGCATATTCAT AATAAAGTTATATA
FK029	5' CDK8 aa1	pAceBac1	multiple	CTTCCATGACCGGTGGCC AGCAGATGGGCATGGACT ATGACTTTAAAGTGAAG
FK030	3' CDK8 aa403	pAceBac1	multiple	CAGAAGTCCGATTCGATC CTATCAGTACCGATGTGT CTGATG

ID	Description	Overhang	Usage	Sequence 5' – 3'
FK034	3' MED12 aa1227	pFL	multiple	GTACTTCTCGACAAGCTT CTACTATCA GTAGCGTCCAAATATGTT GGTAC
FK036	pFL linearization (targets SV40)		multiple	TGATAGTAGAAGCTTGTC GAGAAG
FK037	3' MED12 aa2048	pAceBac1	2	GATTCGAAAGTCCGATTC GATCCTATCATAGGATGG CTGTTGAACGGAC
FK038	5' T7	pIDK, pIDS	multiple	GAAGACTTGATCACCCGG GATCTCGAGCCATGGCTT CCATGACCGGTG
FK039	3' Cyclin C aa283	pIDK, pIDS	multiple	CAGAAGTCCGATTCGATC CTATTAAGATTGGCTGTA GCTAGAGTTC
FK040	pIDK, pIDS, pUCDM, pSPL linearization (targets p10 reverse)		multiple	GGCTCGAGATCCCGGGTG
FK041	5' MED12 aa1	pFL	multiple	ATGGCTTCCATGACCGGT GGCCAGCAGATGGGCATG GCGGCCTTCGGGATC
FK043	5' T7	pAceBac1	multiple	ATTATTCATACCGTCCCA CCATCGGGCGCGATGGCT TCCATGACCGGTG
FK044	3' Cyclin C aa283	pIDC	multiple	GCGCGCTTCGGACCGGGA TCCTATCAAGATTGGCTG TAGCTAGAGTTCT
FK045	pAceBac1, linearization (targets polh)	pIDC	multiple	GATCCGCGCCCGATGGTG
FK046	pAceBac1, linearization (targets SV40)	pIDC	multiple	TGATAGGATCCCGGTCCG AAGCGC
FK049	5' Strep	pIDK, pIDS	multiple	AAGACTTGATCACCCGGG ATCTCGAGCCTGGTCACA CCCTCAATTCGAG
FK052	3' MED12 aa1227	pAceBac1	3	ATTCGAAAGTCCGATTCG ATCCTATCACACAGCCTT GAGAACAGCAAAC
FK053	pAceBac1, linearization (targets polh)	pIDC	multiple	CGCGCCCGATGGTGGGAC
FK057	5' Cyclin C	pIDK	28	TCAGAAGTCCGATTCGAT CCTATCAAGATTGGCTGT AGCTAGAGTTCTG

ID	Description	Overhang	Usage	Sequence 5' – 3'
FK060	3' MED12 aa1395	pAceBac1	4	ATTCGAAAGTCCGATTCG ATCCTATCACTCTGCTGA CTGTTGGAAAAC
FK062	3' CDK8 aa403	pAceBac1	multiple	TAGATTCGAAAGTCCGAT TCGATCCTATCATCATTT CTTCAACGGGGGTCC
FK067	3' MED12 aa1195	pAceBac1	26	ATTCGAAAGTCCGATTCG ATCCTATCAAGGCTTGTT TCCATCAGACTG
FK068	3' MED12 aa1100	pAceBac1	27	ATTCGAAAGTCCGATTCG ATCCTATCAGCACAAGGC CTTAAGCACTC
FK069	3' Cyclin C	pIDK	28	TATGCATCAGAAGTCCGA TTCGATCCTATCATTTCT TCAACGGGGGTCC
FK087	5' MED12 aa1	pAceBac1	multiple	ATTATTCATACCGTCCCA CCATCGGGCGCGATGGCG GCCTTCGGGATC
FK090	Plasmid linearization (targets TEV-T7)		multiple	GGAAGCCATCTGGAAGTA CAGGTTCTC
FK091	3' MED12	pAceBac1	41	GAAGCCATCTGGAAGTAC AGGTTCTCATCCTTCTGG TTCACTTGGGG
FK093	3' MED12	pAceBac1	43	GAAGCCATCTGGAAGTAC AGGTTCTCAAGCAGGTCA CTAAAGGGAG
FK142	3' MED12 Codon opt. aa1114	pAceBac1	76	TTCGAAAGTCCGATTCGA TCCTATCACAGCAGGTCG TTGAAACCGC
FK146	3' MED12	pAceBac1	80	GAAGCCATCTGGAAGTAC AGGTTCTCAGACCACCTG ACCTCCACAG
FK095	pIDK, pIDS, pUCDM, pSPL linearization (targets HSV TK polyA)		multiple	TGATAGCAGCTGATGCAT AGCATG
FK114	5' MED12 Codon opt. aa1	pAceBac1	66	TATTCATACCGTCCCACC ATCGGGCGCGATGGCAGC ATTCGGCATTCTC
FK115	3' MED12 Codon opt. aa1227	pAceBac1	66	GGAAGCCATCTGGAAGTA CAGGTTCTCCACTGCTTT CAACACTGCGAAC
FK116	5' MED13 Codon opt. aa1	pFL pAceBac1	multiple	TATTCATACCGTCCCACC ATCGGGCGCGATGAGCGC ATCTTTCGTGCC
FK117	3' MED13 Codon opt. aa2174	pAceBac1, pFL	multiple	AGCCATCTGGAAGTACAG GTTCTCGAGCATGTTCAT AATGAAGTTGTAG
FK118	5' MED13 Codon opt. aa1	pAceBac1 pFL	multiple	GCAGATGGGCGAGAACCT GTACTTCCAGATGAGCGC ATCTTTCGTGCC

ID	Description	Overhang	Usage	Sequence 5' – 3'
FK124	5' MED12 Codon opt. aa1	pIDS	multiple	AGATGGGCGAGAACCTGT ACTTCCAGATGGCAGCAT TCGGCATTCTC
FK126	3' MED12 Codon opt. aa1227	pAceBac1	66	TTCGAAAGTCCGATTCGA TCCTATCACACTGCTTTC AACACTGCGAAC
FK127	5' CDK8 Codon opt. aa1	pAceBac1	68	GATGGGCGAGAACCTGTA CTTCCAGATGGACTACGA CTTTAAAGTGAAG
FK129	3' CDK8 Codon opt. aa403	pAceBac1	68	TCGAAAGTCCGATTCGAT CCTATCACTTCTTAAGAG GTGGGCCTTG
FK133	3' MED13 Codon opt. aa2174	pFL	72	CGAAAGTCCGATTCGATC CTATCAGAGCATGTTCAT AATGAAGTTGTAG
FK135	3' CDK8 Codon opt. aa403	pUCDM pIDC	multiple	ATTCCGCGCGCTTCGGAC CGGGATCCTACTTCTTAA GAGGTGGGCCTTG
FK137	3' Cyclin C Codon opt. aa283	pUCDM, pSPL	multiple	CCGCATGCTATGCATCAG CTGCTATCAAGACTGCGA ATAGGAGCTGTTC
FK139	5' MED12 Codon opt. aa1	pIDS	117 117M1	AAGACTTGATCACCCGGG ATCTCGAGCCATGGCAGC ATTCGGCATTCTC
FK144	5' CDK8 Codon opt. aa1	pUCDM pIDC	multiple	TCCCACCATCGGGCGCGG ATCTAGATGGACTACGAC TTTAAAGTGAAGC
FK145	5' Cyclin C Codon opt. aa1	pUCDM, pSPL	multiple	TGATCACCCGGGATCTCG AGCCATGGCTGGTAACTT CTGGCAATC
FK153	3' MED13 Codon opt. aa390	pAceBac1	86	GAAGCCATCTGGAAGTAC AGGTTCTCGTTCTGGGCG CGGTTCATG
FK154	3' MED13 Codon opt. aa500	pAceBac1	87	GAAGCCATCTGGAAGTAC AGGTTCTCGCTGATGACC AGACGCTGG
FK155	3' MED13 Codon opt. aa545	pAceBac1	88	GGAAGCCATCTGGAAGTA CAGGTTCTC
FK172	3' CDK8 Codon opt. aa359	pUCDM pIDC	multiple	TCCGCGCGCTTCGGACCG GGATCCTAGAGGAACTCC CTCTTAGGATAAG
FK177	5' UTR CDK19		CDK19 template	GAGGCGGCTGTTGGAGAA G
FK178	3' UTR1 CDK19		CDK19 template	AAGTGTGCTCTGGGACTG AG
FK167	5' CDK19 aa1	pAceBac1 pSPL	multiple*[1]	ATGGGCGAGAACCTGTAC TTCCAGATGGATTATGAT TTCAAGGCGAAG
FK168	3' CDK19 aa439	pAceBac1 pSPL	multiple	TTCCGCGCGCTTCGGACC GGGATCCTACTTCTTGTT TGGAGGCACCTG

ID	Description	Overhang	Usage	Sequence 5' – 3'
FK170	3' CDK19 aa359	pSPL pIDC	multiple	TCCGCGCGCTTCGGACCG GGATCCTAAAGGAATTCT CGTTTGGGGTATG
FK183	5' CDK19 aa1	pIDC	137	TCATACCGTCCCACCATC GGGCGCGATGGATTATGA TTTCAAGGCGAAG
FK188	5' UTR MED12L		MED12L template	GAGGGAGTCTGTCTGCAA AG
FK189	3' UTR MED12L		MED12L template	TGTCAAAGAAATGAAAAA AAGGGAC
FK190	5' MED12L aa1	pAceBac1	41L 43L	CATACCGTCCCACCATCG GCGCGATGGCCGCCTTC GGGCTTC
FK191	3' MED12L aa100	pAceBac1	41L	AGCCATCTGGAAGTACAG GTTCTCATCTTTAGCATT AACTTGTGGTTTC
FK192	3' MED12L aa352	pAceBac1	43L	AGCCATCTGGAAGTACAG GTTCTCAAGAAAATCTGA GAAGGCCAGC
FK193	5' UTR STAT1		STAT1 template	TGTCTAGGTTAACGTTCG CAC
FK194	3' UTR STAT1		STAT1 template	GGCCTTTCTTTCATTTCC CTAG
FK195	5' STAT1 aa639	pGEX4T1	EC6	CTGGTTCCGCGTGGATCC CCGGAACTTTCTGCTGTT ACTTTCCCTG
FK196	3' STAT1 aa750	pGEX4T1	EC6 EC7	GCGCGAGGCAGATCGTCA GTCAGTCATACTGTGTTC ATCATACTGTCGA
FK197	3' UTR2 CDK19		CDK19 template	GTTTTCCTCCCATGTGTA TGAG
FK200	3' MED12 aa91	pAceBac1	multiple	AAGCCATCTGGAAGTACA GGTTCTCGCGACCAGTGT CAGGAAGG
FK201	5' STAT1 aa639	pGEX4T1	EC7	CGGATGAAAACCTGTACT TCCAATCCCTTTCTGCTG TTACTTTCCCTG
FK202	3' MED12 aa295	pAceBac1	104	GAAGCCATCTGGAAGTAC AGGTTCTCGCGGGACAGG TATGCAGAC
FK203	3' MED12 aa303	pAceBac1	105	GAAGCCATCTGGAAGTAC AGGTTCTCCCGTGTACAG AAGTAGGCAAG
FK207	3' CDK8 Codon opt. aa464	pUCDM pIDC	multiple	TCCGCGCGCTTCGGACCG GGATCCTATTAATAACGA TGGGTTTGGTGTG
FK209	5' Cyclin C Codon opt. aa1	pAceBac1	108	TTCATACCGTCCCACCAT CGGGCGCGATGGCTGGTA ACTTCTGGCAATC

ID	Description	Overhang	Usage	Sequence 5' – 3'
FK212	3' MED12 Codon opt. aa100	pIDS	117 117M1	TATGCATCAGAAGTCCGA TTCGATCCTAGTCCTTCT GGTTGACCTGTG
FK214	MED12 linearization aa32	MED12	41M1-5 41M11 41M14	CTTCTGTTTGGGGTCCTG AG
FK215	5' MED12 E33Q	FK214	41M1	CAGGACCCCAAACAGAAG CAGGATGAACTGACGGCC TTGAATGTAAAAC
FK216	5' MED12 D34N	FK214	41M3	CAGGACCCCAAACAGAAG GAGAACGAACTGACGGCC TTGAATGTAAAAC
FK217	5' MED12 E35Q	FK214	41M5	CAGGACCCCAAACAGAAG GAGGATCAACTGACGGCC TTGAATGTAAAAC
FK218	5' MED12 E33Q/D34N	FK214	41M2	CAGGACCCCAAACAGAAG CAGAACGAACTGACGGCC TTGAATGTAAAAC
FK219	5' MED12 D34N/E35Q	MED12	41M4	CAGGACCCCAAACAGAAG GAGAACCAACTGACGGCC TTGAATGTAAAAC
FK224	Cyclin C linearization aa97	Cyclin C	79aM4-6	TACTTTGCTGGCAAGAAA CACGC
FK225	5' Cyclin C E99Q	FK224	79aM4	GCGTGTTTCTTGCCAGCA AAGTAGAGCAGTTTGGCG TAGTCTCAAATAC
FK226	5' Cyclin C E98Q	FK224	79aM5	GCGTGTTTCTTGCCAGCA AAGTACAGGAGTTTGGCG TAGTCTCAAATAC
FK227	5' Cyclin C E99Q/E98Q	FK224	79aM6	GCGTGTTTCTTGCCAGCA AAGTACAGCAGTTTGGCG TAGTCTCAAATAC
FK229	3' MED12 aa69	pAceBac1	125	GAAGCCATCTGGAAGTAC AGGTTCTCGATCTTGGCA GGATTGAAGCTG
FK230	5' MED12 aa6	pAceBac1	126	TCATACCGTCCCACCATC GGGCGCGATGATCTTGAG CTACGAACACCGG
FK231	5' MED12 aa11	pAceBac1	127	TCATACCGTCCCACCATC GGGCGCGATGCACCGGCC CCTGAAGCG
FK232	5' MED12 aa23	pAceBac1	128	TCATACCGTCCCACCATC GGGCGCGATGGATGTTTA CCCTCAGGACCC
FK234	5' MED12 aa29	pAceBac1	129	CATACCGTCCCACCATCG GGCGCGATGCCCAAACAG AAGGAGGATGAAC
FK236	5' MED12 E33A	FK214	41M6	CAGGACCCCAAACAGAAG GCGGATGAACTGACGGCC TTGAATGTAAAAC

ID	Description	Overhang	Usage	Sequence 5' – 3'
FK237	5' MED12 E33L	FK214	41M7	CAGGACCCCAAACAGAAG CTGGATGAACTGACGGCC TTGAATGTAAAAC
FK238	CDK8 Codon opt. linearization aa64	CDK8	79aM7	ACAAGCGCTCATGGATAT ACCCG
FK239	CDK8 Codon opt. linearization aa149	CDK8	79aM8	GTGCAGGACCCAATTCGC G
FK240	CDK8 Codon opt. linearization aa177	CDK8	79aM9	TGCAAAGCCCATATCGGC AATT
FK241	5' CDK8 Codon opt. R65Q	FK238	79aM7	GGTACGGGTATATCCATG AGCGCTTGTCAGGAGATT GCCCTGTTGCGTG
FK242	5' CDK8 Codon opt. R150Q	FK239	79aM8	TTACACGCGAATTGGGTC CTGCACCAGGACTTGAAA CCCGCTAACATAC
FK243	5' CDK8 Codon opt. R178Q	FK240	79aM9	AAAATTGCCGATATGGGC TTTGCACAGCTCTTCAAC AGTCCCCTGAAAC
FK244	MED12 linearization aa29	MED12	41M8-10	GGGGTCCTGAGGGTAAAC ATC
FK245	5' MED12 K30A	FK244	41M8	TGTTTACCCTCAGGACCC CGCGCAGAAGGAGGATGA ACTGACGGCCTTG
FK246	5' MED12 Q31A	FK244	41M9	TGTTTACCCTCAGGACCC CAAAGCGAAGGAGGATGA ACTGACGGCCTTG
FK247	5' MED12 K32A	FK244	41M10	TGTTTACCCTCAGGACCC CAAACAGGCGGAGGATGA ACTGACGGCCTTG
FK220	CDK8 Codon opt. linearization aa195	CDK8	79aM10-11	AGCCAAAGGTTTCAGGGG AC
FK248	5' CDK8 Codon opt. T196D	FK220	79aM10	CCCCTGAAACCTTTGGCT GATCTCGATCCTGTCGTC GTAGATTTCTGGT
FK249	5' CDK8 Codon opt. T196A	FK220	79aM11	CCCCTGAAACCTTTGGCT GATCTCGATCCTGTCGTC GTAGCTTTCTGGT
FK250	CDK8 Codon opt. linearization aa30	CDK8	79aM12-14	TCCCCTACCGACTTTGCA GC
FK251	5' CDK8 Codon opt. T31D	FK250	79aM12	GCTGCAAAGTCGGTAGGG GAGATTATGGTCATGTAT ACAAGGCCAAG
FK252	5' CDK8 Codon opt. T31A	FK250	79aM13	GCTGCAAAGTCGGTAGGG GAGCTTATGGTCATGTAT ACAAGGCCAAG
FK253	5' CDK8 Codon opt. Y32F	FK250	79aM14	GCTGCAAAGTCGGTAGGG GAACGTTCGGTCATGTAT ACAAGGCCAAG

ID	Description	Overhang	Usage	Sequence 5' – 3'
FK256	CDK8 Codon opt. linearization aa359	CDK8	79aM15-16	GAGGAACTCCCTCTTAGG ATAAG
FK257	5' CDK8 Codon opt. T360A	FK256	79aM15	CTTATCCTAAGAGGGAGT TCCTCGCTGAAGAGGAAC CTGACGATAAG
FK258	5' CDK8 Codon opt. T360D	FK256	79aM16	CTTATCCTAAGAGGGAGT TCCTCGACGAAGAGGAAC CTGACGATAAG
FK259	Cyclin C Codon opt. linearization aa180	Cyclin C	79aM17-18	GACAATACGCCAAGCTAA TGG
FK260	5' Cyclin C Codon opt. N181A	FK259	79aM17	CATTAGCTTGGCGTATTG TCGCCGACACTTACCGTA CGGATC
FK261	5' Cyclin C Codon opt. D182A	FK259	79aM18	CATTAGCTTGGCGTATTG TCAACGCCACTTACCGTA CGGATC
FK262	5' MED12 L36R	FK214	41M11	CTCAGGACCCCAAACAGA AGGAGGATGAACGGACGG CCTTGAATG
FK265	MED12 Codon opt. linearization aa32	MED12	117M1	CTTCTGCTTAGGGTCTTG CGG
FK266	5' MED12 Codon optimized E33Q	FK265	117M1	CAAGACCCTAAGCAGAAG CAGGACGAACTGACCGCC CTG
FK267	MED12 linearization aa42	MED12	41M12-13	TTTTACATTCAAGGCCGT CAGTTC
FK268	5' MED12 Q43P	FK267	41M12	ACTGACGGCCTTGAATGT AAAACCTGGTTTCAATAA CCAGCCTGCTGTC
FK269	5' MED12 G44S	FK267	41M13	ACTGACGGCCTTGAATGT AAAACAAAGTTTCAATAA CCAGCCTGCTGTC
FK270	5' MED12 D34Y	FK214	41M14	CAGGACCCCAAACAGAAG GAGTACGAACTGACGGCC TTGAATGTAAAAC
FK273	CDK8 Codon opt. linearization aa409	CDK8	79dM1-6	TGGAGGAACCACTCTAAC CTTC
FK274	5' CDK8 Codon optimized T410D	FK273	79dM1	GTTAGAGTGGTTCCTCCA GACACAACTTCTGGAGGA CTGATC
FK275	5' CDK8 Codon optimized T410A	FK273	79dM2	GTTAGAGTGGTTCCTCCA GCCACAACTTCTGGAGGA CTGATC
FK276	5' CDK8 Codon optimized S413D	FK273	79dM3	GTTAGAGTGGTTCCTCCA ACCACAACTGACGGAGGA CTGATCATGACATCC
FK277	5' CDK8 Codon optimized S413A	FK273	79dM4	GTTAGAGTGGTTCCTCCA ACCACAACTGCCGGAGGA CTGATCATGACATCC

ID	Description	Overhang	Usage	Sequence 5' – 3'
FK278	5' CDK8 Codon optimized T410D/S413D	FK273	79dM5	GTTAGAGTGGTTCCTCCAGACACAACTGACGGAGGACTGTCATGACATCC
FK279	5' CDK8 Codon optimized T410A/S413A	FK273	79aM6	GTTAGAGTGGTTCCTCCAGCCACAACTGCCGGAGGACTGATCATGACATCC
FK280	3' CDK19 aa502	pIDC	137	ATTCCGCGCGCTTCGGACCGGGATCCTAGTACCGGTGGGCCTG
pGEX rev	pGEX4T1 linearization (please note that this oligo was designed by Silke Spudeit)		EC6	TTCCGGGGATCCACGCGGAACC
Smed3 rev-TEV vs. SiS2	pGEX4T1 linearization (Please note that this oligo was designed by Silke Spudeit)		EC7, 8, 9, 12	GGATTGGAAGTACAGGTTTTCATCCGATTTTGGAGGATGGTCG
pGex for vs. IK112	pGEX4T1 linearization (Please note that this oligo was designed by Silke Spudeit and Dr. Iana Kim)		EC6, 7, 8, 9, 12	TGACTGACTGACGATCTGCCTCGC
FK285	5' UTR BRCA1		BRCA1 template	GGACGGGGGACAGGCTG
FK286	3' UTR BRCA1		BRCA1 template	GTAGAAGGACTGAAGAGTGAG
FK287	5' BRCA1	pGEX4T1	EC9	CGGATGAAAACCTGTACTTCCAATCCCGAAATCCAGAACAAAGCACATC
FK288	3' BRCA1	pGEX4T1	EC9	GCGCGAGGCAGATCGTCAGTCAGTCATCTTTTGTTGACCCTTTCTGTTG
FK291	MED12 linearization aa14	MED12	41M15-16	CAGGGGCCGGTGTTCGTAG
FK292	5' MED12 K15N	FK291	41M15-16	TCTTGAGCTACGAACACCGGCCCCTGAATCGGCCGCGGCTGGGG
FK293	5' MED12 E33K	FK214	41M17	CAGGACCCCAAACAGAAGAAGGATGAACTGACGGCCTTGAATGTAAAAC
FK300	5' MED12 aa1	pIRESneo (EcoRI)	CP3, CP3M1	TAGGCGCGCCATATATAGAAAAATGGCGGCCTTCGGGATC
FK301	3' MED12 aa2177	pIRESneo (EcoRI)	CP3, CP3M1	TTACTAGTGGATCCACTGAACTATTAGTAGCGTCCAAATATGTTGGTAC

ID	Description	Overhang	Usage	Sequence 5' – 3'
FK307	3' MED13 Codon opt. aa947	pFL	141	AGTACTTCTCGACAAGCT TCTACTATCACTTGCCCA CAGTCCAGGAC
FK311	5' UTR CDK3		CDK3 template	CTTCCTGGCCGCCATGTG
FK312	3' UTR CDK3		CDK3 template	TCCCCAGATGCATCCTCT C
FK313	5' CDK3 aa1	pIDC	143	TCATACCGTCCCACCATC GGGCGCGATGGATATGTT CCAGAAGGTAGAG
FK314	3' CDK3 aa305	pIDC	143	CCGCGCGCTTCGGACCGG GATCCTAATGGCGGAATC GCTGCAGC
FK315	CDK8 Codon opt. linearization aa392	CDK8	79aM20-23	GTCCTGATTGCCCGGATG AC
FK316	5' CDK8 Codon opt. S393A/S394A	FK315	79aM20	ACTGGTCATCCGGGCAAT CAGGACGCCGCTCACACA CAAGGCCCACCTC
FK317	5' CDK8 Codon opt. S393D/S394A	FK315	79aM21	ACTGGTCATCCGGGCAAT CAGGACGACGATCACACA CAAGGCCCACCTC
FK318	5' CDK8 Codon opt. T396A	FK315	79aM22	ACTGGTCATCCGGGCAAT CAGGACTCGTCACACGCT CAAGGCCCACCTCTTAAG AAG
FK319	5' CDK8 Codon opt. T396D	FK315	79aM23	ACTGGTCATCCGGGCAAT CAGGACTCGTCACACGAT CAAGGCCCACCTCTTAAG AAG
FK320	CDK8 Codon opt. aa381 linearization	CDK8	79aM24-25	GTGGTTGTTGCCCTGCTG TTG
FK321	5' CDK8 Codon opt. T382A	FK320	79aM24	CAGCAACAGCAGGGCAAC AACCACGCTAATGGAACT GGTCATCCGGGC
FK322	5' CDK8 Codon opt. T382D	FK320	79aM25	CAGCAACAGCAGGGCAAC AACCACGACAATGGAACT GGTCATCCGGGC
FK333	3' MED12 aa60	pAceBac1	155	TGGAAGCCATCTGGAAGT ACAGGTTCTCCTTGGCAC TGCCATGCTCATC
FK334	CDK8 Codon opt. linearization aa384	CDK8	79aM26-27	GTCATCCGGGCAATCAGG AC
FK335	5' CDK8 Codon opt. T385A	FK334	79aM26	CGAGTCCTGATTGCCCGG ATGACCAGCTCCATTAGT GTGGTTGTTGCCC
FK336	5' CDK8 Codon opt. T385D	FK334	79aM27	CGAGTCCTGATTGCCCGG ATGACCGTCTCCATTAGT GTGGTTGTTGCCC

ID	Description	Overhang	Usage	Sequence 5' – 3'
FK337	5' UTR CDK7		150	GCTTTAAGGTAGCTTTAA ATTCGTG
FK338	3' UTR CDK7		150	CTTCTACAGCATTTACTT AATGTTTAC
FK343	5' CDK7 aa1	pAceBac1	150	GATGGGCGAGAACCTGTA CTTCCAGATGGCTCTGGA CGTGAAGTC
FK344	3' CDK7 aa346	pAceBac1	150	TCGAAAGTCCGATTCGAT CCTATTAAAAAATTAGTT TCTTGGGCAATCC
FK281	5' UTR Cyclin H		Cyclin H template	CGGTGGGGGTACGGGTG
FK282	3' UTR Cyclin H		Cyclin H template	GTTTGATATGCTTCCTAC TTCTC
FK283	5' Cyclin H aa1	pGEX4T1	EC8	GGATGAAAACCTGTACTT CCAATCCATGTACCACAA CAGTAGTCAGAAG
FK284	3' Cyclin H aa323	pGEX4T1	EC8	CGCGAGGCAGATCGTCAG TCAGTCATTAGAGAGATT CTACCAGGTCGTC
FK345	5' Cyclin H aa1	pIDC	151	TCATACCGTCCCACCATC GGGCGCGATGTACCACAA CAGTAGTCAGAAG
FK346	3' Cyclin H aa323	pIDC	151	CCGCGCGCTTCGGACCGG GATCCTATTAGAGAGATT CTACCAGGTCGTC
FK339	5' UTR MAT1		MAT1 template	CGCGTCTGAGGGGGCTTG
FK340	3' UTR MAT1		MAT1 template	CTGCACATAGCTATAATT TTATAAGTC
FK347	5' MAT1 aa1	pIDS	152	ACTTGATCACCCGGGATC TCGAGCCATGGACGATCA GGGTTGCCC
FK348	3' MAT1 aa309	pIDS	152	GCATCAGAAGTCCGATTC GATCCTATTAACTGGGCT GCCAGAAAAGC
FK351	3' CDK8 Codon opt. aa424	pUCDM	79e	TTCCGCGCGCTTCGGACC GGGATCCTAGCGCTGATA ATCGGATGTCATG
FK352	3' CDK8 Codon opt. aa371	pUCDM	79f	ATTCCGCGCGCTTCGGAC CGGGATCCTACTTCTTGT CTCCCTTATCGTC
FK353	3' CDK19 aa460	pUCDM	98e	ATTCCGCGCGCTTCGGAC CGGGATCCTAGTGCTGAT AATCCGAGGGC
FK354	3' CDK19 aa371	pUCDM	98f	CCGCGCGCTTCGGACCGG GATCCTAATTCTTGTCAC CTTTTTCTTCAGG

ID	Description	Overhang	Usage	Sequence 5' – 3'
FK360	3' MED12 aa50	pAceBac1	153	TGGAAGCCATCTGGAAGT ACAGGTTCTCAGCAGGCT GGTTATTGAAACC
FK361	3' MED12 aa45	pAceBac1	154	AAGCCATCTGGAAGTACA GGTTCTCGAAACCTTGTT TTACATTCAAGGC
FK371	5' UTR p21		p21 template	TGTGAGCAGCTGCCGAAG TC
FK372	3' UTR p21		p21 template	ACAAACTGAGACTAAGGC AGAAG
FK373	5' p21 aa1	pAceBac1	160	ATTCATACCGTCCCACCA TCGGGCGCGATGTCAGAA CCGGCTGGGGATG
FK374	3' p21 aa164	pAceBac1	160	GGAAGCCATCTGGAAGTA CAGGTTCTCGGGCTTCCT CTTGGAGAAGATC
FK375	5' P21 aa1	pGEX4T1	EC12	TCGGATGAAAACCTGTAC TTCCAATCCATGTCAGAA CCGGCTGGGGATG
FK376	3' P21 aa164	pGEX4T1	EC12	CGCGCGAGGCAGATCGTC AGTCAGTCATTAGGGCTT CCTCTTGGAGAAG
FK377	pAceBac1 linearization (targets TEV)	pAceBac1	Spt5 CT1-6	GGTGCTGAAAACCTGTAC TTCC
FK378	Spt5 linearization	Spt5	Spt5 CT1-6	CAGAAAGCCCTTCCGGCT G
FK379	3' Spt5 aa978	FK377	Spt5 CT6	CTTGGAAGTACAGGTTTT CAGCACCCTGGTCCTCAA ACTTTTCCAGC
FK380	5' Spt5	FK378	Spt5 CT1-6	CCGTTACAGCCGGAAGGG CTTTCTGTTCAAGAGCTT CCCATGTCTG
FK381	3' Spt5 aa518	FK377	Spt5 CT5	CTTGGAAGTACAGGTTTT CAGCACCCAGGTCCCGGG GGAGCA
FK382	3' Spt5 aa593	FK377	Spt5 CT4	CTTGGAAGTACAGGTTTT CAGCACCGTTGTTCTGCT CTGAGTCCAAG
FK383	3' Spt5 aa754	FK377	Spt5 CT3	CTTGGAAGTACAGGTTTT CAGCACCGCCCACCGTGG TGAGCC
FK384	3' Spt5 aa837	FK377	Spt5 CT2	CTTGGAAGTACAGGTTTT CAGCACCCTCATATTCTT CCTCAGCCCG
FK385	3' Spt5 aa978	FK377	Spt5 CT1	CTTGGAAGTACAGGTTTT CAGCACCGTCGCTGGAGT TCTGCTCGA

Oligos used for colony PCRs and Sanger sequencing are listed below.

ID	Description	Sequence 5' – 3'
Seq01	Sumo fwd	ATAACGATATTATTGAGGCTCAC
Seq02	SV40 rev	TATGGCTGATTATGATCCTCTA
Seq09	Sumo fwd2	TACGACGGTATTGAAATTCAAG
Seq10	SV40 rev2	GTTTCAGGTTCAGGGGGA
Seq11	MED12 fwd1	GGAGCAGTTACAGAAGATG
Seq12	MED12 fwd2	CAGTTGAAGTTCGCTGGTC
Seq13	MED12 fwd3	ACATTGACCCTAGTTCCAG
Seq14	MED12 fwd4	GTGTAGTTGAGGCTGAGC
Seq15	MED12 fwd5	ACTTTTGTTGCCATCCTCATC
Seq16	MED12 fwd6	GTGCTCAGCTCTCTAGAG
Seq17	MED12 fwd7	GCTTCGATTCCATCTTCAAG
Seq18	MED12 fwd8	ACTGGCGTCATGGGTTTAG
Seq19	MED12 fwd9	AACAGCAACAGCAGCAGC
Seq20	CDK8 fwd	TGTTACATTCTGGTACCGAG
Seq21	MED13 fwd1	CCTTGCTCAACAGTCTAATAG
Seq22	MED13 fwd2	AATCTCAAGTCAAGAAATGCTG
Seq23	MED13 fwd3	AGAGTTAATGGTGCAATGTAAG
Seq24	MED13 fwd4	TAGTATAGGAGCGCAGTTC
Seq25	MED13 fwd5	GCATCTGTGTTTGCAACATG
Seq26	MED13 fwd6	CCAGAACCACTGCCAATC
Seq27	MED13 fwd7	GCAGGATCCATGTCTACAC
Seq28	MED13 fwd8	GGATACTGTTTATCACATGATC
Seq29	MED13 fwd9	TTAGCTTTCAATCCCAACAATG
Seq31	HSV TK polyA rev	AACACCCGTGCGTTTTATTC
Seq32	p10 fwd	GGACCTTTAATTCAACCCAAC
Seq33	MED13 rev1	TCTATTGGAACGGTGTTTAATG
Seq34	MED13 rev2	CTCATTGGTCTTGTGCTTAG
Seq35	polh fwd	GGAGATAATTAAAATGATAACCATC
Seq36	CDK8 rev	TGGTTCTGACGTTAGTAGTTC
Seq37	Cyclin C rev	TTCAGAGAATACCTGGCATAG
Seq38	T7 terminator rev	GCTAGTTATTGCTCAGCGG
Seq39	MED12 Codon opt. fwd1	CACTAAGTACCTGTGGGAAC
Seq40	MED12 Codon opt. fwd2	CGAGATCGAACAGCAGATC
Seq41	MED12 Codon opt. fwd3	CAGCTCTTCAAAGCTGGAAG
Seq42	MED12 Codon opt. fwd4	CTGATGGAATACTCTCTGTC

ID	Description	Sequence 5' – 3'
Seq43	MED12 Codon opt. fwd5	CTGTGCAACGTGGACGTC
Seq44	MED13 Codon opt. fwd1	TCACCCTGGCTCAGCAG
Seq45	MED13 Codon opt. fwd2	CTGCGTCACAAGAACCTG
Seq46	MED13 Codon opt. fwd3	CAGTGCAAGAAGCCACTG
Seq47	MED13 Codon opt. fwd4	CCCTCTGAGATCAAGGAC
Seq48	MED13 Codon opt. fwd5	CTTCTCTGCTGTCATGAAC
Seq49	MED13 Codon opt. fwd6	TGGAACCCTACGGTTCAC
Seq50	MED13 Codon opt. fwd7	GCAAACCGCTGGTATCTC
Seq51	MED13 Codon opt. fwd8	CAACAGAGCCAGGAGAAAG
Seq52	MED13 Codon opt. fwd9	TCCCCAACATCCTGCAAC
Seq53	Cyclin C Codon opt. fwd1	CTAGAGATCATTCGCGTAATC
Seq54	CDK8 Codon opt. fwd1	AGCCTTCGTATTCGAAGAG
Seq55	LoxP fwd	CTTGGGCAGCAGCGAAG
Seq56	eYFP rev	GGACGAGCTGTACAAGTAG
Seq57	CDK8 Codon opt. fwd2	TTCACTGGTCAGCAACTCG
Seq58	CDK8 Codon opt. rev1	CTACTTGGTGCAAGGCAC
Seq59	Cyclin C Codon opt. fwd2	TCCCTTACAGGATGAACCAC
Seq60	Cyclin C Codon opt. rev1	ACGGATGGTACACGATGAG
Seq61	BstXI fwd	GTATACCCTAGGGGTTATGAT
Seq62	Strep fwd	GTCACACCCTCAATTCGAG
Seq63	Strep rev	CAGGGAACCGGTCTTTTC
Seq64	CDK19 fwd	GATACCAAAATGTCACAACTAC
Seq65	CDK19 rev	GGTGCTTCACAGAGACTTG
Seq66	CDK8 Codon opt. rev2	CGCTTGGCCTTGTATACATG
Seq67	Cyclin C Codon opt. rev2	CTTGACCCATATCCTGGAC
Seq71	Spt5 fwd1	CAGCTGCTCCCAGGAGTC
Seq72	Spt5 fwd2	GTGATCACGGAGGGTGTG
Seq73	Spt5 rev1	CACACCCTCCGTGATCAC
Seq74	Spt5 fwd3	GGCTGTTTGATGCTGAGAAG
Seq75	Spt5 fwd4	GACCTTCCAGGTGCTGAAC
Seq76	Spt5 fwd5	CCCAGACGCCCATGTATG
Seq77	Spt5 fwd6	GGGACACCTACCTGGATAC

Appendix B: Additional cloned plasmids

Additional MED12 and MED12L encoding plasmids, which were not included/did not appear in this study, yet might be useful for further studies, are listed below.

Backbone	Insert	Amino acids/ mutation	5' modification	3' modification	Internal ID
pIRESneo	MED12	1-2177/wt	Flag-HA		CP3
pIRESneo	MED12	1-2177/E33Q	Flag-HA		CP3M1
pAceBac1	MED12	1-2177/E33Q	Strep-SUMO-T7-TEV		1M1
pFL	MED12	1-2177/wt	Strep-SUMO-T7-TEV		11
pAceBac1	MED12	1-2048/wt	Strep-SUMO-T7-TEV		2
pAceBac1	MED12	1-1395/wt	Strep-SUMO-T7-TEV		4
pAceBac1	MED12	1-1227/wt		TEV-T7-Strep	38
pAceBac1	MED12	1-1227/wt		TEV-T7-Strep	56
pFL	MED12	1-1227/wt		TEV-T7-Strep	44
pFL	MED12	1-1227/wt		TEV-T7-Strep	55
pIDS	MED12	1-1227/wt	SUMO-T7-TEV		30
pAceBac1	MED12	1-1195/wt	Strep-SUMO-T7-TEV		26
pAceBac1	MED12	1-1114/wt	Strep-SUMO-T7-TEV		76
pAceBac1	MED12	1-1100/wt	Strep-SUMO-T7-TEV		27
pAceBac1	MED12	1-1005/wt	Strep-SUMO-T7-TEV		77
pAceBac1	MED12	19-295/wt		TEV-T7-Strep	104
pAceBac1	MED12	19-303/wt		TEV-T7-Strep	105
pAceBac1	MED12	11-45/wt		TEV-T7-Strep	154
pAceBac1	MED12	11-50/wt		TEV-T7-Strep	153
pAceBac1	MED12	23-45/wt		TEV-T7-Strep	157
pAceBac1	MED12	23-50/wt		TEV-T7-Strep	156
pAceBac1	MED12	23-60/wt		TEV-T7-Strep	155

Backbone	Insert	Amino acids/ mutation	5' modification	3' modification	Internal ID
pAceBac1	MED12	1-100/wt		TEV-T7-Strep-Flag	41F
pAceBac1	MED12	1-100/E33Q		TEV-T7-Strep-Flag	41FM1
pAceBac1	MED12L	1-100/wt		TEV-T7-Strep	41L
pAceBac1	MED12	1-174/wt		TEV-T7-Strep	124
pAceBac1	MED12	1-224/wt		TEV-T7-Strep	42
pAceBac1	MED12	1-295/wt		TEV-T7-Strep	120
pAceBac1	MED12	1-303/wt		TEV-T7-Strep	121
pAceBac1	MED12L	1-352/wt		TEV-T7-Strep	43L
pAceBac1	MED12	1-540/wt		TEV-T7-Strep	81
pAceBac1	MED12	1-593/wt		TEV-T7-Strep	113
pAceBac1	MED12	1-621/wt		TEV-T7-Strep	82

Additional MED13 encoding plasmids, which did not appear in this study, yet might be useful for further studies are listed.

Backbone	Insert	Amino acids	5' modification	3' modification	Internal ID
pAceBac1	MED13	1-2174		TEV-T7-Strep	58
pFL	MED13	1-2174		TEV-T7-Strep	57
pIDS	MED13	1-2174	SUMO-T7-TEV		29
pIDS	MED13	1-2174	T7-TEV		60
pIDS	MED13	1-1366	SUMO-T7-TEV		31
pIDS	MED13	1-1366	T7-TEV		32
pIDS	MED13	1367-2174	SUMO-T7-TEV		33
pIDS	MED13	1367-2174	T7-TEV		34
pIDS	MED13	1367-2174	T7-TEV		62
pIDS	MED13	1330-2174	SUMO-T7-TEV		35
pIDS	MED13	1330-2174	T7-TEV		36

Backbone	Insert	Amino acids	5' modification	3' modification	Internal ID
pIDS	MED13	1330-2174	T7-TEV		61
pIDS	MED13	1331-1408	T7-TEV		84
pIDS	MED13	1409-2174	T7-TEV		85
pIDS	MED13	1-390	T7-TEV		37
pIDS	MED13	1-390	T7-TEV		63
pAceBac1	MED13	1-390		TEV-T7-Strep	86
pAceBac1	MED13	1-500		TEV-T7-Strep	87
pAceBac1	MED13	1-545		TEV-T7-Strep	88

Additional donor plasmids that encode for full-length Cyclin C in combination with different C-terminally truncated CDK8- or CDK19 variants were listed. These constructs were primarily used for crystallization attempts. However, as we did not obtain diffracting crystals, these constructs are not included in this study.

Backbone	Insert	Amino acid	5' modification	3' modification	Internal ID
pUCDM	Cyclin C CDK8	1-283 1-353			79b
	Cyclin C CDK8	1-283 1-424			79e
	Cyclin C CDK8	1-283 1-371			79f
pUCDM	Cyclin C CDK19	1-283 1-353			98c
	Cyclin C CDK19	1-283 1-460			98e
	Cyclin C CDK19	1-283 1-371			98f

Additional cloned plasmids that could be used for protein production and additional research.

Backbone	Insert	Amino acids	5' modification	3' modification	Internal ID
pIDS	MAT1	1-309			152
pAceBac1	p21	1-164		TEV-T7-Strep	160
pGEX4T1	p21	1-164	GST-TEV		EC12

In the following, C-terminally truncated variants of Spt5 were cloned into pAceBac1 acceptor vector, combined with Spt4, co-expressed and purified to homogeneity. These constructs and resulting DSIF variants, that harbor C-terminally shortened Spt5, were handed out to Vladyslava Gorbovytska and Filiz Kuybu. Furthermore, wild-type NELF and the mutants SV210 and SV211 (Vos et al., 2016) as well as wild-type DSIF was purified and provided for general usage.

Backbone	Insert	Amino acids	5' modification	3' modification	Internal ID
pAceBac1	Spt5	1-978		TEV-Strep	Spt5 CT1
pAceBac1	Spt5	1-837		TEV-Strep	Spt5 CT2
pAceBac1	Spt5	1-754		TEV-Strep	Spt5 CT3
pAceBac1	Spt5	1-593		TEV-Strep	Spt5 CT4
pAceBac1	Spt5	1-518		TEV-Strep	Spt5 CT5
pAceBac1	Spt5	1-399		TEV-Strep	Spt5 CT6

Acknowledgements

Thanks to all students that were part of the CDK8 crew

- Maximilian Seurig – workflow optimization and first MED13 constructs
- Melanie R. Müller – first CDK19 studies and co-purification attempts
- Franziska Langhammer – high throughput MST measurements
- Robin Weinmann – high throughput kinase assays
- Bastian Jahreis – CDK8 autophosphorylation
- Silas Amarell – N-terminal MED13 binding studies
- Meret Kuck – crystallization of CDK8/19 ternary constructs
- Amelie Lindner – p21 binding studies

I really enjoyed to supervise and to teach you all

Dr. Alexander Leitner, Dr. Elisabeth Schneider, Dr. Hung Ho-Xuan and Dr. Iana Kim - thank you for the data for our manuscript

Thanks to Vlada Gorbovytska for an always open ear for my personal and private issues

Katrin Wienchol - I regret the worst decision I've ever made in my life - please forgive me

(Eidesstattliche) Versicherungen und Erklärungen

(§ 9 Satz 2 Nr. 3 PromO BayNAT)

Hiermit versichere ich eidesstattlich, dass ich die Arbeit selbstständig verfasst und keine anderen als die von mir angegebenen Quellen und Hilfsmittel benutzt habe (vgl. Art. 64 Abs. 1 Satz 6 BayHSchG).

(§ 9 Satz 2 Nr. 3 PromO BayNAT)

Hiermit erkläre ich, dass ich die Dissertation nicht bereits zur Erlangung eines akademischen Grades eingereicht habe und dass ich nicht bereits diese oder eine gleichartige Doktorprüfung endgültig nicht bestanden habe.

(§ 9 Satz 2 Nr. 4 PromO BayNAT)

Hiermit erkläre ich, dass ich Hilfe von gewerblichen Promotionsberatern bzw. -vermittlern oder ähnlichen Dienstleistern weder bisher in Anspruch genommen habe noch künftig in Anspruch nehmen werde.

(§ 9 Satz 2 Nr. 7 PromO BayNAT)

Hiermit erkläre ich mein Einverständnis, dass die elektronische Fassung meiner Dissertation unter Wahrung meiner Urheberrechte und des Datenschutzes einer gesonderten Überprüfung unterzogen werden kann.

(§ 9 Satz 2 Nr. 8 PromO BayNAT)

Hiermit erkläre ich mein Einverständnis, dass bei Verdacht wissenschaftlichen Fehlverhaltens Ermittlungen durch universitätsinterne Organe der wissenschaftlichen Selbstkontrolle stattfinden können.

…………………………………………………………………………………………

Ort, Datum, Unterschrift